Design and fabrication of a novel bioactive composite scaffold to induce anterior cruciate ligament regeneration

Tania Citlalli Choreño Machain

Submitted for the degree of:

Doctor of Philosophy

Division of Surgery and Interventional Science

University College London

Declaration

I, Tania Citlalli Choreño Machain confirm that the work presented in this thesis is my own. Where information has been derived from other sources, I confirm that this has been indicated in the thesis.

Signature:

Abstract

Introduction: Anterior cruciate ligament (ACL) injuries are one of the most common sports injuries. The injury entails devastating consequences in a person's quality of life and leads to an early onset of osteoarthritis (OA). The current treatment of choice is associated with an unacceptable rate of donor-site morbidities due to harvesting a tendon from the already injured limb to use as a graft for the surgical reconstruction, but the alternative conservative treatment is associated with up to 87% development of post-traumatic OA. Although various approaches exist, there is currently no ideal choice of graft that could ensure knee stability and address the joint inflammatory state.

Hypothesis: The addition of a biomimetic coating to the only clinically accepted synthetic graft's material will support ligament resident cells growth and enhance ligament-like extracellular matrix deposition that would contribute to ligament healing.

Methods: PET fibres were modified in a two-step process. First, O_2 plasma was used to activate the surface. Next, a bioactive coating was added. Biocompatibility tests under physiologically relevant static and dynamic conditions were executed with mesenchymal stem cells (MSCs) and patient-derived ACL cells.

Results: PET surface was effectively activated by a 1-min O_2 plasma exposure. The 1% chitosan glycidyl methacrylate (CS-g-GMA) / 1% hyaluronic acid (HA) coating of an O_2 plasma pre-treated PET fibrous scaffold provided the maximum enhancement of collagen deposition across all the studies conducted. The effect is sustained in the context of strenuous physical activity and is further increased by low-intensity pulsed ultrasound (LIPUS) treatment at a frequency of 1 MHz, a duty cycle (DC) of 50% and an intensity of 0.5 W/cm^2. The scaffold proved appropriate for the interaction with a MSC line and patient-derived ACL cells from individuals of different ages and gender.

Conclusion: The biocomposite scaffold designed and developed in this thesis combines straightforward methodology, approved materials already in clinical use for different purposes and a favourable response to safe readily available rehabilitation options to improve the outcomes for ligament regeneration.

Impact statement

The current surgical treatment of choice for an ACL complete rupture is restricted for the more physically active and younger patients, leaving a wider population affected by ACL injuries without this benefit. The associated graft donor site morbidities and the absence of certainty for full stability recovery and quality of life limit this option. A synthetic scaffold that provides tissue integration could overcome the current challenges. PET, CS and HA have been used before in ligament tissue engineering (TE). Nevertheless, no previous research has employed the manufacturing protocol, materials with the chemical modification, mixture ratio, and concentration here explored. The bioactive composite scaffold developed and evaluated in this thesis demonstrates the potential for the induction of ligament regeneration supported by its ability to considerably enhance the extracellular matrix deposition of both types of cells found in native ACL tissues. It also effectively sustains these cells through mechanical stimulation encountered in real-life scenarios. The approach of this project incorporates physiologically and clinically relevant materials and methods, reflecting on the advancement of biomaterials and TE approaches for ligament regeneration.

The two-step manufacturing approach here explored proved successful in incorporating physical and chemical cues relevant to ligament tissue. O_2 plasma treatment is an effective technique to activate the PET surface and improve a bioactive coating addition. The interaction between CS-g-GMA and HA at the concentrations and ratio here explored showed a favourable bioactive mixture. The 1% CS-g-GMA / 1% HA coating of a 1-min O_2 plasma pre-treated PET fibrous scaffold supports cell growth and significantly enhances extracellular matrix (ECM) deposition. The results from the dynamic stimulation experiments show promise for an alternative synthetic graft that positively interacts with physiologically relevant mechanical stimulation in promoting ligament tissue remodelling. It offers a promising option for a safe return to sports after surgical reconstruction. From a personalised medicine perspective, the similar

favourable outcomes obtained after using different patient-derived cell populations in the experiments suggest good tolerance despite patient-to-patient variability.

The scaffold proved appropriate for the interaction with an MSC line and patient-derived ACL cells from individuals of different ages and gender. The scaffold here proposed for ligament regeneration offers several benefits. The methodology is easily reproducible, the selected materials are environmentally friendly, and they are relatively low cost. The use of clinically validated and certified materials could expedite further testing and incorporation into clinical settings. Due to the inherent material properties, the scaffold holds the potential for reduced immune responses, inflammatory reactions, and infections, hence improving ligament regeneration.

Further *in vitro* experiments are required with a larger set of patient-derived cells to address the hosts biological responses heterogeneity, particularly in search for the anti-inflammatory potential of the proposed scaffold. With the aim to translate the alternative to a clinical setting, computational biomechanics analyses could be done by using accurate and realistic finite element simulations. As part of a pre-clinical testing stage, the material properties could then be evaluated in relevant *in silico* models employing different surgical techniques and the addition of components such as muscles and synovial fluid to better understand the response of the biomimetic composite ligament scaffold to different physiologically relevant loading regimes and determine the complex cause-effect correlation. Moreover, to advance the pre-clinical stage of the research involving the biomimetic composite scaffold here proposed, naturally occurring disease models of domesticated and companion animal trials could be designed as they would be mutually beneficial for human and veterinary patients, offering the latter an alternative treatment to slow down joint degeneration and reduce pain caused by a chronically deficient limb. This is of particular relevance given that as in humans, ACL (also known as cranial cruciate ligament) injuries are one of the most common orthopaedic injuries in dogs and the injury implies an increased risk of euthanasia, particularly for large and giant breeds [1].

Acknowledgements

In the following paragraphs, I would like to express my gratitude towards everyone who has contributed somehow to the culmination of this project.

Firstly, I would like to thank UCL for hosting my studies and providing innumerable opportunities for my professional and personal growth. Likewise, I am grateful to the Consejo Nacional de Ciencia y Tecnología (CONACYT) for funding my PhD programme, making this work possible.

I would like to express my deepest appreciation to my supervisors. Prof Umber Cheema, I will be forever grateful for the opportunity in accepting me into her group. Her kindness, positivity and guidance have been invaluable. Mr Sujith Konan, I am truly grateful for his support and the occasion to be part of his practice. Dr Pierre Gélat, I appreciate him giving such insightful feedback; his guidance arrived at a crucial time.

I would also like to thank Prof Wenhui Song for providing her expertise and helping shape the dynamic culture work. Dr Eduardo Elizalde Peña, for his direction throughout the synthesis of the materials. I would also like to acknowledge Prof Stefan Guldin and Maximiliano Jara Fornerod from the Department of Chemical Engineering for their assistance and access to their plasma machine. Likewise, my sincere regards to Dr Nikolitsa Nomikou and Hamzah Masood for their kind assistance with the sonoporator device. I extend my gratitude to Dr Richard Thorogate, Dr Robert Palgrave and Dr Nicola Mordan for their training and aid with AFM, XPS and SEM. My appreciation goes to the members of the Division of Surgery, extended to all the people I have had the pleasure to meet and work with at IOMS, CBH and particularly at the Royal Free Hospital, where I had the fortune to get to know such friendly peers. I would also like to recognize the invaluable assistance of Alexandru Chivu, Chau Chong, Evelyn Karageorgiou, Heike Lee-Muller, Katerina McCann, Kathryn Knapp, Sra. Maria, Mark Harrison, and Amir Afrashtehpour. I am very grateful to Dr Amir Gander for being the most considerate manager. Dr Nathan Griffiths, Craig, Diana, Amy, Kyra, Elena,

Akshay, and everyone else at TAPb, working alongside them lovingly enriched my PhD experience. I would also like to acknowledge the help of Paul Harrison from Don Whitley Scientific Limited for his assistance with the TC-3 bioreactor.

My sincere regards to everyone in Prof Umber's group. A special mention to Rawiya Al Hosni, for her invaluable thoughtfulness and assistance whenever I got stuck with anything in the lab. Elena Provaggi, Sara Malferrari and Aida Rivera Navarro, I am very grateful for having been part of the same group as you; I cannot thank you enough for your support. Thank you to Soraya Padilla Lopategui, Medina Guliyeva, Carolina Ramos Rivera, and Krystal Gayle, who made these years incredibly joyful.

My heartfelt gratitude goes to everyone in my family for being ever so present. T.M. for cheering me and providing a loving outsider's academic look whenever I needed it. To my brother, whose points of view keep me grounded and give me perspective. To my friends back home for all their positivity.

Finally, this work is in loving memory of two extraordinary women whose example and encouragement have been essential in my life and throughout this journey. I would also like to dedicate this work to my parents, without whom none of it would have been possible. I owe them my deepest gratitude for being an immeasurable source of inspiration and for their unwavering guidance.

Table of contents

List of figures

Chapter 1

Chapter 2

Chapter 3

Chapter 4

Chapter 5

Chapter 6

Chapter 7

List of tables

Chapter 1

Chapter 2

Chapter 3

Chapter 4

Abbreviations

θ – surface contact angle

2D – two-dimensional

3D – three-dimensional

ACL – anterior cruciate ligament

ACLSCs – anterior cruciate ligament derived stem cells

ACLR – anterior cruciate ligament reconstruction

ADSCs – adipose derived stem cells

AFM – atomic force microscope

ALP – alkaline phosphatase

AMB – anteromedial bundle

ANOVA – analysis of variance

ATR – attenuated total reflectance

bFGF – basic fibroblast growth factor

BMPs – bone morphogenetic proteins

BPTB – bone-patellar tendon-bone

BrdU – 5-bromo-2'-deoxyuridine

BSA – bovine serum albumin

CI – confidence intervals

COL1A1 – gene encoding collagen type I alpha 1 chain

COL3A1 – gene encoding collagen type III alpha-1 chain

Col I – collagen type I

Col III – collagen type III

COL-I – anti-collagen I antibody

COL-III – anti-collagen III antibody

CS – chitosan

CS-g-GMA – chitosan glycidyl methacrylate

DAPI – 4',6-Diamidino-2-Phenylindole, Dihydrochloride

DMMB – dimethylmethylene blue assay

DMEM - Dulbecco's Modified Eagle Medium

DI H2O – deionized water

E – Young’s modulus

ECM - extracellular matrix

Egr1 – early growth response factor

ERK – extracellular signal-regulated kinase

eV – electron volt

FAK – focal adhesion kinase

FBS – fetal bovine serum

FITC – fluorescein isothiocyanate

FTIR – Fourier transform infrared spectroscopy

GAGs – glycosaminoglycans

HA – hyaluronic acid

HH – hedgehog

HIF1α – hypoxia inducible factor 1

HMDS – hexamethyldisilazane

HT – hamstring tendon

IGF – insulin-like growth factor

iMSCs – immortalised mesenchymal stem cells

kHz – kilo Hertz

LARS – ligament advanced reinforcement system

LF – ligamentum flavum

LIPUS – low intensity pulsed ultrasound

MAPK – mitogen-activated protein kinase

MEK – MAPK-ERK kinase

MDs – mean differences

Mkx – Mohawk homeobox

MPa – mega Pascals

MSCs – mesenchymal stem cells

N – Newtons

NHS – National Health Service

OA – osteoarthritis

PBS – phosphate-buffered saline

PCL – polycaprolactone

PDGF – platelet derived growth factor

PDMS – polydimethylsiloxane

PEG – polyethylene glycol

PET – polyethylene terephthalate

PGA – poly (glycolic acid)

PLA – poly (lactic acid)

PLGA – poly (D, L-lactic-co-glycolide)

PLLA – poly-L-lactic acid

PLB – posterolateral bundle

PSR – picrosirius red

PT – patellar tendon

RCT – randomised controlled trial

RF – radio frequency

ROCK – Rho-associated coiled-coil-containing protein kinase

Rq – root-mean-square

Runx2 – runt-related transcription factor 2

Scx – scleraxis

SD – standard deviation

SE – standard error of the mean

SEM – scanning electron microscope

sGAG – sulphated glycosaminoglycans

T – temperature

TA – tibialis anterior

TE – tissue engineering

Tnmd – tenomodulin

TGF-β1 – Transforming growth factor beta

US – ultrasound

Vcan – versican

XPS – X-Ray photoelectron spectroscopy

W - watts

WCA – water contact angle

Z – standard score

Chapter 1

Introduction

1.1 Clinical problem and epidemiology

There are four major ligaments in the human knee connecting the femur to the tibia and providing joint stability. Among them, the anterior cruciate ligament (ACL) is central for the steadiness of the knee. It is also the most frequently injured, particularly during sports. For the sportive population, the incidence of ACL injuries is at its highest during competitions. It is in these settings where more physically and mentally stressful situations are frequently encountered [2]. The mechanism of injury is heavily dependent on the type of physical activity at the time of injury and the playing surface in the case of sports. Generally, a noncontact mechanism is the most reported. It entails no physical contact with any other person at the time of injury. The most common dynamic alignment of the leg when an ACL injury occurs seems to be a “knee-in and toe-out”. The term refers to an outward angulation of the knee – in either an internal or external rotation of the tibia – while the foot moves away from the midline of the body during the loading phase. Both the mechanism and dynamic alignment explain why the incidence of ACL injuries is the highest in sports where sudden deceleration, landing and pivoting manoeuvres are recurring like in skiing, football, basketball, and volleyball [2, 3].

The main challenge from an injury to this intra-capsular ligament is its inability to self-heal. There have been 133 270 cases of anterior cruciate ligament reconstruction (ACLR) reported in England’s national hospital episode statistics (HES) between 1997 and 2017 [4]. From this same registry by Abraham et al. [4], a 12-fold increase in England’s national rate of ACLR was found. The incidence grew from 2.0/100 K population (95% CI 1.9 to 2.1) in 1997–1998 to 24.2/100 K (95% CI 23.8 to 24.6) in 2016 – 2017. More recently, the HES from 2018/ 2019 have listed an incidence of 6.8%

for spontaneous disruption of ligament of the knee as the primary diagnosis by outpatient attendance [5]. Nowadays, ACLR is one of the most common orthopaedic surgical procedures. Biological grafts are the preferred source of tissue for the surgical reconstruction, specifically autografts. Nevertheless, 0.31% of ACLRs employ synthetic grafts to avoid donor-site morbidity or augment graft size [6]. Compared to natural grafts, currently used synthetic grafts improve patient-reported outcome scores and have less postoperative complications [7], however, they have been associated with long-term inflammatory changes and stiffness attributed to immunological reactions [8].

Still, a set of non-athlete patients often receive a conservative treatment instead of an ACLR. Although the prevalence of ACL injuries lies within a sport setting at about a 5-fold difference, road traffic accidents and activities of daily living also contribute to the epidemiology of ACL tears [9]. ACL injuries predominantly occur in young, physically active patients. For the non-competitive athlete population, surgical reconstruction is often delayed or even set aside in favour of conservative management of the injury. The consensus statement from the British Association for Surgery of the Knee (BASK) and the British Orthopaedic Sports Trauma and Arthroscopy Association (BOSTAA) on the best practice for ACL injuries management [10], notes that the chief indication for ACLR is symptomatic instability. Current innovations in techniques and surgical expertise in the field of paediatric ACLRs have ensured that skeletally immature patients are considered for surgical reconstruction. In this population, a conservative approach seems to be linked to a worse long-term outcome for meniscal or cartilage damage from an unstable joint [11]. These Associations recognise the current lack of evidence for reconstruction reducing the risk of osteoarthritis (OA) or improving long-term function in the absence of instability, for which often the non-athlete population with low functional demands, no sporting interests and the patients' perceived stability of the knee opt for a non-operative treatment involving physical rehabilitation [12, 13]. ACLR appears to prevent to some degree further meniscal injury and therefore decrease future OA rates. The prevalence of post-traumatic OA is 24.5 – 51.2%; its association with chronic anteroposterior instability has long been suggested [14]. This knee instability develops in 8 to 50% of patients after ACLR; in 75 to 87% of those treated conservatively [14]. The psychological and psychosocial implications of the

distressing consequences of an ACL injury are increasingly recognised. The incidence of depression after an ACL diagnosis and the fear of reinjury can be as high as 40% and 50%, respectively [15]. These conditions contribute as much as 60% to an athlete's failure to return to their pre-injury level of play [15]. A group comparing the incidence of meniscal and cartilage injuries in athlete and non-athlete populations concluded that both groups could benefit from early ACLR as no difference in the progression of injuries in athletes and non-athletes was found [13].

Across the world, the projected population growth expects people aged over 65 years to outnumber children younger than five years of age within the next decade [16]. Given that inactivity directly correlates with chronic diseases, governments are now actively encouraging physical activity throughout a person's lifespan. People who join any sporting activity after the age of 65 generally decide to do so either to look after their health or to negotiate the ageing process. Participation in sports as people get older is becoming an identity statement. Sports participation aids to evade the older adult societal stereotype, aiming to exchange it for that of a competitive athlete [17]. In this respect, the Eurobarometer report published in 2018 [18] revealed that 30% and 28% of European citizens over the age of 55, men and women respectively (40% and 37% for the UK), practice exercise or sport. In total, 44% of European citizens aged 15 or older (45% for the UK) are involved at least with some regularity in any type of physical activity outside sports. Interestingly, 69% of these European citizens (70% for the UK) engage in sports or recreational physical activity spontaneously and are not members of any club, which would imply that they practice without an injury prevention plan in place and with heterogenous fitness and health conditions. For the younger population, an Australian report on a large repository of sport registration data from state sporting associations found that nearly a third of all sports participants were aged 10 – 14 years [19].

As more people around the world is encouraged to participate in sport activities and the sports demands are intensifying, the increase in ACL injuries and ACLRs compel the advancement of a ligament graft that can offer a safe and long-lasting return to pre-injury stability and functionality.

1.2 Anterior cruciate ligament structure and ultrastructure

Ligaments are dense regular connective tissues that link together bones to bones. Structurally, hierarchically arranged parallel collagenous fibres form the ligaments (see figure 1.1). The ligament's fibrous architecture is poorly vascularised and populated. Fibroblast cells are the most common type of cells found in a ligament. Other than fibroblasts, a subpopulation of cells positive for α-smooth muscle actin (α-SMA) [20] and two different populations of clonogenic multipotent cells have been isolated from human ACLs [21-25]. MSCs are a heterogeneous fibroblast-like type of stem cells capable of differentiating into a range of mesodermal phenotypes and musculoskeletal tissues including ligaments [26, 27]. Articular MSCs' niche is poorly vascularised and poorly oxygenated. Whitin the ligament, A population of ACL-derived MSCs share characteristics with synovial MSCs [25], which are very sparce within the ECM rather than directly in contact with other cells but receive signalling through transmembrane proteins from underlying cells and their homeostasis is highly regulated by mechanical stress and the interaction with the specific ECM components they produce [27]. Articular MSCs are habitually quiescent but activate in response to injuries [22]. The cellular component receives the blood supply from the epiligament, which also contains the sensory and proprioceptive nerves. The anterior cruciate ligament plays a key role in joint motion. Knee flexion and extension is largely made possible by the strong collagen dense structure that tightly binds the femur and the tibia, preventing an anterior displacement of the tibia and resisting rotational loads, particularly during exercise. Macroscopically, the ACL is formed by the anteromedial bundle (AMB) and the posterolateral bundle (PLB). The bundles originate from the posterior-medial aspect of the lateral femoral condyle and insert at the anterior aspect of the tibial plateau. They are not isometric. During flexion, the AMB extends while the PLB shortens. At knee extension, the ACL has a mean length of 32 mm and a width of 7-12 mm. The ACL is innervated by posterior articular branches of the tibial nerve, and it is vascularised by branches of the middle genicular artery.

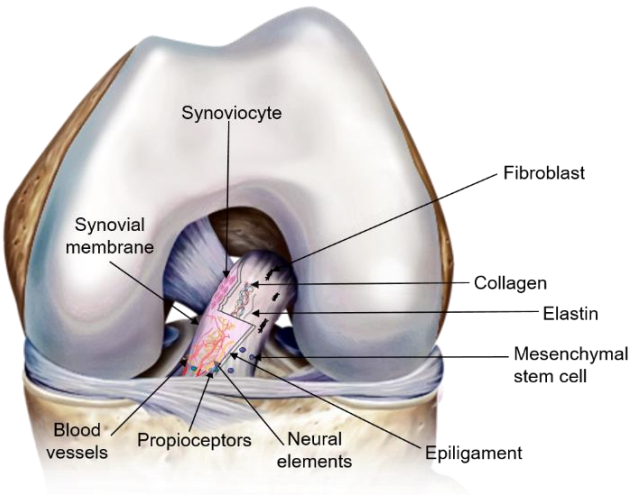

Figure 1.1 Human anterior cruciate ligament gross anatomy and microanatomical histoarchitecture. Image modified from Arthrex Inc with Servier Medical Art under a Creative Commons Attribution 3.0 Unported License.

The ACL ultrastructure is composed of collagen bundles of multiple types (mostly type I) and a matrix made of a network of proteins, glycoproteins, elastic systems, and glycosaminoglycans (GAGs) with numerous functional interactions. Compared to the homogeneity in periarticular tendons, the ACL exhibits distinguishable arrangements of collagen fibres and cell type at its proximal, medial, and distant regions. The greater part of the ACL exhibits a parallel fibre structure with spindle-shaped cells, resembling the tendon composition; conversely, a distinctive trait of ACL histology is the presence of helical and crossing fibres forming non-linear networks. A feature of the insertion sites of the ACL is the disordered loose fibres assembly, populated by fibrochondrocyte-like cells responsible for the deposition of high amounts of GAGs in these regions [28]. Another type of cells observed at the proximal regions of the ACL are mesenchymal stem cells with a marked ability to differentiate into the chondrogenic, osteogenic and adipogenic lineage [24]. Undular fibres – referred to as crimp – and helical fibres – unique to the ACL – can be identified in this tissue. A distinctive ultrastructural characteristic of the ACL is its lamellar layout, which presents changes in fibre orientation from lamellae to lamellae. Also specific to ACL is the smaller (between 50 and 100 nm) and more homogenous distribution of fibril diameters with a mean density of 142.51 ± 57.12 per μm^2, which is 3.8 times that of the hamstring tendon (HT) [28].

The ACL is capable of enduring multiaxial stresses and varying tensile strains due to its complex ultrastructural organization and abundant elastic system. These properties enable it to transfer loads from bone to bone restraining excessive joint displacements when subjected to high stresses [29]. The ultimate tensile force of ACL varies between 600 and 2300 N, according to studies on cadavers [30]. Moreover, each of the two distinct bundles of the ACL present different tangent modulus. Butler et al. reported a tangent modulus of 154 ± 120 MPa for the AMB and 283 ± 114 MPa for the PLB in humans [31], lower from that of the extra-articular ligament medial collateral ligament (MCL) (332 ± 58 MPa) [29].

1.3 Ligament markers

Describing ligaments as either intra-articular or extra-articular is useful given that their ultrastructure varies in response to their anatomical location [28, 29, 32-34]. Compared to tendons and extra-articular ligaments, the anterior cruciate ligament has a higher expression of the genes for decorin, fibromodulin, transforming growth factor (TGF) β1, hypoxia inducible factor 1 (HIF1α), collagen type III (COL3A1), collagen type V and elastin [34, 35]. Still, ligaments and tendons share similarities and are therefore commonly studied together (table 1.1). The gene expression of collagen type I (COL1A1), COL3A1, tenascin-C and scleraxis (Scx) is ordinarily looked for to characterise ligaments. During embryogenesis of ligament tissues, the genes for types I, III, IV, V and VI collagen are upregulated, although they are not specific [36]. Tenascin-C is an extracellular matrix glycoprotein highly expressed during embryogenesis and in sites with high cell turn over or that undergo significant tensile stress [37]. A member of the zinc finger transcription factor's family, the early growth response factor (Egr1), has also been identified as a key factor for ligament formation during embryogenesis [36]. During this same period, versican (Vcan) – a chondroitin sulphate proteoglycan – contributes to ligament development by modulating the expression of Scx and increasing the local concentration of TGFβ. It is present at the ligament-bone interface during foetal development [38, 39]. On the other hand, mature tendon and ligament cells specifically express tenomodulin (Tnmd) and show a transient expression of tenascin-C during active tissue remodelling or pathological state. Scx is a helix-loop-helix major ligament / tendon transcription factor required for the

development of ligaments in the limbs, specific to the formation of connective tissue mediating attachment to bone [36, 40]. Mohawk homeobox (Mkx) is part of the superclass of three amino acid loop extension atypical homeobox genes. It is specifically expressed in ligament / tendon, and it is related to the tissue maturation [36, 41].

	Ligament	**Tendon**	**References**
Characteristic	**Content / expression**	**Content / expression**	[24, 29, 35, 40, 42-51]
Main cellular composition	Fibroblast (Lygamentocyte)	Tenocyte	
Mesenchymal progenitor cell markers	Nucleostemin, SSEA-4, STRO-1, Oct-4, CD29, CD44, CD90 and CD105	STRO-1, Musashi-1, CD146, CD90 and CD44	
Ground substance	20 – 30%	Lower	
Water	60 – 80%	60 – 80%	
Collagen type I	70 – 80%	95 – 99% 103 ± 38 µg / mg dry tissue	
Collagen type III	8%	1 – 5% 17.8 ± 6.6 µg / mg dry tissue	
Collagen type V	12%	Lower	
Collagen amino acids			
Cysteine content	3.3 per 1000 residues	0. 8 - 1.11 per 1000 residues	
Major reducible collagen crosslink	Hydroxylysinonorleucine (DHLNL)	Histidino - hydroxymerodesmosine (HHMD)	
Hydroxylysyl pyridinoline (HP)	0.48 – 0.67 mol/mol of collagen	0.31 – 0.50 mol/mol of collagen	
Lysyl pyridinoline (LP)	0.014 – 0.026 mol/mol of collagen	< 0.01 mol/mol of collagen	
Elastin	5% Ligamentum flavum (LF): 141 ± 7 spectral counts	2% Achilles tendon: 9 ± 8 spectral counts	
Tenascin	LF: 17 ± 15 spectral counts	Achilles tendon: not detected	

Hyaluronan and proteoglycan link protein 1	LF: 47 ± 30 spectral counts	Achilles tendon: 0 ± 0 spectral counts	
HIF1α	Higher	Lower	
GAG	Femoral insertion site > midsubstance > fibular insertion site Most abundant: chondroitin sulphate and dermatan sulphate (DS) MCL : 4.2 ± 1.9 µg sGAG / mg dry tissue	1.2 ± 0.06 – 12.3 ± 4.3 µg / mg dry tissue Most abundant: chondroitin sulphate (0.2 ± 0.2 – 6.9 ± 2.6) and DS (0.8 ± 0.2 – 2.5 ± 1.2) (Mean ± S.D.) Areas subject to compressional force: DS and keratan sulphate	
Proteoglycans	1 %		
Decorin	LF: 278 ± 10 spectral counts	Achilles tendon: 207 ± 30 spectral counts	
Fibromodulin	LF: 51 ± 18 spectral counts	Achilles tendon: 59 ± 14 spectral counts	
Biglycan	LF: 192 ± 8 spectral counts	Achilles tendon: 81 ± 10 spectral counts	
Fibronectin	11 ± 7.0 µg / mg dry tissue	1.6 ± 0.3 µg / mg dry tissue	

Table 1.1 Comparison between ligaments and tendons. All ligamentum flavum and Achilles tendon protein contents are expressed as mean ± SE.

1.4 Ligament extracellular matrix (ECM)

Ligaments are mainly composed of water, with only one third of them corresponding to solid components, primarily collagen at about 75%. Out of this, collagen type I (Col I) accounts for 85% and the rest is made up of types III, VI, V, XI and XIV. Proteoglycans, elastin, and glycoproteins among other proteins, make up the remaining dry weight of a ligament. Characteristically, collagens are molecules composed of three polypeptide chains with the repeating amino acid motif glycine followed by any two other amino acids (Gly-X-Y) contained by one or more regions in each of the chains [52-54].

At an ultrastructural level, the collagen fibres within a ligament are further composed of smaller fibres (figure 1.2). Within the ligament cells, procollagen molecules are

synthesised as procollagen alpha chains on the ribosomes and transported to the rough endoplasmic reticulum where the procollagen molecules assemble through a series of post-translational modifications [55]. Before these molecules are secreted through microtubules into the extra cellular space, they are compressed into secretory vesicles in the Golgi network. Procollagen molecules are subsequently processed so that the triple helical collagen molecules start lining up, resulting in the formation of fibrils. These fibrils then stabilise to form fibres. A critical step in the collagen fibre formation – and what gives rise to its mechanical properties – is the covalent crosslink formation promoted by a specialised enzyme called lysyl oxidase [56].

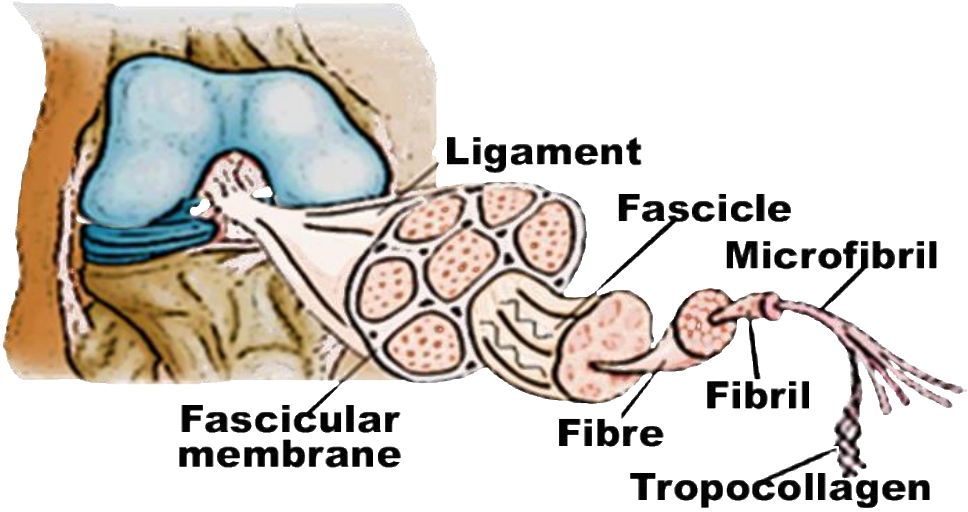

Figure 1.2 Structural hierarchy of a ligament. Image made with Servier Medical Art under a Creative Commons Attribution 3.0 Unported License.

The total content of the amino acids proline and hydroxyproline confers the stability to the collagen triple helix as a result of the cyclic nature of the side chains that restricts flexibility about the peptide bond [55]. Additional stabilisation is provided by the hydroxylation of proline, a process that requires the presence of Fe2+, 2-oxoglutarate, O_2 and ascorbate [55]. Due to spatial arrangement of the collagen molecules, the prolyl hydroxylation only takes place before the assembly of the triple-helical procollagen molecule. Given that collagen denatures at a particularly slow rate and that it only appears to be stable at body temperatures due to kinetic effects, fibre stabilization requires interactions with chaperones and supramolecular assembly for further stabilization [57].

1.5 Ligament injury and healing

Sudden large strains or repetitive low stresses overtime, result in ECM disruption and cellular damage. There are different grades of ligament injuries, from a mild sprain to a complete tear. Intra-articular ligaments such as the ACL face a major challenge for healing after a rupture due to their complex location and interaction with the surrounding tissues. Compared to what is found in knee extra-articular ligament cells, ACL fibroblasts grow slower, produce less collagen, are more susceptible to apoptosis by nitric oxide, and display a reduced response to growth factors [58-60].

The ordinary phases for an extra-articular ligament healing are summarised in figure 1.3. In the first instance, the abrupt interruption of tissue continuity is expected to prompt the generation of a hematoma, inhibited in the case of the ACL due to the exposure to proteolytic enzymes in the synovial fluid once the synovial membrane is broken. During the first 48 to 72 h, the clot formation serves as a scaffold for cells to begin migrating and proliferating. Chemotactic substances are released and immune cells – neutrophils and macrophages – populate the injury site. Synthesis of collagen type III (Col III) increases, along with growth factors such as TGF-β1, IGF, PDGF, BMPs -12 and -13, and bFGF. Gradually, cell differentiation starts taking place and the ECM reorganises, moving from the previous predominantly Col III composition to one dominated by Col I. The ligaments are known to be at their weakest during this period. The Col I to Col III ratio while these phenomena are taking place is of around 5.9 – 12.7. In parallel, the ECM goes through organisation, degradation, and synthesis of components. Maturation of the tissue can take up to 18 months [59, 61, 62].

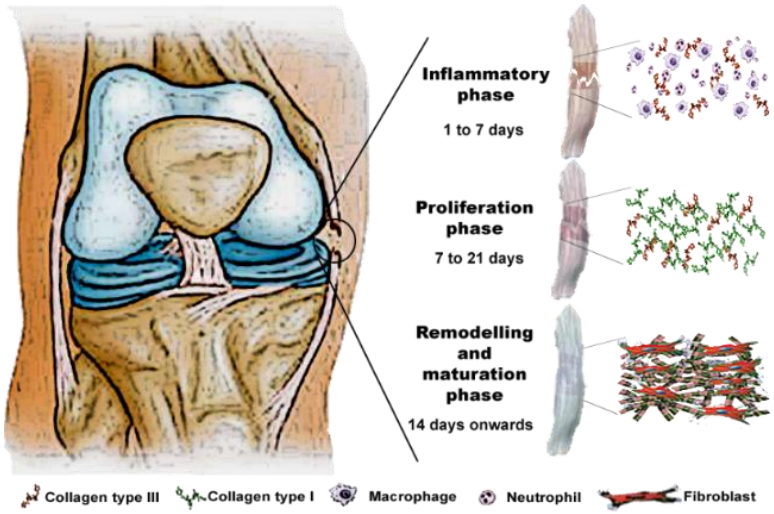

Figure 1.3 Phases of ligament healing. The events that take place in response to ligament injury are illustrated. The initial inflammatory phase encompasses the recruitment of immune cells that prompt the wound healing. Subsequently, the initial ECM production occurs during the proliferative phase. The final remodelling and maturation phase involves a decreased cellularity and increased alignment of both cellular and matrix content, with adhesions and scar tissue formation. Image modified from OrthoInfo by AAOS under a CC BY 2.0.

1.6 Current therapy for ligament injury

As previously stated, the primary healing of the ligament depends on the grade in which the ligament is injured. A nonsurgical treatment could be considered for mild sprains or partial tears, particularly when there is not an urge to go back to sports. Nevertheless, secondary injury to the surrounding structures is common due to recurrent events of instability and persistent inflammation. The gold standard is the surgical replacement of the injured ligament using the patient's own tendon tissue as a substitute graft.

1.6.1 Biological Grafts

Autografts, allografts, and xenografts have been explored as a replacement for a ruptured ACL. Surgeons consider several variables when selecting the most suitable graft for the surgical reconstruction of an ACL rupture. Variables include the patient's expectations, level and intensity of physical activity, age, sex, and pre-operative knee laxity levels [62]. Tendon autografts have been the most accepted treatment. The

preferred autografts are the bone-patellar tendon-bone (BPTB) and HT, although the use of the iliotibial band and quadriceps tendon have been reported. The ACLR practice in some parts of the world benefits using BPTB grafts for people in high-demand physical activities, whereas HT is the preferred graft choice for non-athletes [13]. Differences in the outcomes such as the harm to the donor site, the incidence of graft failure, complications associated and return to sports time between BPTB and HT are under continuous scrutiny. BPTB autograft is often associated with a faster healing rate owing to the bone-to-bone healing potential from the central third of the patella that accompanies the graft. In collegiate sports, it has been associated with a decreased incidence of graft rupture compared to the HT autograft [63]; however, there are multiple donor-site consequences to ponder. The same applies to the HT autograft despite the reduction in donor-site complications [64]. HT autografts are associated with muscle weakness, knee joint laxity and a higher risk of femoral tunnel widening [63, 65-67]. Graft harvesting commonly leads to regional hypoesthesia or dysesthesia as a result of harming the infrapatellar branches of the saphenous nerve when retrieving either BTPB or HT autografts [68]. The presence of somatosensory deficits after ACLR has been associated with a higher incidence of anterior knee pain [69], a morbidity more frequently present after BPTB ACLR [70].

Despite the acceptable success rate of tendon autografts as an ACL replacement, the concomitant morbidities for the harvesting site, as well as the limited tissue availability for secondary reconstructions if needed, have encouraged the search for alternative tissue sources. Therefore, cadaveric tissue – allografts – has been explored as surrogates. Allografts provide the advantages of lessening donor-site morbidity, availability of larger grafts, which in turn reduce the operative time. Nonetheless, their use is associated with higher costs, lengthier graft processing, slower tissue integration and the safety concern of disease transmission [71-74].

The use of tissue from a different species than human as a ligament graft emerged as an alternative to the safety concerns raised by allografts. Infections and unfavourable immunologic responses have largely discouraged the use of xenografts. Immunologic rejection has been addressed in multiple studies, highlighting the cellular and ECM

differences among species, and new options cleaving specific epitopes have resulted in better host immune tolerance. However, an increased infection rate from the use of these tissues in clinical trials do not make xenografts an appealing alternative [75, 76].

1.6.2 Artificial Grafts

To avoid the donor-site morbidity, synthetic devices providing strong stability and a relatively faster return to previous functional sport demands have been tested since the 1970s. These synthetic constructs have been used in various forms, tailored to specific needs such as scaffolds, stents or prostheses [77, 78]. The first generation of artificial ligaments were proven to be less efficient than autografts in terms of stabilizing the knee joint and reducing knee effusion, synovitis, or OA [79, 80]. The latest generation of synthetic devices includes the Ligament Advanced Reinforcement System (LARS), made of two distinct sections to imitate the ACL anatomic structure, and avoid ligament deformation. Some second-generation artificial grafts are still in use; nevertheless, a synthetic substitute for the ligament remains to be found as no current material has been able to replicate the ACL's physical and chemical properties.

1.6.2.1 Synthetic materials used for ligament repair and healing

The development and use of synthetic ligaments were popular during the 1980s, but after a decade of unsatisfactory results characterised by recurrent instability, re ruptures, wear debris, chronic effusions, synovitis and osteolysis, these grafts were withdrawn from regular practice [81-84]. Various synthetic materials have been explored as ligament grafts or reinforcement devices such as:

- Polyarylamide (PAA) [85]
- Poly Lactic Acid (PLA) [86]
- Poly L-lactic acid (PLLA) [87, 88]
- Poly(tetrafluoroethylene) (PTFE) [85, 89]
- Poly (ethylene terephthalate) (PET) [85, 89, 90]
- Polypropylene (PP) [85, 89]
- Poly (lactic acid-co-glycolide) (PLGA) [87, 88, 91]
- Polydioxanone (PDS) [88]

- Poly (glycolic acid) (PGA) [88]
- Poly(ε-caprolactone) (PCL) [88]

By themselves, none has demonstrated either appropriate mechanical properties or tissue integration [81, 82, 92, 93]. Most of the synthetic materials used for ligament reconstruction have disadvantages in the cell-material interactions.

1.6.2.2 Role of PET in ligament reconstruction and regeneration

Artificial grafts made of PET were developed in 1992 under the term LARS. They are CE-marked as a Class IIb medical device [94] and have survived the downfall of the artificial ligaments. The LARS's mechanical properties depend on the number of fibres it is made of. It has an average tensile strength of 4600 N which is about 7.3 times that of an adult native ACL [95]. The LARS tensile strength can be selected for the patient according to the graft's thickness. To illustrate this point, a 60 gauge LARS has a tensile strength of 2,500 N, and 3,600 N correspond to the 80 gauge [96]. A 19-year follow up study of PET artificial ligaments in sportsmen showed a high rate of degenerative OA, suggesting the influence of synthetic ligaments on the early onset of this pathology [97]. The novelty of the LARS is that it has been designed to mimic the mid portion of the ligament and so it is made of two distinctive parts: an extra-articular and an intra-articular. PET artificial ligaments – when used in very well selected patients – have shown no significant difference in the main efficiency outcomes for a ligament reconstruction when compared to autografts up to 2.5 years after the surgery [98]. Despite of the early encouraging data suggesting a faster return to sports, and no significant complications in the short to intermediate-term, long term results have evidenced a subjective patient dissatisfaction with the performance of the PET graft which may be related to the absence of tissue integration [98, 99]. A cohort of 51 patients followed for a minimum of 6 years found a mechanical failure rate of 33.3% [96]. A case series of 72 patients found similar results of 31% rupture rate at 9.5 years of follow up [100]. Despite the 'inertness' of the LARS, a case series of 15 patients from 8 different surgical centres reported a foreign body reaction – associated with chronic synovitis – in 71.42% of the explanted samples sent for macroscopic and histological analysis [101]. Out of their 10 affected LARS, rupture had only occurred in two, three

failed in terms of increased laxity, there was one late-stage infection, a case of revision due to synovitis, one reinjury of the reconstructed knee, and the others were revised for joint stability [101].

1.7 Rationale for this thesis

ACL injuries are one of the most common sports injuries. They can signify the end of a sports person career and lead to a decreased quality of life in the general population, mainly due to an early onset of OA. The current treatment of choice for a complete ACL rupture is associated with an unacceptable rate of donor-site morbidities. Various approaches exist, but there is currently still no ideal synthetic alternative for a graft. There is, however, an artificial graft made of PET. It is approved and certified in Europe, but its use is not advisable in clinical practice for ACLR. It is used for augmentation and in extra-articular ligament repairs. This artificial graft provides a suitable scaffold for an early return to sports due to its tensile strength that supports the joint load through the weak phase of the tissue healing after ACLR. Addressing its absence of tissue integration by rendering it a biomimetic construct via a straightforward methodology would result in an established familiar synthetic graft for ligament reconstruction.

This study aimed to develop a bioactive composite scaffold for ligament TE to provide an adequate microenvironment that supports mesenchymal stem cell viability and ECM synthesis when faced with native conditions, as is the case for grafts after ACLR.

The hypothesis is that a bioactive composite scaffold made from PET fibres coated with a natural biomaterial complex will support ligament resident cells growth and enhance ligament-like extracellular matrix deposition that would contribute to ligament healing.

1.8 Objectives

The objective of this research was to design and develop a three-dimensional (3D) scaffold to promote the proliferation and functionality of resident ligament cells under conditions resembling those of the native ACL. To identify the requirements of a suitable ligament scaffold, a systematic assessment of the scientific validity of the published literature was done. The literature review focused on the current understanding and ongoing clinical and basic research in grafts used for ACLR against relevant core questions. These questions included the native ACL ultrastructural characteristics, its ECM composition, the current graft sources, and the validated manufacturing approaches. The assessment of the demonstrated advantages and limitations of materials used in regenerative medicine regarding their accessibility, clinical familiarity, cost-effectiveness, and environmental impact was considered. Likewise, the appraisal of the outcomes and applicability of the methodology used in the literature aided in defining the physiologically relevant scenarios that a scaffold would encounter considering the context of an *in-situ* TE approach. The scaffold design and experimental plan presented in this thesis were developed according to these findings.

The project can be broken down into the following stages:

1. The completion of a systematic review taking stock of the highest-quality evidence available for ACLR outcomes to reflect on the need for an alternative to the current graft options.
2. The surface modification of a synthetic PET scaffold with O_2 plasma to enhance its bioactivity.
3. The further modification of the O_2 plasma pre-treated 3D PET fibrous scaffold by the addition of a biomimetic CS-g-GMA and HA coating to enhance cell vitality and ECM deposition.
4. The appraisal of the bioactive composite scaffold's capability to support cell growth and ECM under continuous physiological mechanical loading.
5. The study of the effect of LIPUS on stimulating the ligament-like remodelling of the scaffold.

Chapter 2

Systematic review

Aims: To provide an evidence-based analysis of the current graft options for ACLR in terms of the associated adverse outcomes.

Hypothesis: The current graft options present an unacceptably high rate of failure in terms of re-ruptures and knee OA, emphasising the need for a better alternative to the current graft options for ACL repair.

2.1 Introduction

ACL injuries represent 40% of all sports injuries in the United Kingdom [102] and go up to 73% in Switzerland [103]. In context, a 15-year follow-up of 4443 elite European football players [104] revealed an incidence of 3.5% in ACL ruptures. For this cohort, there was a 3.1% ACLR rate and a 4% re rupture rate during the period of study.

An ACL rupture entails devastating consequences in a person's quality of life. The impact of this injury is tightly dependent on the person's age and previous activity level. For instance, it could signify a career ending condition for an athlete or conduct a young patient to a total knee replacement at an earlier age than the average for the general population. A chronic ACL deficient knee is usually accompanied by subchondral sclerosis, meniscal degeneration, and osteochondral defects [105]. Biomarker concentrations of cartilage turnover increase after ACL injury [106]. Among the factors that contribute to the development of post-traumatic osteoarthritis (PTOA) in a knee that has suffered an ACL tear, are instability, alterations to the normal biomechanics of the joint, along with the frequently associated injuries to knee articular cartilage, menisci, and surrounding tissues. Although a surgical treatment – when compared to a non-operative one - has resulted in clinical improvement of joint stability, there seems to be no clear reduction in secondary lesions or degenerative changes in the knee [105]. A

study suggests that ACL tears augment the number of patients with symptomatic knee OA by 30,000 to 38,000 and contribute with an increase of 25,000 to 30,000 total knee arthroplasties per year [107]. Despite the fact that ACLR slightly reduces the lifetime risk of knee OA and its associated costs, a retrospective case series report has evidenced a greater incidence and severity of OA for knees that have undergone ACLR when compared to their non-ACL-injured counterparts [108]. The structural damage in the joint caused by the acute injury to the ACL triggers pathogenic mechanisms that lead to the up-regulation of matrix-degrading enzymes, collagen and proteoglycan synthesis suppression, release of oxidants and inflammatory cytokines, and cell death [109]. Furthermore, an ACLR does not restore the native kinematics of the knee [105, 110], which contributes to the persistent inflammatory state after an ACL injury despite ACLR. In fact, ACLR might evoke a similar inflammatory response to the ACL injury which explains the increased incidence of early-onset OA regardless of the reconstruction [111, 112].

ACL injuries have an implied financial impact on an athlete's career, although it is dependent on whether it is in the context of individual or team sports. After an ACLR, male professional footballers who returned to their previous activity level miss two months of training and 2.5 months of match play [104]. Eliakim et al. [113] estimated the financial impact of players' layoff time on English Premier League teams to be £45 million per season from the injury-related decline in performance. The figure came about from determining the number of days lost to injury leading to the loss of league points and places in the general table, which translated to a loss of income from wage bills and missed prize money. Then again, ACL injuries are not experienced only by professional athletes. There is also a recognised economic burden for them in the general population. As reported by the Swiss Council for Accident Prevention, this amounts to 205 – 257 million US dollars (USD) per year [103]. A Spanish randomised prospective study with a two-year follow-up evidenced a total cost in 2010 euros of €3,250.92 for an ACLR using a single-bundle (SB) hamstring autograft and €4,172.39 for the reconstruction with a double-bundle (DB) [114]. Accordingly, the United States Centre for Disease Control reported an annual work loss cost of $193,447,000 for hospitalised patients with knee sprains/ strains updated for 2010 [115]. Moreover, an

economic analysis published in 2011 [116] showed that the sum of hospital costs plus the fee of a professional surgeon per quality-adjusted life-year (QALY) was $10,326 for an ACLR. For these reasons, the procedure ranks eighth for cost-effectiveness per QALY of various medical treatments, just below neonatal intensive care.

An ACLR surgery can have complications leading to graft failure. Success of the reconstruction relies more on the surgical technique than graft choice [117, 118]. Revisions are usually necessary for complications such as those related to hardware, bone tunnel defects or incorrect tunnel placements. The inferior outcomes present as increased laxity of the graft, a higher graft failure rate and cartilage injuries. Reasons for these outcomes are multifactorial [119]. The heterogeneity of surgical techniques, fixation methods, graft choices, number of graft strands and number of bundles, make assessment of the overall effectiveness of ACLR difficult.

The main question addressed in this chapter was the suitability of the grafts used in ACLR measured by the overall incidence of re-ruptures and early development of OA in young active patients. The outcomes are presented in four follow-up terms from the surgery: up to two years, from three years to five years, from six years to nine years and ten years or more. Evidence of the time elapsed from an ACLR to the onset of major complications after ACLR, will provide a better representation of the effectiveness of the current graft used for ACLR and will help to identify the main limitations that need to be addressed by a ligament scaffold to improve ACLR longer term results.

2.2 Methods

Outcomes of primary ACLR were extracted from randomised controlled clinical trials (RCTs) from 2007 to June 2017. Included studies addressed any type of autograft (harvested from the ipsilateral or contralateral knee; BPTB, HT, tibialis anterior or Achilles' tendons), allograft (regardless of the sterilization process performed on the graft) or synthetic graft.

The inclusion criteria were English-language full text available reports of level I randomised controlled trials that had included patients aged between 16 and 50 years

with a primary unilateral ACL injury and a symptom free contra-lateral knee. Clinically verified unilateral ACL rupture was considered when done by a positive Lachman test and a positive pivot-shift test, an MRI or through a previous diagnostic arthroscopy. The exclusion criteria were trials in which the patients were skeletally immature, other associated ligament (posterior, grade 3 medial or lateral collateral) injury, a history of a previous ACL surgery, a contralateral knee ligament injury, or radiographically verified OA indicated by a grade 2 or above in the Kellgren and Lawrence grading scale.

All ACLRs were considered regardless of the fixation method, graft used, surgical technique or rehabilitation protocol followed. Only studies where standardised grafts were used and studies that addressed either of the primary outcomes of this systematic review were included.

Outcomes were measured based on the criteria in table 2.1.

Primary outcomes	**Secondary outcomes**
1. Incidence of osteoarthritis following ACLR. 2. Incidence of re-ruptures following ACLRs.	1. Other adverse effects and complications after ACLR: • Infection. • Deep venous thrombosis. • Others (hardware problem, cyclops lesion, arthrofibrosis). 2. Autograft donor site morbidities: • Long-term knee pain (visual analogue scale). 3. Objective measures of knee stability (e.g. KT-1000 arthrometer, KT-2000 arthrometer results). 4. Return to pre-injury level of activity/sport participation after ACLR.

Table 2.1 Primary and secondary outcomes.

For the timing of outcomes assessment, the four time set points chosen to strengthen the reliability of comparisons can be found on figure 2.1

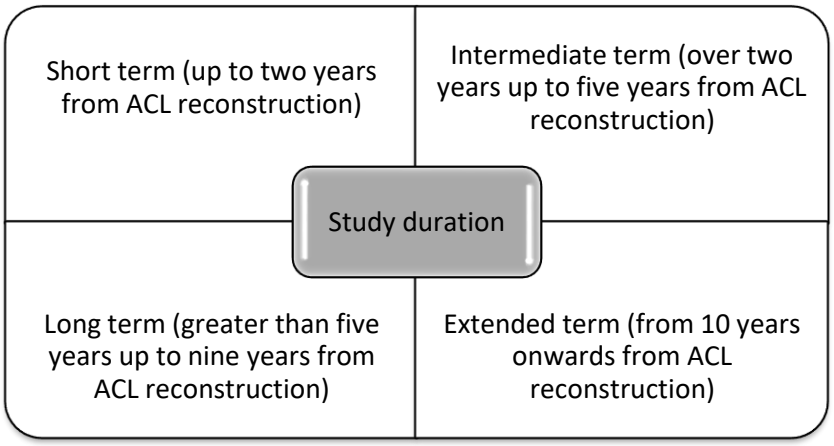

Figure 2.1 Classification of outcomes by duration of the studies.

The electronic database search through health-related bibliographic databases included Pubmed, the Cochrane Central Register of Controlled Trials (CENTRAL), MEDLINE and EMBASE.

The search strategy for the EMBASE database was as follows: Embase Classic+Embase <1947 to 2017 July 14>, Emcare 1995 to present, GEOBASE <1980 to April 2017>, HMIC Health Management Information Consortium <1979 to March 2017>, Journals, Ovid MEDLINE(R) Epub Ahead of Print, In-Process & Other Non-Indexed Citations, Ovid MEDLINE(R) Daily, Ovid MEDLINE and Versions(R)

1 ("anterior cruciate ligament reconstruction" and "surgery" and outcome and randomized controlled and clinical trial).af. (641)

2 remove duplicates from 1 (459)

The details and records for the included trials were extracted using a data collection form and were then entered into Review Manager 5.3.5 software [120]. The RCT were critically appraised as per the guidelines for Consolidated Standards of Reporting Trials CONSORT [121]. The risks of bias were assessed for each study using The Cochrane Collaboration's tool. Each study was given a low, unclear, or high-grade risk of bias for each of the following domains: random sequence generation, allocation concealment, personnel and participants blinding, blinding of outcome assessment, incomplete

outcome data, selective outcome reporting, and other sources of bias whether a particular misguiding information that could affect the outcomes was included). All articles were treated equally, disregarding titles of journals or names of authors.

The results were pooled for trials with comparable groups. Due to the heterogeneity of the data, the random effects model and 95% confidence intervals (CIs) were employed. The information for dichotomous outcomes is presented as risk ratios with 95% CIs, and mean differences (MDs) with 95% CIs for continuous outcomes for the analysis of quantitative data. No values were assumed to present missing data in the analyses. Special attention was given to identify potential mislabelling or non-identification of data relevant to the outcomes included in this review.

There was insufficient data for subgroup analysis to stratify patients by gender, age, injured knee, chronicity of ACL rupture, traumatic versus atraumatic injury, isolated ACL injuries versus accompanying soft tissue lesions, or allografts versus autografts.

2.3 Results

2.3.1 Description of studies

The RCT for ACLR surgeries included adult patients from 15 to 55 years of age, with a mean age of 29.4 years at the time of the surgery. Regarding the gender distribution, 36.4% were female participants and 63.5% were male. The time from injury to surgery ranged from two days to 194 months (median 8.4 months). Figure 2.2 depicts the study flow diagram. ACLR techniques included arthroscopic and open surgery, variations in femoral tunnel placement, number of graft strands, single versus double bundle and different fixation methods. Twenty-seven RCT had their primary outcome as knee stability either rotational or anterior. The studies were carried out in Finland, China, the U.S.A., Australia, Italy, Canada, Germany, Norway, Sweden, Japan, the Czech Republic, Denmark, Iran, the U.K., South Korea and Spain.

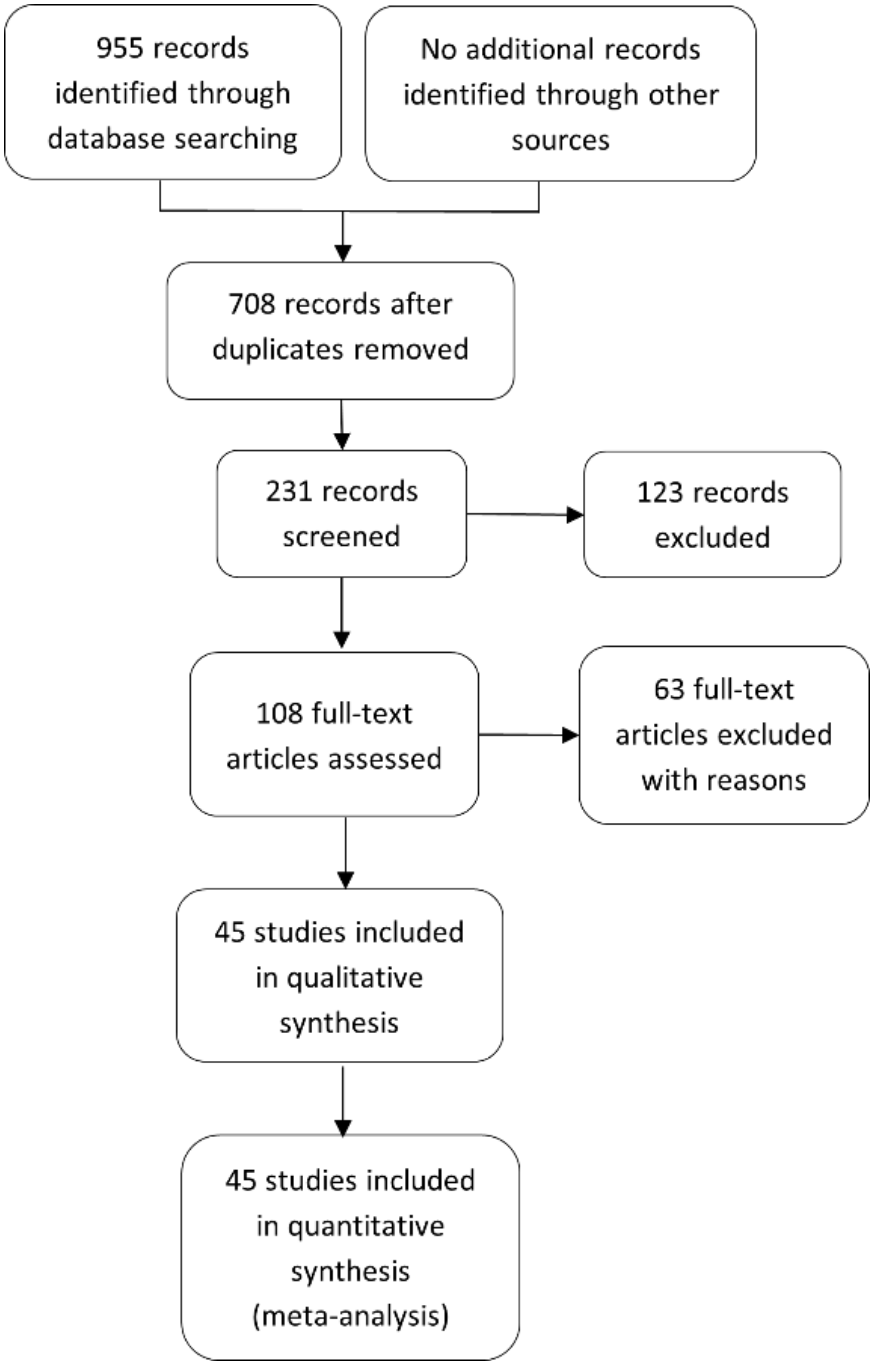

Figure 2.2 Study flow diagram. Out of 955 records initially identified through database searching, 45 were finally considered relevant and were included for both qualitative and quantitative analysis.

2.3.2 Characteristics of included studies

There were two main types of comparisons in the clinical trials, DB versus SB ACLR (10 clinical trials) [122-131], and fixation techniques (10 RCT) [132-141]. In the order of frequency in comparisons within the remaining studies, nine compared the use of hamstring versus bone-patellar tendon –bone autografts [117, 142-149], three compared rehabilitation protocols [150-152], two tested irradiated versus non-irradiated allografts [153, 154]. The following comparisons were found in single studies: BPTB versus iliotibial autografts [155], semitendinosus versus semitendinosus plus gracilis tendon autografts [156], ipsilateral versus contralateral autografts [157], patellar tendon (PT) with or without a synthetic degradable augmentation device [158], doubled tibialis anterior (TA) allograft versus quadrupled HT allograft [159], single-bundle HT versus CaP hybridized autograft [160], PT versus synthetic graft [161], HT autograft versus TA allograft[162], conventional technique versus computer-navigated reconstruction [163], ST/G double strand plus extra-articular sling versus double-bundle autograft [164], and initial graft tension[165]. Regarding mean follow-up times, as expected, most of the studies (24/45; 54%) covered a short-term follow-up which ranged from one up to two years after the index ACLR. Thirteen percent of the studies (6/45) fell into the medium-term criteria and 22% (10/45) comprised the long-term follow-up. The five studies (11%) in the extended term follow-up ranged from ten to fifteen years (see figure 2.3).

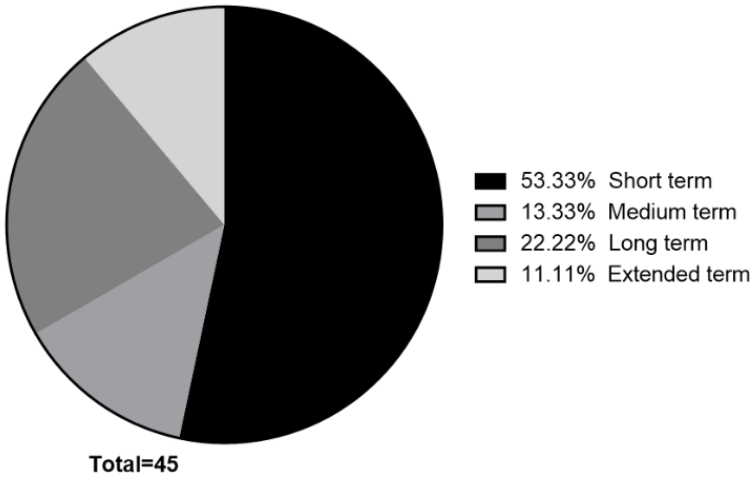

Figure 2.3 Distribution of the included RCT (N = 45) by follow-up terms. More than half of the studies reported a follow-up of the patients only up to two years after ACLR.

2.3.3 Risk of bias

Over 50% of studies were classified as high risk for attrition bias due to incomplete outcome data; particularly important for the long and extended-term studies. Less than 30% of the studies explicitly stated how they addressed a potential performance bias. About 50% were scored as low risk of bias for either random sequence generation or allocation concealment. Nearly 50% of the studies reported as randomisation method the use of “the sealed envelope method”, without giving any more information concerning either use of opaque, randomly numbered envelopes, or information on the random sequence generation. Around 60% of the studies accurately addressed a potential detection bias by explaining how the blinding of the outcome assessment was achieved. Around 70% of the studies reported the outcomes as stated on their methodology, thereby avoiding a reporting bias (see figure 2.4).

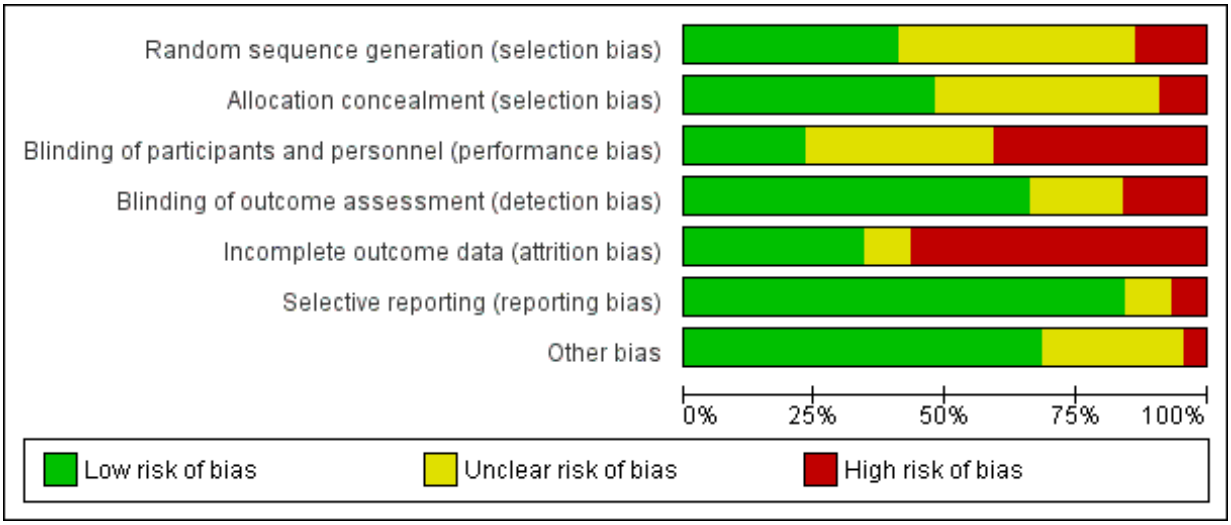

Figure 2.4 Appraisal of the randomised control trials by risk of bias. The highest risk of bias for the studies included was an incomplete report of their outcome data. Figure created with RevMan software.

2.3.4 Meta-analysis main outcomes

Data for pooling individual outcomes were available for a maximum of 45 trials divided by the main outcomes of OA and graft rupture.

2.3.4.1 Osteoarthritis

Eleven trials were included, involving 1176 mostly young physically active adults. Four of those trials provided information regarding the contralateral knee and were included in the pooled comparison of outcomes (see table 2.2). The overall incidence of OA for the autograft subgroup is shown in figure 2.5.

Subgroup	Study	Ipsi. Events	Contra. Events	# Patients	Weight	Risk Ratio	Follow-up term
Autograft		119	37	219	87.4%	3.04 [2.02, 4.59]	
Hamstring tendon							
	Barenius 2014	16	8	29	22.90%	2.00 [1.02, 3.93]	Extended
	Holm 2010	48	12	61	34.30%	4.00 [2.37, 6.75]	Extended
Subtotal (95% CI)				90	57.10%	3.20 [2.12, 4.83]	
Total events		64	20				
Heterogeneity: $Chi^2 = 2.56$, df = 1 (P = 0.11); $I^2 = 61\%$ **Test for overall effect: Z = 5.55 (P < 0.00001)**							
Bone-patellar tendon-bone							
	Barenius 2014	18	6	28	17.10%	3.00 [1.40, 6.42]	Extended
	Holm 2010	34	9	61	25.70%	3.78 [1.99, 7.19]	Extended
Subtotal (95% CI)				89	42.90%	3.47 [2.12, 5.67]	
Total events		52	15				
Heterogeneity: $Chi^2 = 0.21$, df = 1 (P = 0.65); $I^2 = 0\%$ **Test for overall effect: Z = 4.95 (P < 0.00001)**							
Total (95% CI)				179	100.00%	3.31 [2.42, 4.55]	
Autograft Heterogeneity: $Chi^2 = 2.87$, df = 3 (P = 0.41); $I^2 = 0\%$ **Test for overall effect: Z = 7.43 (P < 0.00001)** **Test for subgroup differences: $Chi^2 = 0.06$, df = 1 (P = 0.81), $I^2 = 0\%$**							
Allograft		16	8	152	12.6%	1.99 [0.88, 4.53]	
	Sun 2012	7	4	28	17.10%	3.00 [1.40, 6.42]	Medium
	Tian 2017(13)	9	4	61	25.70%	3.78 [1.99, 7.19]	Long
Heterogeneity: $Tau^2 = 0.00$; $Chi^2 = 0.09$, df = 1 (P = 0.76); $I^2 = 0\%$ **Test for overall effect: Z = 1.65 (P = 0.10)**							
Overall (95% CI)		**135**	**45**	**371**	**100.0%**	**2.98 [2.22, 3.98]**	
Heterogeneity: $Tau^2 = 0.00$; $Chi^2 = 3.94$, df = 4 (P = 0.41); $I^2 = 0\%$ **Test for overall effect: Z = 7.33 (P < 0.00001)** **Test for subgroup differences: $Chi^2 = 0.81$, df = 1 (P = 0.37), $I^2 = 0\%$** **Risk difference: 0.3 (p<0.00001; 95% CI [0.2, 0.3]; SE 0.03)**							

Table 2.2 Incidence and comparison of knee OA. The results were subdivided by the type of graft and to compare the incidence of OA in the index knee against the occurrence in the contralateral knee. Overall, there is a statistically significant higher incidence for the development of knee OA in the originally injured knee. Table generated by RevMan software.

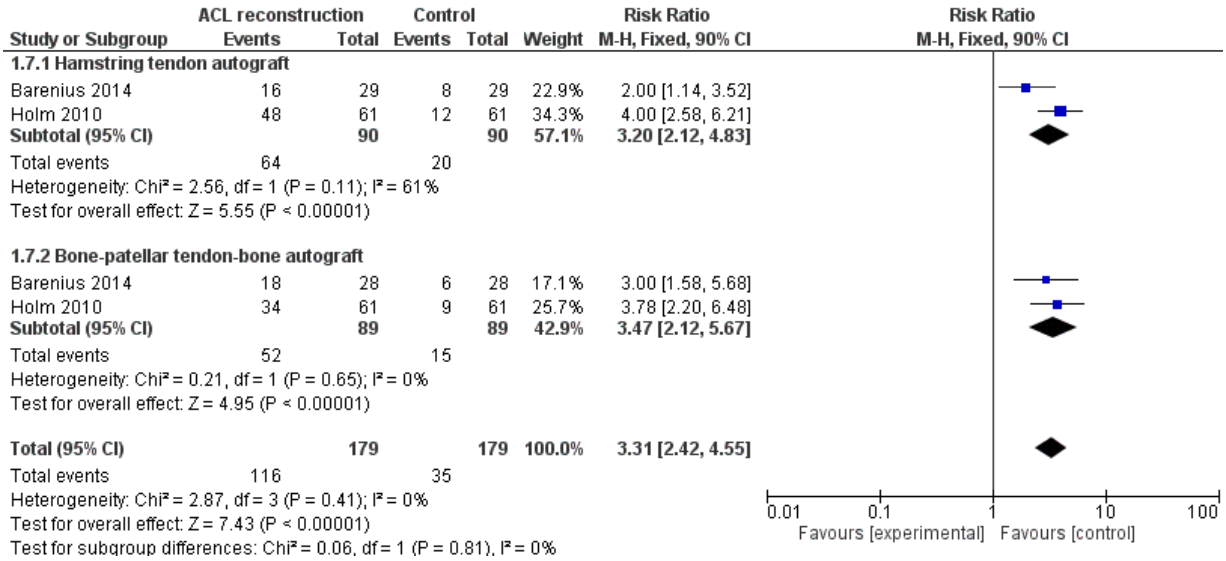

Figure 2.5 Forest plot for incidence of OA by subgroup. ACLR leads to a higher incidence in knee OA for both types of autografts analysed. Graph generated by RevMan software.

2.3.4.2 Graft rupture

Forty-one studies addressed this outcome – either directly or indirectly –. The effect estimate of ruptures is shown in table 2.3. The data were analysed using a random effect model to account for the variance between the studies. The risk ratio - or relative risk - of each subgroup was calculated to find the effect estimate. The data compares the risk of graft rupture among subgroup participants. To quantify the difference of relative risk for graft rupture, a value above 1 signifies an increased risk.

Subgroup	# Studies	Total Patients	Effect estimate	95% CI
Autograft	39	3234	1.32	0.82, 2.12
Hamstring tendon	26	1864	1.76	1.02, 3.04
Bone-patellar tendon-bone	13	612	1.35	0.75, 2.45
Heterogeneity: $Tau^2 = 0.34$; $Chi^2 = 24.72$, $I^2 = 47\%$ (P = 0.03). Test for overall effect: Z = 1.13 (P = 0.26). Test for subgroup differences: $Chi^2 = 0.41$, df = 1 (P = 0.32), $I^2 = 14\%$				
Allograft	3	359	6	0.73-49.51
Test for overall effect: Z = 1.66 (P = 0.10)				
Total (95% CI)	41	3593	1.40	[0.87, 2.23]
Heterogeneity: $Tau^2 = 0.23$; $Chi^2 = 49.10$, df = 32 (P = 0.03); $I^2 = 35\%$ Test for overall effect: Z = 2.61 (P = 0.009) Test for subgroup differences: $Chi^2 = 2.39$, df = 3 (P = 0.49), $I^2 = 0\%$				

Table 2.3 Summary of pooled data of graft rupture. The effect estimates for all the subgroups show a significantly increased relative risk of re-rupture for all the grafts. The table was generated by RevMan software.

The overall incidence of re-rupture for the reconstructed ACL was 5.51%. The incidence of graft rupture within each subgroup was 5.81% for autografts and 2.78% for allografts. Fifteen out of the 40 studies included information on both uninjured and index knee. Table 2.3 shows the summary of these data. When analysed by follow-up term times (see figure 2.6), five studies from the "long" and "extended" terms included information for the index and contralateral knee. The effect estimate was 0.85 [0.50, 1.45] Z = 0.59 (P = 0.55). The overall contralateral knee risk for having an ACL rupture was 0.04. The risk ratio was 1.91 [95% CI 1.44, 2.53] (SE 1.14; Z=4.51; p = 0.0000).

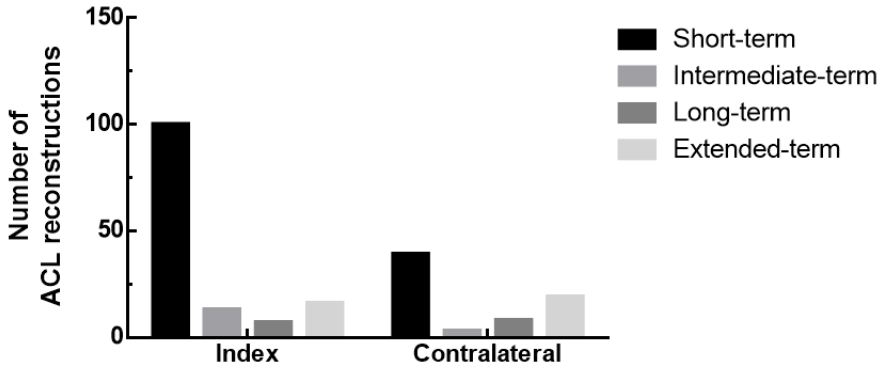

Figure 2.6 Incidence of re-ruptures of the ACL grafts and new ruptures of the contralateral ACL by terms. There was no statistically significant difference between index and contralateral knee at any studied term. N=205.

Two studies mentioned the incidence of traumatic versus atraumatic ACL re-ruptures (figure 2.7), including 784 participants with a risk ratio of 0.39 [95% CI 0.21, 0.1]. Both, hamstring tendon and bone-patellar bone-tendon autografts favoured the traumatic re rupture of the grafts, with an overall effect Z= 2.94 (p = 0.003). There was no significant difference between the subgroups (p = 0.15) I2 = 51.7%.

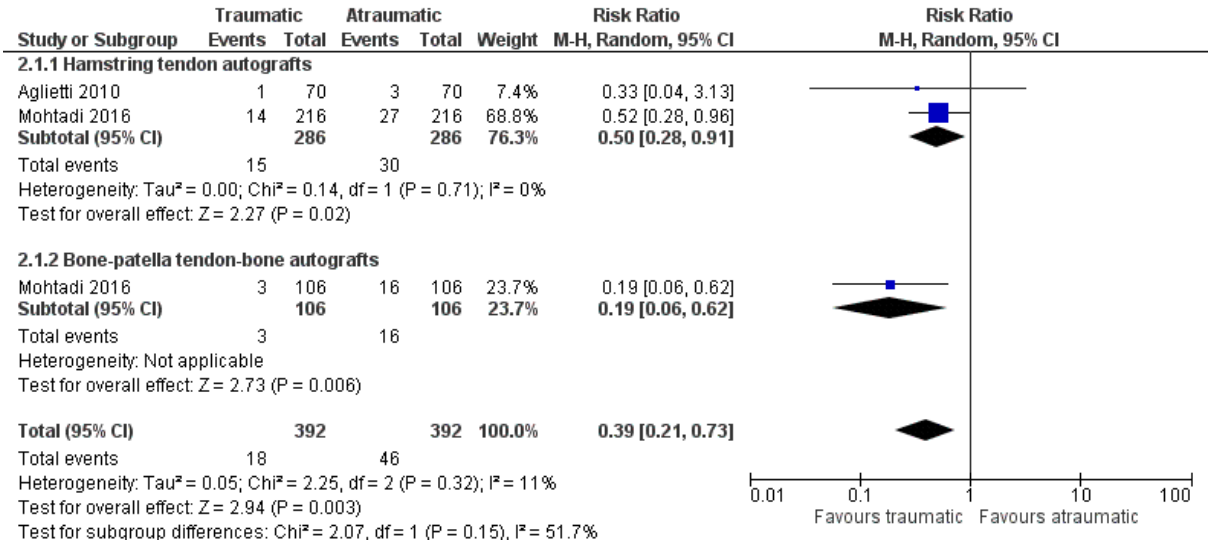

Figure 2.7 Forest plot of traumatic versus atraumatic autograft re-ruptures by type. There was a statistically significant increase in relative risk for presenting a traumatic mechanism of injury for the ruptures reported.

2.3.5 Secondary outcomes

2.3.5.1 Complications

Thirty-one studies reported several complications summarised in figure 2.8. Seventeen reported complications were directly related to the interventions. These are labelled as hardware related and include a fixation pin translocation and the persistent discomfort due to screw fixation. In all these cases, hardware had to be removed. With regards to systemic complications, there was one pulmonary embolism, one laryngospasm and lung oedema. There were also two wound dehiscence events.

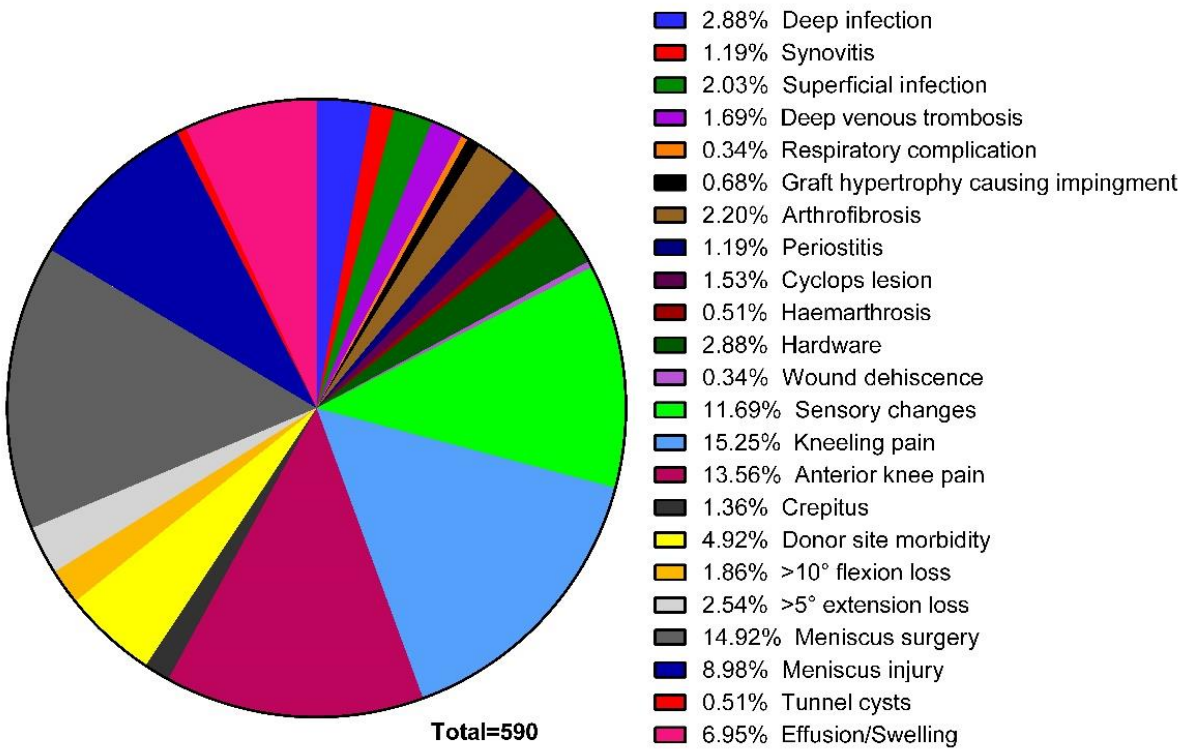

Figure 2.8 The complications reported at the final follow-up of thirty one out of forty-five studies are presented as percentages of the total number of pooled events (590 total events). Kneeling pain, anterior knee pain and sensory changes were the most frequently reported.

Four studies [130, 134, 145, 149] reported anterior knee pain for both the BPTB and HT autografts. The mean number of patients with knee pain at the final follow-up were 10 ± 4 and 5 ± 3 patients respectively. There was no statistically significant difference based on the type of autograft (p = 0.1; 95% C.I. -10.8 to 1.4) Peterson et al. [158] reported 13 patients for the BPTB with a poly (urethane urea) augmentation device and 12 patients with a BPTB autograft without an augmentation device, who presented anterior knee pain at the final 4 years follow-up. Four studies [134, 147-149, 166] reported kneeling pain for both the BPTB and HT autografts. The mean number of patients with kneeling pain at the final follow-up were 10 ± 5 and 8 ± 4 respectively. There was no statistically significant difference for the mean of the studies for the type of graft used (p = 0.6; 95% C.I. -8.136 to 4.936). For donor site morbidities, 69 patients showed sensory changes, one haematoma and 32 various local muscle complications

ranging from mild harvest site pain to different level of strains mainly from the hamstring tendons. Ten studies reported a postoperative infection. Five studies reported a total of thirteen deep infection events for the autograft subgroup and one study reported two for the allograft subgroup. There was one study that reported one event for each subgroup. Four studies reported ten superficial infections for the autograft subgroup and one study reported two for the allograft subgroup.

Return to full competitive sports was overall unrestricted once there was evidence of sufficient recovery of muscle strength, proprioception, and flexibility. There were eight studies [123, 128, 136, 140, 141, 144, 148, 155] where patients were allowed full return to sports after 6 months from surgery. In two studies [129, 131], the patients were allowed to restart sport activities eight months after surgery. In one study [138], contact sports were permitted after nine months from the reconstruction. One study [153] reported a period of 10 to 12 months for their patients to return to full sports activity, and another one [126] reported a lapse of 10 to 11 months after the index surgical procedure. Nine studies addressed the number of participants going back to their pre-injury activity level [123, 128, 136, 142, 144-146, 158, 164]. Out of 428 patients included in these studies, 262 returned to their original activity level (61%). Five percent had to stop any activity and thirty-four percent returned to a lower activity level (see figure 2.9). Five studies [130, 131, 145, 164, 166] reported the time it took for their patients to go back to their full activity level. These studies reported a mean time of 6.7 months.

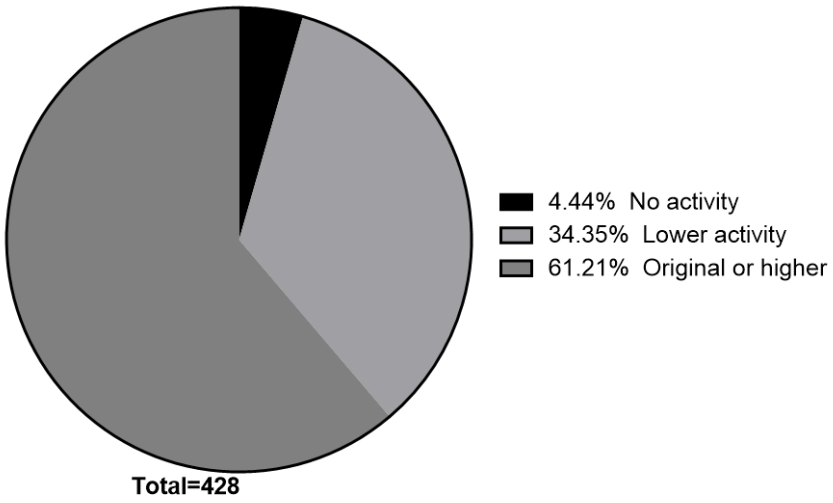

Figure 2.9 Representation of the percentage of patients who returned to their pre-injury activity level, a lower activity level or had to stop their sports activities at the final follow-up. Patients n = 428; studies N = 9.

Articles were analysed based on their results on anterior knee stability measured either with a KT-1000 or a KT-2000 arthrometer. The results were reported in various methodologies. Only 15 articles provided information on the difference in anterior knee laxity by comparing the index knee to the contralateral knee at the final follow-up of each study in the format of 0-2mm, 3-5mm, 6-10 or >10mm (for which n = 0). There were 409 patients with a measurement of knee stability. Seventy-three percent of the patients presented a side-to-side difference of 0-2mm. Seventeen percent recorded a 3-5mm side-to-side difference and ten percent scored a 6-10mm difference in anterior knee laxity. Fifteen studies included a mean side-to-side difference in anterior knee laxity, with a mean difference of 1.6 mm ± 1.7 mm.

2.4 Discussion

This systematic review and meta-analysis included 45 level I randomised controlled trials, which reported follow-up results for 4820 participants. The included trials compared grafts, surgical techniques, and surgery plus rehabilitation protocols, to investigate the reported efficacy of the surgical treatment for anterior cruciate ligament rupture with current grafts available.

The main findings of this review were:

- An incidence of 5.51% (201 / 3644) for graft ruptures following primary surgery.
- An overall incidence of 23.8% for the development of OA (18.5% from 2 up to 5 years after the ACLR and 36.4% for patients after six or more years from surgery).

New ACL ruptures on the contralateral and originally uninjured knee totalled 4.20% (69 / 1641) of patients ($p = 0.04$). For the OA outcome, 12.12% of patients (45 / 371) ($p = 0.00$) developed OA of the contralateral uninjured knee after the primary ACLR. There was a considerably higher percentage of patients who developed OA after ACLR on the index knee (68%) when compared to the contralateral uninjured knee (22%) 10 years after the primary ACLR. A greater incidence and severity of OA as been reported for knees that have undergone ACLR when compared to ACL-injured counterparts [108]. The choice of autograft has been associated with the development of tibiofemoral OA in a prognosis cohort study by Keays et al. [167], situating patients with a BPTB graft at a higher risk of PTOA when compared to those with a HT. PTOA is caused by collagen rupture, which is an irreversible stage, along with a speedy continuous loss of GAGs, contributing to cell death [109]. The persistence of inflammation and increased matrix degradation from the activation of the complement proteolytic cascade and the apoptotic caspase pathway associated with the post-traumatic phase that has been found to happen again after ACLR affect chondrocytes' – key for articular cartilage function – ability to express proteins involved in metabolic pathways [109, 111]. The surgical reconstruction of a torn ACL stimulates the recurrence of an increased release

of IL-6, IL-8 and IL-10 in the synovial fluid [168]. Some efforts to counteract the inflammatory and catabolic cascade of events have taken place in the form of aspiration of the knee and injection of either IL-1 receptor antagonist or corticosteroids. These have resulted in improved patient reported outcomes related to OA and a decrease in collagen breakdown products respectively [169, 170]. Given that an ACL can reduce the secondary injury to the meniscus and cartilage but not necessarily the progression of OA, additional means to address the inflammatory context are required. For this reason, a tissue engineered scaffold for ACL regeneration should include biomaterials with the potential to challenge this persistent inflammatory state. Polysaccharides are natural products with demonstrated pharmacological mechanisms for their anti-inflammatory effects [171]. Therefore, constituents of this group are to be considered for the development of the ligament scaffold presented in this thesis.

Contrary to the trend for OA, the ACL rupture rate levelled after five years for both knees. A five-year cohort study reported a similar trend after reconstruction with bone-patellar tendon-bone autograft. The re-rupture rate reported in this cohort study was 4.3% for the index knee and 5.3% for the contralateral knee [172]. In contrast, a cohort study from 2014, showed a crude rate of ruptures of 2.45% for the index knee and 1.93% for the contralateral knee at 5 years [173]. The only statistically significant differences between graft ruptures and new ACL ruptures in the contralateral knee were found when the outcomes were divided by follow up period after primary surgery. Most of the ACL secondary ruptures occurred within the first two years after reconstruction (short-term). When no trauma or surgical technical error – such as graft placement – can be identified, a biologic failure of graft integration could be the cause of a re-rupture or persistent knee instability. After implantation, a graft undergoes initial necrosis, revascularization, cellular repopulation, deposition of collagen fibres and remodelling – termed ligamentisation – [174-177]. Ligamentisation is the term coined in 1986 by Amiel et al [175] still in use nowadays to refer to the histological and biochemical transformation from a tendon tissue to a substance very similar to normal ACL. It takes 4 to 6 weeks after ACLR for an autograft to undergo revascularization [176]. This phase is prompted by the graft's hypoxia of the initial healing phase [178]. The graft needs to provide a sturdy support to get through the reduction in mechanical strength while the

collagen orientation and crimp pattern are restoring, specially until the vascular density reaches that of an intact ACL about six months afterwards [178]. It is in this scenario where the high ultimate tensile strength, stiffness and reduced water adsorption capacity of PET are useful as a ligament graft [82]. Finding means to enhance angiogenesis and collagen synthesis would be beneficial at this stage to speed up the ligamentisation process. Mechanical stimulation in the form of rehabilitation protocols plays an important role to this end.

As with any surgery, there are accompanying risks to an ACLR. Systemic complications are not consistently reported in connection to an ACLR, and they greatly impact the success rate of the intervention [179, 180]. The incidence of complications is reported here as a secondary outcome. Albeit the correlation of synovitis, effusion, and infection after ACLR with OA is a topic under scrutiny [181, 182]. From the total number of patients analysed for the present review, 25% presented at least one postoperative complication. These complications ranged from mild discomfort to serious systemic and life-threatening conditions such as laryngospasm. There were no significant differences between the subgroups in adverse events and complications. Recognising these complications is not only important for surgical care, but it can also impact the type of graft chosen for the ACL. On this matter, the donor site mobility left from harvesting an autograft for ACLR is well recognised [183]. The review presented here found kneeling pain (15.25%) and anterior knee pain (13.56%) as the most prevalent donor site morbidities with the use of either BPBT or HS autografts. In 2019, a cohort study [183] observed a significantly higher presence of anterior knee pain for the patients with a BPTB autograft, that subsided two years after surgery. Stiffness and patellar fractures where also reported.

There have been forty-one reviews and five Cochrane reviews previously published related to ACLR, but only one review addressed the effectiveness of grafts [184]. The present systematic review only includes studies with the highest level of evidence. It avoids the inclusion of confounders in the results to increase the utility of the data for clinical practice. Therefore, this meta-analysis provides a more precise calculation of the outcomes. Another strength of this study is the rigorous protocol followed, with a

meticulous control of every step of the process, assuring the inclusion of the majority of the RCT reporting secondary ACL ruptures after an ACLR. A search of the MeSH term “anterior cruciate ligament reconstruction” in PubMed from January 2005 to October 2017, shows that only 8% (263 / 3059) of the articles related to ACLR are RCT. This exemplifies, as Svantensson et al. [185] properly demonstrated in their review, that there is a need for additional unbiased and focused research. Even though there have been numerous innovations on the surgical techniques and devices used, the studies are still far from being generalisable [185]. The above review presents the highest quality evidence found on ACLR outcomes.

A primary limitation of the current systematic review carried out in this thesis is the partial availability of data. Pooled data for the secondary outcome of reported complications were available for 2835 (69%) patients, and the data for the main outcomes were available for a maximum of 1833 (45%) patients. In that previous systematic review form 2012, the available data for pooling individual outcomes came from a maximum of 9 trials and 54% of participants [184]. For this reason, the analysis of the results and their translation into clinical implications is complex. Moreover, the evidence can seem controversial given the ample variation of surgical techniques in the included trials. Noteworthy, most of the interventions considered the use of hamstring tendon autografts.

The studies analysed in the above systematic derived from four different continents. For 86.66% of them, the research took place in high-income countries. Despite the contextual site differences, a single experienced surgeon performed most of the operations reported. Three of the included trials were multicentre studies. Still, caution is advised when applying the evidence in different settings. The test for subgroup differences for ACL re-rupture for autografts versus allografts was not statistically significant ($p = 0.17$). The test for heterogeneity was statistically significant ($p = 0.03$). There were insufficient data to perform any further subgroup analyses intended to explore heterogeneity concerning gender, age and pre-injury activity level.

While the search presented in this thesis included various databases, there were two restrictions for this review. Firstly, this area of research is highly active, and secondly, this review only included articles in English. Hence, some trials might have been missed.

There is currently no consensus on the difference in clinical outcomes for the various ACLR techniques. A 2012 Cochrane review [65] looking at double-bundle versus single-bundle reconstruction indicated limited availability of data on the subject but better restoration of knee laxity and possible protection against new injuries with a double-bundle reconstruction. However, a different meta-analysis proved no significant difference in clinical outcome or graft failure in double-bundle versus single-bundle reconstruction. Only two RTC have provided evidence of a statistically significant reduction in the risk of graft failure with a double-bundle technique [67].

All trials were at high risk of bias, which invariably included performance bias. Based on these study limitations and insufficiency of the available data, the quality of evidence for all outcomes was judged as low. In context, Makhni et al. [68] assigned an overall quality score of 2.2 ± 0.9 to articles regarding the ACL. They calculated this score out of a maximum of 5 according to the Jadad score high variability in outcome reporting patterns.

The evidence shows that ACLR may result in effective treatment of ACL complete tears. Most patients maintain an anterior knee laxity difference of 0-2mm compared to their contralateral knee and go back to a pre-injury activity level or even a higher one. Nevertheless, the results of 27% of increased anterior knee laxity and 39% of patients who must either reduce their level of activity or even completely stop their participation in sports are far from ideal.

2.5 Conclusion

The two key aspects evidenced by this systematic review are that both the development of OA and need for a secondary ACLR are more prevalent on the index knee than on the contralateral knee after primary ACLR, regardless of the type of graft used. This observation makes it especially important to emphasise the care needed on the operated knee in the long term since the difference in the incidence of OA compared to the non-operated knee increases with time. Likewise, a reconstructed ACL presents a higher risk of rupture particularly significant within the first couple of years after the primary reconstruction. Moreover, at least one-quarter of the patients experience a complication after the reconstruction with the current graft options. Sensory changes and muscle discomfort should be taken into consideration when advising the patient on the graft options. There is a significant need to design a graft that could enhance tissue integration by supporting cell proliferation from the early hypoxic stage of the initial necrosis, enhances collagen synthesis, addresses the persistence of an inflammatory state, and potentially prevents infectious complications. An alternative source of graft that could replicate the ACL mechanical strength and ultrastructural characteristics could offer a better solution to treat a ruptured ligament.

Chapter 3

Materials and methods

3.1 Materials and equipment

The general materials used throughout this thesis are listed in Table 3.1. Correspondingly, the equipment used in the studies is listed in Table 3.2. All solvents were of analytical grade and were used as received.

Materials	Purchased from
Polyethylene terephthalate fibre, 0.023mm filament diameter, 192 filaments, high tenacity; polyethylene terephthalate clear biaxially oriented film, 0.1mm thick.	Goodfellow Cambridge Ltd., Huntingdon, UK.
Mylar (PET) plastic film, 0.1mm thick.	RS Components Ltd., Northants, UK.
448877 Chitosan, MW 190–310 kDa, deacetylation degree 75 - 85%.	Sigma-Aldrich, Merck Mexico, Naucalpan de Juarez, Mexico.
S0780000 Sodium hyaluronate BRP batch 2.	EDQM Council of Europe, Strasbourg, France.
SCRC-4000™ ASC52telo, hTERT immortalized adipose-derived mesenchymal stem cells, human.	American Type Culture Collection (ATCC), Manassas, USA.
C-12302 normal human dermal fibroblasts (HDF) adult donor.	PromoCell GmbH, Germany
Fetal bovine serum (FBS), 17018029 collagenase type I, DMEM-low glucose media, DMEM-high glucose media PBS.	Gibco Life Technologies, UK.

Trypsin-EDTA, Potassium hydroxide (KOH), ≥ 97.0 % (GC) GMA, acetic acid, pepsin, FAK100 Actin Cytoskeleton / Focal Adhesion Staining, 1,9-dimethyl-methylene blue zinc chloride double salt (DMMB), C9819 chondroitin sulfate A sodium salt, ascorbic acid, antibiotic antimycotic solution, proline, L-cysteine 97%, glycine ACS reagent ≥98.5%, paraformaldehyde (PFA), glutaraldehyde, TritonX-100, Tween-20, Disodium phosphate (Na_2HPO_4), EDTA, Goat anti-Mouse IgG FITC – conjugated AP124F, P5306 papain from papaya latex, ascorbate-2-phosphate, calcium, phosphate, alizarin red solution, cetylpyridinium chloride, 1x insulin-transferrin-selenium supplement, dexamethasone, alcian blue, insulin, isobutylmethylxanthine (IBMX), indomethacin, oil red O stain.	Sigma-Aldrich Chemical Company Ltd., Dorset, UK.
DMEM/F-12 no phenol red, acetonitrile DNA synthesis grade, PrestoBlue assay, 4',6-diamidino-2-Phenylindole, dihydrochloride (DAPI), ProLong® Gold antifade mountant, Whattman® 3MM, Alexa Fluor® 647 phalloidin, black flat-bottom non-sterile 96-well plates, clear flat-bottom nonsterile 96-well plates.	Thermo Fisher Scientific Inc., UK.

Live/Dead cell viability assay, epidermal growth factor (EGF), Quant-iT™ PicoGreen™ dsDNA assay kit.	Invitrogen, Paisley, UK.
Sircol soluble and insoluble collagen assay kits.	Biocolor LTD, Carrickfergus, UK.
Picro Sirius Red Stain Kit, ab260043 recombinant anti-aollagen I antibody, ab184993 recombinant anti-collagen III antibody, ab96885 goat anti-rabbit IgG H&L DyLight® 594.	Abcam, Cambridge, UK.
sc-518082 AF488 scleraxis antibody conjugated to Alexa Fluor® 488, sc-25328 tenascin-C antibody.	Santa Cruz Biotechnology, Inc., Heidelberg, Germany.
TGF-β1, interleukin-6 (IL-6).	PeproTech EC, Ltd., London, UK.
Y27632.	Axon Medchem, Groningen, Netherlands.
Culture flasks and well plates.	Corning Limited, Life Sciences, UK.

Table 3.1 List of materials used for the experimental work presented in the thesis.

Equipment	Origin
Speedy100R laser cutter.	Trotec, Austria.
CLARIOstar® Plus plate reader.	BMG LABTECH, Germany.
Tecan Infinite 200 Pro microplate reader.	Tecan Trading AG, Switzerland.
Orbital shaker S01.	Stuart scientific, UK.
Pico low-pressure plasma system.	Diener Electronics, Germany.
EVOS ® FL auto cell imaging system.	Thermo Fisher Scientific Inc., UK.
Zeiss Fluorescent microscope with Axiocam.	Carl Zeiss Ltd, UK.
Q150RS gold sputter.	Quorum, UK.
EVO MA10 SEM.	ZEISS, Germany.

Table 3.2 List of equipment used for the present work.

3.2 Methods

3.2.1 PET scaffold fabrication

For the fabrication of the two-dimensional PET scaffolds, PET films were cut into 14 mm discs using a laser cutter.

PET filament was used for the fibres and PET films were used for the scaffold support. The scaffold support was made by cutting 14 mm six teeth gear-shaped discs (hollow centre 9 mm) from the PET film using a laser cutter (see figure 3.1). The fibres were wet with deionized water and weaved along the gear teeth.

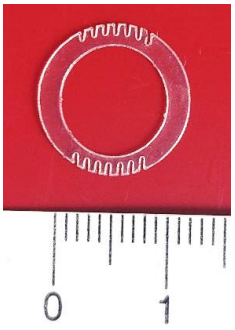

Figure 3.1 PET 3D scaffold frame.

Prior to plasma treatment, all samples were sterilised. Two-dimensional samples were initially washed with de-ionized water and then soaked in 70% ethanol for 30 min, during which they were placed on an orbital shaker. Next, the ethanol was discarded, the samples were washed twice with PBS for 10 min each time and they were air dried under a hood. The 3D fibrous scaffolds were sterilized by autoclaving them for one h and a half at 120˚C.

3.2.2 O_2 plasma surface treatment

For the surface plasma modification, a low-pressure plasma system operating at 40 kHz at 100 W was used. The PET surface was exposed to a consistent fixed power with a gas flow rate of 0.4 mbar, for different exposure times at min 0.5, 1, 2.5, 5 and 10. PET 3D fibre scaffolds were treated with O_2 plasma for 0.5, and 1 min using the same low-pressure plasma system and conditions.

3.2.3 Effect of surface modification on the cellular attachment, proliferation, and collagen production

Biocompatibility was tested by seeding human adipose-derived immortalized mesenchymal stem cells (iMSCs) onto the scaffolds.

Scaffolds were pre-conditioned with DMEM-low glucose media supplemented with 50 µg/mL ascorbic acid, 10%, FBS and 1% penicillin / streptomycin / amphotericin B and incubated at 37ºC for 10 min before seeding. The cells were seeded at a density of 2 x 10^4 cells per 2D scaffold and 4 x 10^4 cells per 3D scaffold. In the 2D experiments, cells were cultured for up to 14 days and for up to 28 days on the 3D scaffolds. Spectrophotometric experiments to assess cell growth and metabolic activity were carried out at days 1, 3, 7, and 14 – with the addition of days 21 and 28 for 3D fibrous scaffolds –. Throughout the cell culture study, 40 % of the medium in each well was replaced with fresh medium every three to four days. Metabolic activity was tested by means of a PrestoBlue assay. The scaffolds were washed in PBS and carefully transferred to new sterile well plates. PrestoBlue reagent was added, and the scaffolds were incubated for 1 h at 37˚C. Fluorescence was measured at an excitation wavelength of 535 nm and an emission wavelength of 615 nm using a plate reader. The fluorescence reading of the no-cell control wells was averaged and then subtracted

from the fluorescence value of each experimental well. The readings were converted into a cell number based on a standard curve generated from the assay of a known number of cells. DNA content was measured using a Pico Green assay. Appropriate standards (0–1 µg/mL) were prepared by diluting Lambda DNA stock solution with Tris-EDTA buffer before the experiment. Accordingly, 100 µL digested sample solution were reacted with 100 µL PicoGreen test solution and subsequently fluorescence intensity was measured at 520 nm using a plate reader.

For all the 2D tests, tissue culture plastic (TCP) was used as positive control and unseeded PET scaffolds as negative control. For all the tests of 3D scaffolds, unmodified PET scaffolds were used as the positive control and unseeded PET scaffolds as the negative control.

3.2.3.1 Cellular attachment

To visualise the cellular morphology and cellular attachment of the iMSC cultured on each scaffold, immunofluorescence staining for the nuclei and actin filaments in the cytoskeleton was performed at 24 h post seeding. The cell media was removed from each well, then scaffolds were washed with PBS. To fix the samples, the cell samples were incubated for 30 min at room temperature with 4% (w/v%) PFA in de-ionized water. Next, the samples were washed again with PBS and the samples were then permeabilized by incubating them for five minutes with 0.1% TritonX-100 in PBS, followed by two more washes with PBS. The samples where then blocked with 1% BSA for 30 min. Phalloidin was added at a 1:40 dilution in PBS and incubated at room temperature in the dark for 40 min. The samples were then washed again with PBS and then DAPI was added and incubated at room temperature in the dark for 10 min in a solution of 1µg/mL. Once the staining solution was decanted and the samples were washed with PBS, the scaffolds were mounted onto a glass slide with antifade mountant. The samples were screened using EVOS fluorescent microscope.

The change in cellular morphology from 4 h to 24 h after seeding was monitored to determine the difference in cell spreading on the treated surfaced. This change was assessed by the deviation of the cell's shape from a circle, which represents a value of 1. The cell circularity was measured using the Image J software to analyse the square

of the perimeter of each cell divided by its area. As the cell morphology becomes more elongated, the value becomes smaller. A systematic survey of the four quadrants was done for the analysis, where at least 25 cells were identified for the comparison.

The morphology of cell adhesion and matrix deposition on the PET fibrous uncoated and coated scaffolds was additionally observed by SEM. The samples of the cell cultures were kept in 2.5% (v/v) of glutaraldehyde for 24 h at 4˚C and dehydrated in a graded series of ethanol concentrations (40%, 70%, 90%, 95%, 100%), for 2 min each. The scaffolds were then left for 24 h in 100 µL of HMDS and gold coated before observation by a SEM.

3.2.3.2 Extracellular matrix production

Collagen production was confirmed qualitatively and quantitatively by using two Picrosirius (PSR) red assays.

To visualise the extent and distribution of the collagen deposition capacity of the seeded iMSCs, the scaffolds were fixed and stained at day 14 using a PSR staining method [186]. With this protocol, collagen is stained in red and can be observed with light microscopy and polarised light microscopy. Birefringence was assessed with a fluorescent microscope to determine the distribution of collagen and potential differentiation between COL I and COL III deposition [187].

The anionic dye in PSR contains sulfonate groups that bind strongly with cationic collagen fibres [188]. Before staining the scaffolds, cells were first fixed in methanol at −20°C overnight. They were then washed with PBS after decanting the methanol and were subsequently stained at room temperature for 4 hours with the dye from the Picro Sirius Red Stain Kit. Excess dye was washed with PBS three times and an additional wash with 0.1% acetic acid. The stained cells were then dried under a hood for spectrophotometric analysis. The PSR solution was eluted in 200 µl of 0.5 M sodium hydroxide per well. The solution was placed on a rocker at room temperature for 1 h before the absorbance was calculated at 555 nm with an Tecan plate reader.

Soluble collagen deposition was quantified by the Sircol soluble and insoluble collagen assays as per the manufacturer’s instructions. The dye binds to the [Gly-X-Y] n helical

structures in collagen. It does not distinguish the specific type of collagen produced by the sample. First, the scaffolds were incubated at 4˚C overnight in a pepsin solution (0.1 mg/ml in 0.5 M acetic acid) to solubilise the collagen. The acid solutions were neutralised, transferred to low protein binding 1.5 ml conical microcentrifuge tubes, incubated at 4˚C for an additional night with and isolation and concentration reagent, and then stored at -20˚C until all the samples were ready for assessment. Figure 3.2 illustrates the protocol followed for the quantitation of soluble collagen from the scaffolds. A standard curve was constructed using 5 µg, 10 µg and 15 µg of the collagen standard solution provided in the kit in de-ionized water prior to the analysis of the samples.

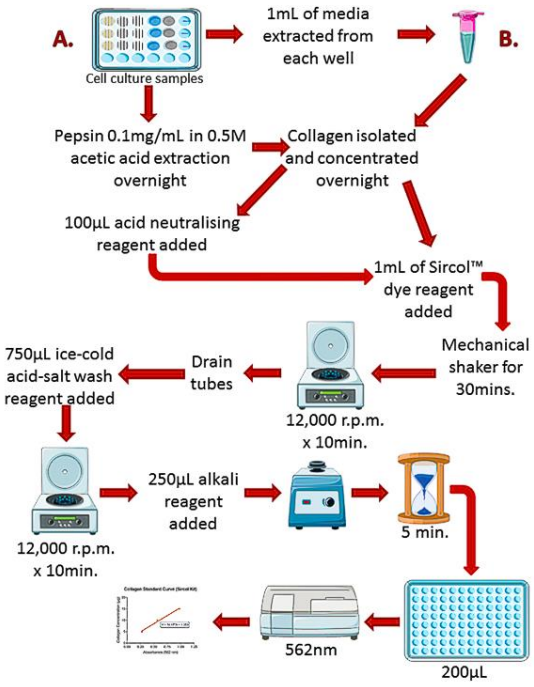

Figure 3.2 Step-by-step graphic representation of the Sircol soluble collagen assay. Image made with Servier Medical Art under a Creative Commons Attribution 3.0 Unported License.

A dimethylmethylene blue assay (DMMB) was used to quantify sulphated glycosaminoglycans (sGAG) in solution. DMMB reagent was prepared by dissolving 16 mg DMMB in 1 L water containing 3.04 g glycine, 1.6 g NaCl and 95 ml of 0.1 M acetic acid. It was then paper filtered using Whattman® 3MM. The pH of this solution was

around 3.0. Bovine chondroitin 4-sulfate was used to prepare standards (0–10 µg/mL) for analysis. The scaffolds were digested enzymatically by adding 1 mL of freshly made papain solution (125 µg/mL) with 10 mM of cysteine in a PBE buffer (100 mM Na2HPO4, 10m M EDTA) and incubating overnight at 60 °C in an orbital incubator. The plates were then stored at -20˚C until all the samples were ready for assessment. For the test, 20 µl of each digestion solution samples were transferred to a 96-well plate. Next, 200 µl of DMMB were added to each sample and the plate was shaken on a plate shaker for 5 sec. The absorbance was immediately read at 525 nm using a CLARIOstar® Plus plate reader.

To evaluate the expression of different ligament related proteins on the iMSC seeded 3D scaffolds, antibodies anti collagen I (COL-I), collagen III (COL-III), tenascin C and Scx were used. At day 14 and 21 the samples were fixed and permeabilized as previously described. The samples where then incubated them for 30 min in 1% BSA, 22.52 mg/mL glycine in PBST (PBS+ 0.1% Tween 20) to block unspecific binding of the antibodies. The primary and secondary antibodies used for this experiment are shown in table 3.3. Titration of the different primary antibodies including the negative controls was conducted prior to the tests. For the staining procedure, primary antibodies were diluted in 1% BSA, 250 µL were added to each 24-well plate sample, and were subsequently incubated overnight at 4°C. The samples were then washed 3 times in 0.1% tween in PBS. Next, the cells were incubated with the secondary antibody in 1% BSA at room temperature for 1 h in the dark. Once the secondary antibody solution was decanted, the samples were washed 3 times with 0.1% Tween 20 in PBS and stained with DAPI for 5 min. The samples were washed 3 times with 0.1% Tween 20 in PBS and were then mounted on glass slides using a fluoromount aqueous mounting media. A Zeiss Fluorescent microscope was used for the assessment of expressed extracellular proteins from the samples.

Primary antibody	Species	Working dilution	Secondary antibody	Working dilution
Anti-Collagen I	Recombinant	1:250	Goat Anti-Rabbit IgG	1:500
Anti-Collagen III	Recombinant	1:100		
Anti-Tenascin C	Mouse monoclonal	1:100	Goat anti-Mouse IgG FITC - conjugated	1:500
Anti-Scleraxis	Mouse monoclonal	1:100		

Table 3.3 Primary and secondary antibodies used for immunofluorescence staining. A summary of the primary and secondary antibodies is presented with their working dilutions.

3.2.4 Analysis of iMSC differentiation on O_2 plasma treated PET samples

Cells were seeded onto PET fibre scaffolds at a density of 40 000 cell/ µL. They were cultured in DMEM-low glucose media supplemented with 50 µg/mL ascorbic acid, 10% FBS and 1% penicillin/streptomycin/amphotericin B for 14 days and then assessed for their ability to retain the iMSCs stemness. Three scaffolds per condition (untreated and 1-min O_2 plasma treated) were stained at day 14 and 21 for osteogenic, chondrogenic and adipogenic differentiation. The ones stained at day 14 were used to assess the scaffold's potential to induce differentiation and to use as negative controls for the ones stimulated with induction media and further cultured. Osteogenic differentiation was assessed using a defined osteogenic growth factor cocktail. The medium was replaced at day 14 with conventional GM supplemented with ascorbate-2-phosphate (57 µmol/L), TGF-β1 (10 ng/mL), EGF (20 ng/mL), IL-6 (10 ng/mL), calcium (3 mmol/L) and phosphate (2 mmol/L). The cells were further culture for 7 days with media changed every 48 h to induce differentiation. They were then stained with alizarin red solution (pH 4.2) and qualitatively assessed by light microscopy. Calcium mineral deposits were quantified by dissolving the incorporated dye with 10% cetylpyridinium chloride for 60 min at room temperature. Absorbance was measured by spectophotometry at 570 nm.

A chondrogenic medium consisting of low-glucose DMEM, 1x insulin-transferrin-selenium supplement, dexamethasone (100 nmol/L), Y27632 (10 µmol/L), ascorbic

acid (50 µg/mL), proline (40 µg/mL) and TGF-β1 (10 ng/mL) was used to culture the seeded scaffolds for 7 days to differentiate the cells down the chondrogenic pathway. Differentiation was evaluated by staining with alcian blue (pH 2.0) overnight at 4˚C.

For adipogenic differentiation, the seeded scaffolds were further cultured for 21 days. The adipogenic differentiation media contained 10% FBS, insulin (1 µg/mL), dexamethasone (0.1 µmol/L), IBMX (4.5 µmol/L) and indomethacin (125 µmol/L). The media was changed every 2 days. Oil Red O stain was used to assess the production of fat droplets. Images were taken with light microscopy.

3.3 Statistical Analysis

Statistical analysis was performed using GraphPad Prism 6.0 (GraphPad Software Inc.) applying one-way or two-way analysis of variance (ANOVA) followed by a Tukey's multiple comparison test. Values are expressed as mean ± SE. Statistical significance is considered when P-values are below 0.05. Error bars in the graphs represent the standard error of the mean (SE). Statistical significance is represented as follows: * = $p < 0.05$, ** = $p < 0.01$, *** = $p < 0.001$.

Aims: To test the effects of a straightforward surface modification of PET with O_2 plasma.

Hypothesis: Low frequency O_2 plasma with the use of a low-pressure system at low power will effectively modify the PET surface and enhance its biocompatibility.

4.1 Introduction

Cell-material interactions at the biological interface are critical for the successful integration of the graft. The material's surface must support the biological functions of native cells while discouraging microbial colonization. The biochemistry, charge, hydrophobicity, roughness/topography, porosity, crystallinity, and stiffness factors of the material's surface affect cell adhesion. To modify these, there are several techniques that can be used, all with advantages and disadvantages. Plasma surface modification is one of them.

When the substrate is an inert polymer, as is the case of PET, chemically reactive functionality in the form of chemical groups or radicals can be generated using plasma treatments. The effects of low frequency (40 kHz) cold plasma treatment on PET fibres have been investigated to enhance cell attachment, proliferation, and extracellular matrix deposition. The effect of O_2 plasma exposure on PET films and woven parallel fibres was investigated. A constant treatment period from 0.5- to 10-min was used for two-dimensional samples and 0.5-and 1-min for 3D samples, with a power of 100 W. Modifications on film's surface structure have been monitored and biocompatibility has been assessed.

4.1.1 Surface modification of PET for ligament regeneration

The surface structure of PET can be modified by using various surface treatment methods such as VUV irradiation [189], wet chemical treatment [190, 191], laser

ablation [192], and cold plasma treatment methods [193]. All these methodologies are useful in modifying the wettability, surface chemistry and roughness. Nonetheless, cold plasma treatments have shown the most promise by affecting only the uppermost surface layer and not altering the material's bulk properties [194, 195].

4.1.2 Plasma treatment for polymer surface modification in ligament regeneration

To understand the effect plasma has on any given surface, it is important to examine what plasma is and how it works. Firstly, plasma is considered as a fourth state of matter. It is a gas in the partial ionized state and behaves as both liquid and gas. When the atoms in the gas become ionised, they produce an electrically conducting medium occupied by an even number of positively and negatively charged particles. The term has been used since 1928, when Langmuir first coined it, and has been thoroughly studied for different applications ever since. Electrons, ions, energy-rich neutrals, molecules, fragments, atoms, and photons compose it. Essentially, a plasma contains an increased number of electrons, ions, atoms, radicals, and complexes. It possesses electrical conductivity, generates a glow when the electrons and ions collide, and forms a magnetic field. In macroscopic dimensions, the number of electrons in a plasma is equal to the number of ions, while in microscopic dimension it charges the space. Because it is usually generated by a constant electrical current, when in a static state, plasma holds high energy with respect to the system's internal energy plus the product of its pressure and volume. The ion shower and recombination of charges is constant over time within the plasma. It has characteristic velocity and energy distributions. It emits a high-energetic vacuum-UV radiation of 2 – 200 nm [196]. Plasma can present at different pressures: low (<100 Pa), atmospheric or high (≥ 1 atm) [197-199]. It is classified as either thermal (or fusion) or non-thermal (also non-equilibrium, or cold) [195, 200]. For surface modification, cold plasma is the most used to preserve the bulk material properties. Cold plasma can be achieved either at atmospheric pressure or at low pressures (< 10 mbar), as used in this thesis [195].

The types of cold plasmas produced at atmospheric pressure are: a) the corona discharge, where the plasma density decreases as it distances from the electrode and

it involves a series of discharges that are not uniform and do not create an arc; b) the dielectric barrier discharge, where a series of swift micro discharges form by a pulsed high voltage between electrodes form an arc that is halted by a dielectric layer; and c) the plasma jet, used to etch or deposit films by ignition of a gas discharge from a continuous gas flow through two concentric electrodes [195, 201]. As opposed to low-pressure plasma, atmospheric plasma does not need a vacuum; it can therefore be applied to tissues directly – which potentially makes it a more portable technology [200, 202]. Nevertheless, low-pressure plasma technology is more applicable to the manufacture of tissue engineered scaffolds given that the discharge can be regulated, therefore it is more reproducible, it requires lower voltage, the discharge is more uniform, it provides high sterilisation and decontamination of the materials, it offers the possibility to use a variety of reagent gases and it can be used to selectively modify the material's surface [200-202].

Low pressure cold plasma can be generated through different types of discharges:

- Direct current (DC) discharge: the application of a constant potential difference between the cathode and anode where the gas is contained generates a continuous current where an electric field accelerates the emitted electrons engendering collisions with the gas atoms and ensuing a glow from the radiation caused by the sequence of excitation collisions and de-excitation. Ionisation collisions also take place, and they are responsible for the self-sustaining plasma, as they generate new electrons and ions by ion-induced secondary electron emission. Compared to electrodeless discharges and settings with time-varying electric field, when the glow discharge is generated by DC, the electrodes are key in the secondary electron emission sustaining the plasma [203].
- Low frequency discharges: characteristically from 40 to 450 kHz. Contrary to radiofrequency (RF), they do not leak to the open atmosphere, but they have higher sheath voltage fluctuations [199, 204]. Their voltage is higher than that of high frequency discharges since it increases to make up for lost ions [205]. The lowest plasma discharge frequency approved as an ISM (Industrial, Scientific,

Medical) band is 40kHz. It is particularly beneficial in providing a higher quality and uniform plasma at a lower cost compared to the higher frequencies, despite its slower etching or coating time. It also outdoes higher frequency discharges as the system required is simpler and it has the highest ion density [205-208]. Etching is controlled by thermal evaporation rather than an atom-scale dissociation found with high-frequency plasma etching processes [209].

- Radiofrequency discharges: these are typically 1–100 MHz, the most used are 13.56 MHz and 27.12 MHz [199, 210-212]. Etching is faster at the standard frequency of 13.56 MHz and is highly dependent on the material to be treated. At this typical RF frequency, the ions gain energy distributed along several RF cycles, narrowing the range in ion energies compared to lower frequencies [209].
- Microwave discharges: are those above 300 MHz, however the reactive gas mixtures are usually exited at either 915 MHz or 2.45 GHz and the power employed is generally in the range of 1 to 60 kW. Etching is the fastest, but the operation requires the most energy [213].
- Pulsed electrical discharges: these are negative or positive pulses lasting ms or ns. They use either DC or RF and have on and off operation cycles. Temperature of the treated material's surface and mean power are reduced compared to continuous discharges, which is useful for the treatment of material with a low melting point [209]. This type of discharges are also particularly useful for plasma polymer coating, to optimise functional group and crosslinking densities [214].
- Laser generated discharges: these are focalised ns or ps pulsed plasma beams [200].

A plasma acts as a conducting fluid where the particles interact not only via collisions, but also through long-range electromagnetic forces. Wavelike phenomena play a critical role in the behaviour of a plasma. Depending on the pressure at which a plasma occurs, its thermal properties change from isothermal at high pressure, to non-isothermal at low pressures. Temperature plays a significant part in the effects of a plasma discharge onto a material's surface. To ascertain the temperature the unit used represents the energy gained by an electron in vacuum when it is accelerated across

one volt of electric potential. This unit is called the electron volt (eV). The temperature measured in electron volts is given by W = T/12000 where T is expressed in kelvins. Given that the energy needed to remove one electron from an atom or molecule, the temperatures required for self-ionisation range from 2.5 to 8 eV [215].

Plasma is a straightforward method to form reactive sites as radicals or functional groups on polymers, forming anchoring sites for further chemical reactions. This chemical modification customarily involves the upper 1 – 10 nm of a surface [216]. The functionalisation of a polymer's surface can be tailored by the selection of the plasma-gas, since the main element or its characteristic groups will be the ones to selectively recombine to the polymer's surface and produce its functionalisation by abstracting H and attaching atoms or fragments of the dissociated plasma gas to the carbon radical sites at the surface. Functionalising a polymer's surface results in enhanced cell attachment and cell spreading, which in turn affect the processes of cell division as well as DNA and protein synthesis [217]. The difficulty of this modification is that there is a broad spectrum of different functional groups formed, and the post plasma introduced oxygen affects the plasma modification. During this process, the interaction of plasma and polymer results in surface charging, surface cleaning, surface functionalisation, etching and emission of degradation products [196, 218].

Referring to plasma-material interactions, there are broadly three types: plasma polymerization, plasma treatment and plasma etching. The first one implies that organic monomers are fragmented and deposited onto a material. Plasma treatment entails the modification of a substrate by the insertion or substitution of chemical functionalities or the creation of radicals for crosslinking or subsequent surface grafting using gases such as Ar, N_2, O_2, NH_3, and CF_4. Materials surface modification can be dominated by any of these processes depending on different factors involved in the process.

As previously mentioned, although PET exhibits a mechanical strength that is comparable to a native ACL, its chemically inert hydrophobic surface translates into low cell attachment [219-221]. Multiple studies have investigated the modification of PET surface by various types of plasma treatment [222]. PET samples treated with O_2 plasma result in the formation of different functional groups and an increased wettability

that correlates with an enhanced cell attachment [222, 223]. When PET is exposed to O_2 plasma gas, atoms or fragments are attached to the polymer's chain (figure 4.1). On the surface, as oxygen species incorporate into the sample's surface, O_2 concentration on it increases, different functional groups form, the surface becomes more hydrophilic, and cell adhesion is enhanced [222, 224, 225]. The effects on the polymer's surface vary depending on the parameters chosen such as gas composition, gas flow, power, pressure, and process time. In a low-pressure and low frequency (40kHz) plasma system such as the one used in this project, gas is excited between two electrodes – one of which is the stainless steel housing of the vacuum chamber - by supply of energy where the ionised gas reacts chemically with the surface.

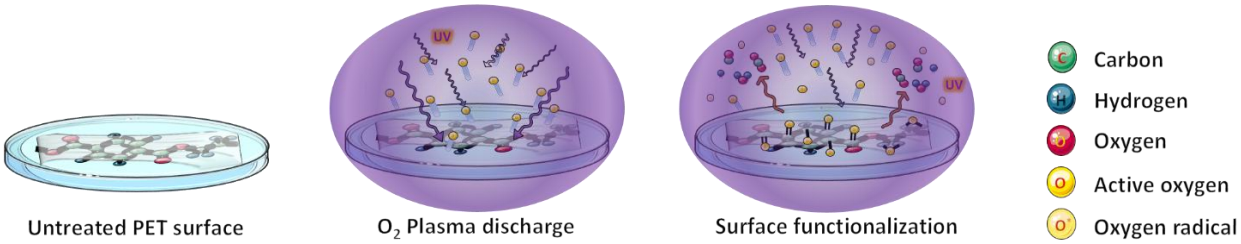

Figure 4.1 Schematic representation of oxygen plasma surface functionalisation. Image made with Servier Medical Art under a Creative Commons Attribution 3.0 Unported License.

Optimal mechanical properties and chemical properties of the bulk are best preserved by avoiding advanced degradation and formation defects that could ensue by prolonged, higher energy plasma exposure.

4.2 Materials and Methods

4.2.1 Surface characterisation

SEM was used to analyse the morphology and structure of the uncoated and coated scaffolds. Samples were air dried, fixed on a stub with double-sided carbon tape and sputtered with a gold layer in a coating system. Examination was performed in a FEI Quanta 200 FEG ESEM apparatus with an accelerating voltage of 10.00 kV.

For the analysis of the effects of PET exposure to oxygen plasma, an X-ray photoelectron spectroscopy (XPS) survey and high-resolution spectra in the regions of C 1s and O 1s for the elemental and chemical state identification were obtained. The data was analysed with the CASAXPS processing software (Casa Software Ltd.). Data was recorded from two different spots from three different samples.

To examine both the surface topography and surface mechanical properties, atomic force microscopy (AFM) was used on the unmodified and modified PET 2D scaffolds. The data collected from this method comes from a deflection translated into voltage that is measured by a detector as the tip of a cantilever interacts with the sample. As the tip scans the surface, a laser beam that is reflected off the cantilever is sensed by a photo detector, allowing to track the vertical and lateral motion of the probe. Compared to surface roughness meassure, the Young's modulus was determined on 1 µm areas using a 16 x 16 pixels force mapping contact mode to ensure the same measurement conditions for all the scaffolds.

Water contact angle measurement was used to assess the wettability of the untreated and treated PET 2D scaffolds. The contact angle is the position at which a liquid interface meets a solid surface. The shape of a small liquid droplet as it rests on a flat horizontal solid surface is then determined by the Young's equation. This equation is used to analyse the interaction between the surface contact angle (θ) and the tension on the surface. The static water contact angles of the PET modified, and unmodified scaffolds were analysed using the sessile drop method using the DSA 100 instrument and ADSA-P drop-shape analysis software (KRUSS, Germany). A 3µL volume of deionized water was dispensed by a syringe pump through a flat tip needle of 0.5 mm

diameter. The average contact angle was calculated using KRUSS drop shape software (version 1.90.0.14). Measurement of a single drop was performed on six independent scaffolds (N = 6).

4.3 Results

4.3.1 O_2 plasma treatment effectively modifies the PET surface

The effect of O_2 plasma treatment on the PET surface topography is shown in figure 4.2 A. The surface changes from the smooth unmodified scaffold to the formation of clusters of particles on the scaffolds treated for 0.5- and 1-min, to a more organised and directional topography for the 2.5-, 5- and 10-min treated scaffolds. The untreated PET scaffold had a WCA of 81.7 ± 6.2°. It reached 22.8 ± 3.3° after 10 min of O_2 plasma exposure. Wettability of unmodified PET scaffolds decreased significantly ($p < 0.01$) when compared to each of the plasma modified scaffolds in a time-exposure dependent manner. The WCA was significantly lower ($p < 0.005$) for the scaffolds treated for 5 and 10 min when compared to the ones treated for 0.5-, 1- and 2.5-min.

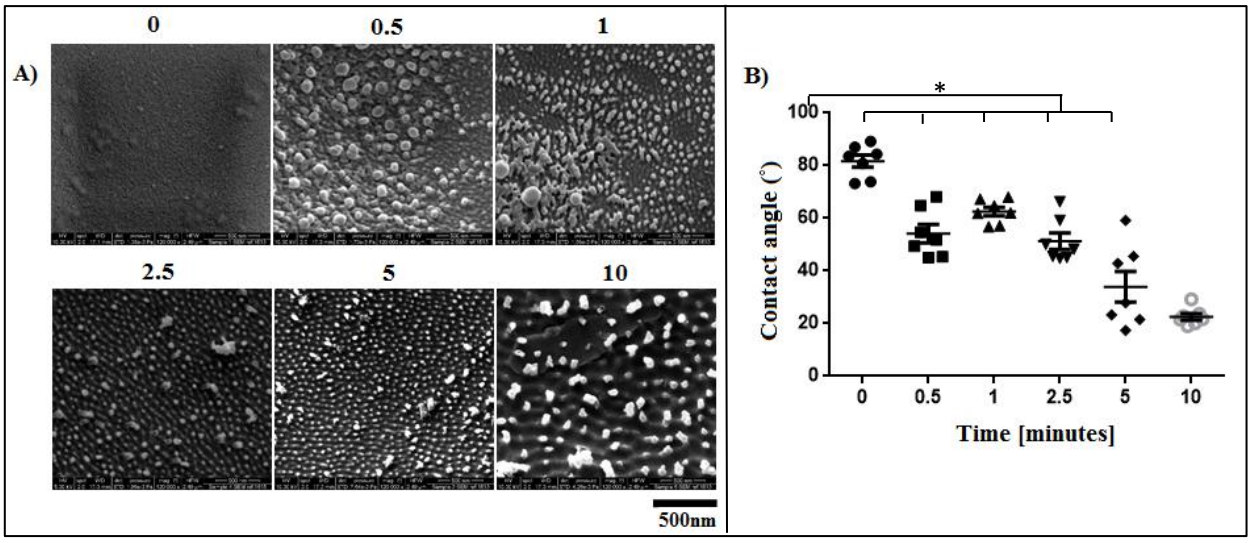

Figure 4.2 Time-dependent effect in minutes of O_2 plasma exposure on PET surface topography as observed in A) SEM and on its wettability as shown by the B) water contact angle. N = 7.

The average roughness (figure 4.3 B) showed a statistically significant difference for the 2.5-, 5- and 10-min treated scaffolds when compared to the baseline ($p < 0.001$). Figure 4.3 C shows no statistically significant difference in the effect of O_2 plasma treatment on the micro mechanical properties ($p > 0.05$). Topographically, the PET surface significantly changed in an exposure time-dependent manner as shown in figure 4.3 A. These images illustrate the significant changes on the PET scaffolds due to O_2 plasma treatment, where the root-mean-square (Rq) surface roughness of the PET films increased from the untreated PET scaffold's 919.0 pm to 10.71 nm on the one exposed to O_2 plasma for 10-min.

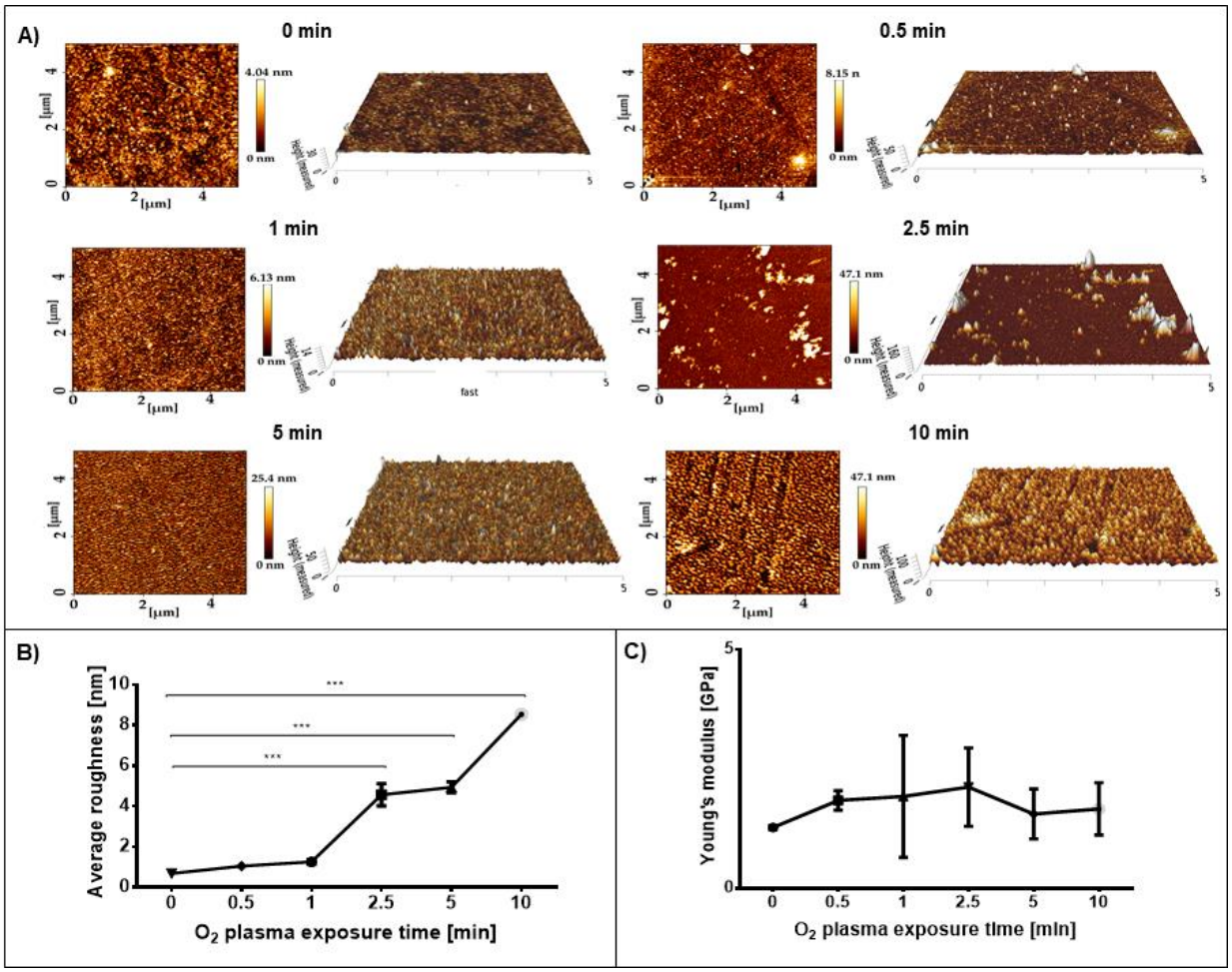

Figure 4.3 Time-dependent effect in minutes of oxygen plasma exposure on PET surface. Changes in topography by A) AFM. Correlation with B) average roughness, and C) Young's modulus. N = 3.

PET compositional changes and surface chemistry before and after O_2 plasma treatment were determined by both XPS survey and high-resolution spectra. Table 4.1 shows normalized carbon and oxygen surface concentrations for the treated and untreated PET scaffolds. Surface carbon concentration decreased in all scaffolds after O_2 plasma treatment in response to an increase in surface oxygen concentration as a factor of time exposure to plasma treatment. The total difference in oxygen concentration was calculated by subtracting the amount of oxygen associated with carbon from the total amount of oxygen from the survey spectra. There was an increase in the atomic percent of this remaining oxygen for all the O_2 plasma treated scaffolds when compared to the untreated scaffold (from 10.38% for untreated PET, to 13.75%, 14.86%, 13.58%, 14.58%, and 10.59% respectively for each of the plasma treatment times). Figure 4.4 shows the components of C 1s from high-resolution spectra of PET scaffolds after O_2 plasma treatment. Table 4.1 lists the surface chemical compositional changes on different surface O_2 plasma exposure times. The intensity of the C–C / C–H component of the plasma treated scaffolds decreased ($p = 0.9$) while the intensity of the carbonyl groups increased for all modified scaffolds when compared to the unmodified PET.

	Atomic concentration (%)		**C 1s component (%)**		
O_2 plasma exposure (min)	**C 1s %**	**O 1s %**	**C-C**	**C-O**	**C=O**
0	56.33	43.67	66.71	19.03	14.27
0.5	51.96	48.04	65.71	19.60	14.69
1	51.49	48.51	66.34	19.23	14.42
2.5	52.23	47.77	65.81	19.54	14.65
5	48.38	51.62	62.96	21.17	15.87
10	49.77	50.23	60.36	22.66	16.99

Table 4.1 XPS data of surface chemical composition changes of PET after O_2 plasma treatment.

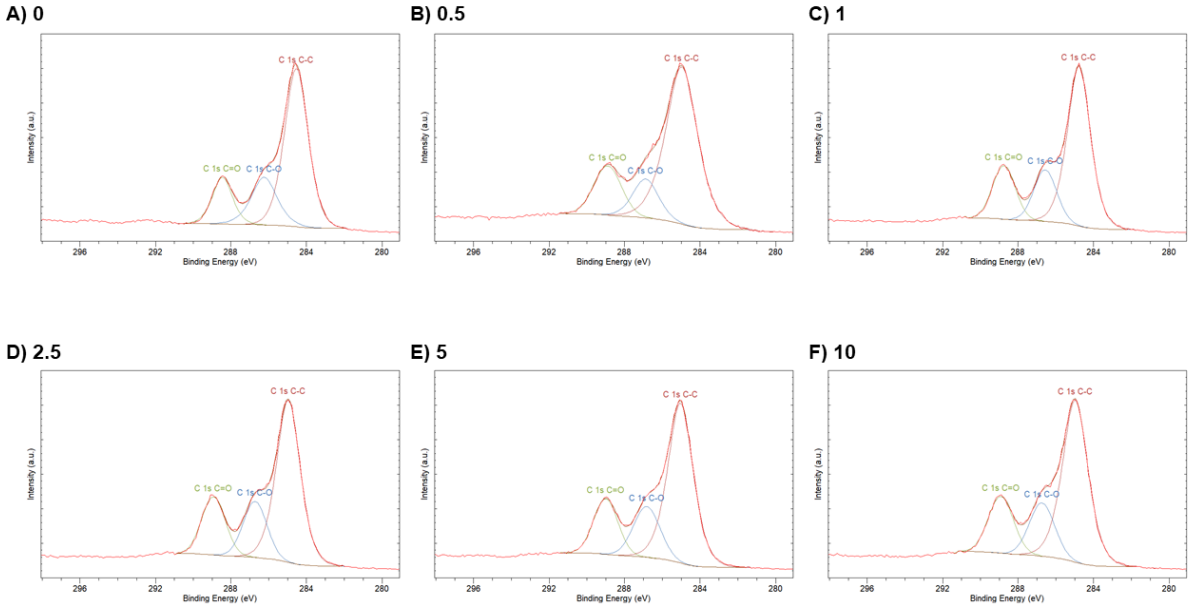

Figure 4.4 XPS C1s spectra and its components of plasma-treated PET scaffolds after different duration in minutes of O_2 plasma exposure. Figure created by CASA XPS software.

The atomic O/C ratio of the scaffold's surface increased in an O_2 plasma time exposure dependent manner, although it did not reach statistical significance ($p = 0.7$). Figure 4.5 shows the changes in the percentage of carbonyl group concentration and O/C ratio as a result of O_2 plasma treatment.

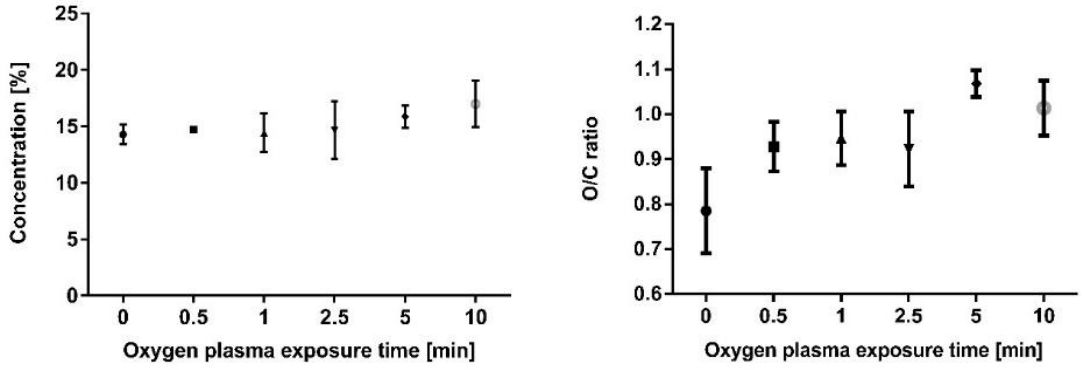

Figure 4.5 Effect of O_2 plasma exposure on carbonyl groups and atomic O/C ratio on untreated and untreated PET films. N = 3.

4.3.2 Effect of surface modification on the cellular attachment, proliferation, and collagen production

4.3.2.1 2D scaffolds

4.3.2.1.1 iMSCs readily attach to O_2 activated plasma PET films

As a measure of cell attachment, circularity was used to assess the cellular interaction with and spreading onto the scaffold's surface (see figure 4.6). After staining the cell for actin cytoskeleton filaments and nuclei, images of the scaffolds were taken in a systematic way to ensure capturing a representative population from the whole scaffold. The cells were counted, and the morphology was analysed with the image processing software. In terms of circularity, there was a significant decrease in cell circularity from 4 to 24 h post seeding; greater for scaffolds treated by 0, 0.5, 1 and 10 min O_2 plasma ($p < 0.0001$), significant also for 2.5 and 5 min-treatments ($p < 0.05$). At 4 h post seeding, the cells on the untreated PET scaffold had a circularity of 0.71 (SE 0.11), which was the closest to the complete circle represented by 1 and evidenced a significantly slower rate of spreading on the surface ($p < 0.0001$). In contrast, cell spreading at 4 h was significantly faster for 2.5-min O_2 plasma treated scaffolds when compared to all but the 5-min treated scaffold ($p < 0.05$).

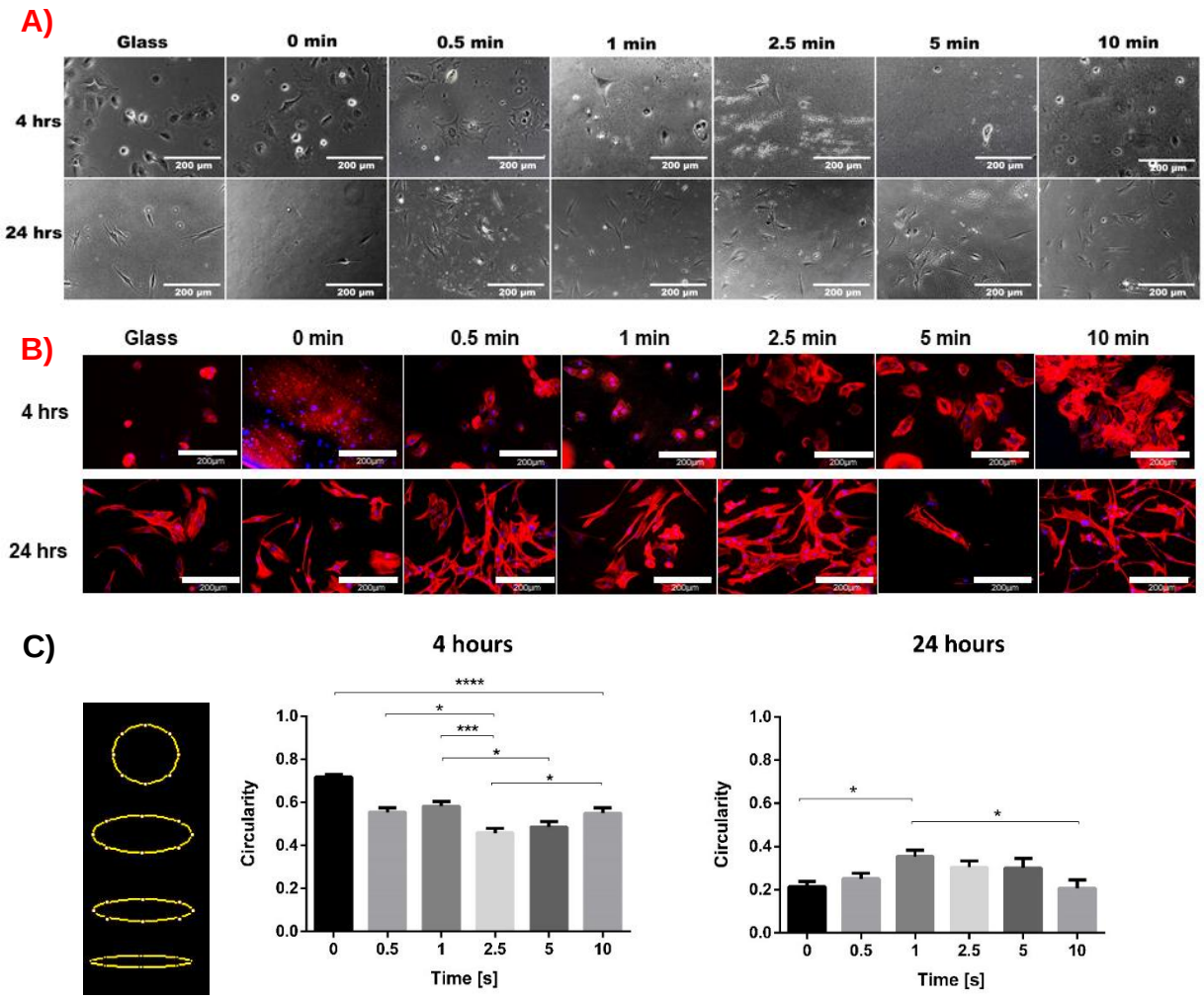

Figure 4.6 Cell circularity 4 h and 24 h after seeding on plasma treated 2D scaffolds. A) Light microscopy representative images; B) nuclear and actin staining of the cells; C) quantification of circularity at 4 h and 24 h after seeding. The closer the number is to the unit, the loss spread the cells are. 1 represents a full circle. N=58 for 4 h and N=25 for 24 h. Bar represents 200 µm.

4.3.2.1.2 O_2 plasma does not have a conclusive effect on iMSC growth on 2D PET

There was a significant increase in DNA content ($p < 0.01$) between day 1 and day 3 for all the conditions except for 5-min O_2 plasma exposure ($p = 0.3$) and the positive control ($p = 0.2$). There was a significant decrease ($p < 0.01$) between day 3 and day 14 for all the conditions except for the positive control ($p > 0.5$). For the PET treated surfaces, there was a significant difference ($p < 0.05$) in cell growth between 0.5-min

and 5-min O_2 plasma exposure at day 3. There was no statistically significant difference ($p > 0.1$) between the treated and untreated PET scaffolds at any time point.

For the metabolic activity by DNA content, there was no statistically significant difference ($p > 0.8$) for treated or untreated PET scaffolds between day 1 and day 3 of cell culture (see figure 4.7). There was a significant increase ($p < 0.001$) in metabolic activity by DNA content for all treated and untreated PET scaffolds from day 7 to day 14. At day 14, the metabolic activity by DNA content was significantly higher ($p < 0.02$) for the PET treated scaffold 0.5-when compared to the 1- and 2.5-min O_2 plasma exposed scaffolds. There was no statistically significant difference ($p > 0.3$) between treated and untreated PET scaffolds at day 14 of cell culture. At day 14, the 10-min O_2 plasma treated PET scaffold showed the highest metabolic activity rate and was significantly increased compared to the metabolic activity displayed by all other scaffolds ($p < 0.001$).

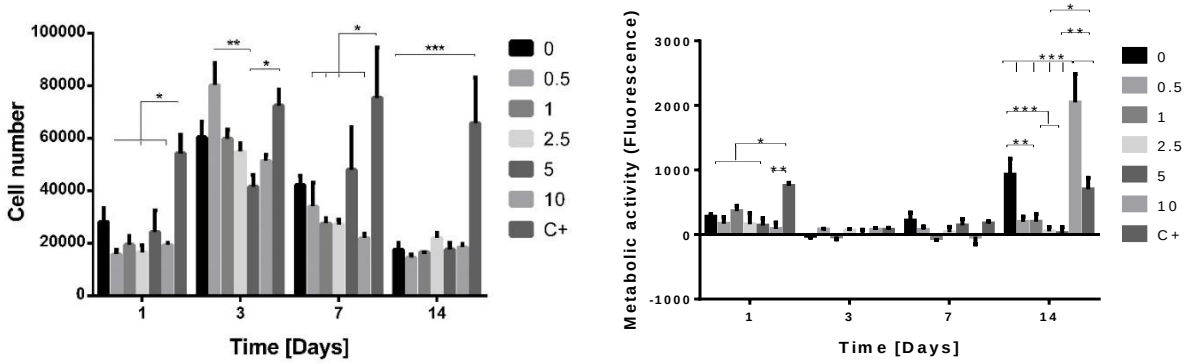

Figure 4.7 iMSCs growth on 2D PET plasma treated scaffolds. Metabolic activity is presented as fluorescence arbitrary units. Labels represent the time in minutes of O_2 plasma exposure from 0 (non-treated) to 10 minutes. C + = TCP. N = 3.

4.3.2.1.3 O_2 plasma PET surface modification marginally increases collagen deposition

Light microscopy observation of untreated and treated scaffolds at day 14 demonstrated a dense cell population, highly confluent in the middle of the scaffolds, with long elongated cellular morphology (see figure 4.8). iMSCs on all scaffolds synthesised and deposited collagen, as evidenced by PSR staining. The cells on the scaffold treated with O_2 plasma for 1-min seem to deposit collagen in a more homogenous manner, when compared to the clusters of stained cells observed in the rest of the scaffolds. Staining was more prominent in scaffolds treated with O_2 plasma for 1-min. Sircol assays showed a non-significant difference in soluble collagen deposition among the scaffolds; nonetheless, iMSCs seeded onto O_2 plasma treated scaffolds, except for the scaffolds treated for 10-min, produced higher amounts of soluble collagen on day 14 when compared to the controls.

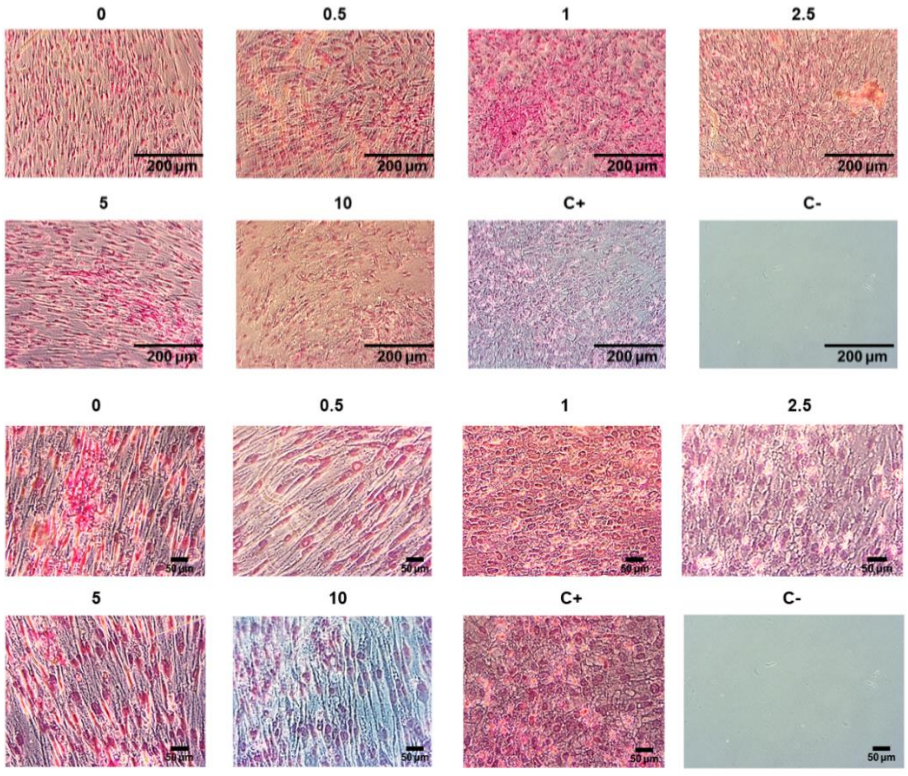

Figure 4.8 Representative images of collagen deposition in untreated and O_2 plasma treated PET 2D scaffolds. Light microscopy after PSR collagen staining on day 14. Bars represent 200µm and 50 µm.

The collagen birefringence was high at day 14 for all scaffolds (figure 4.9). Higher collagen birefringence was observed in all O_2 plasma treated scaffolds when compared to that in the control group. Cellular alignment was evidenced on the 10-min treated scaffold when compared to the shorter exposure time scaffolds. Matrix deposition on O_2 plasma treated scaffolds from 0.5- to 5-min was evidenced.

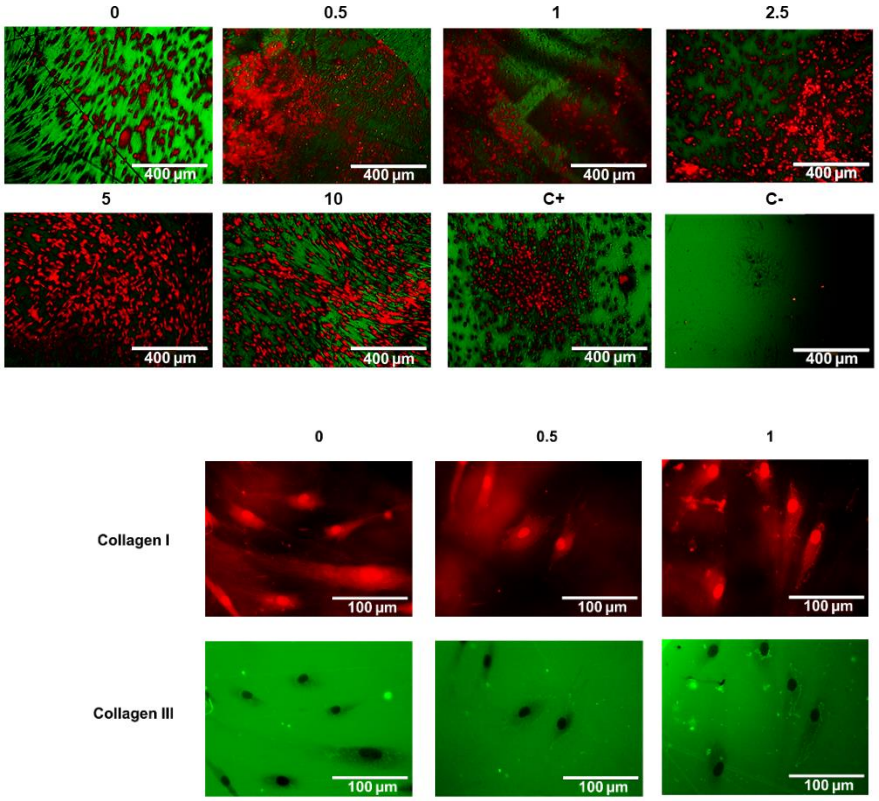

Figure 4.9 Collagen deposition in untreated and O_2 plasma treated PET 2D scaffolds. Birefringence images after PSR collagen staining on day 14. In polarized microscopy, the orange / red tone of the birefringence is given by thick fibres associated with collagen type I and thinner fibres associated with collagen type III appear in a greenish yellow tone. Bars represent 400 µm and 100 µm.

No significant difference was found for the quantification of either collagen or sGAGs among the 2D untreated and plasma treated scaffolds (see figure 4.10).

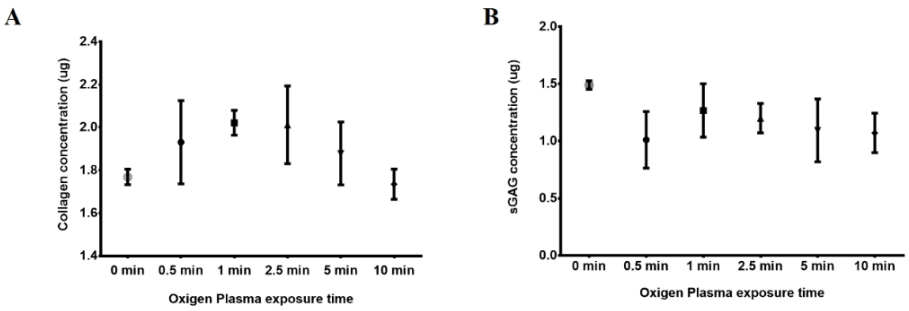

Figure 4.10 Collagen and sGAG deposition in untreated and O_2 plasma treated PET 2D scaffolds at day 7. N = 3.

4.3.2.2 3D scaffolds

4.3.2.2.1 1-min O_2 plasma treatment promotes iMSC growth

At day 7, the metabolic activity by cell number for the 1-min O_2 plasma treated scaffold was significantly higher when compared to the 0.5 min ($p = 0.001$). From day 3 up to day 28, metabolic activity by cell number was higher ($p > 0.9$) for the 1-min treated scaffold. DNA content was higher for 1-min O_2 plasma treated scaffolds from day 7 to day 28, but this was only significantly different at day 21 when compared to the untreated scaffolds and at day 28 when compared to the 0.5-min O_2 plasma exposed scaffolds (see figure 4.11).

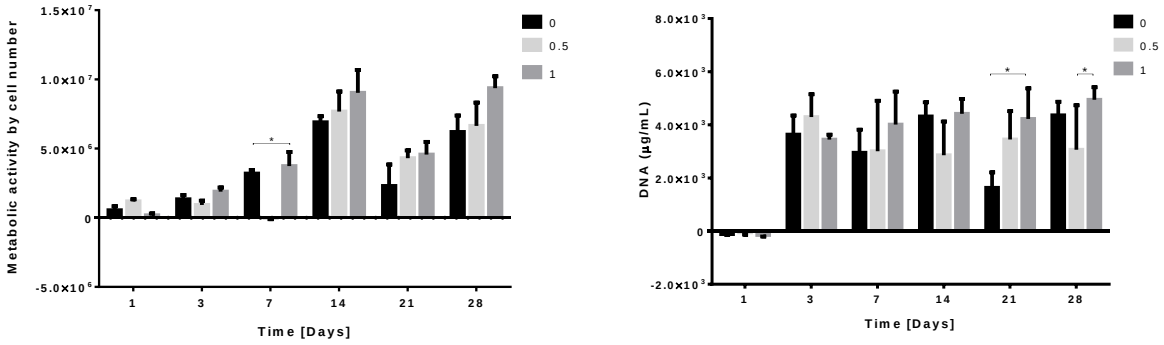

Figure 4.11 Effect of O_2 plasma treatment on cell growth. DNA content and metabolic activity by cell number in untreated (0), 0.5-min O_2 plasma treated (0.5) and 1-min O_2 plasma treated (1) 3D scaffolds. N = 3.

To test whether O_2 plasma treatment could enhance cell growth under physiologically relevant relative hypoxia, the scaffolds were cultured under 5% oxygen tension. At day 21, the 1-min exposed sample demonstrated a statistically significant difference in cell number when compared to both 0 and 0.5-min plasma treated samples (see figure 4.12).

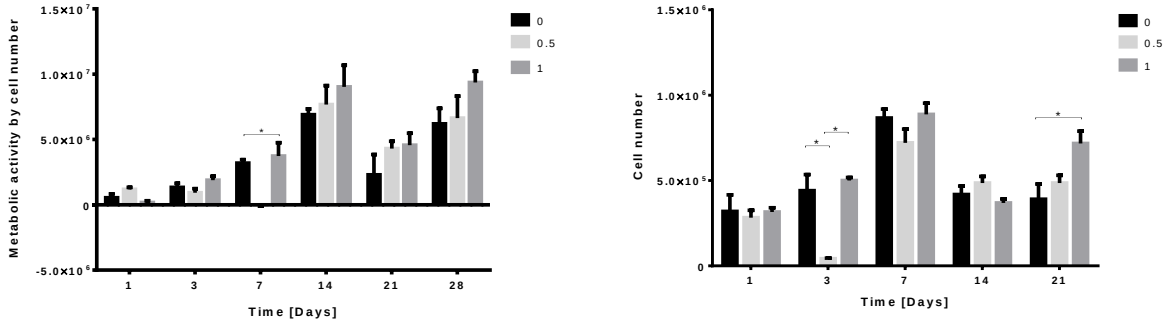

Figure 4.12 Proliferation of iMSCs on 3D fibre untreated scaffolds and scaffolds treated with O_2 plasma for 0.5- and 1-min cultured at an oxygen tension of 5%. N = 3.

4.3.2.2.2 Short-time exposure to O_2 plasma glow moderately promotes ECM deposition

After visualising the location of the collagen deposition on the 3D fibrous scaffolds, the total collagen was quantified by eluting the PSR stain. Total collagen production by DNA content was higher, although not significantly, at all three time points for the 0.5-minute treated scaffolds and for both plasma-modified scaffolds at days 14 and 28 ($p > 0.08$) when compared to the unmodified scaffold (see figure 4.13). There was no significant difference between 0.5- and 1-min O_2 plasma exposed scaffolds ($p > 0.5$), however total collagen production was higher for the 0.5-min treated scaffolds at all three time points.

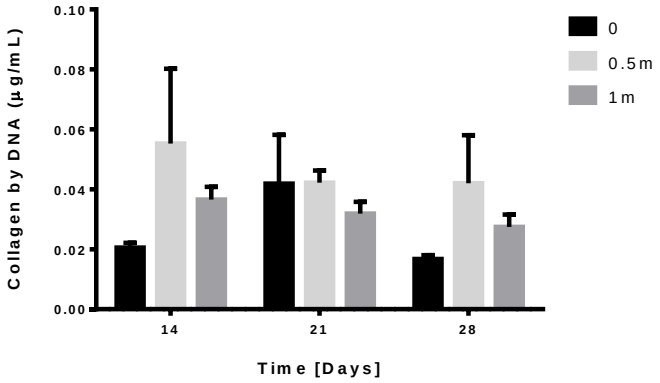

Figure 4.13 Collagen concentration by DNA content from eluted PSR staining from seeded scaffolds cultured in normoxia. N = 3.

Short-time O_2 plasma treatment comparatively improves iMSC functionality in relative hypoxia. With an oxygen tension of 5%, collagen deposition was enhanced for the iMSCs seeded onto the 1-min O_2 plasma treated scaffolds at both 14 and 21 days compared to the non-treated scaffolds under the same conditions (figure 4.14), although the increase only reached significance at day 14 ($p < 0.05$). After normalising by cell number, collagen deposition on the scaffolds treated for 1 min with O_2 plasma was significantly higher in physiologic hypoxia culture at day 14 ($p < 0.0001$) but the effect was inverted by day 21, when the non-treated and plasma treated scaffolds in normoxia showed a significantly higher collagen deposition when compared to their counterparts cultured in physiologic hypoxia ($p < 0.001$).

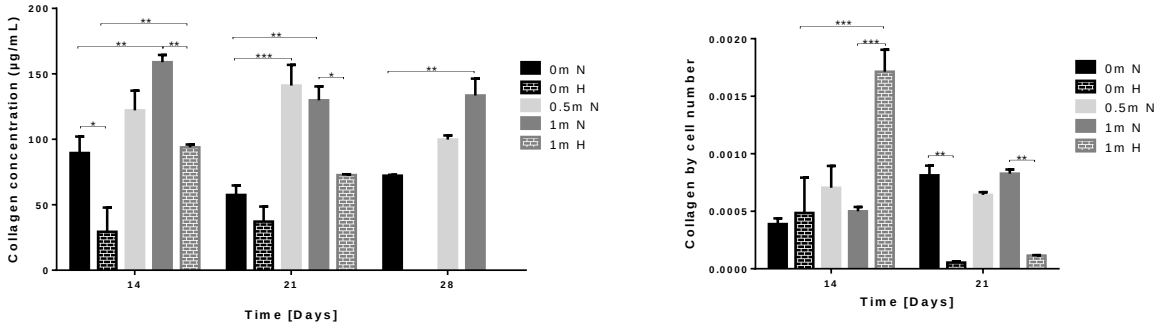

Figure 4.14 Total collagen production from eluted PSR staining and collagen concentration by cell number for seeded 3D fibrous scaffolds untreated and treated with O_2 plasma for either 0.5-min or 1-min cultured in normoxia (N) and physiologic hypoxia (H). N = 3.

The soluble collagen and sGAG deposition were quantified following incubation of unmodified and O_2 plasma treated scaffolds with either an acid/pepsin or a PBE/papain extraction solution (see figure 4.15). There were no significant differences for ECM proteins deposited among the scaffolds. Cells on the 1-min treated scaffold produced slightly higher amounts of sGAG at all time points when compared to the untreated and 0.5-min treated scaffolds.

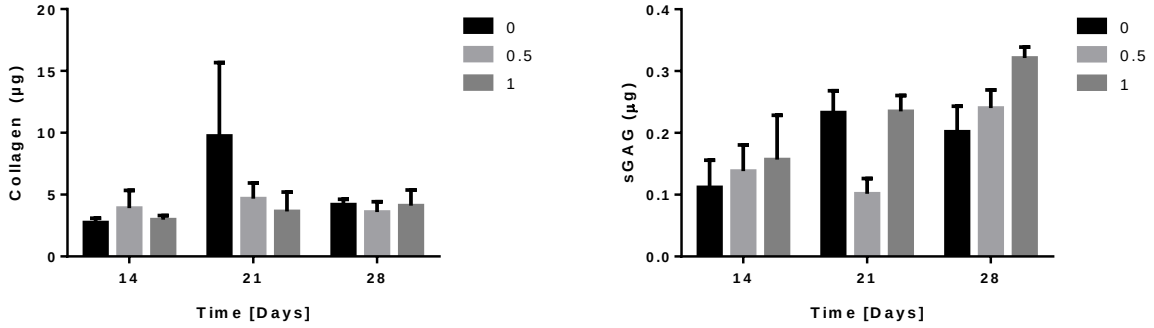

Figure 4.15 Quantification of extracted soluble collagen and sGAG production per scaffold. N = 3.

iMSCs attached, proliferated, and effectively deposited collagen onto the fibrous scaffolds as can be seen in figure 4.16 and figure 4.17, where representative images of the untreated and treated scaffolds at days 14, 21 and 28 are shown. Cells formed 3D colonies with cellular bridges from day 14.

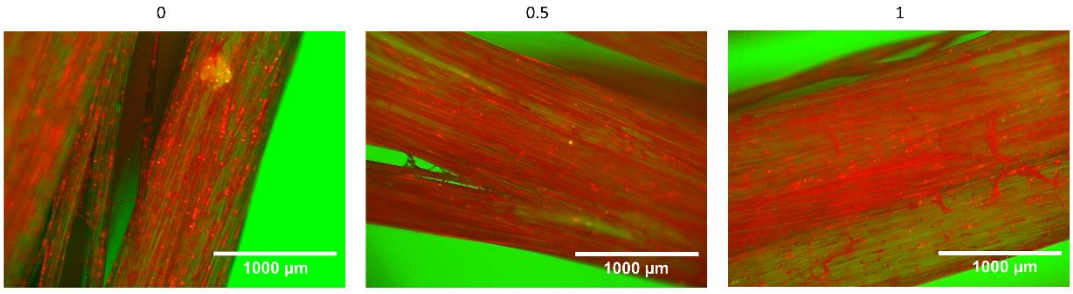

Figure 4.16 Representative birefringence images of collagen deposition after PSR staining. Bar represents 1000 µm.

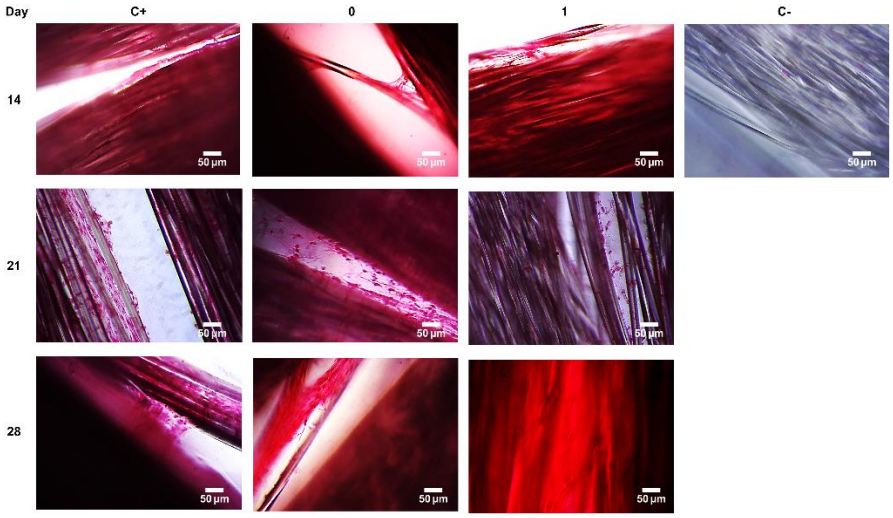

Figure 4.17 Representative light microscopy images of collagen deposition after PSR staining of seeded scaffolds at days 14, 21 and 28. Bars represent 50 µm.

DAPI staining and fluorescence imaging of the iMSCs revealed their homogenous distribution throughout both the untreated and 1-min O_2 plasma-treated scaffold and cellular alignment along the fibres (figure 4.18 and figure 4.19). Immunofluorescence for human COL - III revealed a positive signal through different planes of the scaffold in both conditions.

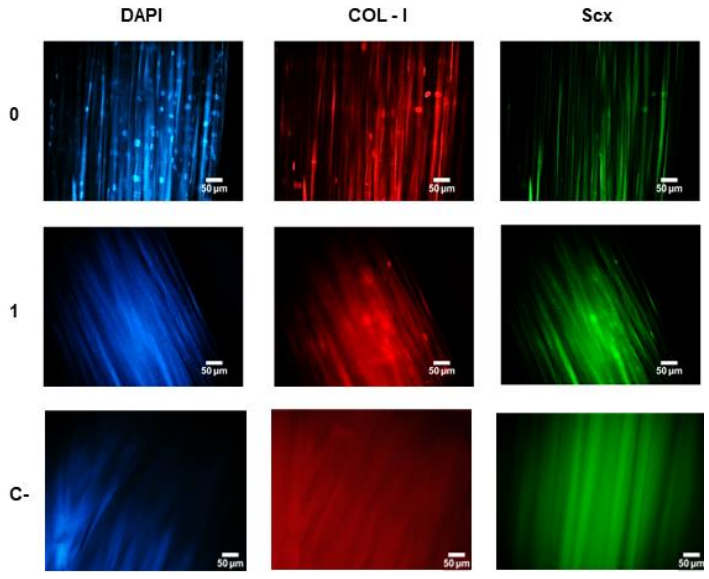

Figure 4.18 Immunofluorescence staining of iMSC on PET scaffolds untreated and coated with 1-min O_2 plasma treatment at day 14 for ligament markers COL-I and Scx.

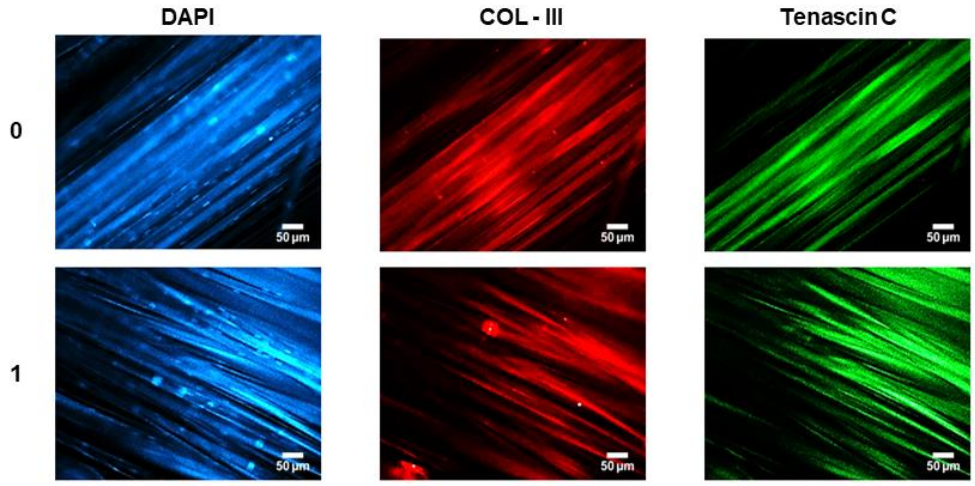

Figure 4.19 Immunofluorescence staining of iMSC on PET scaffolds untreated and coated with 1-min O_2 plasma treatment at day 28 for ligament markers COL-III and tenascin C.

4.3.2.2.3 Low-pressure, low-frequency and low-temperature O_2 plasma treatment supports iMSCs stemness

The effect of the plasma treatment on the capacity of the cells to retain their stemness was assessed qualitatively and quantitatively. For the qualitatively results regarding the potential for osteogenic differentiation, both plasma-treated scaffolds stained positive for alizarin red. The 1-min O_2 plasma treated scaffolds showed calcium deposition comparable to the positive control after cells were cultured with the bone differentiation media (see figures 4.20 and 4.21).

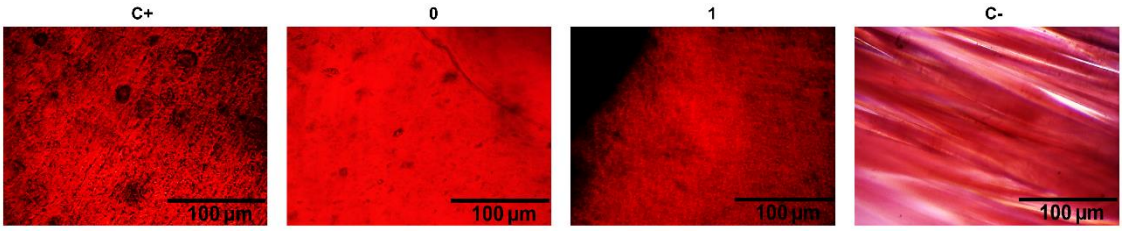

Figure 4.20 Osteogenic differentiation. Alizarin red staining after 21 days of untreated (0) and 1-min O_2 plasma treated (1) seeded scaffolds cultured with osteogenic media. The negative control is PET 1-min O_2 plasma-treated seeded scaffold with DMEM full media (C-). N=3. Bars represent 100 µm.

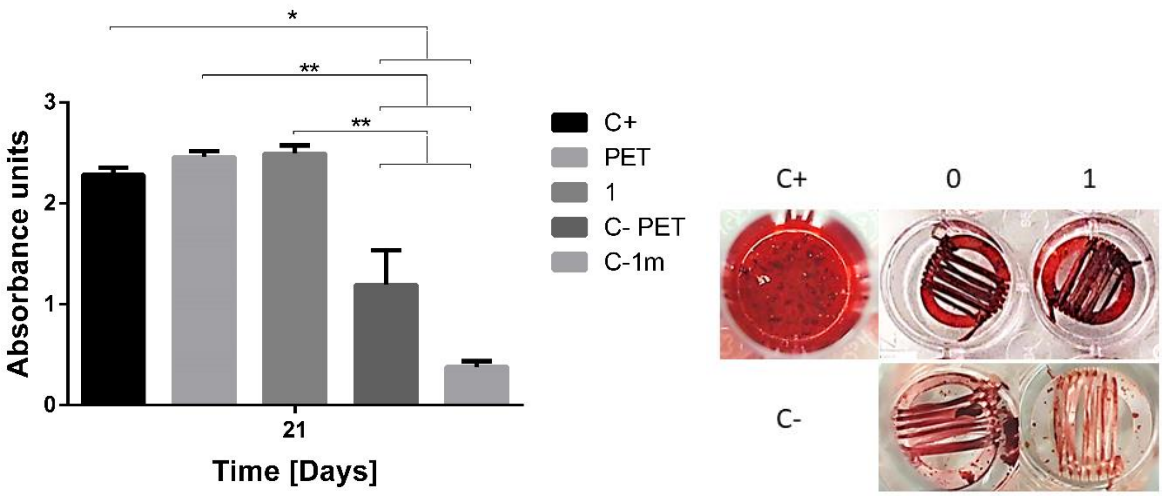

Figure 4.21 Quantification of osteogenic differentiation. Alizarin red staining after 21 days of seeded scaffolds cultured with osteogenic media and their controls with experimental media. N = 3, * = $p < 0.05$.

After culture with chondrogenic differentiation media, the cells for both the untreated and 1-min O_2 plasma treated scaffolds stained positive for Alcian blue (see figure 4.22). The cellular morphology was different from the PET fibrous scaffolds when compared to the positive control as can be seen in figure 4.23.

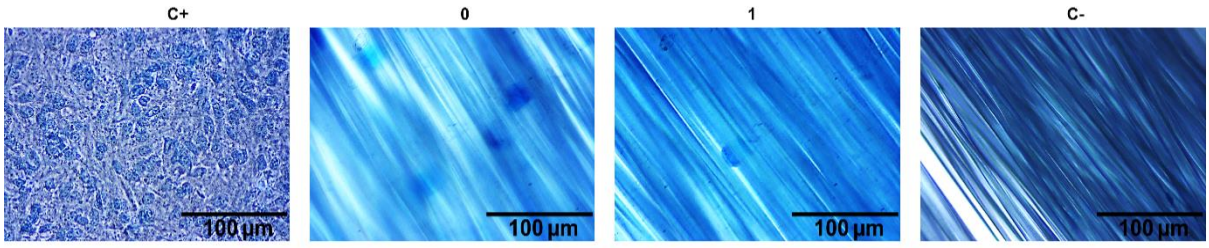

Figure 4.22 Chondrogenic differentiation. Representative images of scaffolds stained with Alcian Blue after culturing iMSCs on 2D TCP surface (C+), untreated PET scaffolds (0) or 1-min O_2 plasma treated scaffolds (1) with chondrogenic differentiation induction media, and on 1-min O_2 plasma treated scaffolds without differentiation induction media (C-). Bar represents 100 µm.

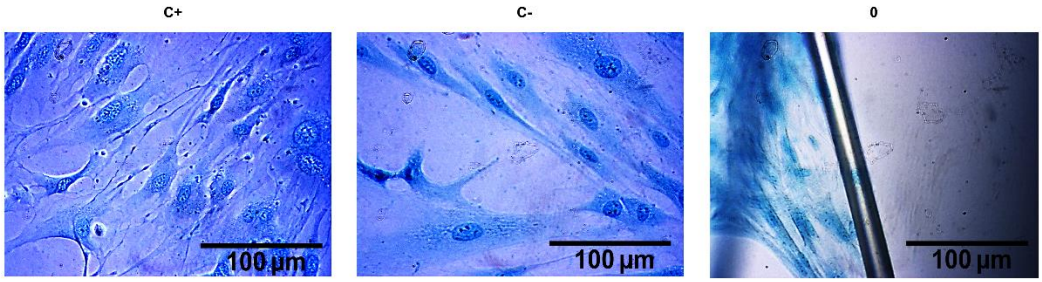

Figure 4.23 Chondrogenic differentiation morphology. Representative images of iMSC morphology with Alcian Blue staining with (C+) and without (C-) chondrogenic differentiation induction media. Bar represents 100 µm.

Fat droplets were observed on both, untreated and 1-min O_2 plasma treated scaffolds (see figures 4.24 and 4.25).

Figure 4.24 Adipogenic differentiation. Macroscopic photography of PET seeded scaffolds cultured with adipogenic induction media.

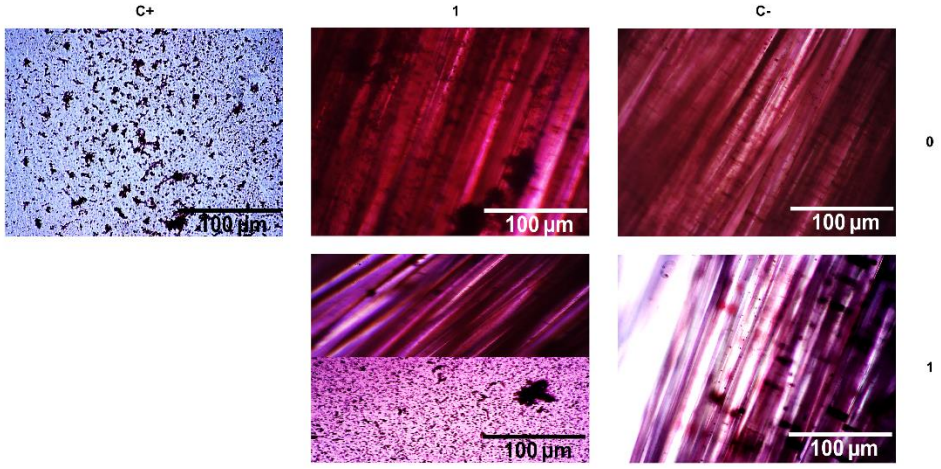

Figure 4.25 Adipogenic differentiation. Representative images of the scaffolds cultured for 21 days with adipogenic differentiation induction media. Bar represents 100 µm.

4.4 Discussion

PET scaffolds have been used for ACLR since the 1990's [226]. Despite its promising debut with apparently successful short-term outcomes and a faster return to physical activities for patients treated, these grafts have not provided a better alternative to the current gold standard reconstruction with either HT or BPTB. Re-ruptures with the PET grafts often occur in the mid-section due to the inefficient tissue take over. In the past couple of decades, various PET graft surface modifications have been tested to improve the cell-material interaction. O_2 plasma can be used to produce either one of four surface modifications: functionalisation, deposition, etching or crosslinking depending on the power, time and type of exposure [227]. Unmodified PET is used as the control given that it is the material used for the only current clinical synthetic graft in use. To enhance cellular proliferation and ECM deposition onto PET scaffolds, O_2 plasma was used as it is a straightforward modification that effectively induces surface functionalisation.

PET is a well-known hydrophobic synthetic material with a WCA above 70° [228]. The experiments carried out in this thesis confirmed that the untreated PET scaffold surface was hydrophobic, with a contact angle of 81.7 ± 6.2°. In line with what has been reported in worldwide literature [229], due to the increase of both surface energy (by the addition of polar groups) and surface roughness after O_2 plasma treatment, the scaffolds surface became hydrophilic. At the longest exposure time, assessment became more difficult, as the water drop spread across the scaffolds surface. PET wettability was effectively affected by oxygen plasma exposure in a time-exposure dependent manner.

O_2 plasma has an effect on the upper 100 nm of a surface from the first few seconds after exposure [230]. As evidenced by the SEM analysis, untreated PET films have a relatively smooth appearance that markedly changes with a prolonged exposure time. Small bubble-like structures appeared after O_2 plasma exposure. These have been reported before [231], and are described as products of material degradation and etching. This etching is also responsible for the increase in average roughness and appearance of the characteristic hill-valley structure in AFM [232]. Average roughness

in our study is comparable to what has been reported for similar time exposure to O_2 plasma [222, 232]. Roughness and topography orientation are effectively modified by O_2 plasma, with both 0.5- and 1-min treatments providing an increase in both parameters without resulting in etching or a weaker Young's modulus.

Radiofrequency (range from ~20 kHz to ~300 GHz) and treatment time are critical factors in the type of effect that the plasma treatment will have on any surface. There is no single best option of said parameters for the activation or functionalisation of PET substrates to encourage ligament regeneration. Most studies reported in the literature employ machines constructed by the research team, thus making the data less standardised. From those using commercially available machines, due to their applicability for a wider range of surface modification and faster etching times, higher power and radiofrequencies devices operating at 13.56 MHz tend to be favoured in the experiments [233]. Here, a low-pressure system using a low radiofrequency and low power demonstrates that O_2-containing polar functional groups are introduced early after the substrate's exposure to the O_2 plasma glow. As the surface wettability changes in a time exposure-dependent manner, the effect of O_2 plasma treatment with a low-pressure plasma system on the introduction of oxygen-containing polar functional groups becomes more evident. Wettability is most affected by the amount of hydroxyl and carboxyl groups on a substrate's surface [234], as it is represented by the findings from the present study. The increase in hydrophilicity on the scaffolds correlates with their gain in carboxyl groups as shown in the XPS results. XPS (also known as electron spectroscopy for chemical analysis, ESCA) was used to analyse the elements and their binding energy on the PET surface. The technique provides information of a surface's chemical modification by measuring and recording a spectrum of the kinetic energy and number of electrons released from the top 0 to 10 nm. It was used to determine the chemical bonding. Identifying the elements present on PET's surface was possible as it can detect the energy needed to cause a core electron in an atom to be emitted after absorbing an x-ray beam which is unique to each element. Although not significantly, the amount of oxygen species increases as the exposure to the O_2 plasma increases. Likewise, the carboxyl compound percentage concentration reaches its highest at 10-min with an increase of 2.27% in the C 1s component when compared to the untreated

PET scaffold. The same 10-min time point has the lowest contact angle recorded in these experiments, with a 58.9° decrease compared to the untreated scaffold. Regarding polarity, an increase of the O/C ratio directly relates to the amount of polar functional groups on the substrate's surface. The O/C ratio does not increase after 5-min O_2 plasma treatment. After 1-min O_2 plasma treatment, there is an increase of 0.16 in the O/C ratio, which is higher than for 0.5- and 2.5-minute treated samples but lower than both 5- and 10-min treated. These results contrast with the findings of Recek et al. [230] where a 0.5-min exposure using a higher frequency system and power at 13.56 MHz and 150 W, respectively, was sufficient to saturate the PET's surface. In line with these findings and despite a lack of statistically significant changes in O/C ratios among their samples, Stular et al. [235] agreed that exposure to O_2 plasma for more than 0.5-min did not offer significant benefit for the functionalisation of a PET fabric, O/C ratio, or further deposition of a gel at 27.12 MHz and ~3 kW. The conclusion was explained as the interference of the thermal effects becomes more important with increasing exposure times. Even at the low power used in the present thesis experiments, the temperature raised from ~25°C at 0.5-min to over 40°C after 5 min of plasma treatment. At higher temperatures, polar functional groups deteriorate. Interestingly, their study showed a basal O/C ratio of their selected PET fabric at 0.31 – compared to this thesis results of 0.78 – and a similar atomic O/C ratio for the samples treated for 0.5- and 1-min, with theirs showing only a 0.02 and 0.04 lower O/C ratio respectively [235]. O_2 plasma exposure introduces polar groups onto a surface as early as 10 s, but literature highlight how application- specific is an optimal time and how it in turn highly dependent on the system chosen for said application. Short exposure times in the range of 5 s to 30 min have been tested by various groups [233]. The outcomes in the present chapter also favour the 0.5- and 1-min O_2 plasma exposure times in terms of surface morphology functionalisation, despite the variation of results when compared to higher power and frequency systems [236, 237].

After concluding that O_2 plasma treatment in the range of 0.5- to 10-min effectively modifies the chemical composition, wettability, and morphology of PET in a time dependent manner, the next step was to investigate the effect of these changes in iMSC behaviour. Mesenchymal stem cells were chosen for the experiments given their

presence in the native ACL stump, which is the site most closely in contact with an implanted graft after ACLR and it is from this tissue where native cells would migrate to infiltrate the graft. In the native ACL, the fibrous ECM provides biological cues that account for its structure and function. Different fibre diameters influence cell migration and proliferation differently and provide the forming tissue with a more natural dynamic growth. When studying the cellular bioactivities on a graft *in vitro*, the responses observed follow those of the proliferation and ligamentisation phases of the *in vivo* faith of the grafts. The initial increase in cell proliferation is followed by a slight decrease in growth as culture progresses, in line with the slow return of cellularity to values of the intact ACL a few months after surgical reconstruction. The first indication of PET biocompatibility was the observation of cell attachment at 4 h post-seeding for all scaffolds and further adaptation to each of the surfaces. In its untreated form, the PET scaffold's surface was smooth. The gradual roughening after O_2 plasma exposure became a micro patterning that iMSCs identified as physical cues both for attachment and spreading. On the observed scaffolds, cell spreading began earlier for all treated scaffolds when compared to the untreated ones as noted by the average cell circularity of the cytoskeleton phalloidin stained scaffolds. As expected, the more pronounced and oriented pattern on the 5- and 10-min treated scaffolds provided physical cues in the forms of grooves that stimulated an earlier cell attachment and cell spreading. At 24 h post seeding, the mean cell circularity for the iMSCs on all the scaffolds was significantly lower than one ($p < 0.0001$). The cells readily adapted after 24 h on the scaffolds treated for 10 min, presenting a circularity of 0.20 ± 0.03 ($p < 0.001$). This can be explained by the added chemical and physical cues of both the increased polarity of the surface and the enhanced topography [238].

Two-dimensional (2D) cell culture is helpful for an initial assessment of cell behaviour under homogenous conditions. It enables the evaluation of the effect of single factors on cell behaviours, the O_2 plasma surface modification in this case, but at the expense of physiological mimetic cues that regulate the cellular activity *in vivo* [239-241]. Cells display differences in morphology, attachment, proliferation, rate and migration when cultured in 3D substrates, as opposed to 2D. Fibroblast-like cells are known to mechanically sense their environment and model their ECM in alignment with the

collagen fibrils network [239, 242-244]. The ligament structural arrangement of collagen fibres of different diameters arranged in a slightly parallel manner, provides the native cells the physical stiffness and orientation cues that induce the further synthesis of ligament ECM proteins and further maintenance of the ligament environment. To mimic that sort of disposition, for the fabrication of the 3D PET scaffolds the arrangement of the fibres was designed to provide spacing for the cells to migrate within the scaffold. The parallel fibre alignment was chosen as it is known to guide the cells into a ligamentogenic differentiation [245]. Tissue ingrowth is a crucial end point for a synthetic ligament after reconstruction. Although native intra articular ligaments are characterised by low cellularity, an artificial graft should be capable of favouring cell adhesion, migration, and growth. Parallel to the 2D results, there were no statistically significant differences in proliferation when comparing the modified and unmodified scaffolds. Nevertheless, the plasma activation of PET fibres with O_2 plasma glow for 1-min, improved cell proliferation at the later time points. This confirmed the hypothesis that a straightforward surface activation of the PET substrate would improve cell vitality. Slightly hydrophilic surfaces – as opposed to hydrophobic – and increased oxygen content promote MSC and fibroblast-like cell attachment and proliferation [246-248], which explains the findings in this chapter. Changes in the elastic modulus and roughness of PET's surface on the fibrous scaffold from the treatment would provide supplementary information to examine the impact of the physical cues introduced by O_2 plasma treatment on iMSCs growth on the 3D scaffolds. Impaired access to the AFM for the testing of the fibrous scaffolds was a limitation towards this end. Considering that the low-frequency and low-power cold plasma methodology chosen – compared to other settings – provide a more homogenous treatment of the surface, thus less variance for the topography, and in agreement with the information obtained from the SEM observations, the changes in roughness were expected to be similar to those found for the 2D scaffolds. In a study where PET fibres were treated with O_2 plasma at 0.15 mBar and 50 W, there was a 1.25-fold increase in roughness from 0.5 min to 1 min, which compares to the results shown in this chapter where there was a 1.20-fold increase in the 2D PET scaffold's roughness for the same exposure time [249].

However, Wei et al. 2.89-fold increase in roughness from non-treated to 0.5 min treated contrasted to the 1.54-fold increase demonstrated by the results in this thesis [249].

The complexity of the ACL goes beyond its ultrastructure and anatomical position. Historically, it was believed that a unique population of fibroblasts formed the cellular component of the ACL. It is now accepted that the type of resident cells depends on the ACL region that they inhabit, fibroblasts being more present closer to the tibial ligament insertion, as opposed to the chondrocyte-like residing in the fibrocartilaginous distal region [21]. ACL derived stem cells (ACLSCs) – a type of MSCs – have also been isolated from the ligament remnants. These have demonstrated a potential to differentiate in accordance with their site of residence[21, 250]. In the context of graft maturation, the capacity of a scaffold to support the MSCs differentiation into a ligament-like cell validates its effectiveness as an option for a ligament surrogate. The production of the right ECM to reflect the ligamentisation of the scaffold is crucial. This thesis evaluated the deposition of total collagen and sGAGs, as well as the expression of the ligament markers Scx, tenascin-C, COL-I and COL-III. It is known that both topography and surface chemistry modulate collagen synthesis[251]. Our results show a moderate increase in collagen deposition as a result of O_2 plasma treatment at earlier time points for both 2D and 3D scaffolds, correlating with the initial remodelling phase. The same trend was evidenced for sGAG. The interaction of collagens with GAGs in the ECM on an ACL greatly influences its structure and function. For this reason, determining the effect of the surface modification of the PET scaffolds on GAG deposition is part of the analysis of the ligamentisation process in this and the following chapters. The information on GAG deposition contributes to widening the picture already given by collagen for the appraisal of whether the seeded cells are converting their environment into an ACL-like structure or not. Of the four primary groups of GAGs, hyaluronic acid (HA) is the only one processed in the plasma membrane without going through a sulfation step. HA is part of the components of the proposed bioactive composite scaffold explored in the following chapters of this thesis. Therefore, quantification of GAG needed to exclude the contribution of HA. In a study comparing the effect of surface chemical modifications against topographic modifications, where they included the use of oxygen plasma, O_2 plasma had the least effect on total

collagen deposition, regardless of topography and normalising by cell number [251]. In their study, just as in ours, the cells synthetised more collagen on the most favourable surface chemistry, rather than the surface with the most groves. However, the production of ECM was not robust enough to favour O_2 plasma as a single effective modification, which corroborated our hypothesis that a second step would be needed to enhance the bioactivity of the scaffold. The results of this thesis show that O_2 plasma glow in a low-pressure system operating at a low frequency and low power for 1-min, introduced the most balanced amount of chemical and topographical changes to the PET substrate and therefore it was chosen for further biological experiments.

The above experiments support the use of O_2 plasma treatment as a straightforward surface modification method to bioactivate the PET surface and sustain MSCs vitality and functionality under atmospheric oxygen tension, which is the standard cell culture condition. Oxygen tension is a key factor that influences the dynamic microenvironment in which stem cells live [27]. *In vitro* cell culture at an oxygen tension of 5% is considered physiologic hypoxia since MSC typically reside in an environment with 1.5 to 4.2% O_2 in the bone marrow [252, 253]. Experimentally, MSCs exhibit a higher proliferation rate in hypoxia after their first passage conditioned in low oxygen tension. For their expansion, an oxygen tension between 1 and 10% is recommended to speed-up cell-doubling time and for the cells to retain their stemness [252, 253]. They preserve their homeostasis by reducing their mitochondrial oxygen uptake. Compared to MSC culture in normoxia (21%), hypoxia enhances MSCs proliferation, self-renewing capacity, along with the increasing the expression of genes that prompt injury repair and limit inflammation. The upregulation of VEGF and suppression of genes associated with apoptosis (BCL-2, CASP3), as well as IL-8 downregulation contribute to the initiation of tissue regeneration by MSCs in hypoxia. In accordance with the aim of the present project of replicating the characteristics that the designed scaffold would encounter in vivo, examining the MSCs response on the scaffold in hypoxia resembles more the expected 0.4–2.3% O_2 found in injured tissue [253]. Importantly, when the ACL is torn it endures a period of relative hypoxia, as it loses the vascular supply and goes through an inflammatory phase. Similarly, a graft for ACLR endures a period of avascular necrosis right after implantation, while the revascularisation of the tissue

takes place [254, 255]. To test the effect of the PET fibrous scaffold's surface activation by O_2 plasma, seeded plasma treated scaffolds and their untreated controls were incubated at a 5% oxygen tension for up to 21 days. The results demonstrate that O_2 plasma treatment for 1-min successfully promotes metabolic activity and cellular proliferation at a rate comparable to tissue culture under 21% oxygen levels up to day 7, after which proliferation temporarily drops before retaking its growth course. Longer term cultures in hypoxia have shown better results compared to shorter terms where lower cell growth rate and inflammation have been found [252, 256]. As oxygen species are introduced into the scaffolds' surface during plasma activation, it was expected that cell vitality would be better supported by the activated scaffolds, as was the case. For the ECM deposition, contrary to the lack of significance at 21% oxygen tension, the activated PET surface significantly promoted the collagen synthesis at the second week of cell culture at 5% O_2 tension compared to the untreated PET. At the third week the trend was still in favour of the plasma treatment, but the significance was lost.

On the same line, this research project explored the potential of the iMSCs to retain their capacity to differentiate after a period of growth and adaptation on the 3D fibrous scaffolds. Given that a ligament graft is exposed to specific cues at its distinct regions – namely the contact with native cells and different mechanical stresses –, the differentiation potentials by growth factor supplementation or by the physical cues presented by the PET scaffolds were assessed to investigate the suitability to induce MSCs differentiation to the right lineage according to the stimulus. Ligamentogenic / tenogenic differentiation of MSCs can be initiated by different approaches including scaffolds with modifiable properties dependent on the direction of their axes [257, 258], the addition of growth factor supplements [258-260], mechanical stimulation [260-262], and co-culture with native fibroblasts [263]. Collagens type I and III, tenascin C and scleraxis protein expression was assessed on the scaffolds to determine whether O_2 plasma treatment of PET parallel fibres composed of microfilaments could direct the cells towards a ligamentous phenotype. Ligament cells share markers with other tissues, particularly collagen type I and III. Ascorbic acid – added to the standard culture media to all the experiments presented in this thesis – is one key factor for the collagen deposition that, for instance, initiates the differentiation towards a bone lineage [264].

MSC differentiation *in vitro* occurs during different time frames for different lineages. For the osteogenic differentiation, it takes the MSCs a week in culture with differentiating agents to produce and progressively deposit an ECM primarily composed of collagen. By the end of the second week, the deposited ECM starts to mineralise, bone markers and hydroxyapatite deposits can be detected. Like osteoblasts, ligament fibroblasts' ECM is collagenous and contains proteins such as fibronectin and vitronectin [264]. Collagen is also extensively found in cartilage and vitronectin is involved in chondrocyte adhesion. In contrast, chondrocytes modify their collagen synthesis form type II to type one and their morphology turns into a spindle shape fibroblast-like as opposed to their regular spherical shape when in the presence of fibronectin – they dedifferentiate – [265]. In the results presented in this chapter, the changes in the topography of the PET scaffolds introduced by etching and sputtering from the low-frequency, low-pressure cold O_2 plasma treatment promoted the elongation of the cells as they attached to the surface. Plasma treatment has been shown to facilitate the induction of MSCs differentiation by modulating their cytoskeletal tension from directing cell shape through micropatterning [266]. A study intending to induce chondrogenesis of human BM-MSCs cultured for 14 days with DMEM supplemented with 10% FBS, antibiotic, and 2 mM L-glutamine by the surface modification of either biaxially oriented polypropylene films or nylon-6 sheets by ammonia plasma treatment for 30 s [267], supports the influence of polymer surface characteristics on MSC differentiation. The study found that the treatment not only favoured cell adherence, but it decreased the expression of the chondrocyte hypertrophic phenotype marker collagen type X. The plasma was generated at an operating pressure of 40 Pa, at 20 W power and radiofrequency of 13.56 MHz and it was also associated with a fibroblast-like morphology of the cells on the nylon-6 surface [267]. The cells on plasma-treated nylon-6 did express aggrecan but did not express collagen type II. Collagen type I expression decreased for the plasma-treated surfaces only up to day 7 of culture when compared to the unmodified controls, but there was no suppression at day 14. Interestingly, for the polypropylene films aggrecan and collagen type II expression were suppressed, although collagen type II expression was also absent on the untreated controls [267]. In contrast, the introduction of carboxyl (–

COOH) groups – effectively introduced by O_2 plasma treatment [268] – has been correlated with human MSC chondrogenic differentiation [269]. Mouse osteoblastic cells have also been tested for the enhancement of osteogenic markers expression after nitrogen or air gas plasma treatment of chitosan scaffolds [270]. A dielectric barrier discharge device with an alternating current was used with a duration of 3-, 5- and 10-min. The increased surface roughness and addition of protrusions that resembled nanoparticles after 5-min plasma treatment influenced the cell behaviour and significantly enhanced alkaline phosphatase (ALP) activity and gene expression of ALP and Runt-related transcription factor 2 (Runx2), osterix and osteocalcin when compared to the untreated control [270]. In the experiments here presented, the iMSCs retained their stemness in both untreated and O_2 plasma treated scaffolds and differentiated into the osteogenic, chondrogenic and adipogenic lineages after induction with the corresponding induction media. Notably, the spontaneous differentiation without induction media apparent in the non-treated scaffold but absent in the 1-min O_2 plasma treated scaffold. This was more evident for the osteogenic differentiation and requires further exploration as the osseointegration of an ACL scaffold is one of the most challenging issues for any ligament TE approach. Osteogenic differentiation is the most studied for plasma treated surfaces, particularly in dentistry. Nandakumar et al. found no effect of plasma treatment on osteogenic protein expression after seven days of culture, but found an upregulation of osteogenic genes for a 30-min oxygen plasma exposure of electrospun poly (ethylene oxide terephthalate)/poly (butylene terephthalate) scaffolds [271]. Higher mRNA expression of HIF1α and HIF-2α have been suggested as signalling pathway triggers for the retained stemness [256]. Studying the effect on MSC differentiation of O_2 plasma activation of PET by means of the low-pressure system at low-frequency and low-power under hypoxic condition remains part of future work.

4.5 Conclusion

Low-pressure O_2 plasma treatment effectively modifies the hydrophobic and smooth PET surface. It offers a fast straightforward method for the surface modification of the PET ACL ligament scaffolds, supports cellular proliferation, and enhances collagen deposition. Additionally, the treatment could serve as an interfacial bonding layer for subsequent material adhesions to further increase the achieved bioactivity.

Chapter 5

The effect of a CS-g-GMA / HA coating of PET and on iMSC's behaviour

---

Aims: To develop a bioactive coating composed of CS-g-GMA and HA to enhance the bioactivity of the PET O_2 plasma pre-treated fibrous scaffold.

Hypothesis: The iMSCs proliferation rate and extracellular matrix deposition will significantly increase by the CS-g-GMA/ hyaluronic acid coating compared to O_2 plasma treatment alone.

5.1 Introduction

The proposed novel approach to enhance the bioactive functionality of a PET ligament graft is a two-step process to optimise the scaffolds' ability to induce tissue ingrowth, hence ligament regeneration. After activating the inert scaffold's surface, the next step is to add a composite coating to provide the scaffold with a chemical structure closer to a natural ligament. During the first few weeks after implantation, the ligament graft endures an impaired vascular supply, resulting in the weakest period for the graft. It is this period where the PET fibre mechanical properties are most beneficial. Nevertheless, the ECM synthesis and remodelling needs active prompting to regain the tissue's natural functions. From a translational point of view, once implanted, the ligament scaffold needs to be prepared to encounter a hostile environment and promote a healing ACL native cellular behaviour as early as possible whilst interacting with the native components of the surrounding tissues.

The overall aim of this chapter was to assess the effectiveness of a composite bioactive coating on a fibrous polyethene terephthalate scaffold. The bioactive coating intends to enhance the onset of tissue formation and growth through a ligamentisation process.

This process of continuous tissue transformation into one resembling the ACL aims to mimic the intra-articular ligament region's response when encountering the local MSC population after implantation of the scaffold.

5.1.1 PET coatings for ligament TE

In the search for a way to meet the appropriate biological requirements of a ligament graft while providing the stiffness and strength to maintain the knee stability importantly during the vulnerable early healing phase, numerous coatings have been proposed for the synthetic material most used for ligament reconstruction – PET –. A significant detail to consider for a ligament TE approach is to note whether the surface modification aims to elicit ligamentisation of the intra-articular portion, the osseointegration at the attachment sites, or both.

Intra-articular ligament regeneration is a consequential research focus, given that ACL midsubstance tears are the most common location of ACL ruptures [272-274]. An example of research in this area includes a composite coating of HA and cationised gelatin [275]. It has shown *in vivo* an inhibited inflammatory cell infiltration accompanied by a slow but progressive immature tissue ingrowth at 12 weeks after the surgical reconstruction [275]. An approach with more promising results proposed a 0.1% CS / 0.1% HA self-assembled layer-by-layer coating after PET scaffold silanisation to regenerate an extra-articular ligament. Human dermal fibroblasts (HDFs) *in vitro* showed significant short-term attachment, proliferation, and a dense ECM network over the scaffold's surface [276].

5.1.2 Polysaccharides in ligament TE

The TE approach to induce ligament regeneration seeks to mimic as much as possible the native cellular environment. For this reason, natural polymers in the form of polysaccharides provide a compelling biomaterial. Polysaccharides are an integral part of the native ligament ECM. They take part in providing the ACL with its ultrastructural architecture [277]. Long chains of monosaccharide units linked by O-glycosidic bonds form polysaccharides [278]. They are hemocompatible, non-toxic, have a low manufacture cost and are environmentally friendly [279].

Among the polysaccharides, HA and chitosan (CS) stand out as ideal candidates for ligament regeneration due to their structural similarity with extra cellular proteoglycans and their ability to form polyelectrolyte complexes when mixed [280, 281].

5.1.2.1 Chitosan in ligament TE

As part of the promising natural materials for TE, CS has raised special interest. It causes minimal or no harm upon ecosystems or the environment and the presence of acetyl amino groups in chitosan permits chemical modifications to create complex molecular structural designs [282, 283]. It is a partially deacetylated derivative of chitin. Chitin along with its structurally similar polysaccharide cellulose, are the most largely produced organic compounds on the planet [284]. Annually, chitin production by some sea and land invertebrates amounts to approximately 10 billion tons [284, 285]. Food industry waste, for instance, makes for a financially sustainable source for the manufacture of CS.

CS is a linear aminopolysaccharide cationic biopolymer with a high percentage of nitrogen content that exhibits applicable chemical properties such as high hydrophilicity, crystallinity, and high viscosity. It contains abundant reactive groups for cross-linking and chemical activation. Like its precursor – chitin –, CS is insoluble in water and organic solvents due to its high degree of inter- and intrachain hydrogen bonding; nevertheless, it is soluble in dilute aqueous acidic solutions. It possesses ionic conductivity and polyelectrolytes in the presence of an acidic pH (below pH 6.0). It causes suspended solids to form aggregates, interacting with negatively charged molecules. CS also features entrapment and adsorption qualities, and it can form films and adhesive materials to isolate biomolecules. Its biological properties confer CS biocompatibility, bioadhesivity, bioactivity, non-toxicity, biodegradability into non-toxic by-products, adsorbability, antimicrobial activity, antiacid and antiulcer activity, and antitumoral potential [282, 283, 285, 286].

Both chitin and CS can be prepared into multiple presentations including nanofibres, films, membranes, gels, sponges, and scaffolds. As polysaccharides with broad hydrogen bonding, CS and chitin degrade before melting, making it necessary to utilise

an appropriate solvent system to process them for each application [287]. An interesting feature of CS is its inherent feature to form microfibrillar arrangements in the living beings. Among its applications in TE, it has been proven to promote tissue growth and differentiation in tissue culture [288]. Due to the cationic nature of CS, blends with anionic polysaccharides such as HA have proven to generate tight ionic interactions and improve the flexibility of the filaments [289, 290]. Additionally, Tamura et al. reported a higher strength of their polysaccharide filament after coating with CS. CS coatings have been added to PET scaffolds before by means of either single-step [291] or multi-step procedures. For instance, a comparison of DC and RF oxygen plasma discharges showed that a coating of low-molecular-weight CS dissolved in 1% CH_3COOH after synthetic air plasma pre-treatment of a PET film for 10 – 60 s at a flow rate of 20 sccm significantly modified the material's contact angle, surface energy, polar and dispersion components and observed morphology, whereas the addition of the coating to an untreated PET film produced no significant changes [268]. The bio-effects of these modifications demonstrated the successful proliferation of MSCs on the substrates, but no benefit for cell adhesion or proliferation after chitosan immobilization on RF pre-treated films [268]. A combination of CS and phospholipids as a coating for PET-based cardiovascular stents has been explored by pouring the solution onto a PET surface activated with air plasma for 1 min at a RF power of 460 W. The material showed a significant increase in roughness and the addition of crystallic protrusions as opposed to the smooth PET surface showing promise to minimise platelet adhesion and the reduction [292]. Specifically for ligament TE, PET sheets from a LARS have been silanised and subsequently dip-coated in 0.1 wt% and 0.1 wt% HA solutions for 1 min each in a sequential manner to obtain 10 bilayers in a layer-by-layer procedure, prior to ultimate incubation in a calcium phosphate solution [293]. This modification of the PET artificial ligament supported osteoblast attachment, spread and ECM deposition for seven days *in vitro*. The study demonstrated a lower metabolic activity rate for the modified scaffolds but a significantly higher alkaline phosphatase activity [293].

5.1.2.2 Hyaluronic acid in ligament TE

In contrast with CS in terms of chemistry, HA (also known as hyaluronan) is a polyanionic macromolecule. It is a linear non-sulphated GAG consisting of repeating units of β-1,4- D-glucuronic acid–β-1,3-N-acetyl- D-glucosamine. It is present in various tissues and fluids in the human body. Peripheral connective tissues produce HA with a daily turnover of 10-100mg [294, 295]. Its biological function in the extracellular matrices is molecular-weight dependant and conforms to its viscosity, elasticity, lubrication, and water holding high capacity due to its large number of hydroxyl groups. HA takes part in the matrix organisation, morphogenesis, remodelling and wound repair. HA's involvement in these processes is due to its effects on cellular functions such as motility, proliferation, differentiation, signalling, and adhesion. HA is also involved in sequestering growth factors and the cellular synthesis of cytokines, prostaglandin 2 and matrix metalloproteinases (MMPs). MMPs – responsible for matrix degradation – accumulate in the synovial fluid after ACL rupture and their expression – along with that of tissue inhibitors of metalloproteinases (TIMPs) – is increased in ACL fibroblasts compared to MCL fibroblasts. Both factors contribute to the ACLs poor healing ability. [296]. The hyaluronan found in healthy joints is of a high molecular weight (> 800 x 10^3). HA's viscoelasticity is high at this high molecular weight. Its contribution to the tissue's homeostasis is to decrease angiogenesis along with the levels of cytokines, MMPs, and NF-kB. In contrast, HA with a much lower molecular weight increases the concentration of nitric oxide, which is what happens in osteoarthritic joints [297-299]. It is one of the main components of the synovial fluid in a highly polymerised form. HA is secreted by the synovium at 0.2 - 0.6 g / 100 mL. It provides elasticity and elevated viscosity to the fluid [300-302].

As a biomaterial, HA it is considered highly biocompatible as it does not elicit inflammatory or foreign body reactions. It is biodegradable and its properties can be chemically tailored by modifying the carboxylates, hydroxyl groups, or N-acetyl group with etherification, amidation, esterification and crosslinking. By isolating specific molecular weights or depolymerising HA, it can be made into different presentations.

For ligament TE, HA has been used in conjunction with other materials to form hydrogels, sponges, fibres, meshes, coatings, nanoparticles, and microspheres.

An example of HA's application was presented by Seo et al. [303] when they combined collagen and HA to coat a silk scaffold with one of two different techniques. They demonstrated a higher proliferation rate of human ACL cells on the silk scaffold covered with a lyophilized collagen-HA substrate compared to the same scaffold dry coated with collagen-HA. Both scaffolds showed a higher immune response after 3 days of culturing T-lymphocytes when compared to a control with no significant difference between the coating techniques. These artificial ligament grafts were tested *in vivo,* and an inflammatory tissue reaction was observed, with histological evidence of monocytes, an absence of giant cells, granulation tissue, cell migration and neovascularisation for the lyophilized collagen-HA substrate graft [303]. Similar biocompatibility results were found by Majima et al. on a hybrid-polymer fibre CS / 0.1% HA scaffold *in vivo*, with joint stability in animal experiments [281].

In the late 90's, a chemical modification of HA by esterification led to a broad variety of HA polymers termed HYAFF ®. Two variants of these polymers have been most characterised for a multitude of medical applications. HYAFF®7 and HYAFF®11 are respectively ethyl and benzyl esters of hyaluronan [304]. For ligament TE, HYAFF® 11 has been knitted into a multilayer cylindrical ligament scaffold and seeded with sheep BM-MSCs. The results showed sheep BM-MSCs differentiation into fibroblast-like cells *in vitro*, with no upregulation of bone or cartilage markers, and a good integration with the scaffold by expressing CD44, which is the specific receptor for HA [305]. HYAFF® 11 has also been tested as a tendon scaffold by creating a Hyalonect mesh and seeding with either human tenocytes or adipose-derived stem cells and tested under dynamic stretch in a custom-made bioreactor. Both types of cells readily adhered to the scaffold and maintained their phenotypes. After 15 days of 120 minutes a day mechanical stimulation, ADSCs modified their morphology from adipose tissue to one more resembling tendon cells, secreting collagen type I and increasing their tenogenic gene expression. Notably, the authors concluded that ADSCs in their experiments could also

differentiate into “vascular-like cells, creating a capillary-like structure inside the cultured tendon like tissue” [306].

Glycidyl methacrylate (GMA) is an epoxy-functional monomer that facilitates the interaction between materials by free radical polymerisation. It has been used in TE as an effective crosslinking agent, particularly for polysaccharides [307-312]. Here, CS was functionalised with GMA at a stoichiometric molar ratio of 1:4 to enhance its elastic properties, as has been demonstrated in previous works [307, 313, 314].

Worldwide literature highlights the benefits of HA in cell survival and functionality as a coating for ligament fibrous scaffolds of various materials, such as a HA crosslinked coating on poly lactic acid fibres [315]. The mixture of HA and CS has been explored to form a polyelectrolyte multilayer film coating for elastic poly (l-lactide-co-caprolactone) fibres [223], and as a stacked Ch-HA hydrogel coating for PCL aligned/random multiscale fibres [316]. Given the proven biological benefits of HA as a biomaterial and its adequate interaction with chitosan, the blend was selected for the bioactive coating of the PET scaffold.

Due to the lack of reactive groups on the surface of PET, bonding of other materials to its surface requires a pre-treatment to encourage the interaction between their chemical structures [317]. To this end, multiple-step processes have been explored and by different research groups before to improve PET’s bioactivity. A two-step surface modification of the PET scaffold was chosen for the project here presented given the effectiveness that different types of plasma gases, powers and discharge frequencies found in literature have shown for polymer surface modification [214, 317-320]. Cold O_2 plasma pre-treatment of PET in a system working at a low frequency provides a fast, safe, low cost and environmentally friendly technique to ensure that the pre-treatment conforms to the scaffold’s design, providing interfacial adhesion and stability of an introduced coating [214]. For the addition of CS and HA, dip coating was chosen after the literature review indicated that immersion provides a more compact and homogeneous coating over other coating adhesion methods [321, 322]. To ensure the polymeric bonding after O2 plasma pre-treatment, the four stages of dip-coating were followed, namely the scaffolds’ immersion into the CS-g-GMA / HA mixture, the swift

withdrawal of the scaffolds from the solution, drainage of the excess solution and drying at 60 ºC to allow the evaporation of the solvents [322]. The fibres were observed under SEM to evidence that they were impregnated with the solution and the structure remained as fibres as opposed to a single 2D film.

5.2 Materials and Methods

5.2.1 Preparation of the scaffold

The quantities of each reagent are Chitosan (1g), GMA (3.86 g 1:4) and KOH 0.05 M (0.72 g).

CS 1g was dissolved in a 0.4 M acetic acid solution. The material was synthesised with a 1:4 molar ratio and prepared as described in [307] (see figure 5.1). Chemical modification of CS through its reaction with GMA was achieved by mixing the 1% CS solution with 0.05 M KOH at 5% with respect to the total reaction mixture and GMA under constant magnetic stirring and incubating the solution – which had a pH of 3.8 – for 1 h under constant magnetic stirring at 60 ± 1 ºC. The reaction was stopped by cooling down the resulting mixture in an ice bath for 15 min. The solution was precipitated into a white fibrous polymer by decanting drop by drop into 8:1 acetonitrile DNA synthesis grade at 40 ± 2 ºC on a hotplate magnetic stirrer. The temperature was constantly monitored to avoid raising it over 42°C, where the ratio Solution:Acetonitrile shows a significant increase; and the material losses its cotton-like appearance

To prepare the CTS-g-GMA /HA solution, the precipitated CTS-g-GMA fibres were dissolved at 1% weight by volume (w/v) in 0.4 M acetic acid. The solution was kept under magnetic stirring until the chitosan was completely dissolved.

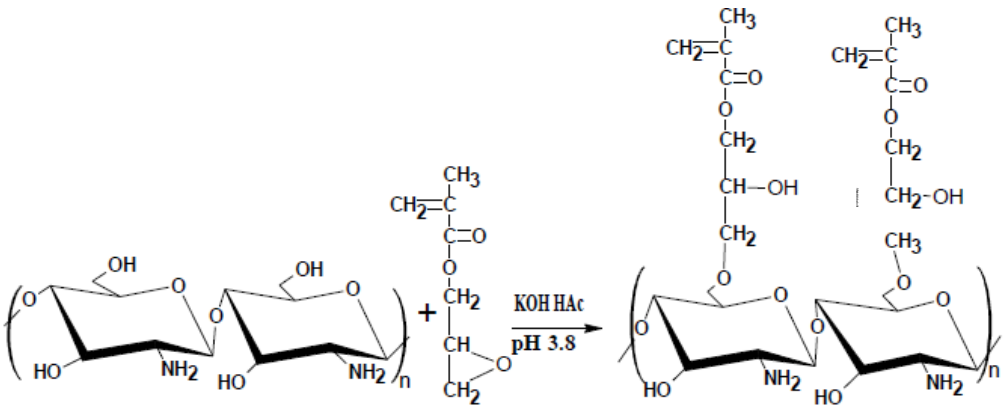

Figure 5.1 Mechanism of chemical reaction for CS-g-GMA as described by Flores Ramirez et al. [307]. Reproduced with permission from the authors.

Separately, HA was dissolved in deionized water at 1% (w/v) and 0.1% (w/v). A solution 1:1 was made with CTS-g-GMA / HA by slowly adding under continuous stirring either the 1% or 0.1% HA solution to a CTS-g-GMA solution.

To prepare the PET fibres dip-coated with chitosan and HA, the PET fibrous scaffolds were exposed to O_2 plasma glow by using a low-pressure plasma system operating at 40 kHz at 100 W, for 0.5- and 1-min with a pressure of 0.4 mbar. The plasma modified PET scaffolds were then dipped in the CTS-g-GMA /HA solution for 1 min. Next, the scaffolds were left in an oven at 60 °C for 3 h to allow the solvent to evaporate. The scaffolds were subsequently washed profusely with sterile deionized water under a culture hood and sterilised by submerging them in 70% ethanol for 30 min, washing them in PBS and air-drying them under the hood.

5.2.2 Scaffold characterisation

SEM of composite scaffolds and their untreated controls sputtered with an ultrathin gold layer was carried out in this chapter with an accelerating voltage of 6 kV.

The 2D uncoated and coated scaffolds were characterized by Fourier transform infrared (FTIR) spectroscopy in the ATR mode. The FTIR spectra of the scaffolds were acquired at a 2 cm^{-1} resolution from 4000 – 400 cm^{-1} with a Fourier transform infrared spectrometer (FT/IR-4000 Jasco, UK). The measurements were normalised relative to the highest intensity peak to generate comparable graphs.

A tension test was employed to determine the tensile strength and modulus of PET modified and unmodified fibres. Uniaxial tension was applied using an Instron-5565 tensile machine. The maximum stress and strain at break together with the Young's modulus were assessed. Briefly, 20mm samples using the cardboard method were prepared. Each sample was then loaded into the grips. Next, the samples were loaded at a speed of 20 mm/min. Eight (N = 8) samples were tested per condition.

5.3 Results

5.3.1 Coating characterisation

The effect of the coating on PET wettability was assessed by water contact angle of a sessile drop. Each of the coating components were tested by themselves and as a 1:1 mixture on the scaffold after 1-min O_2 plasma treatment (see figure 5.2). The WCA of the PET scaffolds was significantly affected by all the coatings ($p < 0.0001$). For the CS component, there was a significant difference on WCA when compared to both the unmodified PET scaffolds and the 1% CS-g-GMA / 1% HA coated scaffolds ($p < 0.01$). The coating with the concentration of 1% for both CS and HA exhibited the lowest WCA, 26.66˚± 0.86.

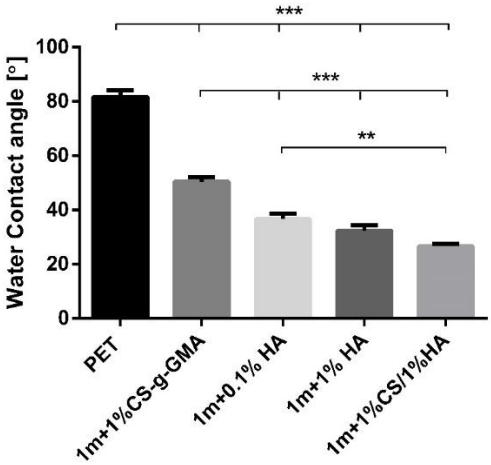

Figure 5.2 Effect of coatings on PET wettability.

The molecular organization of the unmodified and modified PET scaffolds was characterised by FTIR (see figure 5.3). A peak found at 3429 cm^{-1} correlates with the O–H stretching vibration and N–H extension vibration found in CS. The functionalised

scaffold shows peaks due to C=C vibrations at 1505 cm^{-1} and –C=O stretching vibrations at 1713 cm^{-1}.

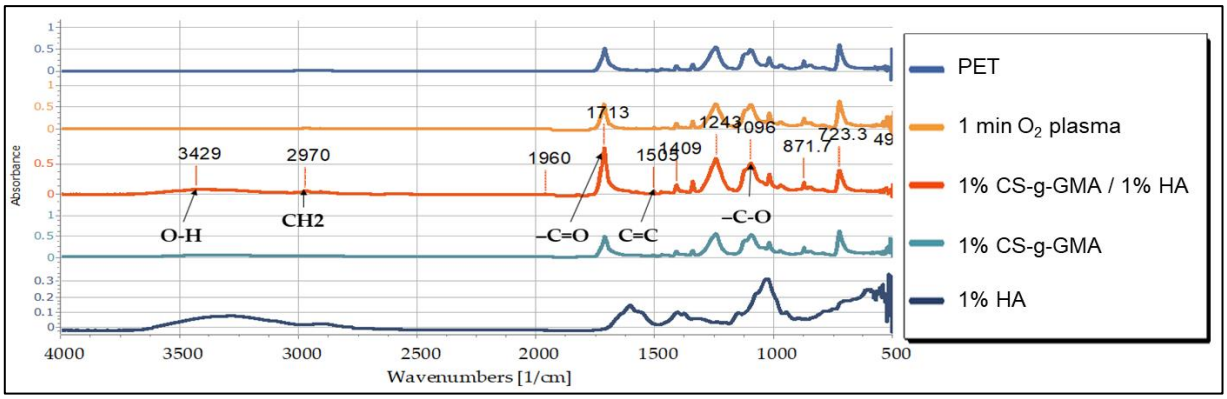

Figure 5.3 Infrared spectrum of absorption for unmodified and modified PET.

Figure 5.4 shows the changes on the surface morphology of the PET fibrosus scaffolds. The unmodified PET fibres have a neatly smooth surface. The coated PET fibres show a patch of roughened appearance conferred by CS and HA aggregates. There is a clear adhesion of the 1% CTS-g-GMA / 1% HA solution to the fibres after O_2 plasma pre-treatment. The mean diameter of PET fibres was 10.472 ± 2.263 µm for the unmodified and 21.022 ± 3.379 µm for the coated fibres.

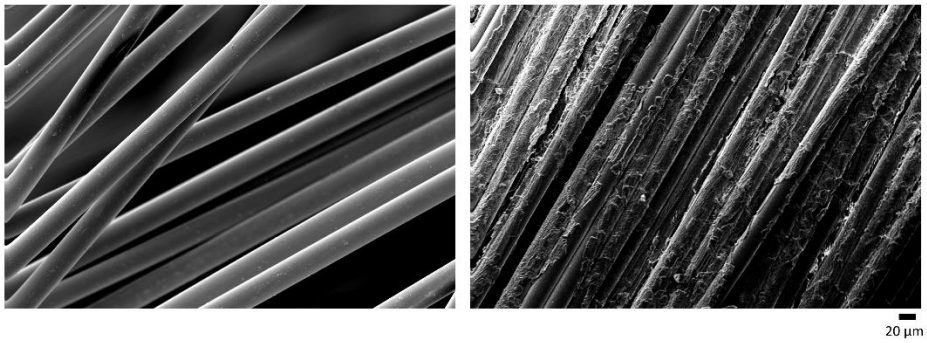

Figure 5.4 SEM representative images of PET fibres untreated and coated with 1% CS-g-GMA / 1% HA. Bar represents 20 µm.

A magnification of the coating adherence to the fibres is shown in figure 5.5. The complex formed by CS-g-GMA and HA distributes on the fibres to form a film on them.

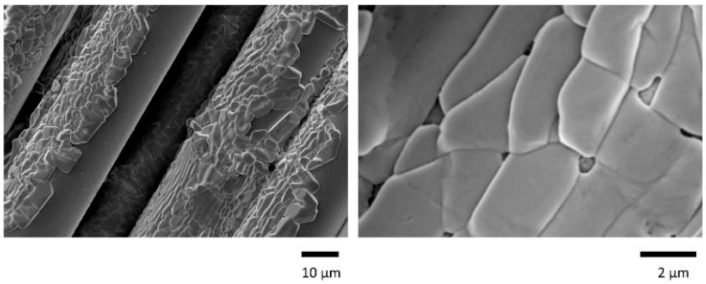

Figure 5.5 SEM representative images of PET fibres coated with 1% CS-g-GMA / 1% HA.

The strains at break of single filaments were measured for a gage length of 20 mm. The maximum stress was calculated as the maximum force divided by initial area. The stress in the fibres at a given load was calculated using the mean diameters measured from the SEM images. The mean stress calculated for the unmodified PET fibres was 0.43 MPa, for the 1-min O_2 plasma treated 0.55 MPa, and 0.13 MPa for the coated fibres. The strain at break for the untreated fibres was 35.43 ± 21.03 and 21.16 ± 9.60 for the coated fibres.

5.3.2 Cellular attachment and proliferation

Cell attachment was observed on the surface of the coated scaffolds at 24 h after seeding by immunofluorescent staining of actin filaments in the cytoskeleton, focal contacts, and the nucleus of the cells (see figure 5.6). Focal contacts of the cell with the fibres were evidenced by the positive staining of focal adhesions with the monoclonal antibody to Vinculin. At 24 h, the cells seem to be orientating in the direction of the fibres.

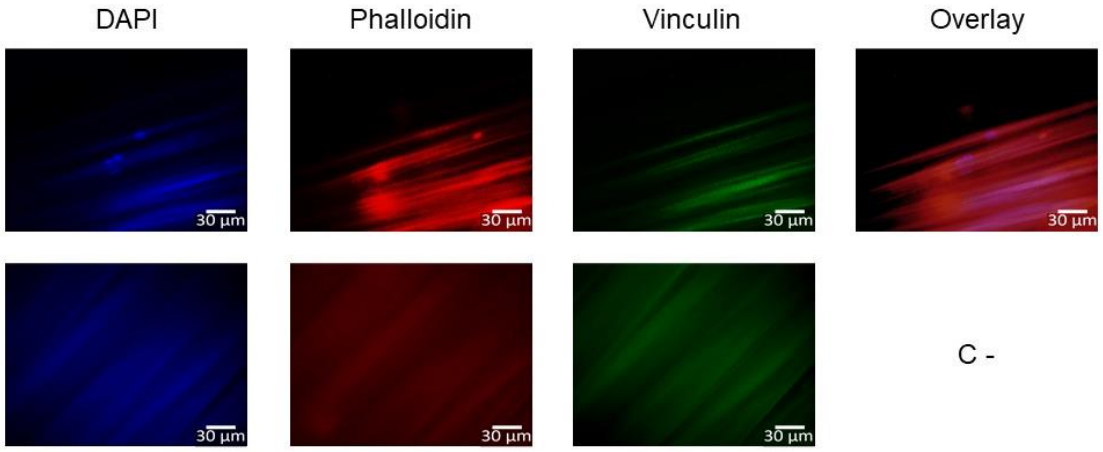

Figure 5.6 Actin cytoskeleton and focal adhesion fluorescence staining after 24 h of seeding iMSCs on PET fibrous scaffolds pre-treated for 1-min with O_2 plasma and coated with 1% CS-g-GMA / 1% HA. Bars represent 30 µm.

To assess the proliferation rate, metabolic activity and DNA were measured from day 1 to day 21 (see figure 5.7). The cell metabolic activity was corrected by calculating the cell number after obtaining a metabolic activity curve. Up to day three of cell culture there was no significant increase for any of the samples. There was a significant increase for all the samples from day 7 to day 14. To investigate the effect of a pre-plasma treatment of the coated scaffolds on the cellular growth, PET fibres were coated with the chitosan solution mixed with either 0.1% or 1% HA solution without surface functionalisation. There was significant effect of pre-plasma treatment at day 21 one, supported by a significant increase in cell numbers from metabolic activity for scaffolds pre-treated for either 0.5- or 1-min and coated with the solution containing 1% HA.

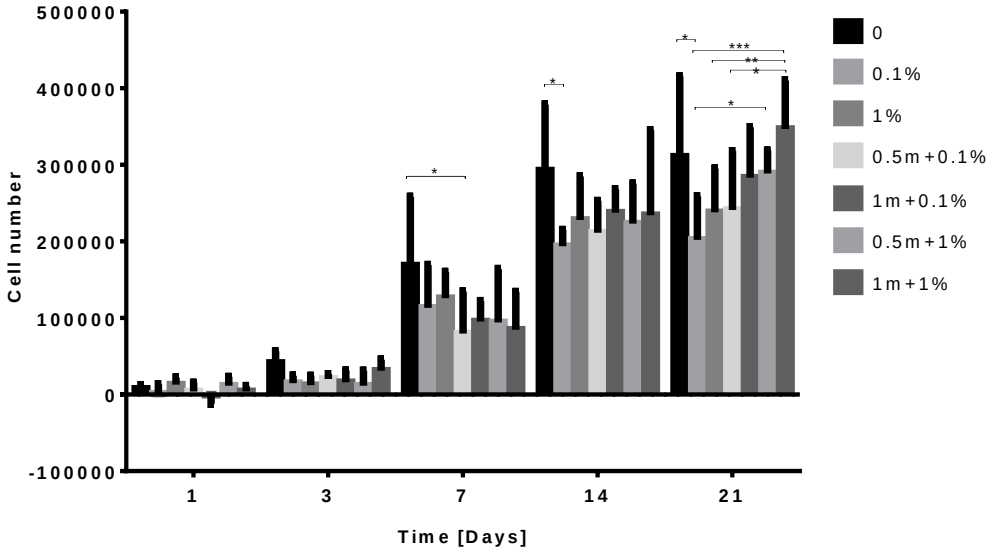

Figure 5.7 Cell growth comparison. The graph shows the iMSC growth during 21 days of culture on untreated PET fibrous scaffolds and scaffolds coated with different concentrations of HA and with different O_2 plasma pre-treatments. The cell number was calculated from the curve of metabolic activity from a known number of cells. N = 6.

The advantage of pre-treating the PET fibres with oxygen plasma glow was concluded. Similarly, a concentration of 1% HA was determined more suitable for our purpose. The 1% CS-g-GMA / 1% HA coated PET scaffolds with an O_2 plasma pre-treatment for either 0.5- min or 1-min were therefore further tested for cell growth, differentiation, and ECM deposition.

There was a significant difference at day 14 favouring cell growth on the unmodified PET scaffold when compared to the coated scaffold pre-treated for 0.5-min ($p < 0.05$) (see figure 5.8).

As per the previous chapter and given the hypoxic nature of the intra-articular joint, the efficacy of the coating for sustaining cell growth and enhancing ECM deposition was tested under a more physiologically relevant oxygen tension of 5%. At day 3 of cell culture, there was a significant difference in cell numbers in favour of the uncoated scaffold, which did not remain for the rest of the experimental time (see figure 5.8 b). By day 28, the iMCs on the coated scaffolds seem to have a better adaptation to the hypoxic conditions.

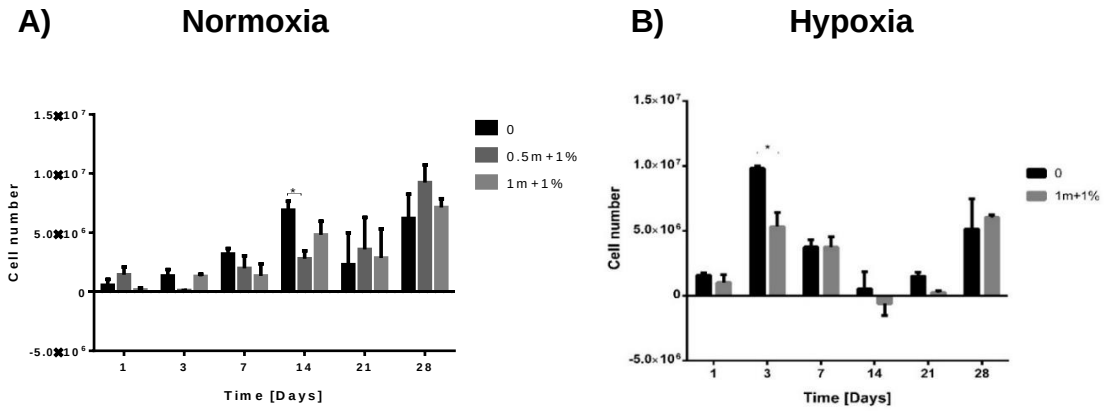

Figure 5.8 iMSC growth shown as cell number from metabolic activity curve in culture in A) normoxia and B) physiologic hypoxia. 0 = untreated PET, 0.5m+1% and 1m+1% = 0.5-min or 1-min O_2 plasma pre-treated PET + 1% CS-g-GMA / 1% HA coating. N = 3.

5.3.3 CS-g-GMA coating enhances ECM deposition on PET fibrous scaffolds

At days 14 and 21, light microscopy images were taken from the scaffolds after staining with PSR to evidence ingrowth by staining the collagen deposition and cellular bridging over time. Figure 5.9 shows representative pictures for each condition.

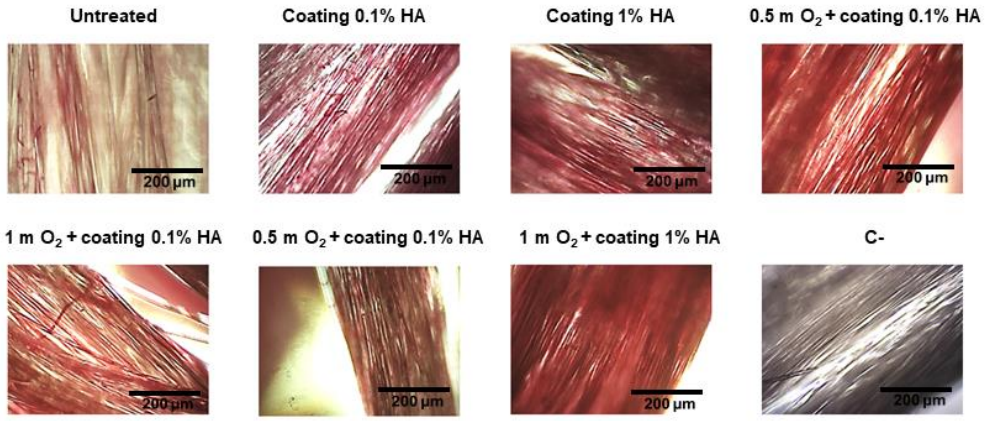

Figure 5.9 Light microscopy representative images of collagen deposition at day 14 on 3D fibrous untreated and treated scaffolds after staining with PSR. Coating refers to the basic coating composed of 1% CS-g-GMA, O_2 plasma pre-treatment is given in minutes. Bar represents 200 µm.

At day 14, the iMSCs had attached and spread on PET untreated and coated fibrous scaffolds as it can be seen from the SEM images in figure 5.10. After 14 days of culture, ECM can be noted covering the fibres of the PET coated and untreated scaffolds. There were areas where cells had proliferated well and were forming cell networks.

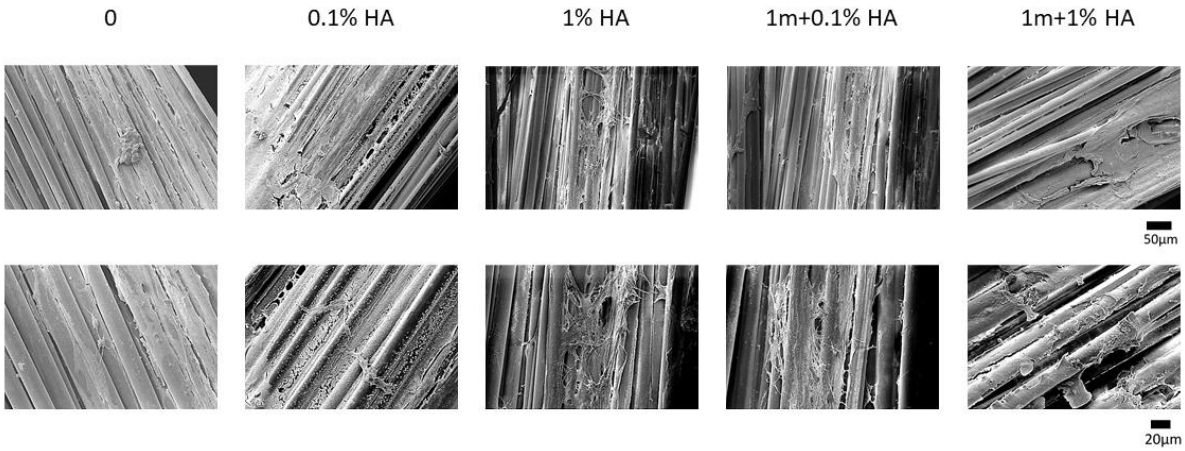

Figure 5.10 SEM representative images of matrix deposition on unmodified and modified PET scaffolds at day 14. All modified scaffolds contain with 1% CTS-g-GMA mixed with either 0.1 or 1% HA and pre-treated or not pre-treated with O_2 plasma.

Further magnification on SEM images from the 1% CS-g-GMA / 1% HA 1-min pre-treated PET fibrous scaffolds to analyse cell-cell and cell-substrate interaction can be seen in figure 5.11. At day 14 of culture, iMSCs have a fusiform morphology, are attached and proliferating along the fibres. iMSCs are also observed proliferating across the fibres forming bridges between them. A fibrillar architecture of the ECM can be seen at a closer look. Due to the dehydration steps during SEM sample preparation, there are apparent areas of cell membrane disruption. Protrusion of bundles of filopodia / lamellipodia can be seen through the spacings between fibres, indicating cell adhesion.

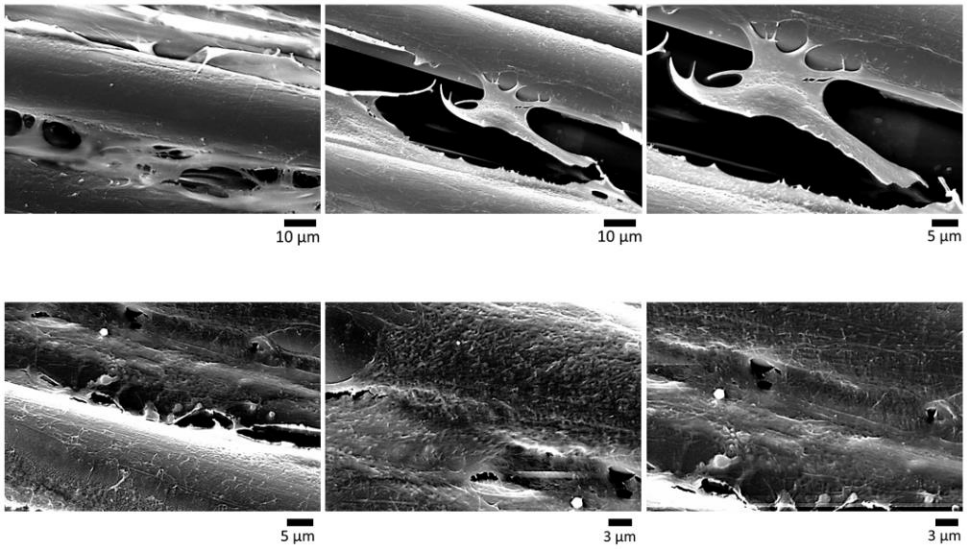

Figure 5.11 Cell-substrate interaction and ECM deposition after 14 days of culture. SEM representative images of matrix deposition on PET fibrous scaffolds coated with 1% CS-g-GMA / 1% HA pre-treated for 1-min with O_2 plasma.

Light microscopy imaging of the scaffolds after staining for collagen deposition evidenced ECM synthesis and showed that the iMSCs clustered to form cell sheets between fibres. Qualitatively, there was less collagen staining in the untreated PET scaffold when compared to the treated scaffolds. For all the seeded scaffolds, the cells appeared to have migrated and proliferated along the fibres. For the coated scaffolds, the staining images also indicated cell migration and proliferation across fibres to form cell bridges that were particularly prominent in the scaffolds with the 1% CS-g-GMA / 1% HA coating (see figure 5.12).

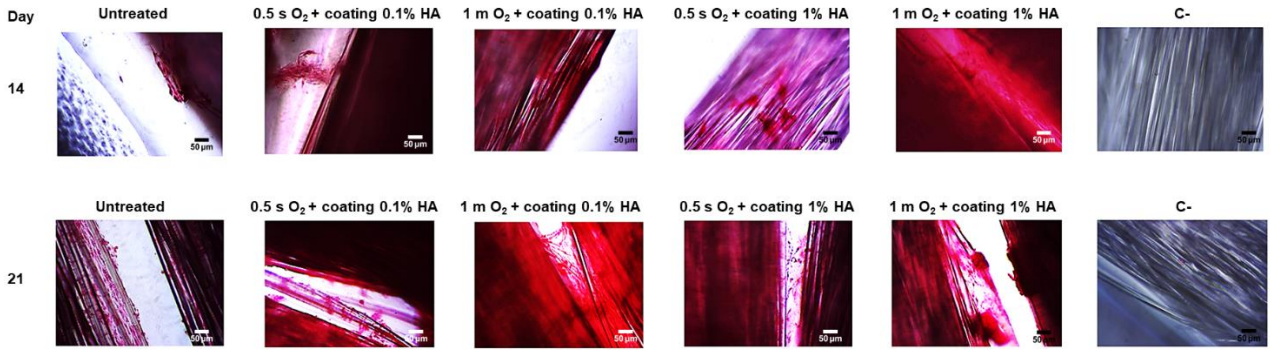

Figure 5.12 Light microscopy representative images of cellular bridging by staining for collagen with PSR. Bar represents 50 µm.

The staining was then eluted, and the results were corrected by subtracting the corresponding negative controls (see figure 5.13). When comparing the coating composition, at day 14, there was a higher collagen deposition for the scaffolds modified with a 1% CST-g-GMA / 1% HA after plasma treatment. There was no significant difference among the treatments (p = 0.35).

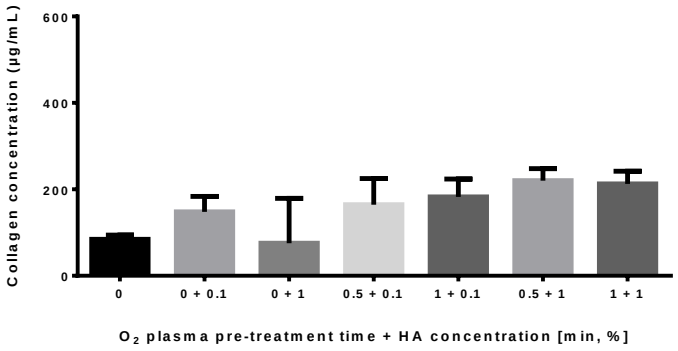

Figure 5.13 Collagen deposition at day 14 in 3D fibrous scaffolds pre-treated with O_2 plasma for 0.5- or 1-min, coated with 1% CS-g-GMA and either 0.1% or 1% HA. N=3. Bar represents SE.

Collagen deposition was then followed from day 14 to day 28 for the plasma pre-treated scaffolds coated with the solution containing 1% HA (see figure 5.14).

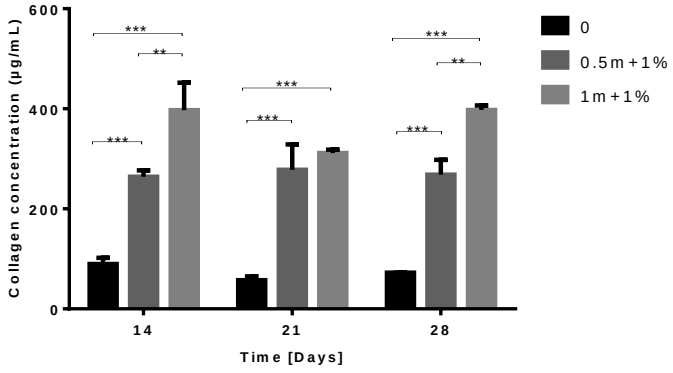

Figure 5.14 Collagen deposition from day 14 to day 28 on the non-treated (0) and O_2 plasma pre-treated PET fibrous scaffolds coated with solution containing 1% HA. N=3.

Regarding the ECM deposition under physiologic hypoxia (see figure 5.15), the collagen concentration on the coated scaffolds at days 14 and 21 was significantly higher ($p < 0.0001$). When corrected for the cell number, the statistically significant

difference remained for day 14 ($p < 0.0001$) but the difference did not reach significance at day 21 ($p = 0.06$).

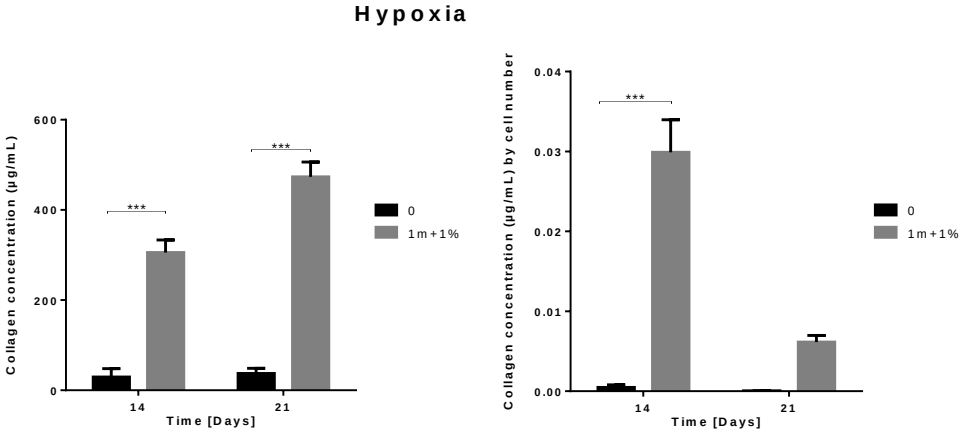

Figure 5.15 Collagen deposition at days 14 and 21 of cell culture at 5% oxygen tension. Non-treated (0) and 1-min O_2 plasma pre-treated coated fibrous scaffolds (1m+1%). N=3.

To quantify the acid-soluble collagen and sGAG deposited on the scaffolds, unmodified and coated scaffolds after O_2 plasma treatment were incubated with either an acid/pepsin or a PBE / papain extraction solution (see figure 5.16). There was a statistically significant increased collagen deposition at day 21 for the coated scaffolds pre-treated for 1-min with O_2 plasma ($p < 0.05$). No other statistically significant differences were noted for acid soluble collagen deposition. For sGAG, there was a statistically significant difference at day 28 in favour of the coated scaffolds pre-treated for 1-min with O_2 plasma ($p < 0.01$).

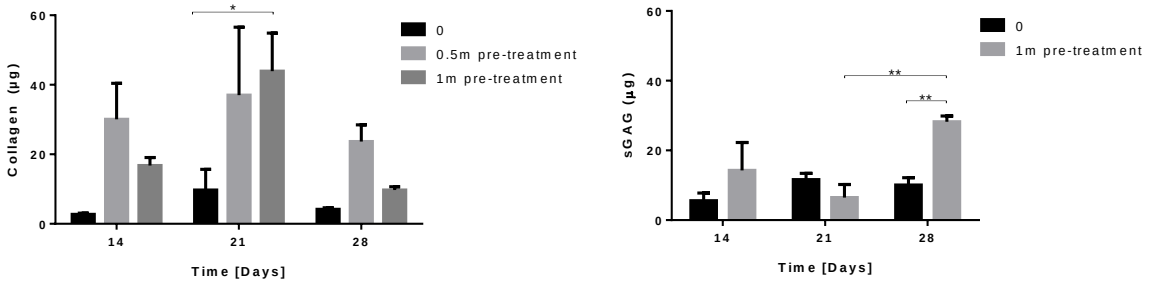

Figure 5.16 Extracted soluble collagen and sGAG quantified at days 14, 21 and 28. Non-treated PET and coated scaffolds with either 0.5 or 1-min O_2 plasma pre-treatment. N=3.

The secretion of ligament ECM proteins on the coated PET scaffold were visualized by immuno-fluorescent staining. The images showed that the deposition of COL-I at day 21 was increased by the 1%Cs-g-GMA/1%HA coating (see figure 5.17). The COL-I, COL-III, tenascin C and Scx deposited on the coated scaffold's surface seemed to align with the fibres.

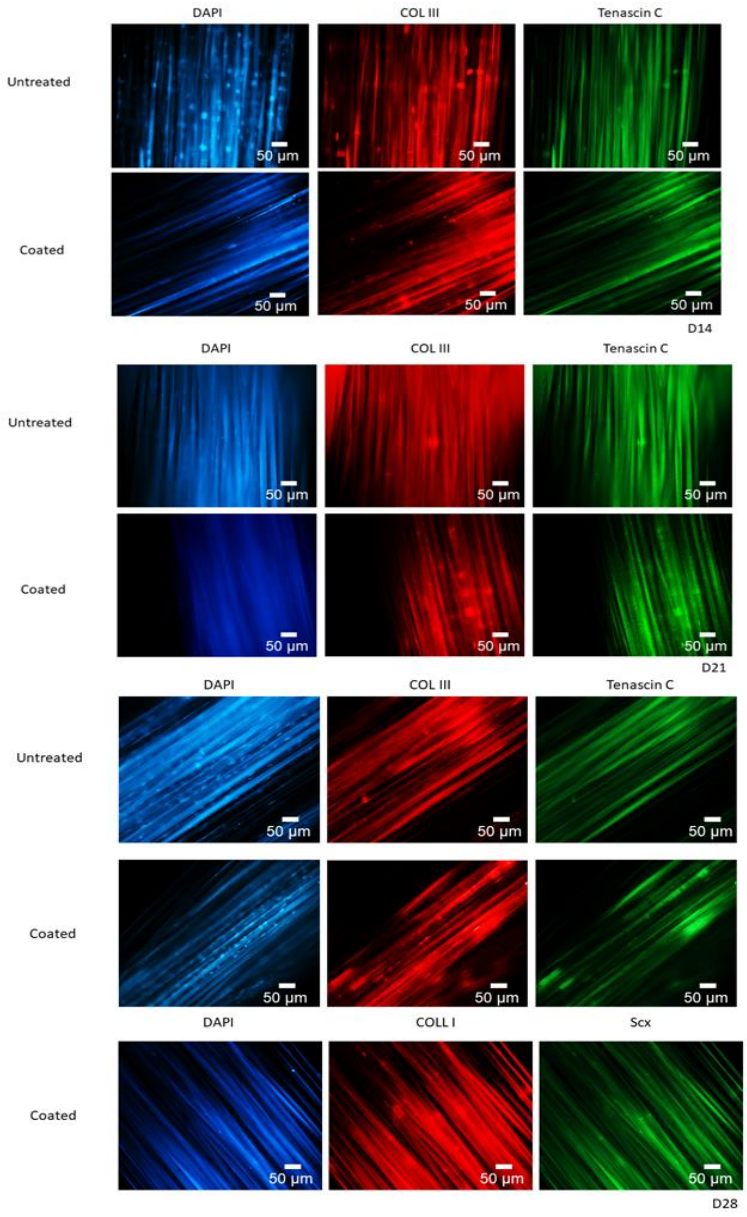

Figure 5.17 Immunofluorescence staining of iMSC on PET scaffold coated with 1-min O_2 plasma pre-treatment + 1% CS-g-GMA / 1% HA at days 14, 21 and 28 for ligament markers COL-I, COL-III, tenascin C and Scx.

5.3.4 Effect of coating on iMSC differentiation capacity

After selecting the scaffold treatment which demonstrated the highest extracellular matrix deposition, the differentiation capacity of the iMSCs was investigated. After a 14-day period of cell growth on the scaffolds under regular experimental conditions, the cells were exposed to either osteogenic, chondrogenic or adipogenic culture media. They were then stained with alizarin red (see figures 5.18 and 5.19), oil red O (see figure 5.20). Scaffolds cultured under regular experimental conditions with no induction media during the same experimental time were used as negative controls.

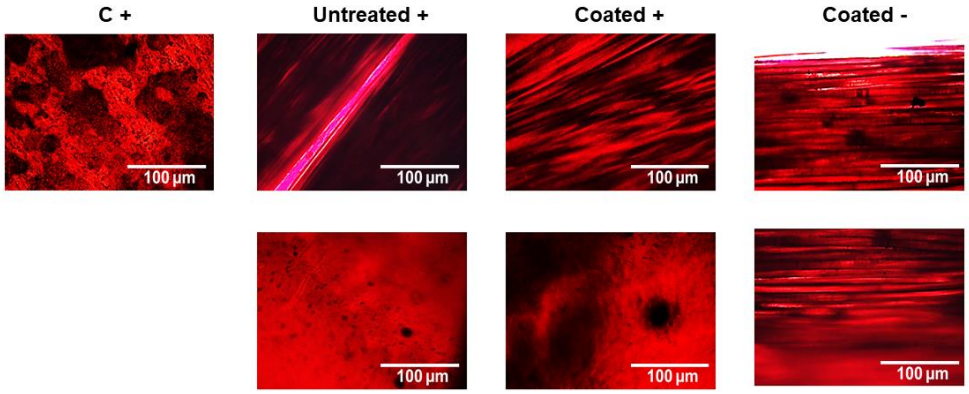

Figure 5.18 Osteogenic differentiation. Alizarin red staining after 21 days of seeded scaffolds cultured with osteogenic induction media (+). The negative control is PET 1-min O_2 plasma-treated and coated with 1% CS-g-GMA / 1% HA seeded scaffold without induction media (-).

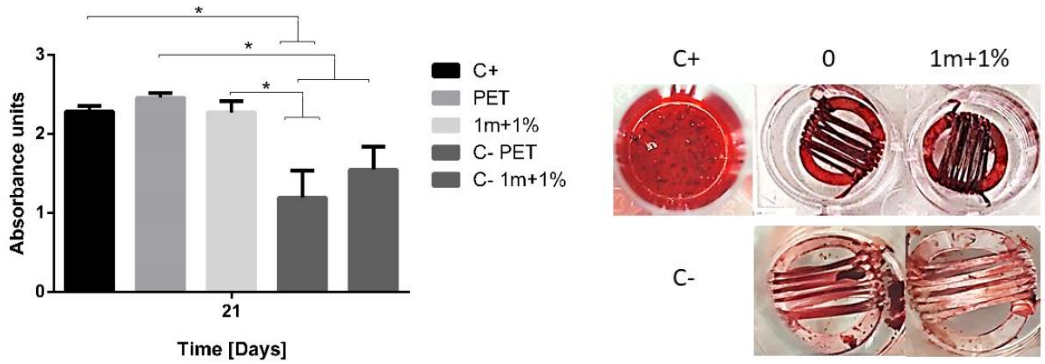

Figure 5.19 Quantification of osteogenic differentiation. Alizarin red staining after 21 days of seeded scaffolds cultured with osteogenic media and their controls with experimental media.

At day 21 after culturing with adipogenic induction media, fat droplets were observed on both, untreated and 1% CS-g-GMA / 1% HA coated scaffolds pre-treated with O_2 plasma (see figure 5.20).

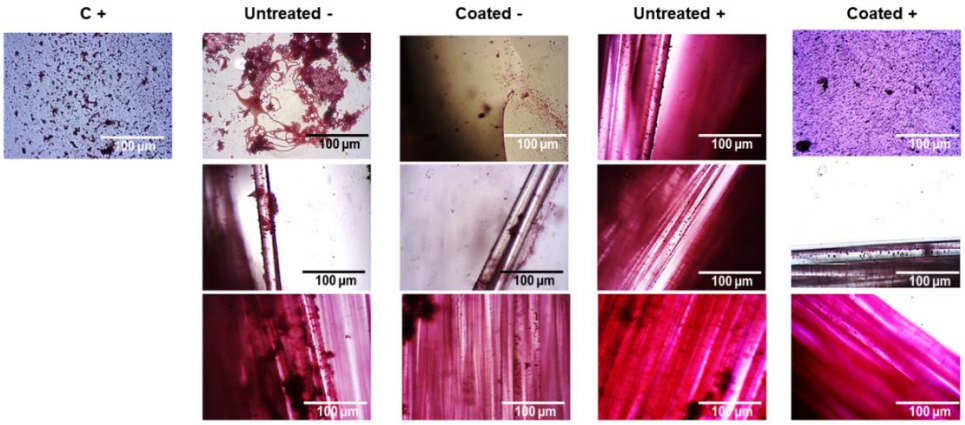

Figure 5.20 Adipogenic differentiation. At day 14, the scaffolds were stained with Oil red O to assess spontaneous differentiation without induction media (-). Additionally, scaffolds were culture for 21 days with adipogenic differentiation induction media (+).

5.4 Discussion

Along with fibres, ligaments are also comprised by a ground substance that provides them their viscous gelatinous appearance. For this reason and due to their structural similarity with extra cellular proteoglycans and their ability to form polyelectrolyte complexes when mixed, HA and CS stand out as ideal candidates for ligament regeneration [280, 281]. Given the proven biological benefits of HA and CS as biomaterials and their complementary interaction, they were both selected for the bioactive coating for the PET scaffold. In this chapter, the effects of a bioactive coating made of CS-g-GMA and HA on improving the bioactivity of a PET fibrous scaffold were tested.

The ionic interaction between CS and HA acid seems promising for ligament TE. The combination of this polysaccharides has shown an improved fibroblast adhesion and deposition of ECM products when compared to the use of chitosan alone [289]. The findings from this chapter supported the effect of chitosan and hyaluronic acid for the promotion of cell proliferation and ECM deposition. The coated scaffolds provided iMSCs with an environment that encouraged the deposition of proteins present in the

native ACL ECM. Moreover, the iMSCs proliferating on the bioactive scaffolds seem to retain their stemness and differentiate according to the specific induction cue. These data support the hypothesis that the addition of a 1 % CS-g-GMA / 1% HA bioactive coating to a 1-min O_2 plasma pre-treated PET fibrous scaffold could enhance ligament regeneration.

In this chapter, the dip-coating procedure used successfully coated the PET scaffolds with a stable layer of CS-g-GMA and HA. The expected average thickness of a single layer after dip-coating is below 0.5 μm, which allows for a relatively quick evaporation and drying stages that lead to the tighter arrangement of the polymeric networks and thus a lower coating porosity [322]. Several factors affect the homogeneity and thickness of the coating from the dip-coating technique. These include the viscosity of the solution, the speed at which the scaffolds are withdrawn from the solution, the evaporation rate of the solvent, the spontaneous contraction of the gel, and the conditions surrounding the withdrawal [322]. For the preparation of the bioactive composite scaffold presented in this thesis, the procedure was optimised to be repeatable and was performed in the same manner for all the scaffolds manufactured. The water contact angle testing on the samples demonstrated no significant variability from batch to batch and the SEM observation of three different coated samples qualitatively corroborated the presence of the similar coated surfaces for the PET fibrous scaffolds. A coating's thickness can be measured with methodologies involving destructive or non-destructive methodologies. SEM is useful in the observation and measurement of coatings with a small thickness, when optical microscopy is not adequate for the analysis of the scaffold's cross-section or if there is low contrast [323]. There are, however, several limitations to this technique, particularly with conventional SEM methodologies and to ensure good quality images. It requires sample preparation for the scaffolds to be conductive and for it to withstand a high vacuum environment and the electron beam irradiation. SEM was also used in this thesis to measure the cross-section of single fibres. It was achieved by observing transversally a fibrous sample cut in half and measuring with the aid of a software that allowed the conversion of pixels in the images into

dimensions as units of length through a scale [323]. The preparation of the sample and the cross-sectional cutting hold the potential of introducing artifacts into the measurements or damaging the scaffold's structure. The FT-IR results show the contribution of HA's abundant content of hydroxyl and carboxyl groups to the coating, with the peak appearing at 3429 cm^{-1} – attributed to the stretching mode of the O-H bond –, and the increase in the peak intensity at 1096 cm^{-1} – due to the –C-O- group – [276, 324]. The peak appearing at 2970 cm^{-1} can be attributed to the vibration of the CH_2 group present in chitosan. Similarly, the increase in the peak intensity at 1713 cm^{-1} can be assigned to the C=O stretching vibration from the carboxylic groups [325]. These differences with the untreated PET spectra suggest the incorporation of CS and HA into the material's surface. Regarding the mechanical properties, similar to the results presented above for this project a study on PET / CS films made via solvent-cast blending showed that an increase in chitosan content resulted in a decrease in tensile strength and elongation at break of PET [326]. In the study by Masoomi et al. despite retaining appropriate tensile strength for food packaging purposes, the PET / CS films became more brittle by adding chitosan. Blending PET and CS with concentrations of 10 and 2 (w/v%) respectively mixed in a 1:99 mass ratio reduced the tensile strength from 50.01 ± 4.8 MPa from PET unblended controls to 44.31 ± 3.9 MPa. Likewise, the elongation at break was reduced from 78.46 ± 8.0% to 54.47 ± 6.3% [326] associated to the weak tensile properties of chitosan. The 1.4-fold decrease in strain at break found in the study by Masoomi et al. compares to what it is reported in the results obtained for this thesis where there was a 1.6-fold decrease in strain at break for the composite scaffolds when compared to the untreated PET ones. In contrast, a different study on a 3D scaffold composed of PET knitted hollow tubes saturated with a 1 wt% chitosan solution and freeze-dried demonstrated an increase in tensile strength of their constructs as a result of the chitosan filling the hollow tubes and reinforcement of them by conferring adhesive properties to the PET plied yarns [327]. The surface properties of polymers hinder the interfacial adhesion to natural polymers. For this reason, the straightforward, non-toxic, cost-effective, and reproducible O_2 plasma treatment was explored in the previous chapter as the first step of the selected two-step surface modification for the PET scaffold. In a study exploring the benefit of treating the surface

of recycled polyethylene / CS composites with polyethylene-graft-maleic anhydride to improve the materials' compatibility, the addition of CS well coated onto the matrix in the presence of the compatibilising agent demonstrated an improved adhesion across the interface and an increased tensile strength in relation to increasing CS loading. [328]. For the experimental results presented in this thesis, the CS-g-GMA / HA coating did not seem to reinforce the PET scaffolds in terms of strain at break, nevertheless, a human tendon fascicle has a failure strain of 17 ± 7% [329].

CS and hyaluronic acid can be chemically modified to enhance their interaction and address specific material needs. For instance, their more water-soluble variations [330] have demonstrated an effectiveness in preventing post-operative fibroblast adhesion to injectable hydrogels [331]. Within the same purpose of manufacturing tissue engineered injectable hydrogels, this CS-HA combination has demonstrated to provide high viability of osteoblasts, chondrocytes, and fibroblasts after being encapsulated in the material [332, 333]. In this chapter, CS was functionalised with the monomer GMA to improve its potential for radical polymerization reactions, prior to synthetising the HA / CS complex solution. The bioactive coating proposed here demonstrated an early cell attachment to the 3D PET scaffolds and a favourable cell growth up to 28 days. An improved cell attachment is of utmost importance in the mechanosensitive and load-bearing ligaments. The iMSCs were found to reorganise their cytoskeleton along the aligned fibres of the scaffold in this chapter, portraying an elongated cell morphology oriented with the fibres. Cell attachment was evidenced by the multiple filopodia and lamellipodia extending from the iMSCs bodies and protruding through the fibres. The hydrophilicity conveyed by the bioactive coating contributes to the cell adhesion as focal adhesion protein expression is increased by hydrophilic surfaces [245]. The results presented in this chapter suggest that cell growth might in fact be enhanced by the 1% CS-g-GMA / 1% HA coating in a longer term compared to the untreated PET fibres, prompting for longer cell culture investigations. Majima et al. [281] reported a similar finding of cell growth – for rabbit PT fibroblasts – reaching significance at day 28 for a 0.1% CS / 0.1% HA fibrous scaffold made by means of a wet-spinning technique. This late increased growth could be in response to the enhanced interaction

of the seeded cells with a more robust ligament-like ECM that presents cell signals improving cell proliferation and differentiation, cell migration, and further cell adhesion.

About ECM production, the 1% CS-g-GMA / 1% HA 1-min O_2 plasma pre-treated PET fibrous scaffold significantly enhanced both collagen and sGAG deposition. The combination of CS and HA at different concentrations has demonstrated an increase in Col I before [276, 281]. This is possibly due to an induced ligamentogenic differentiation from the environment facilitated by the bioactive coating. The coating improved the PET surfaces biocompatibility and hydrophilicity, producing a biomimetic microenvironment for the iMSCs to attach, proliferate, synthesise ligament-like ECM and retain their stemness. The chemical structure of CS-g-GMA and high molecular mass HA used in this chapter have the potential to favourably interact with diverse growth factors, receptors, and adhesion proteins, thus enhancing ligament-like tissue formation. It is hypothesised that the proposed bioactive composite scaffold would be capable of inducing cell migration and chemoattraction of growth factors from the ACL remnant after scaffold implantation.

5.5 Conclusion

The above work has shown an enhanced initial cell attachment to the coated substrates, but cell proliferation is not enhanced by the adhesion of the coating. However, cell growth is sustained in longer-term culture and the significant increase in collagen deposition from the MSCs cells seeded onto the bioactive coated scaffolds supports them as a promising candidate for ligament regeneration.

Chapter 6

Enhanced iMSC collagen deposition on a bioactive composite scaffold for ligament TE under dynamic mechanical stimulation

---

Aims: To evaluate the behaviour of iMSCs seeded onto a bioactive PET fibrous scaffold coated with 1% CS-g-GMA / 1% HA and cultured in a uniaxial mechanical stimulation bioreactor.

Hypothesis: The iMSCs seeded onto the bioactive composite scaffolds will display higher vitality and functionality that the ones on unmodified PET scaffolds when subjected to continuous mechanical stimulation.

6.1 Introduction

Tissues within the musculoskeletal system, including the ligaments, depend on mechanical stimulation to maintain their homeostasis. Native cells in the ligaments possess cell surface receptors in charge of translating stress signals such as compression, torsion, and tension into synthesis of new tissue [334]. These responses are modulated by the duration and intensity of the stimulus. Among several ECM proteins, collagen and Tnmd are upregulated by uniaxial stretching [335]. Ligaments are connected to the ECM by integrins that sense mechanical loading that prompts intracellular signalling. The signalling cascade produced induces the transcription and synthesis of growth factors that in turn generate an autocrine-paracrine response to synthetise collagen [336]. Research from the past few decades has proven the effect of mechanical stimulation on ECM synthesis in connective tissues [337]; nevertheless, there is no clear optimal stimulation pattern specific for ligament TE. As it has been documented that a ligament graft is at a higher risk of reinjury when commencing

rehabilitation, there is a concern for the potential deleterious effects of some specific rehabilitation exercises on generating strain levels that compromise the structural integrity of the graft [338, 339]. For the recovery of the knee after a surgical repair of a torn ACL, there is evidence to support that early joint motion results in a reduction in pain, and in the formation of scar and capsular contractions [338]. While the encouraging feature of the currently approved PET artificial ligament is the earlier return to physical activity, the available long-term data on graft ruptures urges the consideration of different approaches in design and selection of materials to conceive a graft that can enhance the ligamentisation process. This chapter systematically explores the effectiveness of the bioactive coating of a PET fibrous scaffold on supporting the proliferation and functionality of iMSCs under cyclic strain at a fixed frequency using a bioreactor. The impact on extracellular matrix remodelling will be analysed.

6.1.1 Effect of loading on ligament physiology

As with any other tissue, ligament's composition is critical to its mechanical properties and specific to defined anatomical locations [29]. Variations in the frequency and ranges of strain result in microstructural changes that impact the elastic response and the nonlinear viscoelastic behaviour of ligaments [340-342]. In everyday life, the ligaments are subjected to cyclical loading. The tensile strain refers to the change in length of the ACL and is expressed as a percentage. It induces the alignment of cells with their cell bodies and nuclei along the principal strain direction. Ligaments require varied amounts of tensile strains throughout the day to maintain the equilibrium of their structural composition and cellular function [343]. They sustain tensile forces from stretching along their axis, compressive forces particularly at their entheses, and shear forces during sliding in the synovial sheath [344]. MMP expression is directly modified by loading amplitudes [345].

Due to the predominance of collagen in ligament makeup, the regulation of this protein is frequently the focus of dynamic stimulation studies in ligament regeneration [346-350]. The focal interest of previous studies has been gene regulation of collagen, with less data on the protein deposition. Mechanical load promotes changes in ECM content,

hierarchical organization, collagen crosslinking, fibril diameter, fibre orientation, density, and length [351]. The translation of these stimuli into cell biofunctions is facilitated by mechanoreceptors in ligaments.

6.1.2 Mechanoreceptors in ligaments

The sub synovial layer in close contact with the ACL's collagenous fascicles contains a vast neural network [352-354]. Mechanoreceptors such as Pacinian corpuscles, Ruffini, and Golgi tendon organ-like in the human anterior cruciate ligament detect changes in tension, speed, acceleration, direction of movement, and the position of the knee joint [353, 355-358]. The Pacinian and Ruffini corpuscles are encapsulated and myelinated afferent axons [359]. The Ruffini corpuscles are formed of nerve terminals, an incomplete perineural capsule and endoneural connective tissue. They contain mitochondria and vesicles and are in direct contact with the collagenous fibrils [360]. They are stretch receptors responsible for the slow adaptation to small changes when the ligament is under tensile stimulation. This slow adaptation capacity allows them to sustain a prolonged discharge. They are also involved in proprioception [359]. The Pacinian corpuscules, on the other hand, are velocity receptors that conform the fast adaptation neural response. They transfer kinesthesis independently to proprioception [359, 360]. The Golgi corpuscle is a partially encapsulated high-threshold mechanoreceptor that also acts in rapid adaptation to stretching stimulus [361, 362]. Clinical and experimental data show that tension sustained by a ligament activates receptors at different thresholds and that these ligament afferents adapt more readily when the joint draws near to its normal functional range [363].

Free nerve endings, also called bare due to their lack of myelin sheath, are the most abundant neural component in the ACL. The cruciate ligaments have been found to contain more free nerve endings than the patellar tendon or the ligaments and tendons from both the medial and lateral complexes [355]. These neural components respond to compression and stretching of the ACL. They are considered within the nociceptive system, for they respond to inflammatory agents and for the fact that their reaction is triggered when surpassing the normal stimuli threshold [364]. Their significantly greater presence in the ACL in comparison to the rest of the knee stabilising structures

reinforces the importance of the ACL in static and dynamic stability for the resistance to forces, coordination and the manifestation of pain in knee OA [365].

The deformation of these neural networks by tissue loading activates pathways that modulate the expression of various factors involved in cellular functions [366].These sensory properties emphasise the importance of testing any ligament scaffold for mechanical deformation in accordance with physiological loading conditions.

6.1.3 Mechanotransduction

At a cellular level, the mode, magnitude, and direction mechanical of stresses are sensed are sensed and the information is translated via different mediators – represented in figure 6.1 – to adapt ligament cell behaviour. Components from the ECM and the cell interact in response to mechanical loading including nuclear structures, cytoskeletal filaments, membrane surface receptors, channels, processes and other elements, ECM proteins, ligands and binding sites, cell-ECM and cell-cell adhesions.

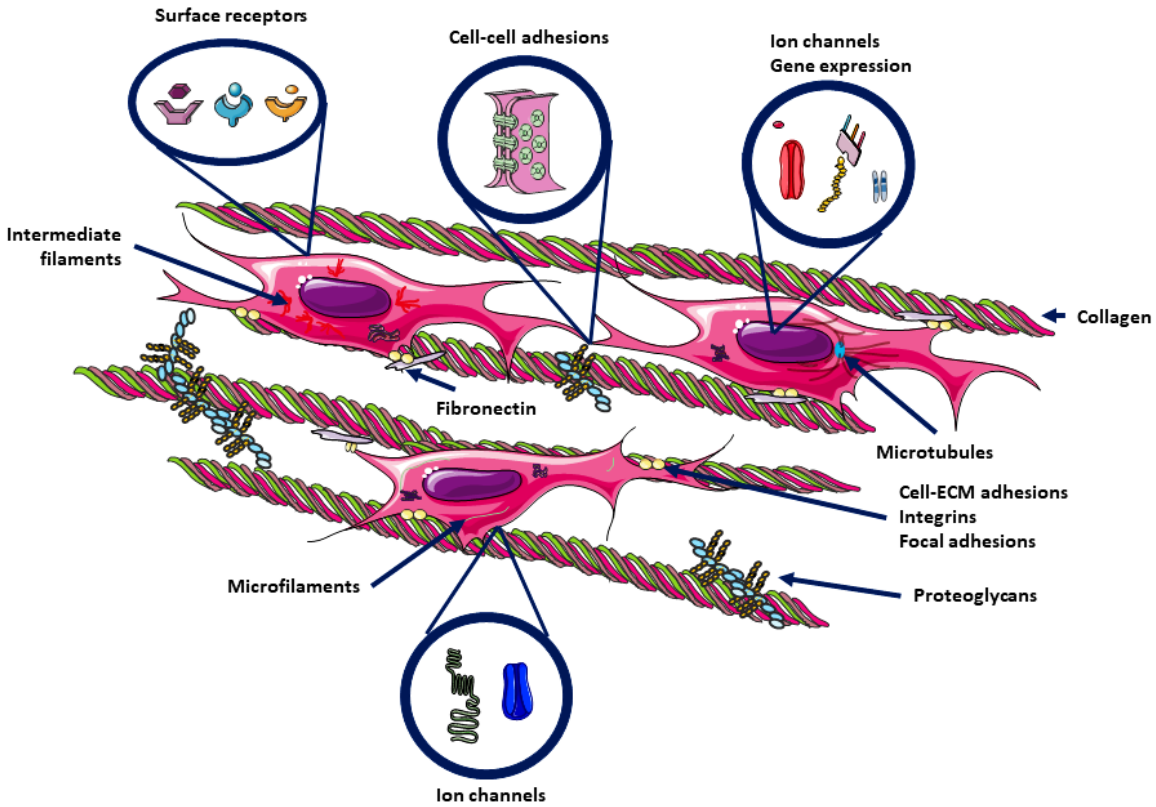

Figure 6.1 Mediators of mechanotransduction. Image made with Servier Medical Art under a Creative Commons Attribution 3.0 Unported License.

Mechanical stimuli regulate various membrane proteins. Extracellular factors such as mechanical stimuli and fluid flow are sensed by primary cilia, which are cell apical surface projections formed of microtubules, leading to the activation of ion flux through the regulation of key signalling pathways that include the hedgehog (HH) and Wnt. The ciliary axoneme houses receptors and mechanosensitive channels [367]. The cellular actin cytoskeleton adapts to the environment by forming specialised protrusions formed by assembling monomeric globular (G)-actin into (F)-filamentous actin. Lamellipodia and filopodia are types of actin-based protrusions found in MSCs and ligament fibroblasts. The lamellipodium is considered the key element in fibroblast-like cell migration in 3D environments. On the other hand, filopodia sense mechanical and chemical cues through their multiple receptors including growth-factor receptors, integrins and cadherins. For this reason, filopodia are believed to control cell-matrix adhesions and motility, stabilising the advancement of lamellipodium. Adhesion sites within the lamellipodium direct protrusion and contractility of fibroblasts [368].

Cell adhesion related molecules transduce mechanical stimuli as intracellular signals. The resident ligament cells sense their ECM environment through transmembrane receptors called integrins. Integrins mediate cell-cell and cell-matrix attachment by modulating cytoskeletal interactions with different combinations of their 18 α and 8 β subunits that specifically bind to different extracellular ligands. Integrins act as well as signal transducers and direct the biochemical signals and cellular forces sensed to regulate cell migration, cell growth, and cell survival [369-372]. Their function depends on the crosstalk with growth factors and other signalling pathways; they initiate different mechanotransduction pathways depending on the isoform and cytoplasmic proteins and the ECM components that are involved [371, 373]. The collagen-binding integrins are β1, α1β1, α2β1, α10β1 and α11β1 [373]. Aside from collagen, other β -integrin ligands present in ligaments are laminin, and fibronectin. ACL fibroblasts possess ß1-chain, α1β1, and α5β1, but lack α2β1, α3β1, α4β1, and the αβ-subunit [369].

Integrin-ECM contacts interact with mechanical stress to activate the phosphorylation of focal adhesion kinase (FAK) and the Rho-dependent assembly of focal adhesion complexes. Integrin gene expression is stimulated by Scx and Mkx, which are activated

by mechanical force [344]. Ligament fibroblasts integrin-mediated adhesions on fibronectin involve cAMP and Ca2+/phospholipid signalling pathways [374]. The protein that connects the actin cytoskeleton to the intracellular domains of integrins is called talin. Talin acts as a shock absorber and molecular switch via the rearrangement of protein domains caused by tensile force. When talin interacts with growth factor receptors, it exposes binding sites for FAK and proteins that stabilise the focal adhesions, as is the case of vinculin. Increased collagen expression on ligament fibroblasts is associated with FAK recruitment to integrin clusters at the cell surface. Integrins interact with extracellular growth factors, growth factor binding proteins and growth factor receptors. For instance, the expression of integrins such as αvβ3, αvβ5, avβ6, and several β1 integrins is upregulated by signalling from TGF-β, mediated by tenascin C [344, 371]. In human ACL cells, uniaxial stretching increases integrin αV and COL1A1 expression by modulating the integrin αVβ3-dependent focal adhesion [372]. Focal adhesions dominate direct mechanotransduction in ligament fibroblasts. These are integrins embedded in the cell membrane and their intracellular adaptor proteins that bind to collagen. For MSCs, focal adhesion complexes upregulate ligament-like gene expression as a result of tensile stretching. Nuclear deformation affecting FAK leads to the activation of transcription factors YAP and TAZ, which sense mechanical stress [344, 371].

Ligamentisation implies the aligned fibrillar collagen deposition by resident cells, this process is facilitated by physiologic loading of the tissue. In MSCs, this collagen assembly and the speeding up of collagen deposition is mediated by the mechanosensitive cation channel transient receptor potential vanilloid 4 (TRPV4) [375]. TRVP4 also modulates the force that is transmitted across vinculin and calcium permeability [344, 375]. Stretch-sensitive ion channels activate as the cell membrane deforms. Piezo proteins are one of such channels. When they are activated, they allow the cells to sense mechanical stress by permitting the entrance of calcium into the cytoplasm. Calcium flux is associated with focal adhesions and cell-cell signalling [344]. Ca2+ flux is involved in fibrillogenesis by regulating cell motility, transduction of extracellular stimuli, gene transcription and protein expression. Oscillations in Ca2+ levels affect MSCs migration and differentiation processes [375]. Changes in the ECM

induced by mechanical stimulation modulate ligament cell behaviour indirectly by the interaction of mechanosensitive ECM components such as fibronectin and tenascin C, which can concentrate cytokines and damage associated molecular patterns at the ligament fibroblast surface in response to abnormal mechanical stresses to trigger cell death and the subsequent tissue repair process [344].

Cell-cell signalling induced by mechanical stresses occurs through communication via intercellular gap junctions at the cells' cytoplasm. In fibroblasts, gap junction communication is formed when hemichannels called connexons come into direct contact with a neighbouring cell's connexon and complete the intercellular channels that then cluster into gap junction plaques. These hemichannels are formed by proteins called connexins – with their four transmembrane domains – and they facilitate the transportation of metabolites, secondary messengers, and ions. Unpartnered open hemichannels enable ATP, glutamate, and NAD+ release into the extracellular space in response to mechanical stress [376, 377].

In tendons, cells oriented along collagen fibres express connexin 43 gap junctions, which mediate the mechanical loading inhibitory effect on the tenocyte's collagen synthesis. In contrast, tenocytes connexin 32 has a diffuse location pattern and is thought to have a stimulatory effect on collagen synthesis [378].

6.1.4 Bioreactors in ligament regeneration

Bioreactors in ligament TE intend to incorporate mechanobiological cues to mimic the tissue's environment. Published data on the use of bioreactors in ligament TE includes a wide range of devices from custom-made to commercially available systems. However, they all share key elements and coincide in providing a sterile environment for cell culture where a mechanical stimulus in the form of a linear displacement is caused by applied tensile forces. The majority of works in tensile bioreactors involve uniaxial stretching of the sample, normally holding fixed an end of the sample while the other end is shifted by a linear actuator [379]. This type of stimulation complies with the load transfer from bone to bone along the normal longitudinal direction of the ligament. Some mechanical parameters explored in these types of bioreactors include stiffness, ultimate tensile load, ultimate elongation, and energy absorbed at failure [380, 381].

Cells within the ligaments adapt differently to different forces. Therefore, the study of a single force application aids to understand specific induced cell behaviours. Other types of bioreactors involve the application of tensile load to culture plates with flexible rubber bases [347, 382]. This type of bioreactor has enabled the study of stretch activated ion channels and the activation of pathways linked to the intracellular microtubular cytoskeleton [383]. More comprehensive tension-torsion bioreactors have also been used to represent the physiologic daily stresses to which a native ligament is routinely subjected [384, 385].

6.1.5 Induced ligamentisation with mechanical stimuli

Cyclic stretching increases the expression and synthesis of fibronectin and elastin, as well as collagen types I and III. Dynamic loads in the range of 5–15% strain increase the MSCs production of collagen type I [379]. Dynamic culture at low frequencies (≤ 0.6 Hz) and low strain (< 5%) have shown an increase in cell density, increased cell adhesion, increased collagen I protein expression, an improved cell alignment in the direction of the fibres with an enhanced migration to the inner part of the fibrous samples and a ligament-like cell morphology – extended and fusiform – [386-388]. Accordingly, uniaxial cyclic stretching at 1 Hz and 8% strain has been proven to induce tenogenic differentiation of human mesenchymal stem cells without triggering the expression of osteoblastic, chondrogenic, or adipogenic marker genes [389]. Along the same line, Altman et al [261] demonstrated selective induced ligamentisation of human-derived BMSC after 21 days of combined tensile-compressive and torsional loading with a frequency of 0.0167 Hz and a translational strain of 10%. The multidimensional strain promoted cell alignment in the direction of loading, a ligament-like cell morphology, the immunohistochemical expression of COL-I, COL-II and fibronectin, as well as the mRNA expression of COL1A1, COL3A1 and tenascin-C [261]. Mechanical stimulation at a frequency of 1 Hz and 5% strain in the form of cyclical stretching in the long axis significantly upregulated the expression of the following genes in human-derived ACL fibroblasts: COL1A1, COL3A1, fibronectin and tenascin C [349].

6.2 Materials and Methods

6.2.1 PET scaffolds

To mimic the midsubstance of a native ligament, the fibrous component of the scaffolds was arranged to adopt a crimped parallel conformation once mounted on the bioreactor chambers. It consisted of 30 loose PET filaments anchored manually under equivalent tension to a PET frame as with the experiments in the previous chapters. The scaffold was designed to be within the mean adult human ligament dimensions, measuring 32 mm H x 12 mm L.

6.2.2 Bioreactor working conditions

An EBERS TC-3 mechanical stimulation bioreactor (Don Whitley Scientific, Spain) was used to apply dynamic stimulation to individually clamped PET unmodified and modified scaffolds. The TC-3F deformation system used for this study was composed of a single tension compression chamber, a TC3-F Control Software, rod like sample grips, chamber port, load cell with a maximum capacity of 50 N, a central attachment and lateral adjustable attachment kit to provide support and transmit motion between the actuator and the chamber (see figure 6.2). The bioreactor was kept in a vertical position inside a NUAIRE CO_2-Air Jacketed Incubator at 37˚C, with a relative humidity of 95% and CO_2 level of 5%. A 22 µm filter was incorporated to the chamber to ensure sufficient gas exchange.

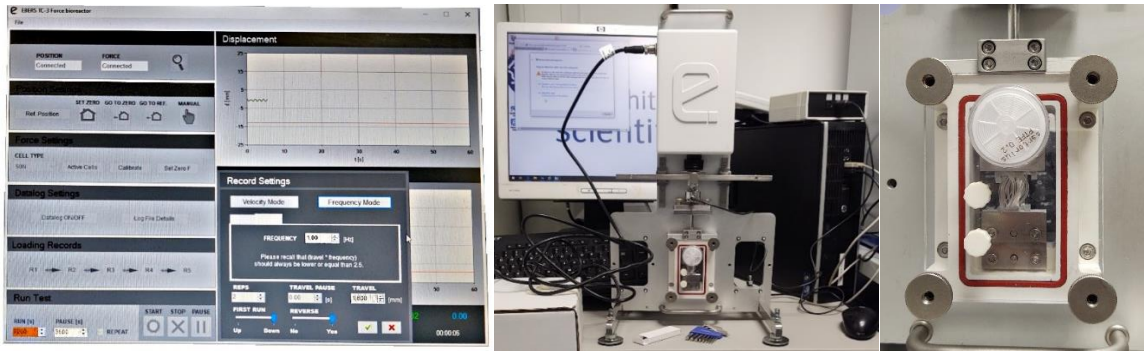

Figure 6.2 EBERS TC-3 software, cyclic tensile bioreactor, and its single chamber.

Three conditions were tested: a) unmodified PET scaffold as control, b) PET scaffold treated for 1-min with O_2 plasma, and c) 1-min O_2 plasma pre-treated PET scaffold

impregnated with 1% CS-g-GMA / 1% HA solution. The cyclic tensile strain was set at 5% at a frequency of 1 Hz. The samples were subjected to cyclic strain for 2 h (cycle 7200 s - pause 3600 s), 8 runs a day for either 24 or 48 h (see figure 6.3). Six scaffolds were tested for each condition, 3 of which were in static culture and 3 of which were in the dynamic culture regime. The separable bioreactor parts were sterilized by autoclaving at 120°C for 22 min prior to use.

In addition, a one-cycle experiment was done to compare the effect of a frequency of 0.5 Hz versus 1 Hz on ECM deposition on the coated scaffolds. A short run of one cycle at 0.5 Hz was also performed on untreated samples as a control.

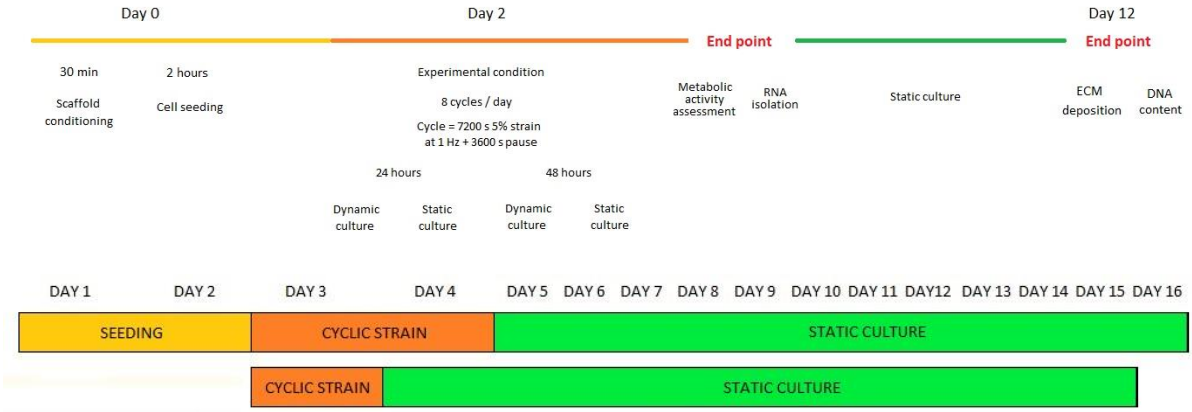

Figure 6.3 Experimental plan timeline. The scaffolds were subjected to either 8 or 16 cycles commencing on the second day after cell seeding and static incubation. The first end point was right after the last cycle stopped. The second end point was 12 days afterwards.

6.2.3 Cell culture

Cell culture was carried out as described in Chapter 3. The scaffolds were seeded with 500 000 iMSCs in total (cell density of 75 000 cells/ cm^2). The cells were left to attach for 2 h before full standard culture medium was added. They were then incubated in static standard culture conditions for two days before the start of the experiments. For each test condition, one scaffold was then carefully placed into the bioreactor, and one was kept in the 6-well plate.

6.2.4 Spectrophotometric assays

To assess cell viability after the dynamic culture regimes, a PrestoBlue assay was carried out as previously described. After carefully transferring the scaffolds in the dynamic and static cultures, one third of each scaffold was cut from the whole, washed in PBS and placed into a sterile 6-well plate. Figure 6.4 is a schematic representation of the scaffold's sectioning. After metabolic activity reading on the day of the dynamic culture regime termination, the scaffolds were further cultured in static conditions for 12 days. On day 12 after the bioreactor regime, the scaffolds were removed from their wells, divided in two equal parts and each part was transferred to a sterile 24-well plate for the assessment of extracellular matrix deposition.

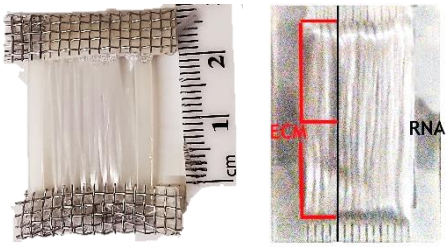

Figure 6.4 Scaffold used for the bioreactor experiments and schematic representation of the experimental purpose for each section of the scaffold.

Quantification of sGAG in the unmodified and modified scaffolds was performed with DMMB assay as previously described.

The same solution was used to determine the DNA content by using the Quant-iT PicoGreen dsDNA Assay Kit as a measure of cell growth and sustained vitality twelve days after mechanical stimulation.

Soluble and insoluble collagen deposition were quantified by the Sircol soluble and insoluble collagen assays (Biocolor Ltd., UK) as per the manufacturer's instructions. Collagen was solubilised and calculated as previously described. A normalisation factor was applied to standardise the measurements among the samples by dividing each sample's weight by the highest weight value – which was given a value of 1 –, and then dividing the µg of collagen by the weight normalisation factor to achieve a value of the µg per gram of scaffold.

For the quantitation of insoluble collagen following cold acid-pepsin to soluble denatured extraction, all the scaffolds were weighed, 20 mg of each residual scaffold

were taken and placed into screw capped collagen round bottom 2 mL digestion tubes. The scaffolds were incubated in a temperature-controlled water bath at 65˚C for 3 h after adding 1 mL of fragmentation reagent. To facilitate sample digestion, the tube contents were vortexed at 30-min intervals during incubation. Next, the tubes were centrifuged for 10 min at 12,000 r.p.m. Denatured collagen standards were prepared (0-60 µg). For the test, 100 µL of the transparent supernatant of each sample were transferred to 1.5 mL conical microcentrifuge tubes, Sirius red dye reagent was added, and the samples were processed in the same manner as the soluble collagen samples. The standards for both insoluble collagen and soluble collagen assay were read using the same microplate reader and the same settings. For the insoluble collagen data, a correlation factor of 2.2 was applied to adjust the denatured collagen dye binding (45%) to that of native collagen.

6.3 Results

6.3.1 Forces and displacement

The same 5% strain was applied in both 24- and 48-h regimes, which was equivalent to a 1.6 mm displacement (see figure 6.5).

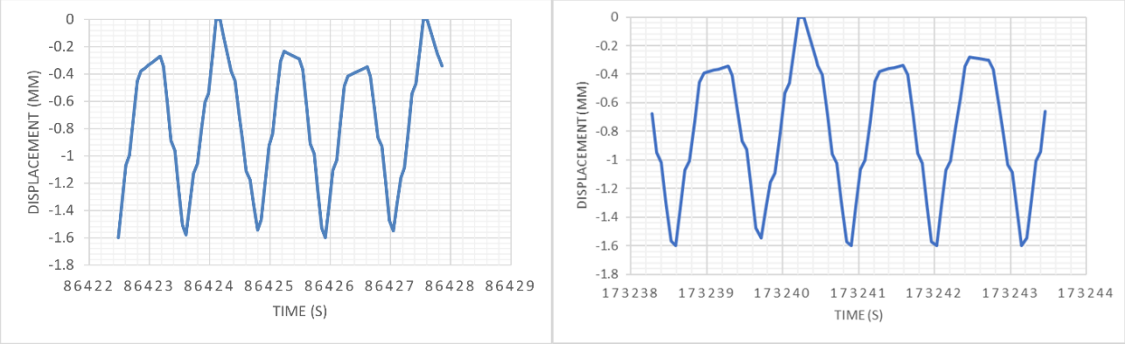

Figure 6.5 Representative graphs of a 24- and a 48-h regime strain applied.

The forces applied to samples were measure after calibrating the 50 N load cell located at the top of the actuator. Figure 6.6 illustrates the profile of forces applied on scaffolds as an average for the readings of the triplicates throughout the entire duration of their respective dynamic culture regimes.

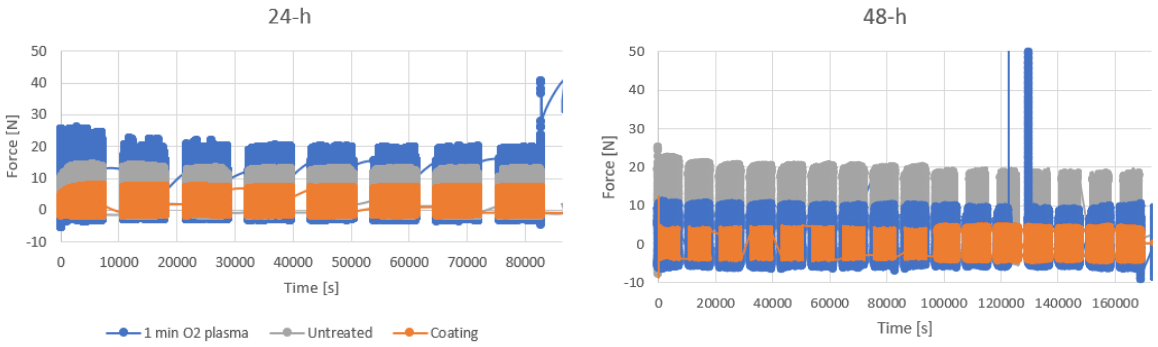

Figure 6.6 Force profile of 24- and 48-h regimes. Average of forces applied to the scaffolds throughout their dynamic regimes. Gray = untreated; blue = O_2 plasma treated; orange = biocomposite scaffolds with CS-g-GMA / HA coating. N = 3.

The forces applied remained constant for the different conditions, although differences were recorded for the modified and unmodified scaffolds. For the 24-h regime, the mean recorded forces were 2.33 ± 1.52 N, 4.16 ± 2.42 N, and 1.34 ± 1.08 N for untreated, O_2 plasma treated and coated scaffolds respectively. For the 48-h regime, the mean forces were 3.42 ± 2.97 N, 1.44 ± 0.60 N, and 0.6 ± 0.33 N for untreated, O_2 plasma treated and coated scaffolds respectively (see figure 6.7). A cross sectional area of 72 mm^2 was calculated for the scaffolds considering their area as an I section with the following formula:

$$Area = 2 * W * t_1 + (H - 2 * t_1) * t_2$$

Where W = width, H = height and t = thickness. The peak stress was calculated dividing the maximum force registered from the software during the loading by the cross-sectional area. There were no significant differences in peak stresses among the samples or between the regimes. To investigate the potential occurrence of conditioning of the scaffolds during the cyclic loading, measurements of the mean peak stress during the first hour of the regimes were contrasted with the same at the last hour of each regime. A relaxation of the scaffolds was apparent, with the following reduction in the applied stresses for the 24-h regime: 42.91 ± 14.40 for untreated

scaffolds; 50.90 ± 16.66 for the ones treated for 1-min with O_2 plasma; and 10.04 ± 7.925 for the coated scaffolds. No significant difference in stress relaxation among the scaffolds was found ($p > 0.05$).

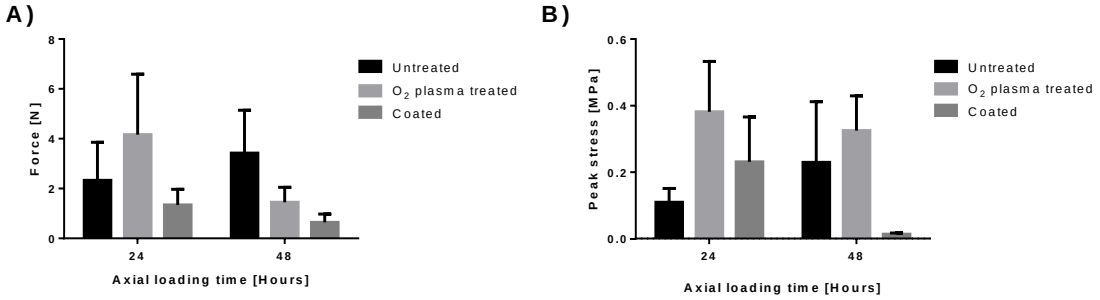

Figure 6.7 Mechanical loads applied during the axial loading regimes. A) Mean force and B) mean peak stress loads during cyclical tensile strain. The force applied on each scaffold for each axial loading regime was measured using a 50 N load cell. N = 3 except for the untreated scaffolds at 24 h and the coated scaffolds at 48 h where N = 2.

6.3.2 Uniaxial tensile loading for eight or sixteen cycles does not significantly enhance iMSC viability

Results from PrestoBlue assay from the 24-h regime showed increased viability in cells seeded onto the untreated PET scaffolds in both the static and dynamic cultures, as well as a non-statistically significant ($p = 0.9$) higher viability in the scaffolds under static conditions (see figure 6.8). There was a non-statistically significant time-dependent increase ($p = 0.9$) in cell viability as evidenced by the increased metabolic activity for the 48-h regime groups when compared to the ones in the 24-h regime. In the static groups, the increase in cell vitality was as follows: 2-fold for untreated scaffolds, 1.6-fold for O_2 plasma treated, and 9-fold increase for coated scaffolds. In the 48-h regime, there was a statistically significant ($p < 0.01$) difference between the untreated scaffolds in the static culture versus the dynamic culture. There was no other significant difference between static and dynamic metabolic activities for neither regime.

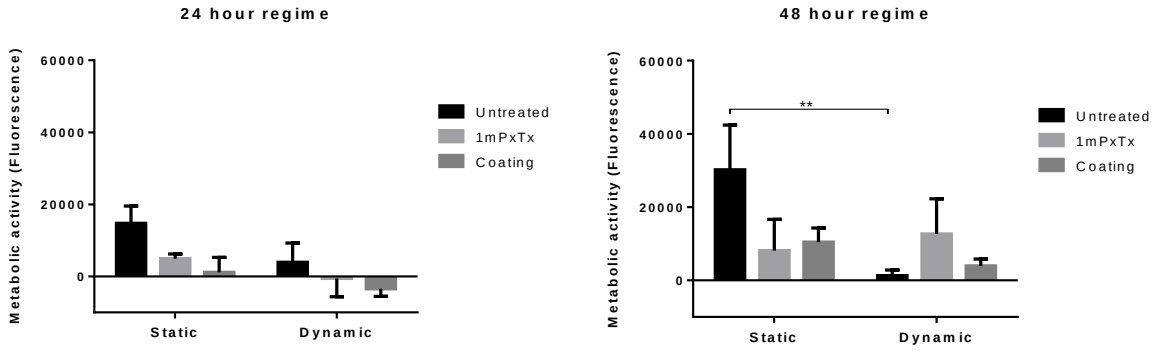

Figure 6.8 Metabolic activity after 24- or 48-h culture. iMSCs reduction of the resazurin-based PrestoBlue assay is presented as fluorescence arbitrary units. N=3.

Cell viability was sustained through the last endpoint of tissue culture as demonstrated by the DNA content on the scaffolds at day 12 after mechanical stimulation (see figure 6.9). Quantification of DNA at day 12 after either regime showed no significant differences in the 24-hour stimulation groups. For the 48-h stimulation groups, the DNA content for the scaffolds modified by 1-min O_2 plasma exposure was significantly higher ($p = 0.01$) in dynamic cultured samples versus the unmodified scaffolds. There were no other significant differences, although the DNA content was slightly higher in the static versus dynamic culture ($p = 0.6$).

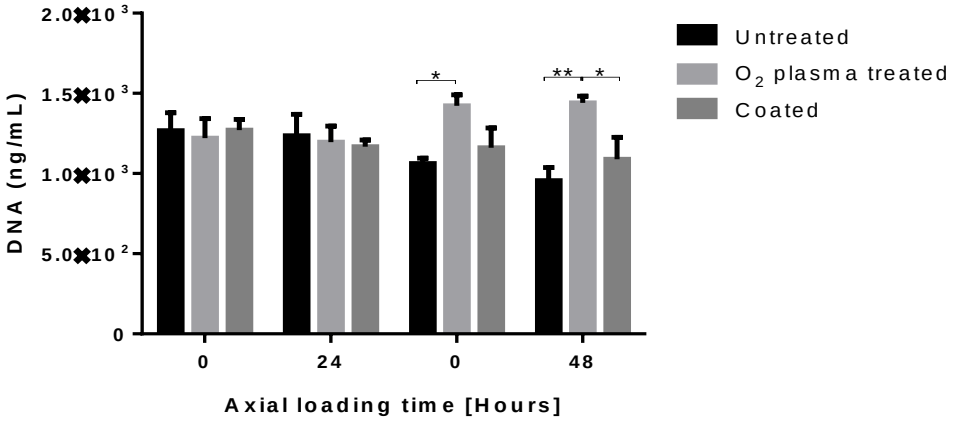

Figure 6.9 DNA content on PET scaffolds in static and dynamic culture. Significant difference was only found in the 48-hour regime. N=3.

6.3.3 Bioactive coating significantly enhanced collagen deposition as opposed to dynamic stimulation

Collagen deposition was significantly higher for the PET scaffolds coated with 1% chitosan-g-GMA/ 1% HA when compared to untreated and 1-min O_2 plasma treated samples ($p < 0.05$). There was no significant difference between static and dynamic culture groups, although the collagen deposition was slightly higher in the dynamic culture groups when compared to the static ones. After normalising the soluble collagen deposition data by grams of tissue (see figure 6.9), there was a statistically significant difference in the deposition on coated scaffolds versus untreated and plasma treated in both static and dynamic groups in the 24-h regime ($p < 0.0001$ and $p < 0.0005$ respectively) and 48-h regime ($p < 0.002$ and $p < 0.02$ respectively). There was a significant difference for the soluble collagen deposition on the coated scaffolds between the 24- and the 48-h regime for the static group ($p = 0.01$). There was no significant difference between the static and dinamyc groups for collagen deposition ($p > 0.9$).

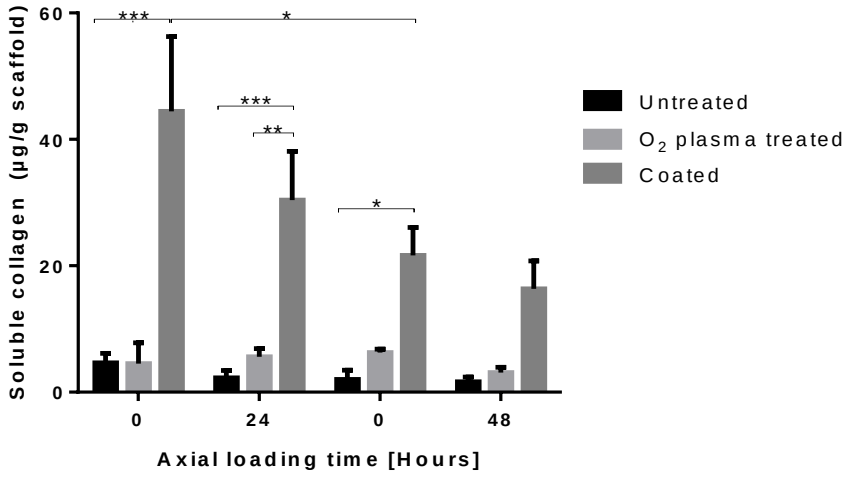

Figure 6.9 Soluble collagen deposited onto untreated, treated scaffolds and their controls at day 12 after their respective stimulation regimes. The coated scaffolds enhanced soluble collagen deposition despite the detrimental effect of the prolonged cycle loading. The data is presented as collagen content normalised by scaffold's weight. 0 = static control for each mechanical stimulation regime. N=3.

When comparing the effect of frequency and time of mechanical stimulation on collagen deposition, there was a decreasing trend in both dynamic and static groups with time and frequency (see figure 6.10). No statistically significant difference was found between dynamic and static cultures. In the dynamic coating group, there was a significant decrease in collagen deposition for both long-time regimes at 1 Hz when compared to the 2-h regime at 50 Hertz.

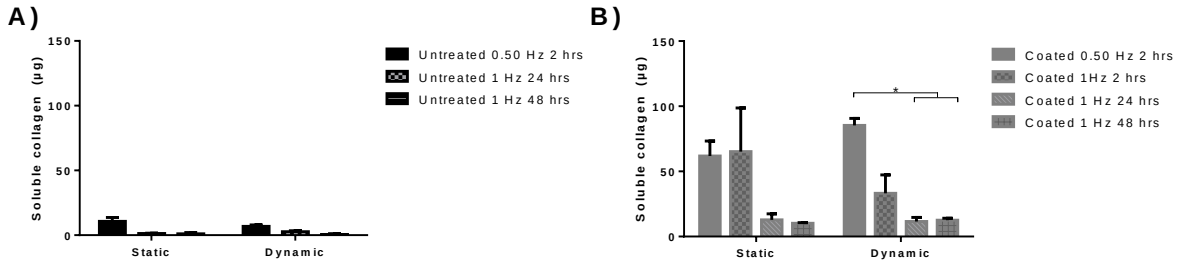

Figure 6.10 Comparison of soluble collagen deposition in A) untreated and B) coated scaffolds with different frequency and duration of the cycle regimes. The graphs show the effect of two physiologically relevant frequencies of cyclic loading. N=3 except for the coated scaffolds at 0.50 Hz where N=2.

The insoluble collagen was measured from 20 mg of the remaining scaffold's weight after soluble collagen extraction (see figure 6.11). For the 24-h regime, there was a significantly higher deposition of insoluble collagen on the coated scaffolds when compared to the O_2 plasma treated ones ($p = 0.01$).

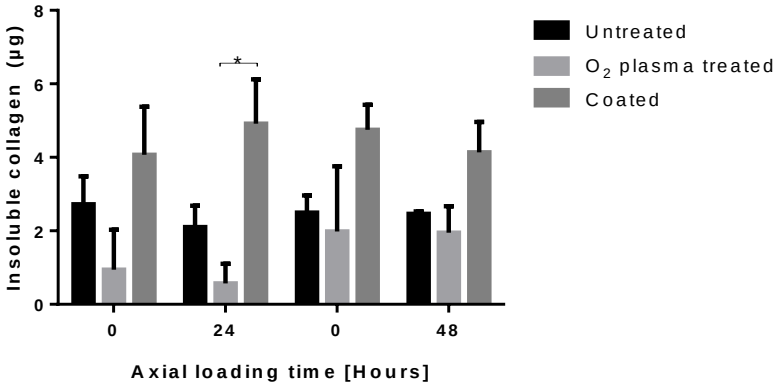

Figure 6.11 Insoluble collagen per 20 mg of scaffold. The effects of mechanical stimulation on the deposition of crosslinked collagen, reflecting maturation of the tissue. N=3.

In contrast with the effect on collagen deposition, dynamic stimulation did increase sGAG deposition for untreated and coated scaffolds in the 48-h regime (see figure 6.12). There was no statistically significant difference for the deposition of sGAG among the conditions in neither 24- nor 48-h regimes (p = 0.3).

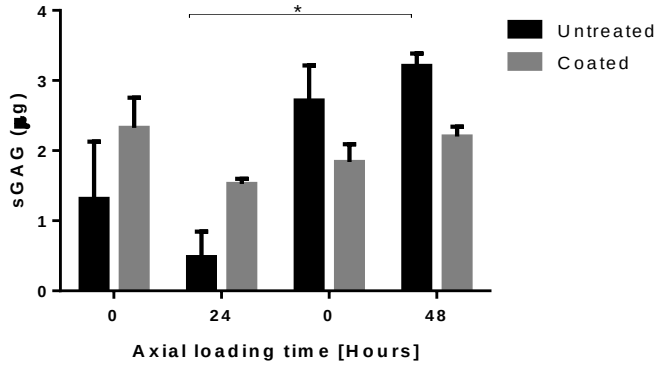

Figure 6.12 sGAG deposition at day 12 after loading regime. Analysis of sGAG production using DMMB assay showed that sGAG deposition had a contrasting response between the two prolonged cyclic load regimes. N=3.

6.4 Discussion

The static testing of the PET fibrous scaffold coated with 1% CS-g-GMA / 1% HA has presented suitable compatibility with iMSCs and a significant enhancement of their collagen deposition, along with favouring the expression of other ligament markers. The main expected outcome of a scaffold intended as a ligament surrogate for ACLR is for it to support the recovery of functionality of the tissue to ensure a safe return to pre-injury levels of activity. Early joint mobility is recognised as pivotal for a satisfactory maturation of the ligament graft after ACLR [150, 390]. Testing a potential tissue engineered ligament construct in dynamic culture offers more translatable information on how an engineered construct will affect cell behaviour once implanted. This thesis investigated the suitability of a 1% CS-g-GMA/1% HA coating of the PET fibrous ligament scaffold to sustain cell proliferation and deposition of ligament-like ECM under the influence of sustained uniaxial cyclic loading using an in vitro system (TC-3 EBERS) to control the amplitude and frequency of the displacement. The regimens of mechanical load used in this study were slightly detrimental for metabolic activity and

did not significantly enhance the deposition of collagen and other matrix proteins. Conversely, the 1% CS-g-GMA/1% HA coating did significantly increase the deposition of matrix proteins by iMSCs.

The ACL is both neurosensory and mechanically crucial to maintain knee stability. The neural components located mostly at the tibial end of the ACL confer it the task of sensing and informing the brain of the joint and limb's position, speed and acceleration in respond to tensile changes [391]. It has been extensively demonstrated that its resident cells are mechanoresponsive as well as the beneficial effect of physiologically adequate loads for ligament regeneration. Longitudinal tensile testing has been systematically used to represent the ligament material behaviour given that the main function of a ligament is to transmit tensile forces. Two actions routinely take place around an ACLR, namely the isometric and cyclic preconditioning of a graft at ACLR as well as post-operative rehabilitation. Both of which apply uniaxial loads to the ACL surrogate. Therefore, despite not providing the full multidimensional range of motions to the graft, a bioreactor delivering uniaxial cyclic mechanical loading still offers an acceptable and valuable approach to understanding the cellular behaviour on substrates subjected to physiologically relevant loading regimes. There is still some debate on the most appropriate rehabilitation protocol after ACLR where the aim is to take athletes to their pre-injury state and ability to sustain strains of 12-15% [343, 392] in correlation with the maximum tensile strain tolerated by the native ACL. In this study, all scaffolds in the dynamic groups were subjected to a 5% strain, which is in line with the Lachman test at 150 N load, which is the clinical examination of choice to evaluate the ACL [393] and with isometric contraction quadriceps-strengthening exercise at 15° [394]. Additionally, it has been suggested that shorter displacements are more beneficial for cell proliferation and ECM synthesis as the frequency of motion is increased, else, a decrease in both outcomes is expected [343]. Since the strain applied remained constant and it is proportional to the force applied, changes in the composition and cross-sectional area of the scaffolds were made evident by the force readings. The results also confirm the differences in stress for the purely PET scaffolds compared to the coated scaffolds, which showed an increase in cross-sectional area. The force applied on the scaffolds remained largely constant for each condition,

however, in both length regimes, the forces applied on the scaffolds to achieve the 1.6 mm displacement was reduced for the coated scaffolds when compared to the untreated and O_2 plasma treated. The difference was more pronounced in the 48-h regime, were a 5.7-fold decrease for the coated scaffolds was evidenced when comparing the average force applied on them against that for the untreated PET scaffolds.

After an injury, healing is promoted by the formation of new tissue as the cells synthesize, secrete and deposit ECM. In engineered 3D cultures, after the cells encounter the substrate and adhere, they release soluble proteins that affect subsequent cell signalling and function. As they expand in culture, they deposit ECM and, as a result, the amount of released growth factors and cytokines on the substrate progressively increase. At the same time, as the cortical tension is reduced, more cadherins are expressed, the intercellular adhesion becomes stronger and the attachment more stable [395, 396]. This succession of events is particularly relevant for dynamic cultures given that the adhesion process is mechanosensitive [397]. On this basis, the bioreactor experiments in this chapter were designed to begin following a two-day static incubation period to allow the iMSCs to adjust to their environment. Similar incubation periods have been followed by diverse groups prior to mechanical stimulation of 3D constructs for ligament TE [337, 398-401].

As a measure of viability and cell proliferation, the reduction power of the seeded iMSCs of the resazurin-based solution showed a general increase in metabolic activity after 48 h in culture when compared to the 24-h regime ($p = 0.03$). For the cells on the untreated scaffolds in static culture, there was a 48% increase in metabolic activity. In comparison, the increase in this parameter for the cells on the coated scaffolds was of 10.92%. For the coated scaffolds, there was a decrease in proliferation for the dynamic group in the 24-h regime, but the maintenance of viability under the dynamic conditions explored in this study was demonstrated by the statistically significant difference in metabolic activity ($p = 0.05$) between the 24-h regime and the 48-h regime and the absence of a significant difference when compared to the untreated scaffolds under dynamic culture ($p = 0.2$ for 24-h regime, $p = 0.3$ for 48-h regime). Our results of a

decrease in mesenchymal stem cells proliferation for untreated and coated scaffolds at 5% stain and 1 Hz cyclic stretch are similar to those found from Sun et al. [343]. In contrast, the scaffolds only treated with oxygen plasma treatment showed a 1.2-fold increase in metabolic activity in dynamic culture when compared to their static controls.

To maintain their biomechanical properties, ligaments respond to mechanical stimulation by sustaining adaptive changes that affect the continuous degradation and synthesis of extracellular matrix components [402]. As this response is directly related to the increase or decrease in loading, both amplitude and frequency in a bioreactor system play a substantial role in collagen and sGAG deposition. sGAGs closely interact with proteoglycans in ligaments to reinforce the structural stability of collagen fibrils and stimulate the cell migration enhancing tissue repair [47]. Experiments with decellularised tendons and flexible-bottom culture plates [385, 403] have shown that there is an effect of mechanical stimulation on the synthesis of sGAGs. Since the sGAG content differs with levels of physical activity, it was relevant to consider the effect of prolonged cyclic loading on their deposition. Mechanical stimulation modulates extracellular matrix formation of the musculoskeletal connective tissues[404-407]. Soluble and insoluble collagen were quantified to investigate whether the mechanical stimulation regimes chosen would amplify the enhancement of collagen deposition evidenced on the previous chapter. It is known that as a ligament graft matures, there is a balance of soluble and insoluble collagen. Therefore, the effect on both newly deposited and crosslinked collagen deposited onto the bioactive scaffolds were quantified. In a human experiment, a one-hour regime of intensive knee activity showed a 1.7-fold increase in the synthesis of collagen in tendons [404]. Ligaments adapt to loading by a controlled matrix turnover response to loading. While normal physical activity has been shown to lead to collagen synthesis and deposition, mechanical overload can cause fatigue and damage to the matrix [408]. Ligament cells transduce excessive mechanical stress into the inhibition of gap junction permeability, which in turn inhibits collagen synthesis [378]. In accordance with these data, the results presented in this chapter demonstrated that on the proposed composite scaffolds, a single 2-h cycle of mechanical stimulation at 0.5 Hz had a 2.56-fold increase in soluble collagen deposition when compared to the same 2-h cycle at 1 Hz. Moreover, the 1 Hz

regime lasting 2-h demonstrated a 2.87-fold increase in soluble collagen deposition when compared to the 24-h regime at the same 1 Hz. Our results provide information to support the benefit of formulating the immediate regular rehabilitation sessions after ACLR with exercises proven to be limited to 5% strain at 0.5 Hz for two hours [339, 409, 410]. A non-statistically significant decrease in collagen deposition was found when increasing the frequency of the mechanical load to 1 Hz, resembling that from running stride frequency in humans. Although a significant increase in soluble collagen deposition was found throughout the regimes for the bioactive composite scaffold when compared to the untreated PET controls, there was a marked decrease in this deposition as the cycles increased from one to eight and 16. In contrast, insoluble collagen did not seem to be affected by mechanical stimulation.

The analysis of temporal expression of ligament-specific genes after mechanical stimulation has consistently evidenced an increase in COL-I, COL-III and tenascin-C that is linked to the times of mechanical exposure and culture. However, given that nearly all studies focus on short time or spaced tension cycles, more information is needed to substantiate the deleterious effect of axial cyclic loading past certain thresholds. The correlation of gene expression with our finding on ECM protein deposition was planned for this chapter. Two-thirds of the scaffolds were separated for RNA extraction immediately after the end of each bioreactor regime's last cycle to analyse the regulation of synthetic and degrading biochemical pathways promoted by the explored loading regimes. As the previous static tests demonstrated an enhanced ECM protein expression, it was hypothesised that there would be an increase in ligament related genes and a decrease in catabolic markers from the cells seeded onto the bioactive scaffolds in response to the mechanical stimulation. Supported by what other studies have reported. A conventional RNA isolation protocol was followed; however, time-constraint challenges arose with the optimisation of the RNA extraction from the bioactive coating of the fibrous scaffolds. In polysaccharide-rich biomaterials, nucleic acids form ionic complexes with the matrix that lead to a low yield of RNA. This outcome could be due to RNA loss by either entraining it to the discarded phase during phase separation or co-precipitating with the RNA [411-413]. Alternative options to the conventional guanidinium thiocyanate are part of an ongoing investigation. The use of

an extraction buffer based on cetyltrimethylammonium bromide has proven to produce sufficient RNA with good purity for downstream applications from MSCs embedded in chitosan matrices, agarose matrices and pure collagen gels [411, 414]. To overcome starch / polysaccharide solidification, another method to test is an SDS-Phenol based extraction and RNA precipitation with sodium acetate and LiCl [412].

6.5 Conclusion

Continuous and prolonged uniaxial cyclic strain at 1Hz has a negative effect on initial MSC viability. A 2-h period of mechanical stimulation at 0.5 Hz further enhances the MSC collagen deposition onto PET fibrous scaffolds coated with 1% CS-g-GMA / 1% HA. The proposed bioactive composite scaffold enhanced collagen deposition by MSC cells under dynamic and static conditions and supports MSC viability.

Chapter 7

In vitro effect of low-intensity pulsed ultrasound on viability and ECM deposition by MSCs and ACL cells for ligament TE

Aims: To evaluate the effect of low intensity pulsed ultrasound stimulation on the viability and ECM deposition of MSCs and native ligament cells seeded onto the biocomposite scaffolds.

Hypothesis: Low intensity pulsed ultrasound enhances MSC and native ligament cells viability and ECM deposition.

7.1 Introduction

As previously mentioned, ligaments undergo several types of mechanical stresses. Although the dominant force applied to ligaments is the tensile force, these tissues come across shear forces especially during hyperextension and low flexion of the knee [30]. In fact, the discontinuation of the popular use of synthetic ligaments came about mainly due to their inferior resistance to friction that led to abrasive wear [415]. Moreover, ligaments vibrate due to the transferral of shock loads while doing everyday activities such as running or driving, that are minimised by muscles, fat, and vascular components to prevent negative effects of higher vibration amplitudes at prolonged durations [416-420]. Low-intensity pulsed ultrasound (LIPUS) is a therapy used for healing musculoskeletal tissues that interacts with both types of mechanical stimuli.

Outcomes of ACLR depend on a variety of factors that have been mentioned in the earlier chapters of this thesis. Some of the unfavourable outcomes are tied to the

selection of the graft. The proposed bioactive composite scaffold has been proven to enhance ECM deposition by MSCs, which are a population of cells that can be found in the remnant of the injured ACL. At present, athletes and the general population alike are increasingly aware of ACL injuries and their treatment. This situation makes it even more possible to find a viable thick ACL stump at the time of ACLR. Migration of both stem cells and native mature fibroblasts is expected after implantation of the graft when combining it with a remnant preservation [421] or remnant incorporation [422] ACLR. These surgical techniques are promising in terms of graft healing as they enhance cell proliferation, revascularisation and regeneration of the proprioceptive organs in the bioactive composite scaffold [423]. Since native ACL cells have been shown to differentiate according to their location within a graft, the ideal maturation of the bioactive graft could be achieved by promoting migration of the native cells from the ACL stump and infiltration assisted by the rehabilitation techniques. One such promising rehabilitation technique is LIPUS.

To aid healing after ACLR, LIPUS has been used as part of the rehabilitation protocols [424]. The use of LIPUS in the present thesis also offers an additional dynamic stimulation scenario to explore the influence of our proposed bioactive composite scaffold on cell behaviour under physiologically relevant conditions. LIPUS is gaining interest as it could be an accessible therapy for patients recovering from an ACLR. Therapeutic ultrasound (US) for soft tissues has mainly been studied in animal models, and it had shown to increase cellular activity, ultimate tensile strength, and stiffness of healing tendons as well as to reduce OA markers [425-427]. Highly relevant to the successful return to sports for an athlete is their interest in actively participating in their recovery [428]. The fact that LIPUS is considered a safe treatment for soft tissue healing due to it being non-invasive and having minor thermal effects [429, 430], make it a very promising tool for ACL injury rehabilitation and warrants the investigation of its effect in the bioactive composite scaffold’s ligamentisation [429].

7.1.1 Graft healing after ACLR

After ACLR, the ACL graft goes through four phases of healing to culminate in tissue integration [24, 431]. At first, the graft undergoes ischaemic necrosis during the acute inflammatory process characterised by hypocellularity. During the early necrotic stage, cytokines such as tumour necrosis factor- (TNF-) α, IL 1-β, IL-6, and chemokines are released from the remnant tissues and some host immune cells – particularly neutrophils and macrophages – along with the local native MSCs begin to migrate towards the graft [432]. As cell recruitments starts to occur and chronic inflammation sets in, revascularisation of the graft starts to happen. Cell migration and proliferation follows, with the accompanying persistent release of growth factors and further chemoattractants. During this remodelling stage, the ECM is synthetised. There is hypercellularity consisting of mesenchymal stem cells and short-lived activated fibroblasts. At first, the amount of small collagen fibres increases in comparison to the large ones. At the insertion sites, Sharpey-like fibres form to integrate the graft to the bone. Finally, the ligamentisation phase ensues with the maturation of collagen and transformation into a native-like ACL tissue. [431, 432]. This last phase never fully concludes in a replica of the original ACL tissue, although cellularity and mechanical properties come close in most cases [433]. Osseointegration happens with the mineralisation of the proximal and distal ends of the graft, while at the midsubstance small collagen fibres replace the previously abundant large ones [432].

7.1.2 Native ligament cells in remaining ACL stump

As mentioned before, the different regions of an ACL hold different compositions of cells. Proximal to the tibial ligament insertion the ACL cells' morphology resembles chondrocytes the most. The midsubstance of the ligament is typically inhabited by fibroblasts with a high expression of the basal ligamentous differentiation-related genes COL1A1 and tenascin C [21, 434]. Nucleated cells from the ACL stump have been successfully isolated and identified as MSC after demonstrating that they possess multilineage differentiation potential, surface markers – were negative for CD34 –, adherence ability and an MSC morphology [24, 25]. Another subset of stem cells, vascular-derived positive for CD34, has been identified in the ACL stump [434]. Native

ACL cell distribution along the graft relies on the relation and regulation between stem cells and their local microenvironment.

7.1.3 Ultrasound in medicine

Ultrasound refers to acoustic waves in the frequency range above 20,000 Hz. Acoustic waves are mechanical radiations originated from the rapid motion of molecules within a compressible medium such as fluids [435]. Whitin an ultrasound transducer, a piezoelectric crystal – employed in most cases – deforms when a voltage produces a mechanical strain on it, leading to the conversion of electric to acoustic energy [436-438]. The pressure wave generated by US is transmitted to the tissue by molecular vibrations and collisions [438]. When referring to the use of US, the power – expressed in watts – indicates the total amount of energy in the US beam and the intensity – expressed in watts/cm^2 – denotes the US delivery rate per unit area of the transducer's surface [436].

Acoustic waves travel at about 1,540 m/s in tissues – which is affected by the lipid and protein tissue contents –. As the US beam encounters resistance the waves are reflected and scattered, causing wave attenuation. Attenuation is the decrease in US waves while they travel through the medium. It is also caused by absorption, when part of the energy is converted into heat [439, 440]. US generates mechanical forces called acoustic radiation forces (ARF) when momentum is deposited into the medium as it passes through, most notable at higher intensities and pulse durations. The transference of energy by US occurs as heat generation, with the application of ARFs and in acoustic cavitation when US interacts with bubbles [440, 441]. US propagation is sustained by the interchanging cycles of compression and expansion undergone by the molecules of the transmitting medium [442].

The use of US in healthcare encompasses diagnosis, surgical and medical treatment. The differences in frequency and intensity ranges are wide among it uses. For diagnostic purposes, the intensity is low to avoid heating the tissues excessively and it ranges from 0.5 – 5 W/cm^2 with frequencies in the range of 3 to 100 MHz. In surgery, it is used as an ablation technique in the form of shock waves and the intensity

employed fall within the range of 0.05 – 27,000 W/cm^2. In the context of high frequency destructive ultrasound for tissue irradiation, an intensity of 10,000 W/cm^2 has been applied for the ablation of cancerous tissue [443]. Concerning the therapeutic use of ultrasound, the usual range of intensity utilised is 30 to 70 W/cm^2 with frequencies ranging from 0.02 to 20 MHz [444-446]. In LIPUS, US has on / off cycles to minimise heating effects. To neutralise reflexion of the waves at the interface between soft tissues and air, water, oils, or gels are used as coupling media [436].

7.1.3.1 Therapeutic ultrasound

Therapeutic US is classified according to its biophysical thermal or non-thermal effects [447, 448]. The thermal effects of US are caused when applying a continuous US at intensities around 1-300 W/cm^2 by absorption in the tissues of the energy produced by the sound waves [437]. When US is applied, the vibrational energy is converted into heat. As the tissues absorb this energy, the US waves are reduced in amplitude as a function of the distance travelled through the tissue. Therefore, the type of tissue treated defines the intensity required. The physiologic influences of thermal ultrasound are an increased tissue temperature, increased collagen extensibility, increased blood flow, increased enzymatic activity, decreased muscle guarding, increased nerve conduction velocity, increased pain threshold [436]. The non-thermal effects are a result of cavitation, microstreaming, and acoustic streaming [449]. Depending on the intensity, duration and continuity of US waves, the cells can experience mild membrane disruptions, deformation, short-lived membrane poration, or lysis [442]. The reason for the bioeffects of ultrasound being heterogenous is the happening of non-inertial cavitation. This phenomenon occurs when microbubbles or gasses dissolved in the fluid medium, continuously oscillating in response to the changes in acoustic cyclic pressure, change their shapes and sizes and collapse, generating convective motion, liquid jets, and shear stresses along their path. The impact of this phenomenon on cells depends on the distance between the cells and these events [442].

7.1.3.2 Mechanism of LIPUS

When cells come into contact with acoustic waves' elastic deformations propagated in the medium, cells experience the ARFs due to pressure gradients, scattering, and absorption as well as from the fluid flow caused by the transfer of the momentum to the medium – or acoustic streaming – [441]. Secondary forces are also present as the waves produce interaction between adjacent particles and force exchange [441]. The vibration triggered by acoustic waves induces membrane and matrix deformations as [450] (see figure 7.1). The complex network of cell organelles senses extracellular stresses through the cell membrane transducing the signal that results in the intracellular effects of ultrasound [442]. In the previous chapter the implication of Ca2+ influx in mechanotransduction was commented. Just as with tensile stretching, ultrasound stimulation increases intracellular Ca2+. With continuous sonication at 1 W/cm^2 and 1 MHz central frequency, it does so by temporarily permeabilising the cell membrane, causing nuclear pore complex (NPC) opening and allowing the passage of macromolecules [451]. The effect of the mechanical effect of LIPUS vary according to the parameters chosen for the delivery of the stimulus and it is still not fully understood whether they are the result of direct transduction to the nucleus or through the cytoskeleton, or to what extent the biological effect observed is a result from the externally applied forces or as a response to the internally generated forces – the deformation of the matrix – [442, 452].

After ACLR, LIPUS has been mostly used to treat the tendon-bone interface. LIPUS is an established therapy for bone healing. It has been shown to increase the levels of alkaline phosphatase, osteocalcin secretion and enhance the expression of osteogenic genes cbfa-1/RUNX2 and osterix [453]. Osteogenic differentiation has also been evidenced, with a significant increase in the expression of bone morphogenic proteins BMP-2, BMP-4 and BMP-6 after LIPUS [453]. In bone fracture healing, an increase in the levels of SDF-1 and CXCR4 expressions in MSCs have been demonstrated after applying LIPUS at 1.5 MHz and 0.3 W/cm^2 [453]. This effect results in MSC migration to the fracture site, which was associated with an increase of local and serum stromal cell-derived factor-1 (SDF-1) level [454, 455]. SDF-1 is a chemokine of stem cell

migration before proliferation and expansion in the bone marrow. In the ligament, SDF-1 seems to play a crucial role in cell homing [456]. An increased level in SDF-1α expression in synovial fluids has been detected up until the first month after an ACL injury, when it is most crucial to fulfil its role in attracting leukocytes to the injured site [457].

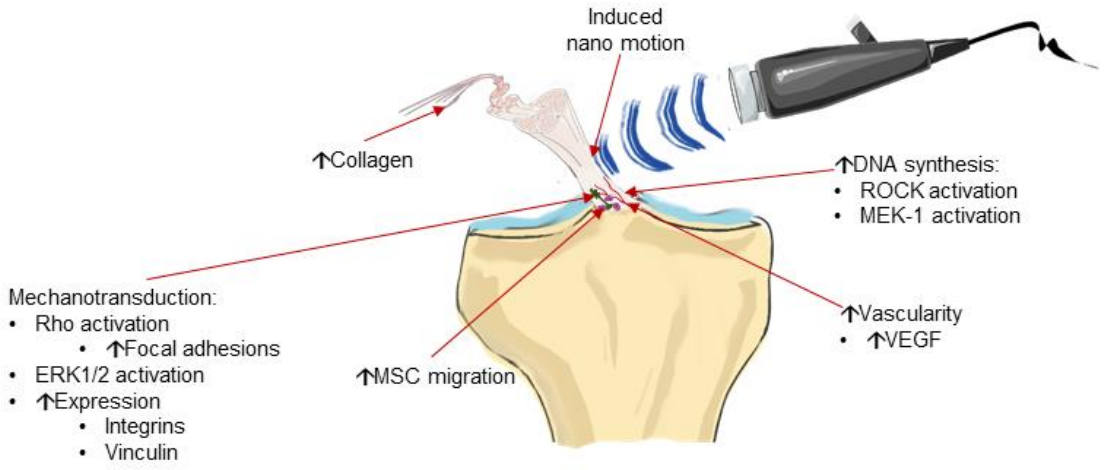

Figure 7.1 Mechanism and effect of LIPUS in ligament healing. Clinically, a LIPUS transducer is placed on the skin above the healing ligament and the ultrasound waves emitted produce nano motion in the tissue. Integrins in the tissue translate the motion into a chemical cascade. Image made with Servier Medical Art under a Creative Commons Attribution 3.0 Unported License.

7.1.3.3 LIPUS in ligament rehabilitation

Just as with exercise, certain intensities of LIPUS heighten cellular metabolism and direct cell adaptation. LIPUS has been used at intensities ranging from 0.1 to 1 W/cm^2 for the treatment of soft tissue injuries with promising results. It has demonstrated to alter tissue biomechanical properties, improve collagen alignment, and stimulate cell proliferation [458]. Among the effects of LIPUS observed regarding ACL tendon-bone graft stimulation, local blood perfusion and angiogenesis are improved, it enhances cartilage maturation, promotes the proliferation of osteoblasts and the osteogenic differentiation of MSCs [459].

At present there have not been any studies reporting on the effects of LIPUS on an ACL tissue engineered scaffold. The interest in LIPUS and its role in treating ligament injuries is increasing. Nonetheless, research efforts to date have focused on bone-tendon healing, giving no information on the effects of LIPUS on a ligament graft's midsubstance [459, 460]. Its widespread use by physiotherapies for soft connective tissue injuries has shown benefits such as an improved rate of healing and tissue strength [461]. In vitro, bone protein synthesis and enhanced calcium uptake have been demonstrated. The analysis of the effect of LIPUS on the growth and ECM deposition of human mesenchymal stem cells and ACL cell will contribute to expand the knowledge of cellular processes involved in the ligamentisation of a tissue engineered graft and the information presented here can inform new strategies to improve wound healing of damaged tissues.

7.2 Materials and methods

7.2.1 Isolation and culture of ACL-derived cells

Human ACL fibroblasts were isolated from ACL tissue obtained from skeletally mature patients undergoing either an ACLR or a total knee replacement at University College Hospital (London, UK). Informed consent for the use of the discarded and anonymised material was obtained from each patient prior to each ligament specimen collection (Ethics approval G12-42506). The human adult ACL tissues were transported in sterile saline solution at room temperature. The excised ACL tissues (N = 14) were each separately minced into small pieces approximately 1 to 2 mm^3, washed 3 times in PBS, and then digested with 0.4% collagenase type I (0.4% w/v) in DMEM / F-12 supplemented with 10% FBS and 1% penicillin / streptomycin / amphotericin B (standard medium) on continuous gentle rocking agitation overnight at 37ºC. Cells were centrifuged at 1000 g for 5 minutes and resuspended in medium, passed through a 70-µm pore size nylon filter, washed 3 times with the same medium and seeded in individual T-25 flasks. Isolated cells from each patient were separately cultured for 2 – 3 days in the standard DMEM/F-12. Cells were passaged and monitored for differences in morphology and growth rate. They were frozen and stored in liquid nitrogen until required for the experiments. No cells were pooled for any experiment.

7.2.2 Cell culture

Human ACL cells between passages 3 - 4 were used throughout the initial experiments for comparison against HDF. Wells and scaffolds were pre-conditioned with full media and incubated at 37 ºC for 10 min before seeding. The cells were seeded at a density of 2 x 10^4 cells/cm^2 either directly onto the 24-well plates TCP surface or PET films and cultured using culture DMEM/F-12 supplemented medium as previously stated.

Immunohistochemistry was performed at day 7 to assess the fibroblast expression of COL – I and COL – III.

HDF were used to compare the ACL cells isolated from human samples to the typical fibroblast morphology and fibroblast collagen deposition. The cells were seeded onto 2D surfaces – TCP and untreated PET films – and examined with light microscopy and fluorescent microscopy to appraise actin and nuclear staining, and immunocytochemistry.

Human ACL cells and iMSCs were seeded as described in previous chapters onto 14 mm PET fibrous scaffolds unmodified and coated with 1% CS-g-GMA/ 1% HA after 1-min O_2 plasma pre-treatment. The seeded scaffolds were incubated at 37 °C in a 5% CO_2 incubator for two days before beginning the experiments.

7.2.3 Ultrasound devices

After careful analysis of the literature on the previous use of LIPUS for soft tissue experiments, a frequency of 1 MHz was selected for the peer reviewed benefits published for musculoskeletal tissues [438]. For the initial experiments, a sonoporator SP100 (Sonidel, UK) was used (see figure 7.2 A). The operating frequency was set to 1 MHz and the LIPUS was applied with a 2 cm^2 transducer with an effective radiation area (ERA) of 1.5 cm^2. The ERA refers to the cross-sectional area of the ultrasound beam. Each well was treated with for 30 s with a US power density of 0.5 W/cm^2, and a duty cycle (DC) of either 25% or 50% at a pulse repetition frequency of 100 Hz. Ultrasound gel was used to mediate the contact between the ultrasound transducer and the bottom of individual wells of the 24-well plates. After obtaining preliminary results favouring a 50% duty cycle, a Sonopuls 490 (Enraf Nonius, NL) was used to further

test the effect of different intensities of 0.5 W/cm^2, 0.3 W/cm^2, 0.1 W/cm^2 at a set DC of 50% for the same cycle duration of 30 s and same frequency of 1 MHz (see figure 7.2 B). The Sonopuls 490 was also used for the treatment of cells cultured in an incubator with an oxygen tension of 5%.

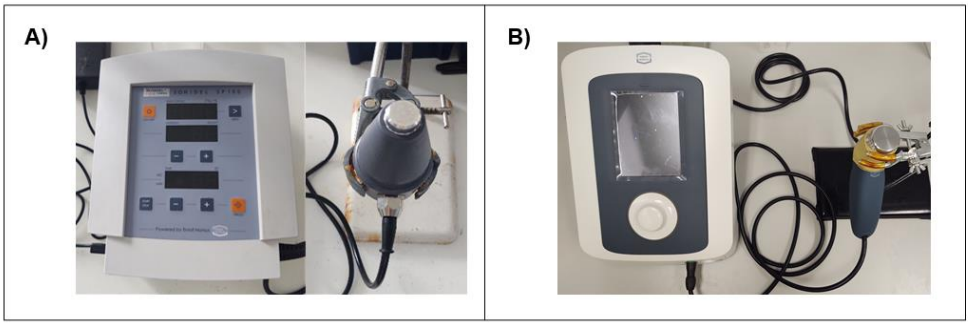

Figure 7.2 LIPUS devices. Individual wells were treated with LIPUS at a frequency of 1 MHz and varying duty cycles and intensities with either a A) SP100 sonoporator or a B) Sonopuls 490 LIPUS device.

7.2.4 Assessment of LIPUS effects on bioactivity

Prior to culturing the cells to test growth and ECM production, a cell viability assay was carried out with LIVE/DEAD™ Viability/Cytotoxicity Kit at day 1 after a pre-culture period of either 1 or 2 days, and after LIPUS treatment on a pilot duration treatment of either 30 s or 1 min. This test was conducted to ensure that cells remained attached and did not undergo apoptosis after the mechanical stimulation provided by the close contact with the LIPUS transducer. For the test, the cells were first washed with 1 mL PBS. Next, 200 µL of the LIVE/DEAD™ reagent (2 mM Calcein AM, and 4 mM EthD-1 solution diluted in tissue-culture grade PBS) was added to each sample and they were incubated in the dark at room temperature for 40 min. The cells were washed with PBS and fluorescent images were taken using an inverted EVOS fluorescence microscope. It is a stablished fact that variations in cellular behaviour and response to any stimulus exist among living organisms [462]. In clinical settings, this applies to treatment tolerance responses from patient to patient. *In vitro*, experiments with primary cells must account for this variation for the purpose of translatability of the results. To address this matter, the variations of DNA content from three different patients were

analysed for a 21-day culture period. A Pico Green assay was used as previously described.

For the LIPUS experiments, metabolic activity was evaluated for a 14-day period with a PrestoBlue assay to monitor cell growth. Cell morphology, interaction with the scaffolds and ECM deposition was assessed by SEM imaging at days 1, 7 and 14 for iMSC and at days 1 and 14 for ACL cells. Collagen deposition was assessed at day 14 after LIPUS treatment via a Sircol soluble collagen assay. sGAG deposition was assessed with a DMMB assay. For each treatment, nine scaffolds (N=9) were seeded with human ACL cells at passages 6-8 and nine scaffolds (N = 9) with iMSCs for the 1% CS-g-GMA / 1% HA PET fibrous scaffolds and their untreated controls.

7.3 Results

7.3.1 Cell isolation

7.3.1.1 Isolated cells from human ligament specimens display a fibroblast phenotype

Morphology of the ACL cells retrieved from human ruptured and intact ACL samples was assessed by light microscopy (see figure 7.3). The ACL cell morphology started to become spindle shape fibroblast like from passage 3 – 4 for all the isolated samples (N = 14).

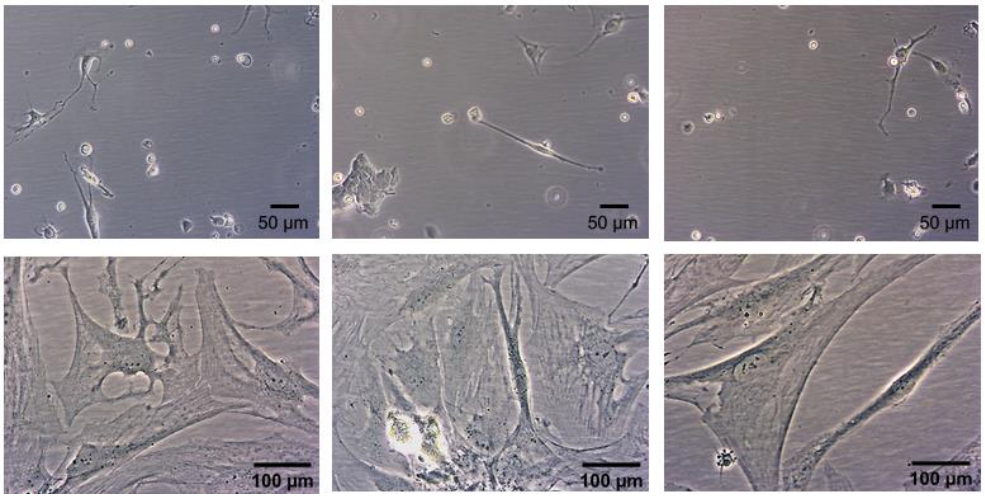

Figure 7.3 Human ACL cell morphology after isolation until confluence and before the first passage.

Statistically significant variations in DNA content from sample to sample occurred for the 2D test on TCP. Akin to the results shown in chapter 4 of this thesis, the cells grow at a higher rate on surfaces that are less hydrophobic than PET (see figure 7.4). Other than the considerable discrepancy in cell growth for the cells seeded onto different substrates, there seem to be no significant heterogeneity in DNA content throughout the period of culture for the ACL cells seeded onto PET films. Cells from two patients were used for the subsequent experiments. The cells were not pooled.

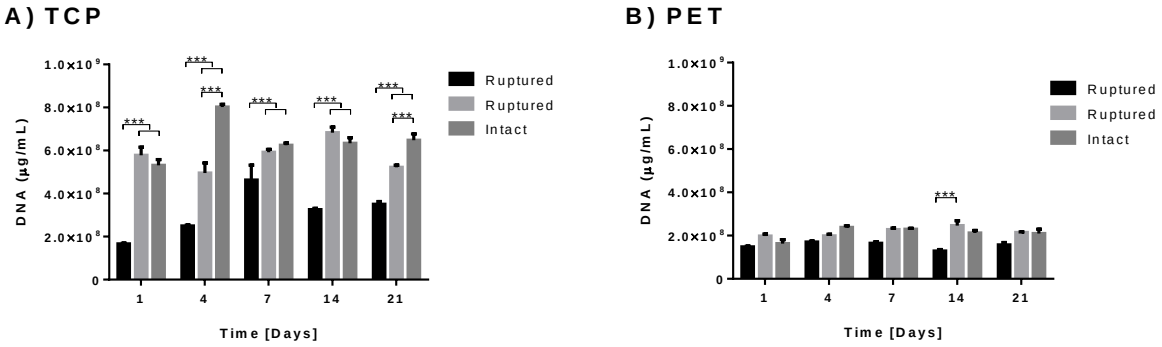

Figure 7.4 Variability in human ACL cells growth. Comparison of DNA content up to 21 days in culture of three different patient samples, two from younger patients who underwent an ACLR for a torn ACL and one older patient from a TKR with an intact ACL. Cells were seeded at the same density either directly onto 24-well plates or on PET films. N = 3. *** = $p < 0.001$.

For the comparison of human dermal fibroblasts and ACL cells from intact and ruptured ligaments, fluorescent staining with phalloidin and DAPI was used to assess cell morphology after 24 h of cell seeding at passage 3 on PET unmodified 2D scaffolds (see figure 7.5). Qualitatively, a higher cellular attachment was displayed by human dermal fibroblasts, compared to ligament cells. Ligament cells from ruptured ligament specimens seem to have a more elongated shape at 24 hours compared to HDFs.

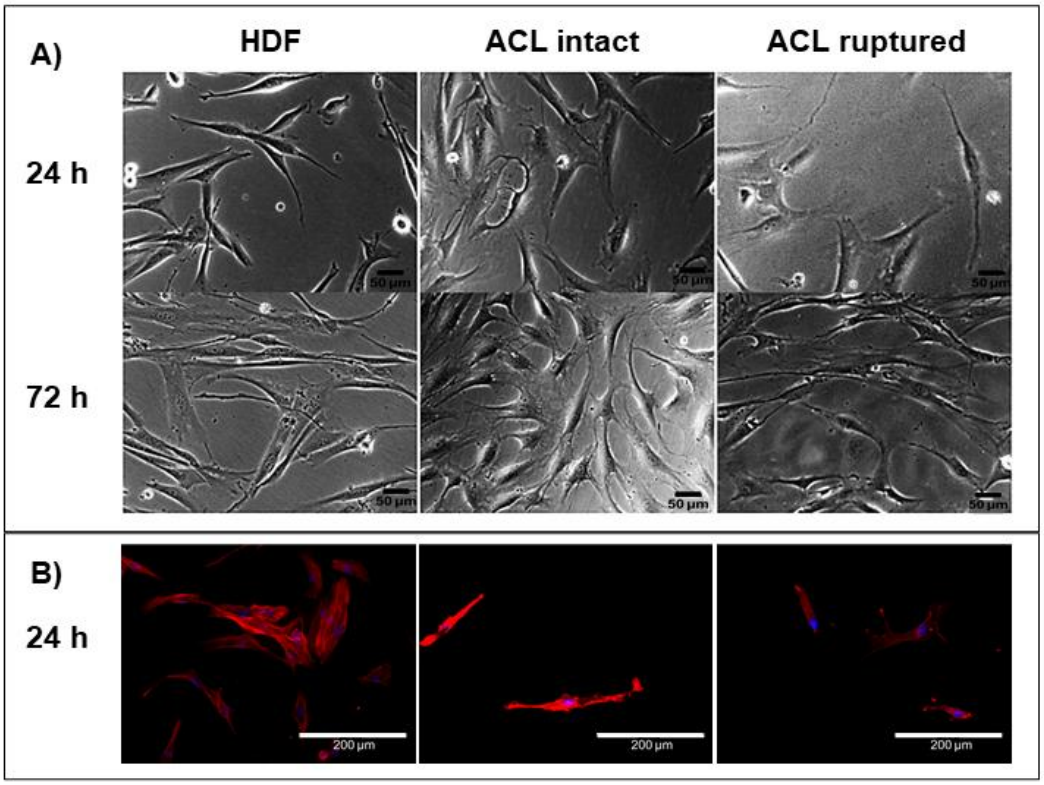

Figure 7.5 Representative images of fibroblast cells on PET films. A) Light microscopy and B) nuclear and actin fluorescent staining illustrating the cell morphology of the human dermal fibroblasts, compared to ACL cells from intact and ruptured ligaments on PET scaffolds at 24 h and 72 h. Scale bars represent 50 µm and 200 µm. All cells were at passage 4.

After 7 days of cell culture of HDF and human ACL cells on 24-well plates – TCP substrate – at passage 3, the cells were fixed and stained for COL-I and COL-III to confirm their fibroblast bioactivity. At this early stage in cell culture, both COL-I markers were present on the ligament-derived cells (see figure 7.6).

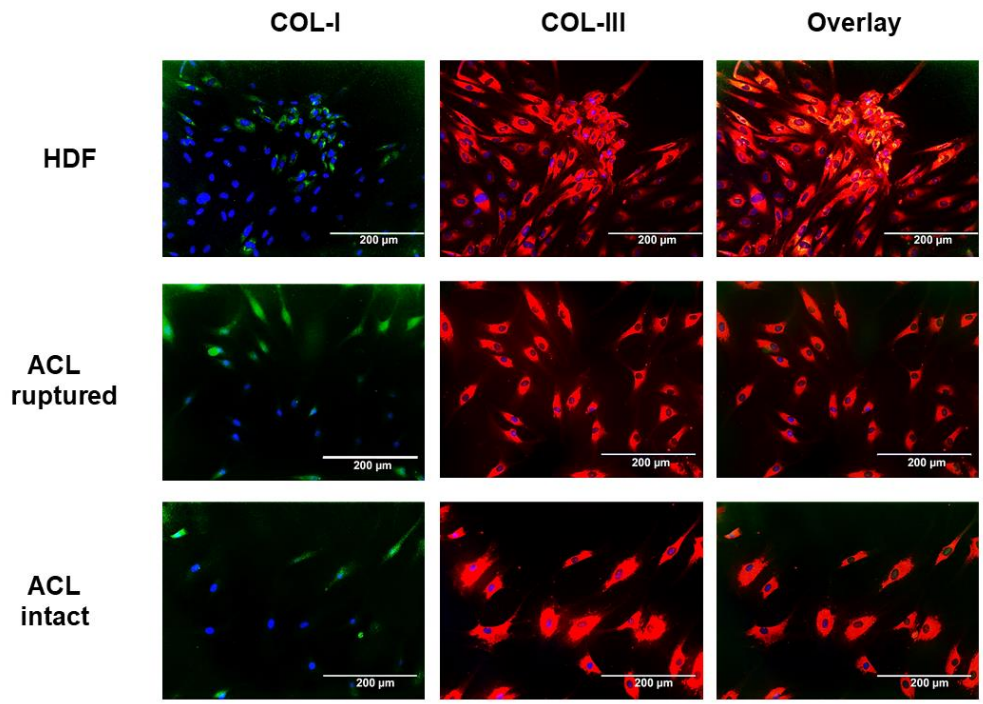

Figure 7.6 Comparative immunocytochemistry of fibroblast cells. Representative fluorescence images of HDF and ACL cells derived from ruptured or intact ligaments at day 7. Fluorescence images showed COL-I, COL-III and overlay of the fluorescence stains as fibroblast markers. Scale bars represent 200 µm.

7.3.2 LIPUS stimulation with an intensity of 0.5 W/cm^2 does not negatively affect the cell attachment of iMSCs or ACL cells

A fixed frequency of 1 MHz with an intensity of 0.5 W/cm^2 was used with a duty cycle of either 25% or 50%. Cell viability on the scaffolds for both duty cycle regimes applied was confirmed by visualisation of live/dead staining 24 h after the LIPUS treatment. Figure 7.7 shows representatives images from the live/dead staining of iMSc at day 1 after LIPUS treatment. After two days of pre-culture in static conditions, the cells remain viable and well attached to the scaffolds after 30 s of LIPUS treatment at 1 MHz, with an intensity of 0.5 W/cm^2 and a DC of either 25% or 50%.

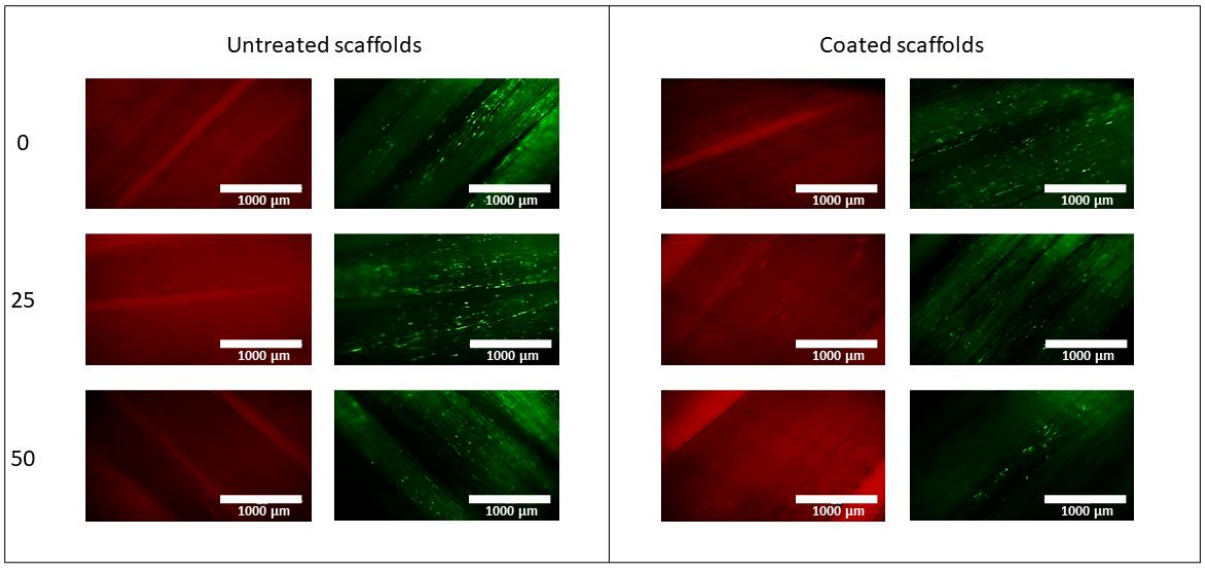

Figure 7.7 Cell attachment viability. Live / Dead staining of iMSCs on bioactive composite scaffolds and untreated PET scaffolds at day 1 after LIPUS treatment at 0 (no LIPUS), 25% or 50% DC.

The seeded scaffolds were analysed with SEM to discern the effect of the mechanical stimulus generated by a power density of 0.5 W/cm^2 with different DC. At day 1 after LIPUS, the cells and the controlled and treated scaffolds showed evidence of attachment, with cell spreading and the presence of bundles of filopodia and lamellipodia. Figure 7.8 illustrates the cell-fibre interaction observed on the 1% CS-g-GMA / 1% HA 1-min O_2 plasma pre-treated scaffolds.

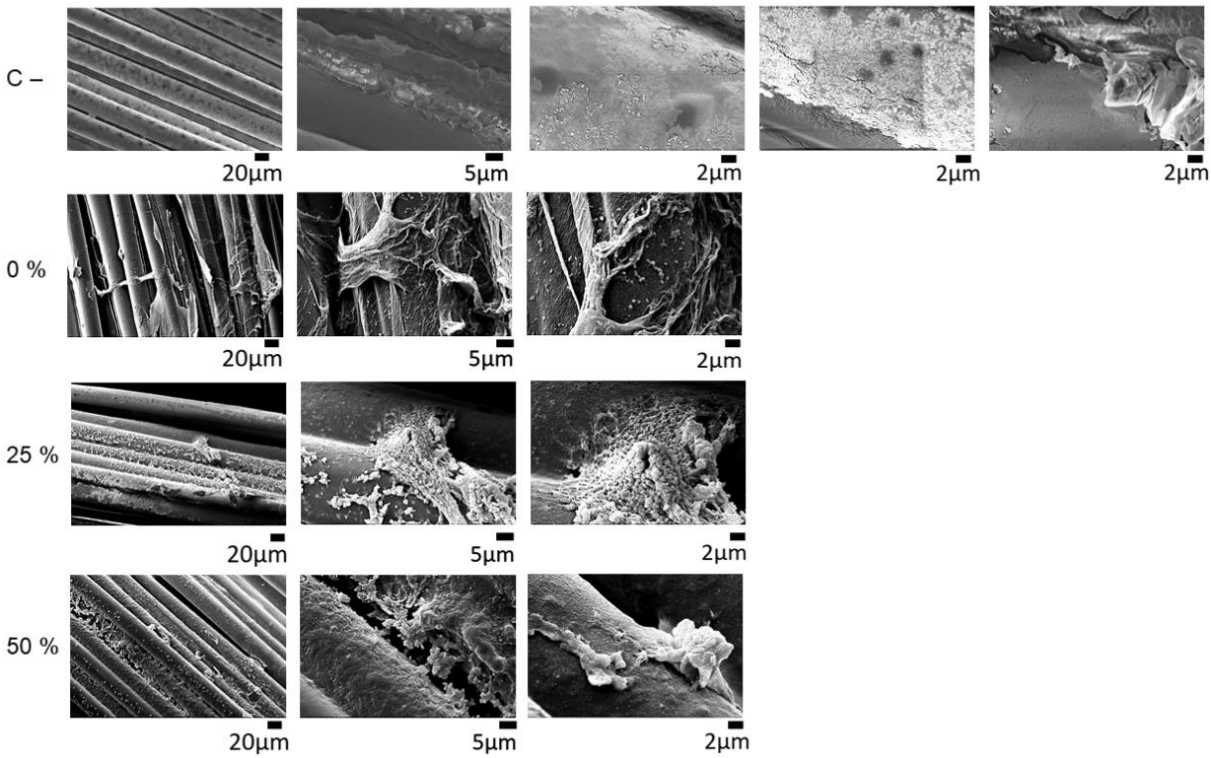

Figure 7.8 Effect of LIPUS on iMSC – bioactive composite scaffold interaction at day 1 after treatment with either 0% (non-LIPUS control), 25% or 50% DC, at 1 MHz during 30 s. Unseeded bioactive composite scaffolds were used as the negative control.

Regarding the metabolic activity, there was no significant difference among the non-LIPUS, 25%-LIPUS or 50%-LIPUS treated scaffolds at day 1. Nonetheless, at day one, LIPUS treatment seems to slightly increase cell proliferation on both the untreated and coated scaffolds (see figure 7.9). On the bioactive composite scaffolds, there was no significant difference between 25% duty cycle LIPUS treatment and no treatment. There was, however, a significant decrease in metabolic activity for cells treated with 50% duty cycle compared to no-LIPUS and 25%-LIPUS ($p < 0.01$ and $p < 0.001$, respectively). From day 3 to day 14, iMSC growth followed the same trend found in previous chapters. There was a statistically significant difference between the metabolic activity for the cells on the untreated scaffolds compared to the bioactive composite scaffolds ($p < 0.001$).

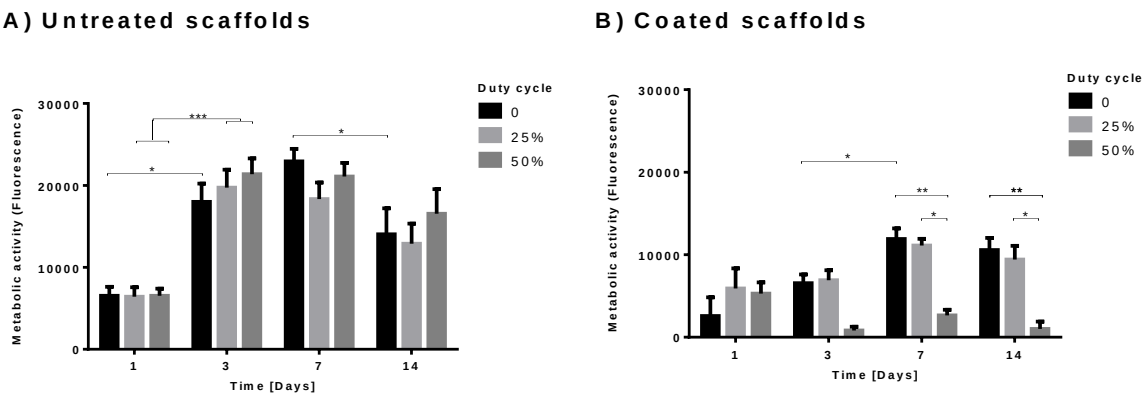

Figure 7.9 Effect of LIPUS on iMSC growth up to day 14. Metabolic activity presented as fluorescence arbitrary units for cells seeded onto A) untreated and B) scaffolds coated with 1% CS-g-GMA / 1% HA treated with LIPUS with an intensity of 0.5 W/cm^2 and either 0 (non-LIPUS control), 25% or 50% DC. N=9.

7.3.3 LIPUS enhances ECM deposition from both iMSCs and ACL cells

The ultimate purpose of LIPUS in ACL physiotherapy is the healing of the tissue. The graft's healing can be monitored by the remodelling changes occurring with the ECM deposition as the cells adapt the environment to help them fulfil their functions. The effect on the scaffolds' remodelling of the generally accepted LIPUS treatment with an intensity of 0.5 W/cm^2 was monitored with SEM. Figure 7.10 displays the qualitatively noticeable enhancement of matrix deposition with the bioactive coating on the PET scaffolds. Increased matrix deposition can be seen on the scaffolds treated with LIPUS as opposed to the non-LIPUS controls. The observation suggests that there is a benefit for applying a 0.5 W/cm^2 LIPUS intensity at a DC of 50% in terms of matrix deposition.

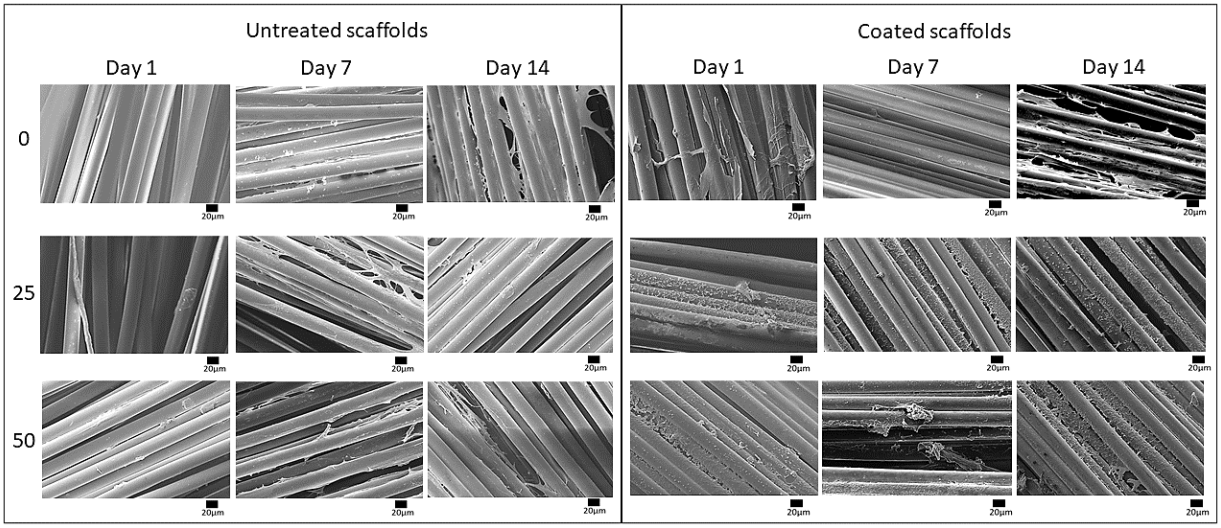

Figure 7.10 iMSC scaffold remodelling. SEM representative images of ECM deposition and cell organisation on the scaffolds after LIPUS treatment with a duty cycle of 0% (non-LIPUS control), 25% and 50%.

Likewise, cell attachment and deposition were evidenced by SEM for the ACL cells from day 1 after LIPUS stimulation. Figure 7.11 shows representative images of the interaction between the ACL cells and the bioactive coated scaffolds at day 1 and day 14.

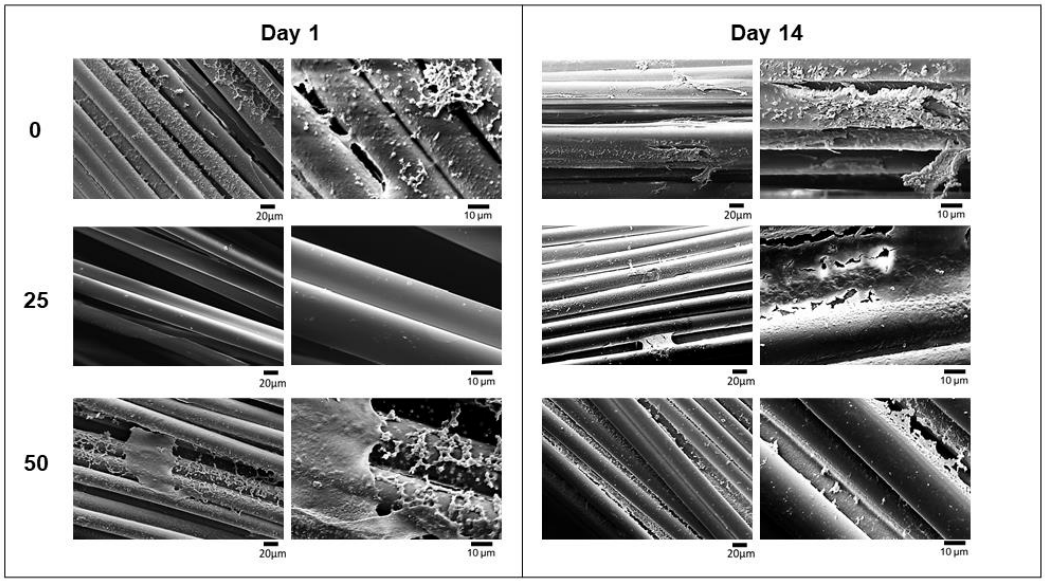

Figure 7.11 ACL scaffold remodelling. SEM representative images of ECM deposition and cell organisation on the bioactive coating scaffolds after LIPUS treatment with a duty cycle of 0% (non-LIPUS control), 25% and 50%.

In terms of functionality, there was a significant increase in soluble collagen deposition for the scaffolds treated with 50% duty cycle LIPUS when compared to their static controls ($p < 0.05$). The trend of increase in collagen deposition after LIPUS treatment was also evident for the untreated scaffolds, although it did not reach statistical significance. Notably, there was a significant difference between coated scaffolds and their untreated control for every condition in terms of collagen deposition, favouring the bioactive scaffold (see figure 7.12). For the MSCs, there was a 4.98-fold increased collagen deposition for the composite scaffolds after LIPUS treatment with a 50% DC when compared to the control PET fibres treated with the same LIPUS regime. This discrepancy between collagen deposition on the untreated controls and composite scaffolds after LIPUS treatment at 50% DC was higher for the ACL cells, with a 16.97-fold difference. Human ACL cells on 1% CS-g-GMA / 1% HA O_2 plasma pre-treated PET fibrous scaffolds significantly deposited a higher concentration of collagen compared to their untreated control for every condition. There was no significant difference among untreated scaffolds' collagen deposition.

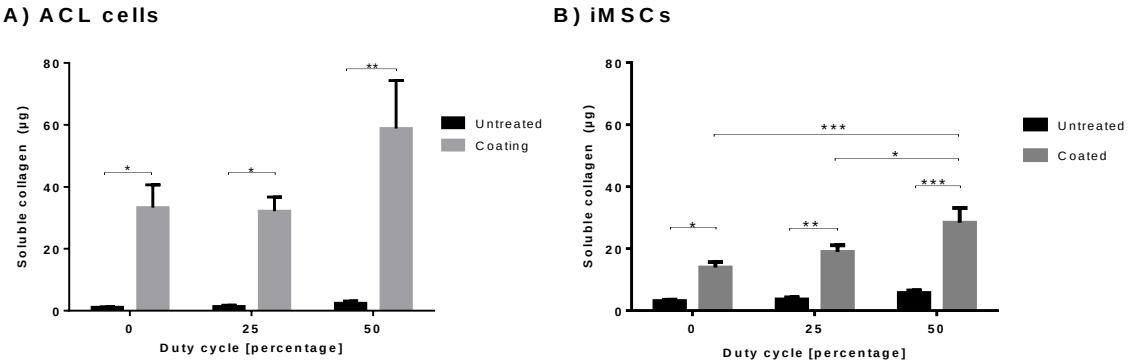

Figure 7.12 Effect of a 0.5 W/cm^2 intensity LIPUS treatment on soluble collagen deposition for both cell types per scaffold. 0 (non-LIPUS control), 25% or 50% DC. N=9.

7.3.4 Effect of LIPUS on iMSCs and ACL cells cultured with an oxygen tension of 5%

Given that during the early inflammatory phase of a ligament's graft healing process the tissue is subjected to a hypoxic environment, the effect of LIPUS on cell viability and functionality was investigated in cell culture with a 5% O_2 tension. Concerning functionality there was no significant difference in collagen deposition for the iMSCs

(see figure 7.13) between LIPUS or no LIPUS (p>0.5). There was a considerable difference between untreated and treated scaffolds (** p < 0.01, *** p < 0.001). Conversely, statistical significance was reached by the LIPUS treatment with an intensity of 0.5 W/cm^2 only for the cells seeded onto the bioactive coated scaffolds compared to the non-LIPUS ones (p < 0.05). The LIPUS treatment for the native ACL cells seems to amplify the beneficial effect of the bioactive coated scaffold in terms of collagen deposition under low oxygen tension conditions. The soluble collagen deposition for the ACL cells on the bioactive coated scaffolds was significantly higher than that of the untreated scaffolds (p < 0.001).

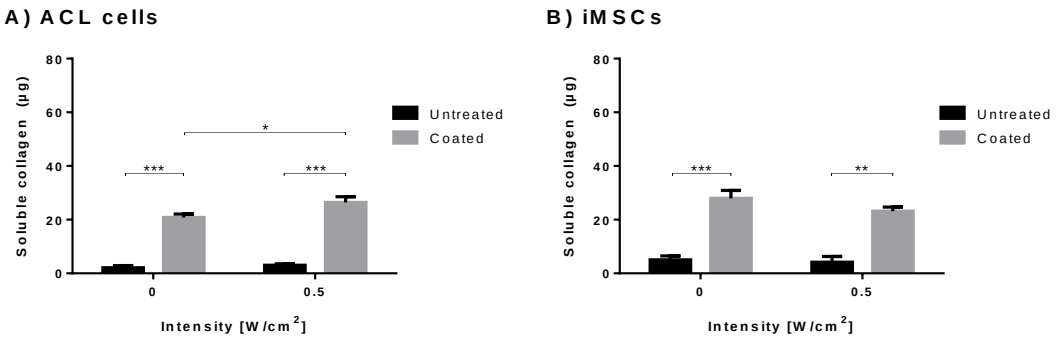

Figure 7.13 Collagen deposition per scaffold of under hypoxic conditions at day 14 after LIPUS. N=9.

7.3.5 Effect of LIPUS intensity on cell growth and ECM deposition

After documenting a beneficial effect on ECM of LIPUS with a 50% DC, different intensities were studied to possibly identify an intensity that could further amplify ECM deposition. Additional intensities of 0.1 W/cm^2 and 0.3 W/cm^2 were selected in line with current clinical practices. The effect of the varied LIPUS intensities for a 50% duty cycle was first tested on iMSCs seeded on 24-well plates to reduce the variables that could act as confounders for the actual effect of the dynamic stimulus. There was no significant difference in terms of metabolic activity between LIPUS and no LIPUS or among different intensities (p > 0.05). There was a significant growth from day 3 to day 7 for all the conditions, smaller between the scaffolds treated with an intensity of 0.3 W/cm^2 compared to the rest of the conditions (p < 0.05 compared to p < 0.001). At day

14 a decline in cell numbers was observed, in correlation with the cell growth plateau. This tendency was unaffected by any LIPUS or no LIPUS treatment (see figure 7.14).

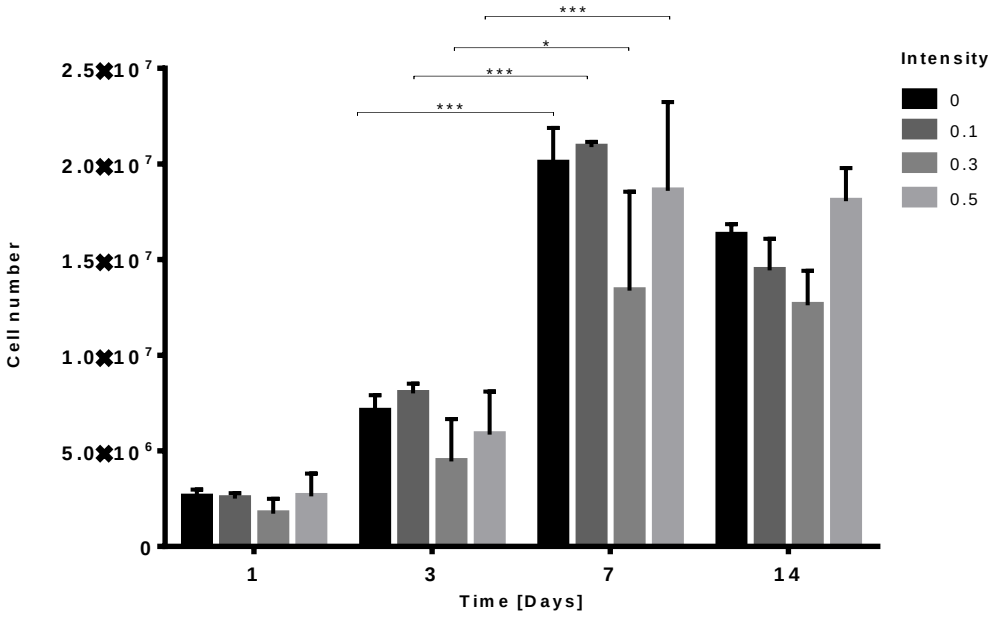

Figure 7.14 Effect of varied intensities of LIPUS on iMSC growth. Cells seeded on 2D TCP individual wells on 24-well plates. A fixed 50% duty cycle was applied with intensities (power density) of 0 (non-LIPUS control), 0.1, 0.3 or 0.5 W/cm^2. The cell number was calculated from a curve of metabolic activity from a known number of cells. N=3.

Collagen deposition at day 14 after treatment was not affected by 30 s of LIPUS with any of the intensities tested for the frequency of 1 MHz and 50% DC ($p = 0.72$). Nonetheless, collagen deposition was higher for all LIPUS treatments when compared to the non-LIPUS wells (see figure 7.15). The lowest power density studied (0.1 W/cm^2) induced a 2.55 increase in collagen deposition compared to the non-LIPUS wells ($p > 0.9$). A bigger sample is required to corroborate these findings.

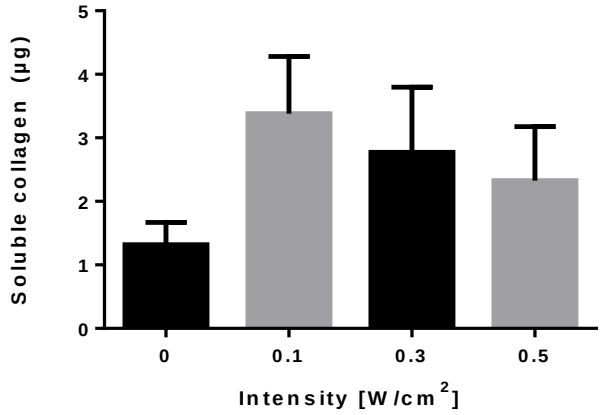

Figure 7.15 Effect of LIPUS intensity on iMSC collagen deposition per well. Cell seeded onto 24-well plates. N=3.

Contrary to the data provided by the 2D TCP experiments, both bioactive coated and untreated scaffolds extracted soluble collagen content was positively affected by LIPUS (see figure 7.16). Significantly lower collagen deposition was observed for coated scaffolds for 0.3 W/cm^2 when compared to both no-LIPUS and 0.5 W/cm^2 ($p < 0.05$, $p < 0.0001$). There was an increase for untreated scaffolds after LIPUS compared to no-LIPUS, although it did not reach statistical significance ($p > 0.05$). For the scaffolds seeded with iMSCs, the highest collagen deposition was achieved on the bioactive coated scaffolds stimulated with a LIPUS intensity of 0.5 W/cm^2. The collagen deposition was, however, not significantly higher to that achieved with the intensity of 0.1 W/cm^2 which also slightly enhanced the collagen deposition by the cells seeded onto the untreated scaffolds. The effect of the bioactive coated scaffold is still superior in enhancing collagen deposition, as the difference is still significant in favour of the coated scaffolds within this group treated with a 0.1 W/cm^2 power density ($p < 0.05$).

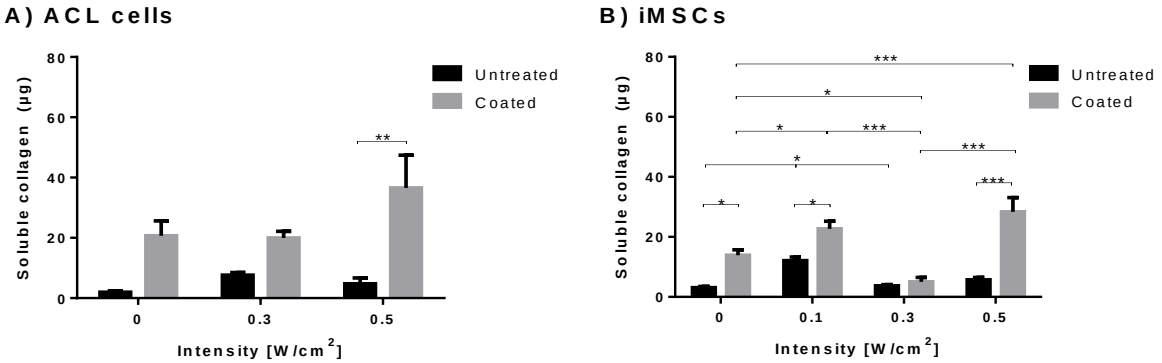

Figure 7.16 Effect of varied LIPUS intensities on iMSCs and ACL cells collagen deposition per scaffold. A fixed 50% duty cycle was applied with intensities of 0 (non-LIPUS control), 0.1, 0.3 or 0.5 W/cm^2 to A) ACL cells and B) iMSCs. At day 14 after stimulation, collagen was solubilised, extracted, and quantified with a colorimetric assay. N=9.

An important component of the ACL ECM, though smaller in proportion to collagen, GAGs are involved in the healing process of connective tissues [463]. Relevant to ACLR, sGAGs are a key factor in the cascade of cellular events of inflammation [464]. Noteworthy, there was no correlation of the results here demonstrated on sGAG deposition when comparing ACL cells behaviour against that of iMSCs (see figure 7.17). LIPUS at 1 MHz and 50% DC with an intensity of 0.05 W/cm^2 induced the ACL deposition of sGAGs onto the untreated PET fibrous scaffolds, but it did not do so for the bioactive coated scaffolds. This difference was non-statistically significant in the ACL cells. For the same intensity parameter, there was a substantial reduction in sGAG deposition when compared to the non-LIPUS bioactive coated scaffolds ($p < 0.05$). There was also a decrease in sGAG deposition for the untreated scaffolds seeded with iMSCs, although it was marginal. For the iMSCs in general, LIPUS at the selected parameters seems to negatively impact sGAG deposition onto the untreated PET fibrous scaffolds. For the coated scaffolds, an intensity of 0.3 W/cm^2 demonstrated a minor increase of these polysaccharide compounds ($p > 0.05$).

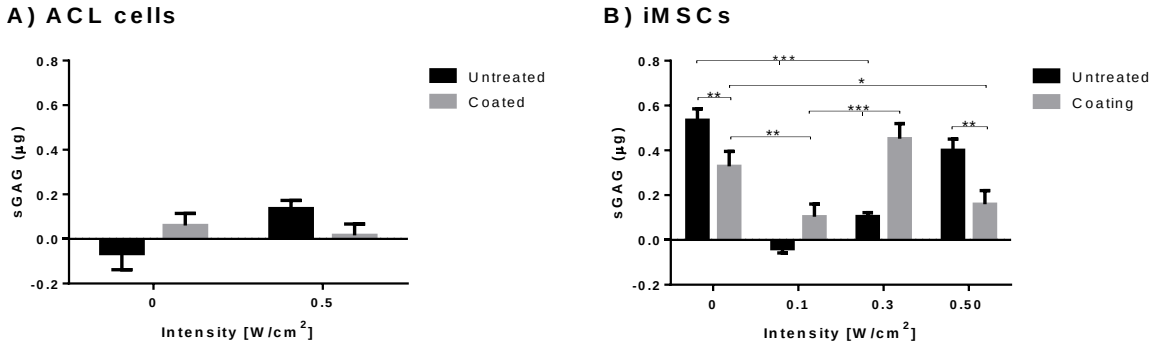

Figure 7.17 Effect of varied LIPUS intensities on iMSCs and ACL cells sGAG deposition per scaffold. A fixed 50% duty cycle was applied with intensities of 0 (non-LIPUS control), 0.1, 0.3 or 0.5 W/cm^2 to A) ACL cells and B) iMSCs. At day 14 after stimulation, sGAGs were extracted and quantified with a colorimetric assay. N = 9.

7.4 Discussion

The purpose of this chapter was to investigate the effect of direct mechanical stimulation in the form of LIPUS on the two populations of cells native to an ACL. In a first instance, successful isolation of ACL cells from patient-derived samples was achieved. LIPUS parameters were selected from the few available reports of its proven effects *in vitro* for ligament healing and supported by the current use of LIPUS in clinical practice. The above presented results demonstrated that LIPUS does not have a detrimental effect on cell attachment of iMSCs or ACL cells and that it enhances collagen deposition. The significant increase in collagen deposition after treating the bioactive coated scaffolds with LIPUS provides further evidence of the beneficial effect of the 1% CS-g-GMA / 1% HA coating of the O_2 plasma pre-treated PET fibres for the enrichment of the ligament-like ECM on the scaffolds.

Despite the poor cellularity and vascularity in the midsubstance of the ACL, this ligament possesses a regenerative potential from its torn remnant that could be harnessed for tissue repair by the bioactive composite scaffold proposed in this thesis. Along with the materials and methods selected for the development of the scaffold, the approach of *in situ* TE could be a simple and efficient manner to fast-track the clinical acceptance and adoption of the proposed scaffold to replace the injured ACL. If

combined with a remnant preservation technique for ACLR, the biological augmentation provided by the MSCs that naturally reside in the ACL stump *in situ* [465] could be potentiated for ACL healing by the biochemical cues supplied by the combination of the CS-g-GMA and hyaluronic acid in the manner here proposed. MSCs and ligament cells have been utilised as a source for ligament TE before [466]. Here the behaviour of MSCs and ACL fibroblasts – the two types of ligament native cells – was interrogated to understand how another form of mechanical stimulation could potentiate the healing enhancement initiated by the bioactive composite scaffold.

Mechanical stimulation is required for ligament healing. In soft tissue regenerative medicine, acoustic ultrasound has been proposed for several types of therapies [424, 436, 467, 468]. Despite being one of the most common treatments for injuries to tendons and ligaments, the fundamental research evidence for the benefit of ultrasound treatment in these contexts is scarce. LIPUS has been approved for the treatment of non-union bone fractures for the past two decades [467]. It is from that application that the use of LIPUS has expanded, and the parameters extrapolated to adjacent tissues. LIPUS promotes MSC and fibroblast proliferation [469, 470]. The results from this chapter demonstrated that, while minimal, LIPUS at a frequency of 1 MHz, an intensity of 0.5 W/cm^2 and a DC of either 25% or 50% boosts MSC proliferation and metabolic activity during the first days even after a short 30 s treatment. The effect seems to remain for a DC of 50 with an intensity of 0.1 W/cm^2 and to catch on for an intensity of 0.5 W/cm2. Qualitative evidence of cell adhesion and proliferation was also presented for both ACL cells and MSCs. A study on MSC osteogenic cell commitment by LIPUS stimulation [470] showed an increase in proliferation at 14 days on + 7 days off stimuli. Most in vitro studies applied LIPUS in a range of minutes, from 1 to 20 min. To this end, special tailored automated devices have been manufactured. The regulation of distinct markers for various cell lines are time dependent. A study investigating the effect of LIPUS on the recovery of MSCs from human umbilical cord [471] concluded that 40 kHz frequency, with a 50% DF and 25 – 35 mW/cm^2 for 100 s was not significantly inferior to no LIPUS in cell proliferation compared to 300 s and 600 s, where the cell viability was significantly lower. The same study found a stimulation time-dependent elongation of morphology. Similarly, MSCs treated with LIPUS at a frequency of

1.5 MHz, 20% DC and an intensity of 0.3 W/cm^2 intensity showed a progressive increase in dsDNA content compared to untreated controls that remained constant after LIPUs stimulus stopped [472]. In this thesis, the stimulus was manually applied to individual wells for a shorter period, allowing to determine whether the brief nano motions induced by the acoustic vibration are sufficient to produce any effect on MSCs or ACL cells behaviour. An experimental setting of increasing exposure times and stimulation at different intervals would help better map the effect of LIPUS on cell proliferation.

Mechanical stimulation of any sort is related to collagen synthesis by ligament resident cells [473]. MSC have shown an increased deposition of collagen I [472]. In connective tissues, healing fibroblasts express nitric oxide (NO), it enhances collagen synthesis and its delivery in clinical trials has shown and enhanced clinical recovery in tendons [474]. In vitro, the synergistic use of shear stress and US significantly increases NO production that might be beneficial for the healing ligament graft as it increases mechanosensitivity [475]. Nevertheless, in osteocyte-like cells, the combination of fluid flow and LIPUS for more than 3 h has demonstrated an increase in the expression of connexin 43, PGE_2 [476, 477], while beneficial for bone formation, might be detrimental in association to OA, which is something to keep in mind when selecting the duration of the stimuli. The enhancement of collagen deposition by the bioactive composite scaffold presented in this thesis has been stablished from previous chapters. In this chapter, the addition of a mechanical stimulus different from the tensile stretching explored in the last chapter proved beneficial for ECM deposition. Notably, soluble collagen production is significantly increased by LIPUS with different DCs and intensities under 21% and 5% oxygen tension culture conditions. Quantification of specific sGAGs would be highly beneficial in understanding their role in ACL graft healing. For instance, the accumulation of GAGs has been reported in pathologies such as chronic patellar tendinopathy and this is thought to be due to over sulphation of the GAGs [478, 479].

7.5 Conclusion

There is an evident trend of increase in collagen deposition after LIPUS treatment. As demonstrated in previous chapters, the bioactive scaffold significantly encourages the deposition of collagen. This effect was further improved with LIPUS. This chapter showed that the combined use of the 1% CS-g-GMA / 1% HA PET composite scaffold and LIPUS treatment could be a useful therapeutic approach to accelerate ligament healing.

Chapter 8

Discussion

The research conducted for this thesis endeavoured to develop a biomimetic tissue engineered scaffold to address the persistent challenges of the current ligament grafts used for the surgical reconstruction of ACL tears. The continuing rise of the occurrence and awareness of ACL injuries and their surgical management increase the demand for a tissue sparing alternative. Based on the advancements in natural biomaterials and TE, this project aimed to build on the surface modification of the only accredited synthetic graft in clinical practice to transform the material into a bioactive setting for the enhancement of ligament tissue integration. As previously discussed, cellular behaviour can be prompted by physical cues as much as by chemical cues [480]. Despite not being a biodegradable material, as a clinically known material PET works for the basis of a ligament synthetic insert as it exhibits appealing mechanical properties for a load-bearing ligament graft to provide joint stability during the weakest period for any graft after ACLR. Throughout this thesis, the literature review and experimental data has supported the knowledge that the smooth and chemically inert surface of PET benefits from the addition of functional groups via a cold O_2 plasma discharged at a low frequency and low power, as well as from the bioactive CS and HA coating that as a whole, improved the cell viability and functionality.

The choice of immortalised adipose derived-MSCs for the experimental development of this thesis followed the intention to optimise the methodology for the scaffold's manufacture with cells that would be found in a native ligament, with a potential for differentiation in response to different biochemical or physical cues and that would retain their potency over multiple passages. MSCs cytoskeleton adapts to the substrate onto which they are seeded by altering their cytoskeleton, which in turn affects their synthesis of diverse growth factors and proteins that modify their microenvironment.

The experiments here presented aimed to encourage MSCs to produce a ligament-like ECM. This was done initially through the introduction of topographic and chemical modifications to the originally inert surface of PET scaffolds. In the last two chapters, mechanical stimulation was incorporated based on the literature demonstrating the crucial role of mechanical stresses on ligament differentiation and the knowledge of the high mechanosensitivity that MSCs exhibit [481]

The process of developing the scaffold here proposed followed a methodological approach to enable the individual analysis of the particulars of each of the steps. In this manner, the project offered helpful insight into the applicability of distinctive techniques for ACL TE. The use of gas plasma technology for regenerative medicine is a rapidly evolving topic. The suitability of the treatment needs to address a precise objective as the working parameters selected for each exposure heavily determine its usefulness for different surface modifications. For this thesis, a low-pressure system operating at a low-frequency and low-power proved effective to activate PET scaffolds and the adhesion of a bioactive coating. O_2 plasma treatment also proved advantageous as a surface cleaning technology. Despite the controlled and minimised exposure of the scaffolds post-treatment with no additional sterilisation to avoid altering the modified surface, no infections occurred on the scaffolds at any time point during cell culture. The integration of various technologies for the assembly, their assessment, and the examination of the bioactive capabilities of the scaffold successfully indicated the response that the bioactive composite scaffold might elicit from native MSCs and ACL cells after implantation in an ACLR. The two mechanical stimulation settings here presented were chosen to facilitate the translation of the technology proposed, given that they relate to physiologically relevant scenarios. The data gathered throughout this thesis supports the potential for the 1% CS-g-GMA / 1% HA PET composite scaffold to induct ligament regeneration.

8.1 Future directions

Due to time constraints and limited access to specific equipment, some sections of this thesis had to be modified, leaving some experiments as part of future work. It is the case of gene expression for all the experimental chapters involving the bioactive coating. The protocol to obtain an acceptable RNA yield out from the polysaccharide encapsulation is under optimisation.

The purpose of this thesis was to create an alternative with the potential to be fast-tracked through the necessary validation steps, expecting to be able to reach patients in a shorter term. The choice of materials, scaffold manufacturing technique and intent for an *in situ* TE approach followed that judgement. The experimental plan considered left unexplored additional processes given the vast options for scaffold manufacturing. It was within the plan to compare the suitability of manufacturing systems to develop the bioactive composite scaffold. The first of such approaches was electrospinning. Electrospun scaffolds contain fibres in the nanometre scale as opposed to the micrometre fibres employed in this thesis [482]. Both MSCs and fibroblasts sense and behave differently depending on the fibre sizes and differences in material stiffness [243]. CS and HA have been electrospun before [483, 484]. Combining CS-g-GMA with HA via different systems has the potential for producing stable and mechanically suitable fibres. Doing so could lead to forgoing the non-biodegradable PET. Exploring the fabrication of a 1% CS-g-GMA / 1% HA fibrous scaffold with or without PET via electrospinning – or the modification of a wet-spinning technique – remain part of future work to evaluate the relevance in biological effects and mechanical properties of these materials at different fibre scales.

Within the same design topic, another direction for improving the bioactive scaffold here presented is plasma technology. Plasma technology is an ever-evolving field that holds enormous potential for ligament TE. The chemical modification of CS in plasma systems is under scrutiny to find more environmentally friendly and straightforward [485, 486] ways to produce water-soluble chitosan to expand its malleability. Plasma induced polymerization of CS-g-GMA and HA could be explored to provide a more homogenous coating for the PET fibres and control the variability of cellular responses.

In terms of variable cellular responses, a limitation of this thesis was that testing with patient-derived ACL cells was only completed for two different individuals. It remains part of future work to enlarge the sample size to determine a more statistically accurate effect of the PET 1-min O_2 plasma pre-treated fibres coated with 1% CS-g-GMA / 1% HA on native cells proliferation and ECM deposition. Moreover, the variability in gene expression for a representative population would provide valuable information regarding the translatability of the system.

Changes in gene expression through time after intervention and for specific mechanical stimulation regimes would provide the means to validate the effects seen with protein deposition. Interrogating gene expression profiles on the interaction between the resident ligament cells and the bioactive composite scaffold object of this thesis would provide a guide to improve the results obtained and understand the phase of graft healing to which the results correspond. Some of the parameters to explore through gene expression in future work are cell signalling, ECM remodelling, inflammation, and adaptation to hypoxia.

Different types of mechanical stimulation are required to test and validate a ligament tissue-engineered scaffold in more physiologically relevant scenarios. The availability of a single chamber uniaxial mechanical stimulation bioreactor limited the options. A modified bioreactor could offer a combination of stimuli, such as the addition of rotational mechanical stimuli. A larger sample of mechanically stimulated seeded scaffolds is needed for a more comprehensive assessment. This thesis provided a much-needed look into the effects of strenuous mechanical stimulation for intraarticular ligaments. There is a gap in this research area that could better inform injury prevention and physical rehabilitation protocols.

Physical rehabilitation is fundamental for ACL graft maturation. The feasibility of applying LIPUS treatments in ambulatory and home-based settings make LIPUS a prominent tool for ligament healing. The results here obtained from a single short cycle were promising. Lengthier regimes and different intervals of LIPUS are required to broaden the picture of the impact this treatment can have on a newly transplanted tissue-engineered ligament surrogate. The effects of LIPUS on MSC differentiation also

need to be measured. LIPUS is known to augment the tensile strength of ligament grafts. One of the tests left aside due to the tight schedule was the mechanical testing of seeded samples after treatment with LIPUS. The correlation of this data with the evidenced matrix deposition is part of ongoing work.

Graft maturation is of utmost importance to ensure a person's return to pre-injury functionality. This thesis focused on inducing regeneration of the ligament's midsubstance as it is the most common site of graft failure. Nevertheless, as it can be gathered for the extensive research effort on the area, for a graft to be fully functional, the enthesis needs to be addressed. The logical future direction for the work here presented is the incorporation of differentiated regions to the scaffold. Current graft failure also happens at the bone insertions, and the tunnel enlargement is caused – among other reasons- by the lack of osseointegration. The 1% CS-g-GMA / 1% HA bioactive coating demonstrated that given the right stimulus, it enhances osteogenic differentiation. Further assessment is needed in this area and fibrocartilage induction. The design of the scaffold could be greatly improved by co-culturing native cells with expected neighbouring cells such as synoviocytes, osteoblasts and endothelial cells. The use of a multi-chamber bioreactor could aid to adjust the conditions for this sort of experiment. It would provide a more biomimetic environment.

Chapter 9

Conclusion

The synthetic alternative for an ACL surrogate designed and developed in this thesis combines straightforward methodology, approved materials already in clinical use for different purposes and the incorporation of safe readily available rehabilitation options to improve the outcomes of ACLRs. Investigating the cellular responses to each of the steps of the scaffold's development from 2D, to 3D, to actual anatomical size and to physiologically relevant stimuli, this research project provides a thoughtful approach for the creation of a tissue engineered ACL graft. The biomimetic potential of the 1% CS-g-GMA / 1% HA composite PET fibrous scaffold was validated by the visualisation of the cell-substrate interaction and ECM deposition onto the scaffolds. The cells used in this project further validate the results here presented, as they are representative of the targeted native tissue.

ACLR is currently a treatment option restricted for the more physically active and younger patients, while there is evidence that demonstrates its benefit for a wider population affected by ACL injuries. The current surgical gold standard limits the extension of this option mainly due to the associated graft donor site morbidities and the absence of certainty for full recovery of stability and quality of life. The systematic review conducted at the beginning of this thesis substantiated the need for an alternative to the existing ACL grafts. Reflecting on the advancement of biomaterials and TE approaches for ligament regeneration, this thesis sought to incorporate physiologically and clinically relevant materials and methods.

Concerning the design and development of the novel scaffold, the two-step manufacturing approach proved successful in incorporating physical and chemical cues relevant to ligament tissue. O_2 plasma treatment is an effective technique to activate PET surface and to improve the addition of a bioactive coating. The interaction

between CS-g-GMA and HA at the concentrations and ratio here explored, showed a favourable bioactive effect in terms of supporting cell growth and enhancing ECM deposition. The 1% CS-g-GMA / 1% HA coating of a 1-min O_2 plasma pre-treated PET fibrous scaffold provided the maximum enhancement of collagen deposition across all the studies conducted. The heightening of collagen deposition is sustained by this novel bioactive composite scaffold despite a context of strenuous physical activity, which makes it more promising for an athlete's return to sports prospective. The effect on collagen deposition for the scaffold is further increased by LIPUS treatment at a frequency of 1 MHz, a DC of 50% and an intensity of 0.5 W/cm^2. The scaffold proved appropriate for the interaction with a MSC line and patient-derived ACL cells from individuals of different ages and gender. A fitting ACL graft can be made by combining the ultimate tensile strength provided by paralleled arranged loose fibres with the bioactive cues from a polysaccharide complex coating that mimics the ligament's ground substance. The graft is environmentally friendly, easy to manufacture, relatively low cost, it uses clinically validated and certified materials and it hold the potential for reduced immune responses, inflammatory reaction, and infections due to the coating composition.

Chapter 10

References

1. Engdahl, K., et al., *The epidemiology of cruciate ligament rupture in an insured Swedish dog population.* Scientific Reports, 2021. **11**(1): p. 9546.
2. Kobayashi, H., et al., *Mechanisms of the anterior cruciate ligament injury in sports activities: a twenty-year clinical research of 1,700 athletes.* J Sports Sci Med, 2010. **9**(4): p. 669-75.
3. Yu, B. and W.E. Garrett, *Mechanisms of non-contact ACL injuries.* Br J Sports Med, 2007. **41 Suppl 1**(Suppl 1): p. i47-51.
4. Abram, S.G.F., et al., *Anterior cruciate ligament (ACL) reconstruction and meniscal repair rates have both increased in the past 20 years in England: hospital statistics from 1997 to 2017.* British Journal of Sports Medicine, 2020. **54**(5): p. 286-291.
5. Secondary Care Analysis, N.D., *NHS Digital, Hospital Episode Statistics for England. Outpatient statistics, 2018 - 2019.* 2019, NHS Digital part of the Government Statistical Service.
6. Ayman Gabr, A.D.M., Fares Haddad, *The National Ligament Registry The Sixth Annual Report (2020)* in *The UK National Ligament Registry* 2020: National Ligament Registry.
7. Sun, J., et al., *Autografts vs Synthetics for Cruciate Ligament Reconstruction: A Systematic Review and Meta-Analysis.* Orthopaedic Surgery, 2020. **12**(2): p. 378-387.
8. Bashaireh, K.M., et al., *The Effectiveness of Autograft Used in Anterior Cruciate Ligament Reconstruction of the Knee: Surgical Records for the New Generations of Orthopedic Surgeons and Synthetic Graft Revisit.* Orthop Res Rev, 2020. **12**: p. 61-67.
9. Sayampanathan, A.A., et al., *Epidemiology of surgically managed anterior cruciate ligament ruptures in a sports surgery practice.* Journal of Orthopaedic Surgery, 2017. **25**(1): p. 2309499016684289.
10. British Association for Surgery of the Knee (BASK), B.O.S.T.a.A.A.B., *Best Practice for Management of Anterior Cruciate Ligament (ACL) Injuries* 2020, British Orthopaedic Association.
11. Dunn, K.L., K.C. Lam, and T.C. Valovich McLeod, *Early Operative Versus Delayed or Nonoperative Treatment of Anterior Cruciate Ligament Injuries in Pediatric Patients.* J Athl Train, 2016. **51**(5): p. 425-7.
12. Grevnerts, H.T., et al., *PATIENTS FOCUS ON PERFORMANCE OF PHYSICAL ACTIVITY, KNEE STABILITY AND ADVICE FROM CLINICIANS WHEN MAKING DECISIONS CONCERNING THE TREATMENT OF THEIR ANTERIOR CRUCIATE LIGAMENT INJURY.* Int J Sports Phys Ther, 2020. **15**(3): p. 441-450.
13. Joseph, C., et al., *Is ACL reconstruction only for athletes? A study of the incidence of meniscal and cartilage injuries in an ACL-deficient athlete and non-athlete population: an Indian experience.* Int Orthop, 2008. **32**(1): p. 57-61.
14. Krause, M., et al., *Operative Versus Conservative Treatment of Anterior Cruciate Ligament Rupture.* Dtsch Arztebl Int, 2018. **115**(51-52): p. 855-862.

15. Padaki, A.S., et al., *Prevalence of Posttraumatic Stress Disorder Symptoms Among Young Athletes After Anterior Cruciate Ligament Rupture.* Orthop J Sports Med, 2018. **6**(7): p. 2325967118787159.
16. United Nations, D.o.E.a.S.A., Population Division, *World Population Prospects 2019*, in *United Nations*. 2019: Online Edition.
17. Jenkin, C.R., et al., *Sport and ageing: a systematic review of the determinants and trends of participation in sport for older adults.* BMC Public Health, 2017. **17**(1): p. 976.
18. Commision, E., *Eurobarometer*, Y. Education, Sport and Culture, Editor. 2018.
19. Eime, R.M., et al., *Age profiles of sport participants.* BMC Sports Sci Med Rehabil, 2016. **8**: p. 6.
20. Brune, T., et al., *In vitro comparison of human fibroblasts from intact and ruptured ACL for use in tissue engineering.* Eur Cell Mater, 2007. **14**: p. 78-90; discussion 90-1.
21. Lee, J.K., et al., *Anterior cruciate ligament remnant cells have different potentials for cell differentiation based on their location.* Scientific Reports, 2020. **10**(1): p. 3097.
22. Ogata, Y., et al., *Anterior cruciate ligament-derived mesenchymal stromal cells have a propensity to differentiate into the ligament lineage.* Regenerative Therapy, 2018. **8**: p. 20-28.
23. Steinert, A.F., et al., *Mesenchymal stem cell characteristics of human anterior cruciate ligament outgrowth cells.* Tissue Eng Part A, 2011. **17**(9-10): p. 1375-88.
24. Fu, W., et al., *Mesenchymal stem cells reside in anterior cruciate ligament remnants in situ.* International Orthopaedics, 2016. **40**(7): p. 1523-1530.
25. Huang, T.F., et al., *Isolation and characterization of mesenchymal stromal cells from human anterior cruciate ligament.* Cytotherapy, 2008. **10**(8): p. 806-814.
26. Caplan, A.I., *Mesenchymal Stem Cells: Time to Change the Name!* STEM CELLS Translational Medicine, 2017. **6**(6): p. 1445-1451.
27. Kurenkova, A.D., et al., *Niches for Skeletal Stem Cells of Mesenchymal Origin.* Frontiers in Cell and Developmental Biology, 2020. **8**(592).
28. Zhu, J., et al., *Ultrastructural and Morphological Characteristics of Human Anterior Cruciate Ligament and Hamstring Tendons.* The Anatomical Record, 2012. **295**(9): p. 1430-1436.
29. Woo, S.L., et al., *Biomechanics of knee ligaments: injury, healing, and repair.* J Biomech, 2006. **39**(1): p. 1-20.
30. Marieswaran, M., et al., *A Review on Biomechanics of Anterior Cruciate Ligament and Materials for Reconstruction.* Applied Bionics and Biomechanics, 2018. **2018**.
31. Butler, D.L., et al., *Location-dependent variations in the material properties of the anterior cruciate ligament.* Journal of Biomechanics, 1992. **25**(5): p. 511-518.
32. Kharaz, Y.A., et al., *Variations in internal structure, composition and protein distribution between intra- and extra-articular knee ligaments and tendons.* J Anat, 2018. **232**(6): p. 943-955.
33. Nagineni, C.N., et al., *Characterization of the intrinsic properties of the anterior cruciate and medial collateral ligament cells: an in vitro cell culture study.* J Orthop Res, 1992. **10**(4): p. 465-75.
34. Schulze-Tanzil, G., *Intraarticular Ligament Degeneration Is Interrelated with Cartilage and Bone Destruction in Osteoarthritis.* Cells, 2019. **8**(9).
35. Little, D., et al., *Proteomic differences between male and female anterior cruciate ligament and patellar tendon.* PLoS One, 2014. **9**(5): p. e96526.
36. Asahara, H., M. Inui, and M.K. Lotz, *Tendons and Ligaments: Connecting Developmental Biology to Musculoskeletal Disease Pathogenesis.* J Bone Miner Res, 2017. **32**(9): p. 1773-1782.
37. Giblin, S.P. and K.S. Midwood, *Tenascin-C: Form versus function.* Cell Adh Migr, 2015. **9**(1-2): p. 48-82.

38. Higuchi, T., et al., *Versican contributes to ligament formation of knee joints.* PLoS One, 2021. **16**(4): p. e0250366.
39. Yamamoto, M., et al., *Cartilage attachment morphology of the fetal cruciate ligaments of the knee: an immunohistochemical study using human fetal specimens.* Okajimas Folia Anat Jpn, 2016. **93**(2): p. 67-72.
40. Schweitzer, R., et al., *Analysis of the tendon cell fate using Scleraxis, a specific marker for tendons and ligaments.* Development, 2001. **128**(19): p. 3855-66.
41. Nakamichi, R., K. Kataoka, and H. Asahara, *Essential role of Mohawk for tenogenic tissue homeostasis including spinal disc and periodontal ligament.* Mod Rheumatol, 2018. **28**(6): p. 933-940.
42. Lim, J.I., Y.-C. Na, and W.-K. Lee, *Preparation of elastic chitosan/poly(l-lactide-co-ε-caprolactone) macroporous scaffolds by acetylation and particulate leaching.* Journal of Porous Materials, 2017. **24**(4): p. 997-1002.
43. Markatos, K., et al., *The anatomy of the ACL and its importance in ACL reconstruction.* Eur J Orthop Surg Traumatol, 2013. **23**(7): p. 747-52.
44. Fujii, K., et al., *Biochemical properties of collagen from ligaments and periarticular tendons of the human knee.* Knee surgery, sports traumatology, arthroscopy : official journal of the ESSKA, 1994. **2**(4): p. 229-233.
45. Fujii, K., et al., *Biochemical properties of collagen from ligaments and periarticular tendons of the human knee.* Knee Surg Sports Traumatol Arthrosc, 1994. **2**(4): p. 229-33.
46. McKee, T.J., et al., *Extracellular matrix composition of connective tissues: a systematic review and meta-analysis.* Scientific Reports, 2019. **9**(1): p. 10542.
47. Ryan, C.N.M., et al., *Glycosaminoglycans in Tendon Physiology, Pathophysiology, and Therapy.* Bioconjugate Chemistry, 2015. **26**(7): p. 1237-1251.
48. Hasegawa, A., et al., *Cellular and extracellular matrix changes in anterior cruciate ligaments during human knee aging and osteoarthritis.* Arthritis Research & Therapy, 2013. **15**(1): p. R29.
49. Bi, Y., et al., *Identification of tendon stem/progenitor cells and the role of the extracellular matrix in their niche.* Nature Medicine, 2007. **13**(10): p. 1219-1227.
50. Riley, G.P., et al., *Glycosaminoglycans of human rotator cuff tendons: changes with age and in chronic rotator cuff tendinitis.* Annals of the Rheumatic Diseases, 1994. **53**(6): p. 367-376.
51. Kohler, J., et al., *Uncovering the cellular and molecular changes in tendon stem/progenitor cells attributed to tendon aging and degeneration.* Aging Cell, 2013. **12**(6): p. 988-999.
52. Kadler, K.E., et al., *Collagens at a glance.* J Cell Sci, 2007. **120**(Pt 12): p. 1955-8.
53. Myllyharju, J. and K.I. Kivirikko, *Collagens, modifying enzymes and their mutations in humans, flies and worms.* Trends Genet, 2004. **20**(1): p. 33-43.
54. Ricard-Blum, S. and F. Ruggiero, *The collagen superfamily: from the extracellular matrix to the cell membrane.* Pathol Biol (Paris), 2005. **53**(7): p. 430-42.
55. Myllyharju, J., *Intracellular Post-Translational Modifications of Collagens*, in *Collagen: Primer in Structure, Processing and Assembly*, J. Brinckmann, H. Notbohm, and P.K. Müller, Editors. 2005, Springer Berlin Heidelberg: Berlin, Heidelberg. p. 115-147.
56. Frank, C.B., *Ligament structure, physiology and function.* J Musculoskelet Neuronal Interact, 2004. **4**(2): p. 199-201.
57. Leikina, E., et al., *Type I collagen is thermally unstable at body temperature.* Proc Natl Acad Sci U S A, 2002. **99**(3): p. 1314-8.
58. Beye, J.A., et al., *Injury-induced changes in mRNA levels differ widely between anterior cruciate ligament and medial collateral ligament.* Am J Sports Med, 2008. **36**(7): p. 1337-46.
59. Chun, J., et al., *Cultures of Ligament Fibroblasts in Fibrin Matrix Gel.* Connective Tissue Research, 2003. **44**(2): p. 81-87.

60. Young, K., et al., *Extracellular matrix content of ruptured anterior cruciate ligament tissue.* Knee, 2011. **18**(4): p. 242-6.
61. Teh, T.K., S.L. Toh, and J.C. Goh, *Aligned fibrous scaffolds for enhanced mechanoresponse and tenogenesis of mesenchymal stem cells.* Tissue Eng Part A, 2013. **19**(11-12): p. 1360-72.
62. Yang, G., B.B. Rothrauff, and R.S. Tuan, *Tendon and ligament regeneration and repair: clinical relevance and developmental paradigm.* Birth Defects Res C Embryo Today, 2013. **99**(3): p. 203-222.
63. Spindler, K.P., et al., *Anterior Cruciate Ligament Reconstruction in High School and College-Aged Athletes: Does Autograft Choice Influence Anterior Cruciate Ligament Revision Rates?* Am J Sports Med, 2020. **48**(2): p. 298-309.
64. Frank, R.M., et al., *ACL Reconstruction Basics: Quadruple (4-Strand) Hamstring Autograft Harvest.* Arthrosc Tech, 2017. **6**(4): p. e1309-e1313.
65. He, X., et al., *Clinical Outcomes of the Central Third Patellar Tendon Versus Four-strand Hamstring Tendon Autograft Used for Anterior Cruciate Ligament Reconstruction: A Systematic Review and Subgroup Meta-analysis of Randomized Controlled Trials.* Injury, 2020. **51**(8): p. 1714-1725.
66. Samuelsen, B.T., et al., *Hamstring Autograft versus Patellar Tendon Autograft for ACL Reconstruction: Is There a Difference in Graft Failure Rate? A Meta-analysis of 47,613 Patients.* Clin Orthop Relat Res, 2017. **475**(10): p. 2459-2468.
67. Yang, X.G., et al., *Network meta-analysis of knee outcomes following anterior cruciate ligament reconstruction with various types of tendon grafts.* Int Orthop, 2020. **44**(2): p. 365-380.
68. Mouarbes, D., et al., *Lower donor-site morbidity using QT autografts for ACL reconstruction.* Knee Surgery, Sports Traumatology, Arthroscopy, 2020. **28**(8): p. 2558-2566.
69. Inderhaug, E., T. Strand, and E. Solheim, *The impact of sensory deficits after harvesting hamstrings autograft for ACL reconstruction.* Knee Surgery, Sports Traumatology, Arthroscopy, 2015. **23**(4): p. 1060-1064.
70. Guglielmetti, L.G.B., et al., *Prospective and Randomized Clinical Evaluation of Hamstring Versus Patellar Tendon Autograft for Anterior Cruciate Ligament Reconstruction in Soccer Players.* Orthop J Sports Med, 2021. **9**(9): p. 23259671211028168.
71. Bottoni, C.R., et al., *Autograft Versus Allograft Anterior Cruciate Ligament Reconstruction: A Prospective, Randomized Clinical Study With a Minimum 10-Year Follow-up.* Am J Sports Med, 2015. **43**(10): p. 2501-9.
72. Iosifidis, M.I. and A. Tsarouhas, *Allografts in Anterior Cruciate Ligament Reconstruction*. Sports Injuries. 2010 Nov 12:421-30. doi: 10.1007/978-3-642-15630-4_58.
73. Li, Y., et al., *Tissue-Engineered Decellularized Allografts for Anterior Cruciate Ligament Reconstruction.* ACS Biomaterials Science & Engineering, 2020. **6**(10): p. 5700-5710.
74. Razi, M., et al., *Allograft or autograft in skeletally immature anterior cruciate ligament reconstruction: a prospective evaluation using both partial and complete transphyseal techniques.* Journal of Orthopaedic Surgery and Research, 2019. **14**(1): p. 85.
75. Van Der Merwe, W., et al., *Xenograft for anterior cruciate ligament reconstruction was associated with high graft processing infection.* Journal of Experimental Orthopaedics, 2020. **7**(1): p. 79.
76. Zaffagnini, S., et al., *Anterior cruciate ligament reconstruction with a novel porcine xenograft: the initial Italian experience.* Joints, 2015. **3**(2): p. 85-90.
77. Davarinos, N., B.J. O'Neill, and W. Curtin, *A Brief History of Anterior Cruciate Ligament Reconstruction.* Advances in Orthopedic Surgery, 2014. **2014**: p. 706042.
78. Ficek, K., et al., *Bioresorbable Stent in Anterior Cruciate Ligament Reconstruction.* Polymers (Basel), 2019. **11**(12).

79. Batty, L.M., et al., *Synthetic devices for reconstructive surgery of the cruciate ligaments: a systematic review.* Arthroscopy, 2015. **31**(5): p. 957-68.
80. Satora, W., et al., *Synthetic grafts in the treatment of ruptured anterior cruciate ligament of the knee joint.* Polim Med, 2017. **47**(1): p. 55-59.
81. Chen, T., J. Jiang, and S. Chen, *Status and headway of the clinical application of artificial ligaments.* Asia Pac J Sports Med Arthrosc Rehabil Technol, 2015. **2**(1): p. 15-26.
82. Legnani, C., et al., *Anterior cruciate ligament reconstruction with synthetic grafts. A review of literature.* Int Orthop, 2010. **34**(4): p. 465-71.
83. Li, H., et al., *Biologic Failure of a Ligament Advanced Reinforcement System Artificial Ligament in Anterior Cruciate Ligament Reconstruction: A Report of Serious Knee Synovitis.* Arthroscopy: The Journal of Arthroscopic & Related Surgery, 2012. **28**(4): p. 583-586.
84. Muren, O., L. Dahlstedt, and N. Dalén, *Reconstruction of acute anterior cruciate ligament injuries: a prospective, randomised study of 40 patients with 7-year follow-up. No advantage of synthetic augmentation compared to a traditional patellar tendon graft.* Arch Orthop Trauma Surg, 2003. **123**(4): p. 144-7.
85. Guidoin, M.-F., et al., *Analysis of retrieved polymer fiber based replacements for the ACL.* Biomaterials, 2000. **21**(23): p. 2461-2474.
86. Narayanan, G., et al., *Poly (lactic acid)-based biomaterials for orthopaedic regenerative engineering.* Adv Drug Deliv Rev, 2016. **107**: p. 247-276.
87. Ge, Z., et al., *Characterization of knitted polymeric scaffolds for potential use in ligament tissue engineering.* J Biomater Sci Polym Ed, 2005. **16**(9): p. 1179-92.
88. Leong, N.L., F.A. Petrigliano, and D.R. McAllister, *Current tissue engineering strategies in anterior cruciate ligament reconstruction.* Journal of Biomedical Materials Research Part A, 2014. **102**(5): p. 1614-1624.
89. Batty, L.M., et al., *Synthetic Devices for Reconstructive Surgery of the Cruciate Ligaments: A Systematic Review.* Arthroscopy: The Journal of Arthroscopic & Related Surgery, 2015. **31**(5): p. 957-968.
90. Jonathan Seymour Mulford, D.C., *Anterior cruciate ligament reconstruction: a systematic review of polyethylene terephthalate grafts.* ANZ Journal of Surgery, 2011. **81**(11): p. 785-789.
91. Sahoo, S., S. Lok Toh, and J.C. Hong Goh, *PLGA nanofiber-coated silk microfibrous scaffold for connective tissue engineering.* Journal of Biomedical Materials Research Part B: Applied Biomaterials, 2010. **95B**(1): p. 19-28.
92. Gisselfält, K., B. Edberg, and P. Flodin, *Synthesis and properties of degradable poly(urethane urea)s to be used for ligament reconstructions.* Biomacromolecules, 2002. **3**(5): p. 951-8.
93. Wang, C.-H., et al., *Effects of Artificial Ligaments with Different Porous Structures on the Migration of BMSCs.* Stem Cells International, 2015. **2015**: p. 702381.
94. Newcastle and York External Assessment Centre, M.T.E.P., NICE, *LARS for reconstructing damaged intra-articular cruciate knee ligaments*, N.I.f.H.a.C. Excellence, Editor. 2015, NICE: NICE guidelines. p. 1-39.
95. Tulloch, S.J., et al., *Primary ACL reconstruction using the LARS device is associated with a high failure rate at minimum of 6-year follow-up.* Knee Surgery, Sports Traumatology, Arthroscopy, 2019. **27**(11): p. 3626-3632.
96. Pan, X., et al., *Bone–patellar tendon–bone autograft versus LARS artificial ligament for anterior cruciate ligament reconstruction.* European Journal of Orthopaedic Surgery & Traumatology, 2013. **23**(7): p. 819-823.
97. Ventura, A., et al., *Synthetic grafts for anterior cruciate ligament rupture: 19-year outcome study.* Knee, 2010. **17**(2): p. 108-13.

98. Jia, Z.Y., et al., *Comparison of artificial graft versus autograft in anterior cruciate ligament reconstruction: a meta-analysis.* BMC Musculoskelet Disord, 2017. **18**(1): p. 309.
99. Parchi, P.D., et al., *Anterior cruciate ligament reconstruction with LARS™ artificial ligament results at a mean follow-up of eight years.* Int Orthop, 2013. **37**(8): p. 1567-74.
100. Iliadis, D.P., et al., *LARS Artificial Ligament Versus ABC Purely Polyester Ligament for Anterior Cruciate Ligament Reconstruction.* Orthop J Sports Med, 2016. **4**(6): p. 2325967116653359.
101. Sinagra, Z.P., et al., *Foreign Body Reaction Associated With Artificial LARS Ligaments: A Retrieval Study.* Orthop J Sports Med, 2018. **6**(12): p. 2325967118811604.
102. Secondary Care Analysis, N.D., *Hospital Accident and Emergency Activity - 2015-16. Excel tables and charts*, J. Winter, Editor. 2017, NHS.
103. Boards, S.M. *Rupture du ligament croisé antérieur: traitement opératoire ou conservateur?* 2009 [cited 2017 September]; Available from: http://www.medical-board.ch/index.php?id=809&L=1.
104. Waldén, M., et al., *ACL injuries in men's professional football: a 15-year prospective study on time trends and return-to-play rates reveals only 65% of players still play at the top level 3 years after ACL rupture.* Br J Sports Med, 2016. **50**(12): p. 744-50.
105. Simon, D., et al., *The Relationship between Anterior Cruciate Ligament Injury and Osteoarthritis of the Knee.* Advances in Orthopedics, 2015. **2015**: p. 928301.
106. Svoboda, S.J., et al., *Changes in Serum Biomarkers of Cartilage Turnover After Anterior Cruciate Ligament Injury.* The American Journal of Sports Medicine, 2013. **41**(9): p. 2108-2116.
107. Mather, R.C., et al., *Societal and Economic Impact of Anterior Cruciate Ligament Tears.* Journal of Bone and Joint Surgery-American Volume, 2013. **95a**(19): p. 1751-1759.
108. Leiter, J.R.S., et al., *Long-term follow-up of ACL reconstruction with hamstring autograft.* Knee Surgery, Sports Traumatology, Arthroscopy, 2014. **22**(5): p. 1061-1069.
109. Punzi, L., et al., *Post-traumatic arthritis: overview on pathogenic mechanisms and role of inflammation.* RMD Open, 2016. **2**(2): p. e000279.
110. Gao, B., M.L. Cordova, and N. Zheng, *Three-dimensional joint kinematics of ACL-deficient and ACL-reconstructed knees during stair ascent and descent.* Human Movement Science, 2012. **31**(1): p. 222-235.
111. Hunt, E.R., et al., *Anterior cruciate ligament reconstruction reinitiates an inflammatory and chondrodegenerative process in the knee joint.* Journal of Orthopaedic Research, 2021. **39**(6): p. 1281-1288.
112. Larsson, S., et al., *Surgical reconstruction of ruptured anterior cruciate ligament prolongs trauma-induced increase of inflammatory cytokines in synovial fluid: an exploratory analysis in the KANON trial.* Osteoarthritis and Cartilage, 2017. **25**(9): p. 1443-1451.
113. Eliakim, E., et al., *Estimation of injury costs: financial damage of English Premier League teams' underachievement due to injuries.* BMJ Open Sport & Exercise Medicine, 2020. **6**(1): p. e000675.
114. Núñez, M., et al., *Health-Related Quality of Life and Direct Costs in Patients With Anterior Cruciate Ligament Injury: Single-Bundle Versus Double-Bundle Reconstruction in a Low-Demand Cohort—A Randomized Trial With 2 Years of Follow-up.* Arthroscopy: The Journal of Arthroscopic & Related Surgery, 2012. **28**(7): p. 929-935.
115. Prevention, C.f.D.C.a. *Data & Statistics (WISQARS™): Cost of Injury Reports*. 2014 September 18, 2014 [cited 2017 October]; Available from: https://wisqars.cdc.gov:8443/costT/.
116. Lubowitz, J.H. and D. Appleby, *Cost-Effectiveness Analysis of the Most Common Orthopaedic Surgery Procedures: Knee Arthroscopy and Knee Anterior Cruciate Ligament Reconstruction.* Arthroscopy-the Journal of Arthroscopic and Related Surgery, 2011. **27**(10): p. 1317-1322.

117. Ahlden, M., et al., *Knee laxity measurements after anterior cruciate ligament reconstruction, using either bone-patellar-tendon-bone or hamstring tendon autografts, with special emphasis on comparison over time.* Knee Surgery Sports Traumatology Arthroscopy, 2009. **17**(9): p. 1117-1124.
118. Fleming, B.C., et al., *The Effect of Initial Graft Tension After Anterior Cruciate Ligament Reconstruction A Randomized Clinical Trial With 36-Month Follow-up.* American Journal of Sports Medicine, 2013. **41**(1): p. 25-34.
119. Wright, R.W., et al., *Descriptive Epidemiology of the Multicenter ACL Revision Study (MARS) Cohort.* American Journal of Sports Medicine, 2010. **38**(10): p. 1979-1986.
120. Centre, T.N.C., *Review Manager* 2014, The Cochrane Collaboration,: Copenhagen.
121. Moher, D., et al., *CONSORT 2010 explanation and elaboration: updated guidelines for reporting parallel group randomised trials.* Bmj, 2010. **340**: p. c869.
122. Adravanti, P., et al., *Single-Bundle versus Double-Bundle Anterior Cruciate Ligament Reconstruction: A Prospective Randomized Controlled Trial with 6-Year Follow-up.* Journal of Knee Surgery, 2017. **30**(9): p. 898-904.
123. Jarvela, T., *Double-bundle versus single-bundle anterior cruciate ligament reconstruction: a prospective, randomize clinical study.* Knee Surgery Sports Traumatology Arthroscopy, 2007. **15**(5): p. 500-507.
124. Nunez, M., et al., *Health-Related Quality of Life and Direct Costs in Patients With Anterior Cruciate Ligament Injury: Single-Bundle Versus Double-Bundle Reconstruction in a Low-Demand Cohort-A Randomized Trial With 2 Years of Follow-up.* Arthroscopy-the Journal of Arthroscopic and Related Surgery, 2012. **28**(7): p. 929-935.
125. Sasaki, S., et al., *Prospective Randomized Study of Objective and Subjective Clinical Results Between Double-Bundle and Single-Bundle Anterior Cruciate Ligament Reconstruction.* American Journal of Sports Medicine, 2016. **44**(4): p. 855-864.
126. Siebold, R., C. Dehler, and T. Ellert, *Prospective randomized comparison of double-bundle versus single-bundle anterior cruciate ligament reconstruction.* Arthroscopy-the Journal of Arthroscopic and Related Surgery, 2008. **24**(2): p. 137-145.
127. Sun, R., et al., *Prospective randomized comparison of knee stability and joint degeneration for double- and single-bundle ACL reconstruction.* Knee Surgery Sports Traumatology Arthroscopy, 2015. **23**(4): p. 1171-1178.
128. Suomalainen, P., et al., *Double-Bundle Versus Single-Bundle Anterior Cruciate Ligament Reconstruction A Prospective Randomized Study With 5-Year Results.* American Journal of Sports Medicine, 2012. **40**(7): p. 1511-1518.
129. Xu, Y., et al., *Prospective randomized comparison of anatomic single- and double-bundle anterior cruciate ligament reconstruction.* Knee Surgery Sports Traumatology Arthroscopy, 2014. **22**(2): p. 308-316.
130. Zaffagnini, S., et al., *Single-bundle patellar tendon versus non-anatomical double-bundle hamstrings ACL reconstruction: a prospective randomized study at 8-year minimum follow-up.* Knee Surgery Sports Traumatology Arthroscopy, 2011. **19**(3): p. 390-397.
131. Zhang, Z., et al., *Double-bundle versus single-bundle anterior cruciate ligament reconstructions: a prospective, randomized study with 2-year follow-up.* Eur J Orthop Surg Traumatol, 2014. **24**(4): p. 559-65.
132. Bjorkman, P., J. Sandelin, and A. Harilainen, *A randomized prospective controlled study with 5-year follow-up of cross-pin femoral fixation versus metal interference screw fixation in anterior cruciate ligament reconstruction.* Knee Surgery Sports Traumatology Arthroscopy, 2015. **23**(8): p. 2353-2359.

133. De Wall, M., et al., *Tibial Fixation in Anterior Cruciate Ligament Reconstruction A Prospective Randomized Study Comparing Metal Interference Screw and Staples With a Centrally Placed Polyethylene Screw and Sheath.* American Journal of Sports Medicine, 2011. **39**(9): p. 1858-1864.
134. Drogset, J.O., et al., *A prospective randomized study of ACL-reconstructions using bone-patellar tendon-bone grafts fixed with bioabsorbable or metal interference screws.* Knee Surgery Sports Traumatology Arthroscopy, 2011. **19**(5): p. 753-759.
135. Harilainen, A. and J. Sandelin, *A Prospective Comparison of 3 Hamstring ACL Fixation Devices-Rigidfix, BioScrew, and Intrafix-Randomized Into 4 Groups With 2 Years of Follow-Up.* American Journal of Sports Medicine, 2009. **37**(4): p. 699-706.
136. Jarvela, T., et al., *Double-bundle anterior cruciate ligament reconstruction using hamstring autografts and bioabsorbable interference screw fixation.* American Journal of Sports Medicine, 2008. **36**(2): p. 290-297.
137. Moisala, A.S., et al., *Comparison of the bioabsorbable and metal screw fixation after ACL reconstruction with a hamstring autograft in MRI and clinical outcome: a prospective randomized study.* Knee Surgery Sports Traumatology Arthroscopy, 2008. **16**(12): p. 1080-1086.
138. Myers, P., et al., *Bioabsorbable versus titanium interference screws with hamstring autograft in anterior cruciate ligament reconstruction: A prospective randomized trial with 2-year follow-up.* Arthroscopy-the Journal of Arthroscopic and Related Surgery, 2008. **24**(7): p. 817-823.
139. Price, R., J. Stoney, and G. Brown, *Prospective randomized comparison of endobutton versus cross-pin femoral fixation in hamstring anterior cruciate ligament reconstruction with 2-year follow-up.* Anz Journal of Surgery, 2010. **80**(3): p. 162-165.
140. Stener, S., et al., *A Long-Term, Prospective, Randomized Study Comparing Biodegradable and Metal Interference Screws in Anterior Cruciate Ligament Reconstruction Surgery Radiographic Results and Clinical Outcome.* American Journal of Sports Medicine, 2010. **38**(8): p. 1598-1605.
141. Stengel, D., et al., *Bioresorbable Pins and Interference Screws for Fixation of Hamstring Tendon Grafts in Anterior Cruciate Ligament Reconstruction Surgery A Randomized Controlled Trial.* American Journal of Sports Medicine, 2009. **37**(9): p. 1692-1698.
142. Aglietti, P., et al., *Anterior cruciate ligament reconstruction: Bone-patellar tendon-bone compared with double semitendinosus and gracilis tendon grafts - A prospective, randomized clinical trial.* Journal of Bone and Joint Surgery-American Volume, 2004. **86a**(10): p. 2143-2155.
143. Barenius, B., et al., *Increased Risk of Osteoarthritis After Anterior Cruciate Ligament Reconstruction A 14-Year Follow-up Study of a Randomized Controlled Trial.* American Journal of Sports Medicine, 2014. **42**(5): p. 1049-1057.
144. Holm, I., et al., *No Difference in Knee Function or Prevalence of Osteoarthritis After Reconstruction of the Anterior Cruciate Ligament With 4-Strand Hamstring Autograft Versus Patellar Tendon-Bone Autograft A Randomized Study With 10-Year Follow-up.* American Journal of Sports Medicine, 2010. **38**(3): p. 448-454.
145. Kautzner, J., et al., *A comparison of ACL reconstruction using patellar tendon versus hamstring autograft in female patients: a prospective randomised study.* International Orthopaedics, 2015. **39**(1): p. 125-130.
146. Maletis, G.B., et al., *A prospective randomized study of anterior cruciate ligament reconstruction - A comparison of patellar tendon and quadruple-strand semitendinosus/gracilis tendons fixed with bioabsorbable interference screws.* American Journal of Sports Medicine, 2007. **35**(3): p. 384-394.
147. Mohtadi, N., et al., *Complications and Adverse Events of a Randomized Clinical Trial Comparing 3 Graft Types for ACL Reconstruction.* Clinical Journal of Sport Medicine, 2016. **26**(3): p. 182-189.

148. Taylor, D.C., et al., *Patellar tendon versus hamstring tendon autografts for anterior cruciate ligament reconstruction: a randomized controlled trial using similar femoral and tibial fixation methods.* Am J Sports Med, 2009. **37**(10): p. 1946-57.
149. Webster, K.E., et al., *Comparison of Patellar Tendon and Hamstring Tendon Anterior Cruciate Ligament Reconstruction: A 15-Year Follow-up of a Randomized Controlled Trial.* American Journal of Sports Medicine, 2016. **44**(1): p. 83-90.
150. Beynnon, B.D., et al., *Accelerated Versus Nonaccelerated Rehabilitation After Anterior Cruciate Ligament Reconstruction A Prospective, Randomized, Double-Blind Investigation Evaluating Knee Joint Laxity Using Roentgen Stereophotogrammetric Analysis.* American Journal of Sports Medicine, 2011. **39**(12): p. 2536-2548.
151. Mayr, H.O., et al., *Rehabilitation results following anterior cruciate ligament reconstruction using a hard brace compared to a fluid-filled soft brace.* Knee, 2010. **17**(2): p. 119-126.
152. Risberg, M.A. and I. Holm, *The Long-term Effect of 2 Postoperative Rehabilitation Programs After Anterior Cruciate Ligament Reconstruction A Randomized Controlled Clinical Trial With 2 Years of Follow-Up.* American Journal of Sports Medicine, 2009. **37**(10): p. 1958-1966.
153. Sun, K., et al., *A prospective randomized comparison of irradiated and non-irradiated hamstring tendon allograft for ACL reconstruction.* Knee Surgery Sports Traumatology Arthroscopy, 2012. **20**(1): p. 187-194.
154. Tian, S.Q., et al., *Arthroscopic anatomic double-bundle ACL reconstruction using irradiated versus non-irradiated hamstring tendon allograft.* Knee Surgery Sports Traumatology Arthroscopy, 2017. **25**(1): p. 251-259.
155. Stensbirk, F., et al., *Iliotibial band autograft versus bone-patella-tendon-bone autograft, a possible alternative for ACL reconstruction: a 15-year prospective randomized controlled trial.* Knee Surgery Sports Traumatology Arthroscopy, 2014. **22**(9): p. 2094-2101.
156. Karimi-Mobarakeh, M., et al., *Role of gracilis harvesting in four-strand hamstring tendon anterior cruciate ligament reconstruction: a double-blinded prospective randomized clinical trial.* Knee Surgery Sports Traumatology Arthroscopy, 2015. **23**(4): p. 1086-1091.
157. McRae, S., et al., *Ipsilateral Versus Contralateral Hamstring Grafts in Anterior Cruciate Ligament Reconstruction A Prospective Randomized Trial.* American Journal of Sports Medicine, 2013. **41**(11): p. 2492-2499.
158. Peterson, L., et al., *Long-term results of a randomized study on anterior cruciate ligament reconstruction with or without a synthetic degradable augmentation device to support the autograft.* Knee Surgery Sports Traumatology Arthroscopy, 2014. **22**(9): p. 2109-2120.
159. Rose, M.B., et al., *A prospective randomized comparison of two distinct allogenic tissue constructs for anterior cruciate ligament reconstruction.* Knee, 2016. **23**(6): p. 1112-1120.
160. Mutsuzaki, H., et al., *Effect of Calcium Phosphate-Hybridized Tendon Graft in Anterior Cruciate Ligament Reconstruction A Randomized Controlled Trial.* American Journal of Sports Medicine, 2012. **40**(8): p. 1772-1780.
161. Ghalayini, S.R.A., et al., *Arthroscopic anterior cruciate ligament surgery: Results of autogenous patellar tendon graft versus the Leeds-Keio synthetic graft Five year follow-up of a prospective randomised controlled trial.* Knee, 2010. **17**(5): p. 334-339.
162. Yoo, S.H., et al., *Comparison of clinical outcomes and second-look arthroscopic findings after ACL reconstruction using a hamstring autograft or a tibialis allograft.* Knee Surgery Sports Traumatology Arthroscopy, 2017. **25**(4): p. 1290-1297.
163. Hart, R., et al., *Outcomes after conventional versus computer-navigated anterior cruciate ligament reconstruction.* Arthroscopy-the Journal of Arthroscopic and Related Surgery, 2008. **24**(5): p. 569-578.

164. Zaffagnini, S., et al., *ST/G ACL reconstruction: double strand plus extra-articular sling vs double bundle, randomized study at 3-year follow-up.* Scandinavian Journal of Medicine & Science in Sports, 2008. **18**(5): p. 573-581.
165. Akelman, M.R., et al., *Effect of Matching or Overconstraining Knee Laxity During Anterior Cruciate Ligament Reconstruction on Knee Osteoarthritis and Clinical Outcomes: A Randomized Controlled Trial With 84-Month Follow-up.* American Journal of Sports Medicine, 2016. **44**(7): p. 1660-1670.
166. Karimi-Mobarakeh, M., et al., *Role of gracilis harvesting in four-strand hamstring tendon anterior cruciate ligament reconstruction: a double-blinded prospective randomized clinical trial.* Knee Surg Sports Traumatol Arthrosc, 2015. **23**(4): p. 1086-91.
167. Keays, S.L., et al., *Factors Involved in the Development of Osteoarthritis after Anterior Cruciate Ligament Surgery.* The American Journal of Sports Medicine, 2010. **38**(3): p. 455-463.
168. Bigoni, M., et al., *Effects of ACL Reconstructive Surgery on Temporal Variations of Cytokine Levels in Synovial Fluid.* Mediators of Inflammation, 2016. **2016**: p. 8243601.
169. Kraus, V.B., et al., *Effects of intraarticular IL1-Ra for acute anterior cruciate ligament knee injury: a randomized controlled pilot trial (NCT00332254).* Osteoarthritis Cartilage, 2012. **20**(4): p. 271-8.
170. Lattermann, C., et al., *A Multicenter Study of Early Anti-inflammatory Treatment in Patients With Acute Anterior Cruciate Ligament Tear.* Am J Sports Med, 2017. **45**(2): p. 325-333.
171. Hou, C., et al., *An insight into anti-inflammatory effects of natural polysaccharides.* International Journal of Biological Macromolecules, 2020. **153**: p. 248-255.
172. Shelbourne, K.D., T. Gray, and M. Haro, *Incidence of Subsequent Injury to Either Knee within 5 Years after Anterior Cruciate Ligament Reconstruction with Patellar Tendon Autograft.* The American Journal of Sports Medicine 2017. **37** (2): p. 246 - 251.
173. Maletis, G.B., M.C.S. Inacio, and T.T. Funahashi, *Risk Factors Associated With Revision and Contralateral Anterior Cruciate Ligament Reconstructions in the Kaiser Permanente ACLR Registry.* The American Journal of Sports Medicine, 2015. **43**(3): p. 641-647.
174. Samitier, G., et al., *Failure of Anterior Cruciate Ligament Reconstruction.* Arch Bone Jt Surg, 2015. **3**(4): p. 220-40.
175. Amiel, D., et al., *The phenomenon of "ligamentization": anterior cruciate ligament reconstruction with autogenous patellar tendon.* J Orthop Res, 1986. **4**(2): p. 162-72.
176. Janssen, R.P. and S.U. Scheffler, *Intra-articular remodelling of hamstring tendon grafts after anterior cruciate ligament reconstruction.* Knee Surg Sports Traumatol Arthrosc, 2014. **22**(9): p. 2102-8.
177. Claes, S., et al., *The "ligamentization" process in anterior cruciate ligament reconstruction: what happens to the human graft? A systematic review of the literature.* Am J Sports Med, 2011. **39**(11): p. 2476-83.
178. Scheffler, S.U., F.N. Unterhauser, and A. Weiler, *Graft remodeling and ligamentization after cruciate ligament reconstruction.* Knee Surgery, Sports Traumatology, Arthroscopy, 2008. **16**(9): p. 834-842.
179. Jameson, S.S., et al., *Complications following anterior cruciate ligament reconstruction in the English NHS.* Knee, 2012. **19**(1): p. 14-9.
180. Abram, S.G.F., et al., *Rates of Adverse Outcomes and Revision Surgery After Anterior Cruciate Ligament Reconstruction: A Study of 104,255 Procedures Using the National Hospital Episode Statistics Database for England, UK.* Am J Sports Med, 2019. **47**(11): p. 2533-2542.
181. Atukorala, I., et al., *Synovitis in knee osteoarthritis: a precursor of disease?* Ann Rheum Dis, 2016. **75**(2): p. 390-5.

182. Makhni, E.C., et al., *Functional Outcome and Graft Retention in Patients With Septic Arthritis After Anterior Cruciate Ligament Reconstruction: A Systematic Review.* Arthroscopy, 2015. **31**(7): p. 1392-401.
183. Rousseau, R., et al., *Complications After Anterior Cruciate Ligament Reconstruction and Their Relation to the Type of Graft: A Prospective Study of 958 Cases.* The American Journal of Sports Medicine, 2019. **47**(11): p. 2543-2549.
184. Tiamklang, T., et al., *Double-bundle versus single-bundle reconstruction for anterior cruciate ligament rupture in adults.* Cochrane Database of Systematic Reviews, 2012(11).
185. Svantesson, E., et al., *Future Perspectives of Anterior Cruciate Ligament Reconstruction.* Operative Techniques in Orthopaedics. **27**(1): p. 79-87.
186. Walsh, B.J., et al., *Microplate reader-based quantitation of collagens.* Analytical Biochemistry, 1992. **203**(2): p. 187-190.
187. Wan, C., Z. Hao, and S. Wen, *A quantitative comparison of morphological and histological characteristics of collagen in the rabbit medial collateral ligament.* Annals of Anatomy - Anatomischer Anzeiger, 2013. **195**(6): p. 562-569.
188. Lattouf, R., et al., *Picrosirius Red Staining: A Useful Tool to Appraise Collagen Networks in Normal and Pathological Tissues.* Journal of Histochemistry & Cytochemistry, 2014. **62**(10): p. 751-758.
189. Kasahara, T., S. Shoji, and J. Mizuno, *Surface Modification of Polyethylene Terephthalate (PET) by 172-nm Excimer Lamp.* Transactions of The Japan Institute of Electronics Packaging, 2012. **5**: p. 47-54.
190. Liu, Y., et al., *Surface modification of polyethylene terephthalate films by direct fluorination.* AIP Advances, 2018. **8**(12): p. 125333.
191. Tavanai, H., *A new look at the modification of polyethylene terephthalate by sodium hydroxide.* The Journal of The Textile Institute, 2009. **100**(7): p. 633-639.
192. Wu, G., et al., *Excimer laser chemical ammonia patterning on PET film.* J Mater Sci Mater Med, 2009. **20**(2): p. 597-606.
193. Ardelean, H., et al., *Effects of different laser and plasma treatments on the interface and adherence between evaporated aluminium and polyethylene terephthalate films: X-ray photoemission, and adhesion studies.* Applied Surface Science, 2005. **243**(1): p. 304-318.
194. Ebnesajjad, S., *17 - Surface Treatment of Fluoropolymers for Adhesion*, in *Fluoroplastics (Second Edition)*, S. Ebnesajjad, Editor. 2015, William Andrew Publishing: Oxford. p. 564-588.
195. Marcandalli, B. and C. Riccardi, *11 - Plasma treatments of fibres and textiles*, in *Plasma Technologies for Textiles*, R. Shishoo, Editor. 2007, Woodhead Publishing. p. 282-300.
196. Friedrich, J., *The plasma chemistry of polymer surfaces : advanced techniques for surface design / [by] Jörg Friedrich*. 2012, Weinheim: Weinheim : Wiley-VCH.
197. Wiesemann, K. *A Short Introduction to Plasma Physics*. 2014.
198. Bauder, U.H., *Properties of high pressure arc plasma.* Applied physics, 1976. **9**(2): p. 105-115.
199. Graham, W.G., *1 - The physics and chemistry of plasmas for processing textiles and other materials*, in *Plasma Technologies for Textiles*, R. Shishoo, Editor. 2007, Woodhead Publishing. p. 3-24.
200. Tabares, F.L. and I. Junkar, *Cold Plasma Systems and Their Application in Surface Treatments for Medicine.* Molecules, 2021. **26**(7): p. 1903.
201. Schutze, A., et al., *The atmospheric-pressure plasma jet: a review and comparison to other plasma sources.* IEEE Transactions on Plasma Science, 1998. **26**(6): p. 1685-1694.
202. Braný, D., et al., *Cold Atmospheric Plasma: A Powerful Tool for Modern Medicine.* International journal of molecular sciences, 2020. **21**(8): p. 2932.

203. Bogaerts, A., et al., *Gas discharge plasmas and their applications.* Spectrochimica Acta Part B: Atomic Spectroscopy, 2002. **57**(4): p. 609-658.
204. Liu, D., et al., *Analysis of double-probe characteristics in low-frequency gas discharges and its improvement.* Rev Sci Instrum, 2015. **86**(1): p. 013504.
205. Dobkin, D.M., *Principles of chemical vapor deposition : [what's going on inside the reactor] / by Daniel M. Dobkin and Michael K. Zuraw*, ed. M.K. Zuraw. 2003, Dordrecht

London: Dordrecht

London : Kluwer Academic Publishers.
206. Mansuroglu, D., *Capacitively coupled radio frequency nitrogen plasma generated at two different exciting frequencies of 13.56 MHz and 40 MHz analyzed using Langmuir probe along with optical emission spectroscopy.* AIP Advances, 2019. **9**(5): p. 055205.
207. Chen, Y., et al., *A Facile, Low-Cost Plasma Etching Method for Achieving Size Controlled Non-Close-Packed Monolayer Arrays of Polystyrene Nano-Spheres.* Nanomaterials, 2019. **9**(4): p. 605.
208. Kutlu, B., A. Al_it, and M. Mutlu, *Surface modification of textiles by glow discharge technique: Part II: Low frequency plasma treatment of wool fabrics with acrylic acid.* Journal of Applied Polymer Science, 2010. **116**: p. 1545-1551.
209. Wilken, L., V. Hoffmann, and K. Wetzig, *Electrical measurements at radio frequency glow discharges for spectroscopy.* Spectrochimica Acta Part B: Atomic Spectroscopy, 2007. **62**(10): p. 1085-1122.
210. Yambe, K., *Property of plasma by radio frequency discharge with the use of multi hollow cathodes.* Journal of Physics: Conference Series, 2008. **106**: p. 012018.
211. Moisan, M., et al., *Low-temperature sterilization using gas plasmas: a review of the experiments and an analysis of the inactivation mechanisms.* International Journal of Pharmaceutics, 2001. **226**(1): p. 1-21.
212. *Capacitive Discharges*, in *Principles of Plasma Discharges and Materials Processing*. 2005. p. 387-460.
213. Nebel, C.E., *Chapter Four - Nitrogen-vacancy doped CVD diamond for quantum applications: A review*, in *Semiconductors and Semimetals*, C.E. Nebel, et al., Editors. 2020, Elsevier. p. 73-136.
214. Thissen, H., *5 - Plasma-based surface modification for the control of biointerfacial interactions*, in *Biosynthetic Polymers for Medical Applications*, L. Poole-Warren, P. Martens, and R. Green, Editors. 2016, Woodhead Publishing. p. 129-144.
215. Potter, S., Kelley, Michael C. and Liley, Bruce Sween., *Plasma*, in *Encyclopedia Britannica*.
216. Grace, J.M. and L.J. Gerenser, *Plasma Treatment of Polymers.* Journal of Dispersion Science and Technology, 2003. **24**(3-4): p. 305-341.
217. Siow, K.S., et al., *Plasma Methods for the Generation of Chemically Reactive Surfaces for Biomolecule Immobilization and Cell Colonization - A Review.* Plasma Processes and Polymers, 2006. **3**(6-7): p. 392-418.
218. Liston, E.M., *Plasma Treatment for Improved Bonding: A Review.* The Journal of Adhesion, 1989. **30**(1-4): p. 199-218.
219. Jurak, M., et al., *Chitosan/phospholipid coated polyethylene terephthalate (PET) polymer surfaces activated by air plasma.* Colloids and Surfaces a-Physicochemical and Engineering Aspects, 2017. **532**: p. 155-164.
220. Ramachandran, B., et al., *A comparative study of polyethylene terephthalate surface carboxylation techniques: Characterization, in vitro haemocompatibility and endothelialization.* Reactive & Functional Polymers, 2018. **122**: p. 22-32.

221. Slepicka, P., et al., *Nano-structured and functionalized surfaces for cytocompatibility improvement and bactericidal action.* Biotechnology Advances, 2015. **33**(6): p. 1120-1129.
222. Recek, N., et al., *Protein Adsorption on Various Plasma-Treated Polyethylene Terephthalate Substrates.* Molecules, 2013. **18**(10): p. 12441-12463.
223. Liu, X., et al., *Mesenchymal stem cell interacted with PLCL braided scaffold coated with poly-l-lysine/hyaluronic acid for ligament tissue engineering.* J Biomed Mater Res A, 2018. **106**(12): p. 3042-3052.
224. Junkar, I., et al., *Influence of oxygen and nitrogen plasma treatment on polyethylene terephthalate (PET) polymers.* Vacuum, 2009. **84**(1): p. 83-85.
225. Lv, J.C., et al., *Environmentally friendly surface modification of polyethylene terephthalate (PET) fabric by low-temperature oxygen plasma and carboxymethyl chitosan.* Journal of Cleaner Production, 2016. **118**: p. 187-196.
226. Mulford, J.S. and D. Chen, *Anterior cruciate ligament reconstruction: a systematic review of polyethylene terephthalate grafts.* ANZ J Surg, 2011. **81**(11): p. 785-9.
227. James, J., et al., *Chapter 11 - Microscopic Analysis of Plasma-Activated Polymeric Materials*, in *Non-Thermal Plasma Technology for Polymeric Materials*, S. Thomas, et al., Editors. 2019, Elsevier. p. 287-317.
228. Junkar, I., M. Modic, and M. Mozeti, *Modification of PET surface properties using extremely non-equilibrium oxygen plasma.* Open Chemistry, 2015. **13**(1).
229. Vesel, A., et al., *Evolution of the Surface Wettability of PET Polymer upon Treatment with an Atmospheric-Pressure Plasma Jet.* Polymers (Basel), 2020. **12**(1).
230. Recek, N., et al., *Adsorption of Proteins and Cell Adhesion to Plasma Treated Polymer Substrates.* International Journal of Polymeric Materials and Polymeric Biomaterials, 2014. **63**(13): p. 685-691.
231. Sasmazel, H.T., S. Manolache, and M. Gümüşderelioğlu, *Functionalization of Nonwoven Pet Fabrics by Water/O2 Plasma for Biomolecule Mediated Cell Cultivation.* Plasma Processes and Polymers, 2010. **7**(7): p. 588-600.
232. Kiruthika, M., K. Nivetha, and G. Shanmugavelayutham, *Physical and mechanical properties of surface modified poly ethylene terephthalate films through low pressure plasma and ultra-violet light.* Materials Research Express, 2019. **6**(11): p. 115350.
233. Levchenko, I., et al., *Plasma and Polymers: Recent Progress and Trends.* Molecules, 2021. **26**(13).
234. Zhou, G., et al., *Effects of Oxygen Element and Oxygen-Containing Functional Groups on Surface Wettability of Coal Dust with Various Metamorphic Degrees Based on XPS Experiment.* Journal of Analytical Methods in Chemistry, 2015. **2015**: p. 467242.
235. Štular, D., et al., *Influence of non-thermal plasma treatement on the adsorption of a stimuli-responsive nanogel onto polyethylene terephthalate fabric.* Progress in Organic Coatings, 2018. **120**: p. 198-207.
236. Jaganjac, M., et al., *Oxygen-rich coating promotes binding of proteins and endothelialization of polyethylene terephthalate polymers.* Journal of Biomedical Materials Research Part A, 2014. **102**(7): p. 2305-2314.
237. Kolar, M., et al., *Covalent Binding of Heparin to Functionalized PET Materials for Improved Haemocompatibility.* Materials (Basel), 2015. **8**(4): p. 1526-1544.
238. Beijer, N.R.M., et al., *Dynamic adaptation of mesenchymal stem cell physiology upon exposure to surface micropatterns.* Scientific Reports, 2019. **9**(1): p. 9099.
239. Dozio, S.M., et al., *Differences in osteogenic induction of human mesenchymal stem cells between a tailored 3D hybrid scaffold and a 2D standard culture.* J Mater Sci Mater Med, 2019. **30**(12): p. 136.

240. Duval, K., et al., *Modeling Physiological Events in 2D vs. 3D Cell Culture.* Physiology (Bethesda), 2017. **32**(4): p. 266-277.
241. Jensen, C. and Y. Teng, *Is It Time to Start Transitioning From 2D to 3D Cell Culture?* Frontiers in Molecular Biosciences, 2020. **7**(33).
242. Baruffaldi, D., et al., *3D Cell Culture: Recent Development in Materials with Tunable Stiffness.* ACS Applied Bio Materials, 2021. **4**(3): p. 2233-2250.
243. Friedl, P. and E.B. Bröcker, *The biology of cell locomotion within three-dimensional extracellular matrix.* Cellular and Molecular Life Sciences CMLS, 2000. **57**(1): p. 41-64.
244. Keely, P. and A. Nain, *Capturing relevant extracellular matrices for investigating cell migration [version 1; peer review: 2 approved].* F1000Research, 2015. **4**(1408).
245. Jenkins, T.L. and D. Little, *Synthetic scaffolds for musculoskeletal tissue engineering: cellular responses to fiber parameters.* npj Regenerative Medicine, 2019. **4**(1): p. 15.
246. Filová, E., et al., *Regionally-selective cell colonization of micropatterned surfaces prepared by plasma polymerization of acrylic acid and 1,7-octadiene.* Physiol Res, 2009. **58**(5): p. 669-684.
247. Bačáková, L., et al., *Adhesion and proliferation of rat vascular smooth muscle cells (VSMC) on polyethylene implanted with O+ and C+ ions.* Journal of Biomaterials Science, Polymer Edition, 2001. **12**(7): p. 817-834.
248. Liu, J.-R., et al., *Low temperature plasma promoting fibroblast proliferation by activating the NF-κB pathway and increasing cyclinD1 expression.* Scientific Reports, 2017. **7**(1): p. 11698.
249. Wei, Q., et al., *Dynamic wetting behavior of plasma treated PET fibers.* Journal of Materials Processing Technology, 2007. **194**(1): p. 89-92.
250. Tomoyuki Matsumoto, S.M.I., Yutaka Mifune, Aki Osawa, Alison Logar, Arvydas Usas, Ryosuke Kuroda, Masahiro Kurosaka, Freddie H. Fu, and Johnny Huard, *Isolation and Characterization of Human Anterior Cruciate Ligament-Derived Vascular Stem Cells.* Stem Cells and Development, 2012. **21**(6): p. 859-872.
251. Wang, P.Y., et al., *Modulation of cell attachment and collagen production of anterior cruciate ligament cells via submicron grooves/ridges structures with different cell affinity.* Biotechnol Bioeng, 2013. **110**(1): p. 327-37.
252. Ejtehadifar, M., et al., *The Effect of Hypoxia on Mesenchymal Stem Cell Biology.* Adv Pharm Bull, 2015. **5**(2): p. 141-9.
253. Antebi, B., et al., *Short-term physiological hypoxia potentiates the therapeutic function of mesenchymal stem cells.* Stem Cell Research & Therapy, 2018. **9**(1): p. 265.
254. Ménétrey, J., et al., *"Biological failure" of the anterior cruciate ligament graft.* Knee Surg Sports Traumatol Arthrosc, 2008. **16**(3): p. 224-31.
255. Corsetti, J.R. and D.W. Jackson, *Failure of anterior cruciate ligament reconstruction: the biologic basis.* Clin Orthop Relat Res, 1996(325): p. 42-9.
256. Griffon, D.J., et al., *Effects of Hypoxia and Chitosan on Equine Umbilical Cord-Derived Mesenchymal Stem Cells.* Stem Cells International, 2016. **2016**: p. 2987140.
257. Bashur, C.A., et al., *Effect of fiber diameter and alignment of electrospun polyurethane meshes on mesenchymal progenitor cells.* Tissue Eng Part A, 2009. **15**(9): p. 2435-45.
258. Olvera, D., et al., *Modulating microfibrillar alignment and growth factor stimulation to regulate mesenchymal stem cell differentiation.* Acta Biomaterialia, 2017. **64**: p. 148-160.
259. Cheng, M.T., et al., *Optimization of culture conditions for stem cells derived from human anterior cruciate ligament and bone marrow.* Cell Transplant, 2014. **23**(7): p. 791-803.
260. Subramony, S.D., et al., *Combined effects of chemical priming and mechanical stimulation on mesenchymal stem cell differentiation on nanofiber scaffolds.* J Biomech, 2014. **47**(9): p. 2189-96.

261. Altman, G.H., et al., *Cell differentiation by mechanical stress.* The FASEB Journal, 2002. **16**(2): p. 1-13.
262. Grier, W.G., A.S. Moy, and B.A. Harley, *Cyclic tensile strain enhances human mesenchymal stem cell Smad 2/3 activation and tenogenic differentiation in anisotropic collagen-glycosaminoglycan scaffolds.* Eur Cell Mater, 2017. **33**: p. 227-239.
263. Li, Y., et al., *Differentiation of Human Amniotic Mesenchymal Stem Cells into Human Anterior Cruciate Ligament Fibroblast Cells by In Vitro Coculture.* Biomed Res Int, 2017. **2017**: p. 7360354.
264. Hanna, H., L.M. Mir, and F.M. Andre, *In vitro osteoblastic differentiation of mesenchymal stem cells generates cell layers with distinct properties.* Stem Cell Research & Therapy, 2018. **9**(1): p. 203.
265. Woodfield, T.B.F., et al., *The regulation of expanded human nasal chondrocyte re-differentiation capacity by substrate composition and gas plasma surface modification.* Biomaterials, 2006. **27**(7): p. 1043-1053.
266. McBeath, R., et al., *Cell Shape, Cytoskeletal Tension, and RhoA Regulate Stem Cell Lineage Commitment.* Developmental Cell, 2004. **6**(4): p. 483-495.
267. Nelea, V., et al., *Selective inhibition of type X collagen expression in human mesenchymal stem cell differentiation on polymer substrates surface-modified by glow discharge plasma.* Journal of Biomedical Materials Research Part A, 2005. **75A**(1): p. 216-223.
268. Demina, T.S., et al., *Plasma Treatment of Poly(ethylene terephthalate) Films and Chitosan Deposition: DC- vs. AC-Discharge.* Materials (Basel), 2020. **13**(3).
269. Curran, J.M., R. Chen, and J.A. Hunt, *The guidance of human mesenchymal stem cell differentiation in vitro by controlled modifications to the cell substrate.* Biomaterials, 2006. **27**(27): p. 4783-4793.
270. Li, Y., et al., *Promotion of osteogenic differentiation by non-thermal biocompatible plasma treated chitosan scaffold.* Scientific Reports, 2019. **9**(1): p. 3712.
271. Nandakumar, A., et al., *Surface modification of electrospun fibre meshes by oxygen plasma for bone regeneration.* Biofabrication, 2012. **5**(1): p. 015006.
272. van der List, J.P., D.N. Mintz, and G.S. DiFelice, *The Location of Anterior Cruciate Ligament Tears: A Prevalence Study Using Magnetic Resonance Imaging.* Orthop J Sports Med, 2017. **5**(6): p. 2325967117709966.
273. Zantop, T., et al., *Intraarticular rupture pattern of the ACL.* Clin Orthop Relat Res, 2007. **454**: p. 48-53.
274. MEI, Y., et al., *Clinical characteristics of 4355 patients with anterior cruciate ligament injury.* Chinese Medical Journal, 2013. **126**(23): p. 4487-4492.
275. Li, H., et al., *The use of layer by layer self-assembled coatings of hyaluronic acid and cationized gelatin to improve the biocompatibility of poly(ethylene terephthalate) artificial ligaments for reconstruction of the anterior cruciate ligament.* Acta Biomaterialia, 2012. **8**(11): p. 4007-4019.
276. Li, H., et al., *The Effect of Layer-by-Layer Chitosan–Hyaluronic Acid Coating on Graft-to-Bone Healing of a Poly(Ethylene Terephthalate) Artificial Ligament.* Journal of Biomaterials Science, Polymer Edition, 2012. **23**(1-4): p. 425-438.
277. Comper, W.D. and T.C. Laurent, *Physiological function of connective tissue polysaccharides.* Physiological reviews, 1978. **58**(1): p. 255-315.
278. Malafaya, P.B., G.A. Silva, and R.L. Reis, *Natural-origin polymers as carriers and scaffolds for biomolecules and cell delivery in tissue engineering applications.* Adv Drug Deliv Rev, 2007. **59**(4-5): p. 207-33.
279. Rinaudo, M., *Properties and degradation of selected polysaccharides: hyaluronan and chitosan.* Corrosion Engineering, Science and Technology, 2007. **42**(4): p. 324-334.

280. de Souza, F.C.B., et al., *Comparative study on complexes formed by chitosan and different polyanions: Potential of chitosan-pectin biomaterials as scaffolds in tissue engineering.* International Journal of Biological Macromolecules, 2019. **132**: p. 178-189.
281. Majima, T., et al., *Chitosan-based hyaluronan hybrid polymer fibre scaffold for ligament and tendon tissue engineering.* Proceedings of the Institution of Mechanical Engineers Part H-Journal of Engineering in Medicine, 2007. **221**(H5): p. 537-546.
282. Brasselet, C., et al., *Modification of Chitosan for the Generation of Functional Derivatives.* Applied Sciences, 2019. **9**(7): p. 1321.
283. Cheung, R.C., et al., *Chitosan: An Update on Potential Biomedical and Pharmaceutical Applications.* Mar Drugs, 2015. **13**(8): p. 5156-86.
284. Kurita, K., *Chitin and chitosan: functional biopolymers from marine crustaceans.* Mar Biotechnol (NY), 2006. **8**(3): p. 203-26.
285. Zargar, V., M. Asghari, and A. Dashti, *A Review on Chitin and Chitosan Polymers: Structure, Chemistry, Solubility, Derivatives, and Applications.* Chembioeng Reviews, 2015. **2**(3): p. 204-226.
286. Rinaudo, M., *Main properties and current applications of some polysaccharides as biomaterials.* Polymer International, 2008. **57**(3): p. 397-430.
287. Ravi Kumar, M.N.V., *A review of chitin and chitosan applications.* Reactive and Functional Polymers, 2000. **46**(1): p. 1-27.
288. Muzzarelli, R.A.A., et al., *Chitosan, hyaluronan and chondroitin sulfate in tissue engineering for cartilage regeneration: A review.* Carbohydrate Polymers, 2012. **89**(3): p. 723-739.
289. Funakoshi, T., et al., *Novel chitosan-based hyaluronan hybrid polymer fibers as a scaffold in ligament tissue engineering.* J Biomed Mater Res A, 2005. **74**(3): p. 338-46.
290. Tamura, H., Y. Tsuruta, and S. Tokura, *Preparation of chitosan-coated alginate filament.* Materials Science and Engineering: C, 2002. **20**(1): p. 143-147.
291. Zemljič, L.F., et al., *Chitosan coatings onto polyethylene terephthalate for the development of potential active packaging material.* Applied Surface Science, 2013. **265**: p. 697-703.
292. Jurak, M., et al., *Chitosan/phospholipid coated polyethylene terephthalate (PET) polymer surfaces activated by air plasma.* Colloids and Surfaces A: Physicochemical and Engineering Aspects, 2017. **532**: p. 155-164.
293. Chen, C., et al., *Preparation and in vitro evaluation of a biomimetic nanoscale calcium phosphate coating on a polyethylene terephthalate artificial ligament.* Exp Ther Med, 2016. **12**(1): p. 302-306.
294. Day, R.M. and M.M. Mascarenhas, *Chapter 7 - Signal Transduction Associated with Hyaluronan*, in *Chemistry and Biology of Hyaluronan*, H.G. Garg and C.A. Hales, Editors. 2004, Elsevier Science Ltd: Oxford. p. 153-188.
295. Zhuo, L., et al., *Chapter 9 - Biological Function of SHAP–Hyaluronan Covalent Complex*, in *Chemistry and Biology of Hyaluronan*, H.G. Garg and C.A. Hales, Editors. 2004, Elsevier Science Ltd: Oxford. p. 205-222.
296. Tang, Z., et al., *Differential expression of matrix metalloproteinases and tissue inhibitors of metalloproteinases in anterior cruciate ligament and medial collateral ligament fibroblasts after a mechanical injury: involvement of the p65 subunit of NF-kappaB.* Wound Repair Regen, 2009. **17**(5): p. 709-16.
297. Asari, A., *Chapter 21 - Medical Application of Hyaluronan*, in *Chemistry and Biology of Hyaluronan*, H.G. Garg and C.A. Hales, Editors. 2004, Elsevier Science Ltd: Oxford. p. 457-473.
298. Li, C., et al., *A review on the wide range applications of hyaluronic acid as a promising rejuvenating biomacromolecule in the treatments of bone related diseases.* Int J Biol Macromol, 2020. **165**(Pt A): p. 1264-1275.

299. Santin, M., *4 - Soft tissue applications of biocomposites*, in *Biomedical Composites*, L. Ambrosio, Editor. 2010, Woodhead Publishing. p. 59-97.
300. Levick, J.R. and J.N. McDonald, *Fluid movement across synovium in healthy joints: role of synovial fluid macromolecules.* Ann Rheum Dis, 1995. **54**(5): p. 417-23.
301. Tamer, T.M., *Hyaluronan and synovial joint: function, distribution and healing.* Interdiscip Toxicol, 2013. **6**(3): p. 111-25.
302. Temple-Wong, M.M., et al., *Hyaluronan concentration and size distribution in human knee synovial fluid: variations with age and cartilage degeneration.* Arthritis Res Ther, 2016. **18**: p. 18.
303. Seo, Y.-K., et al., *Increase in cell migration and angiogenesis in a composite silk scaffold for tissue-engineered ligaments.* Journal of Orthopaedic Research, 2009. **27**(4): p. 495-503.
304. Campoccia, D., et al., *Semisynthetic resorbable materials from hyaluronan esterification.* Biomaterials, 1998. **19**(23): p. 2101-27.
305. Cristino, S., et al., *Analysis of mesenchymal stem cells grown on a three-dimensional HYAFF 11-based prototype ligament scaffold.* J Biomed Mater Res A, 2005. **73**(3): p. 275-83.
306. Vindigni, V., et al., *Preliminary Report of In Vitro Reconstruction of a Vascularized Tendonlike Structure: A Novel Application for Adipose-Derived Stem Cells.* Annals of Plastic Surgery, 2013. **71**(6): p. 664-670.
307. Flores-Ramirez, N., et al., *Characterization and degradation of functionalized chitosan with glycidyl methacrylate.* Journal of Biomaterials Science-Polymer Edition, 2005. **16**(4): p. 473-488.
308. Hong, H., et al., *Cytocompatibility of Modified Silk Fibroin with Glycidyl Methacrylate for Tissue Engineering and Biomedical Applications.* Biomolecules, 2021. **11**(1): p. 35.
309. Baier Leach, J., et al., *Photocrosslinked hyaluronic acid hydrogels: Natural, biodegradable tissue engineering scaffolds.* Biotechnology and Bioengineering, 2003. **82**(5): p. 578-589.
310. Möller, S., et al., *Dextran and hyaluronan methacrylate based hydrogels as matrices for soft tissue reconstruction.* Biomolecular Engineering, 2007. **24**(5): p. 496-504.
311. Inukai, M., et al., *Preparation and Characterization of Hyaluronate-Hydroxyethyl Acrylate Blend Hydrogel for Controlled Release Device.* CHEMICAL & PHARMACEUTICAL BULLETIN, 2000. **48**(6): p. 850-854.
312. Ibrahim, S., C.R. Kothapalli, and A. Ramamurthi, *Characterization of glycidyl methacrylate - Crosslinked hyaluronan hydrogel scaffolds incorporating elastogenic hyaluronan oligomers.* 2011. **- 7**(- 2): p. - 665.
313. Elizalde-Pena, E.A., et al., *Synthesis and characterization of chitosan-g-glycidyl methacrylate with methyl methacrylate.* European Polymer Journal, 2007. **43**(9): p. 3963-3969.
314. Elizalde-Pena, E.A., et al., *Synthesis and characterization of a hybrid (chitosan-g-glycidyl methacrylate)-xanthan hydrogel.* Journal of Biomaterials Science-Polymer Edition, 2013. **24**(12): p. 1426-1442.
315. Araque-Monros, M.C., et al., *Regenerative and Resorbable PLA/HA Hybrid Construct for Tendon/Ligament Tissue Engineering.* Annals of Biomedical Engineering, 2020. **48**(2): p. 757-767.
316. Deepthi, S., et al., *Chitosan–hyaluronic acid hydrogel coated poly(caprolactone) multiscale bilayer scaffold for ligament regeneration.* Chemical Engineering Journal, 2015. **260**: p. 478-485.
317. Strobel, M., et al., *A comparison of gas-phase methods of modifying polymer surfaces.* Journal of Adhesion Science and Technology, 1995. **9**(3): p. 365-383.
318. Learn, G.D., E.J. Lai, and H.A. von Recum, *Nonthermal Plasma Treatment Improves Uniformity and Adherence of Cyclodextrin-Based Coatings on Hydrophobic Polymer Substrates.* Coatings, 2020. **10**(11): p. 1056.

319. Demina, T.S., et al., *Plasma Treatment of Poly(ethylene terephthalate) Films and Chitosan Deposition: DC- vs. AC-Discharge.* Materials (Basel, Switzerland), 2020. **13**(3): p. 508.
320. Siow, K.S., S. Kumar, and H.J. Griesser, *Low-Pressure Plasma Methods for Generating Non-Reactive Hydrophilic and Hydrogel-Like Bio-Interface Coatings – A Review.* Plasma Processes and Polymers, 2015. **12**(1): p. 8-24.
321. Stoleru, E., et al., *Novel procedure to enhance PLA surface properties by chitosan irreversible immobilization.* Applied Surface Science, 2016. **367**: p. 407-417.
322. Pilliar, R.M., *6 - Sol–gel surface modification of biomaterials*, in *Surface Coating and Modification of Metallic Biomaterials*, C. Wen, Editor. 2015, Woodhead Publishing. p. 185-217.
323. Giurlani, W., et al., *Measuring the Thickness of Metal Coatings: A Review of the Methods.* Coatings, 2020. **10**(12): p. 1211.
324. Paul, R. and E. Genescà, *8 - The use of enzymatic techniques in the finishing of technical textiles*, in *Advances in the Dyeing and Finishing of Technical Textiles*, M.L. Gulrajani, Editor. 2013, Woodhead Publishing. p. 177-198.
325. Milosavljević, N.B., et al., *Removal of Cu2+ ions using hydrogels of chitosan, itaconic and methacrylic acid: FTIR, SEM/EDX, AFM, kinetic and equilibrium study.* Colloids and Surfaces A: Physicochemical and Engineering Aspects, 2011. **388**(1-3): p. 59-69.
326. Masoomi, M., M. Tavangar, and S.M.R. Razavi, *Preparation and investigation of mechanical and antibacterial properties of poly(ethylene terephthalate)/chitosan blend.* RSC Advances, 2015. **5**(96): p. 79200-79206.
327. Lin, J.-H., et al., *Polyethylene terephthalate/chitosan tubular knits made by using a freeze-drying method.* Textile Research Journal, 2014. **84**(17): p. 1881-1890.
328. Salmah, H. and A.N. Azieyanti, *Properties of recycled polyethylene/ chitosan composites: the effect of polyethylene-graft-maleic anhydride.* Journal of Reinforced Plastics and Composites, 2011. **30**(3): p. 195-202.
329. Svensson, R.B., et al., *Tensile properties of human collagen fibrils and fascicles are insensitive to environmental salts.* Biophys J, 2010. **99**(12): p. 4020-7.
330. An, L.N.M., et al. *Fabrication of N,O Carboxymethyl Chitosan (NOCC)—Aldehyde Hyaluronic Acid (AHA)—Biphasic Calcium Phosphate (BCP)—Poly (Vinyl Phosphonic Acid) (PVPA) Hydrogel for Bone Regeneration*. 2020. Singapore: Springer Singapore.
331. Li, L., et al., *Biodegradable and injectable in situ cross-linking chitosan-hyaluronic acid based hydrogels for postoperative adhesion prevention.* Biomaterials, 2014. **35**(12): p. 3903-3917.
332. Deng, Y., et al., *Injectable in situ cross-linking chitosan-hyaluronic acid based hydrogels for abdominal tissue regeneration.* Scientific Reports, 2017. **7**(1): p. 2699.
333. Tan, H., et al., *Injectable in situ forming biodegradable chitosan-hyaluronic acid based hydrogels for cartilage tissue engineering.* Biomaterials, 2009. **30**(13): p. 2499-506.
334. Moreau, J.E., et al., *Sequential biochemical and mechanical stimulation in the development of tissue-engineered ligaments.* Tissue Eng Part A, 2008. **14**(7): p. 1161-72.
335. Garcia Garcia, A., et al., *Monitoring mechanical stimulation for optimal tendon tissue engineering: A mechanical and biological multiscale study.* Journal of Biomedical Materials Research Part A. **n/a**(n/a).
336. Kjær, M., et al., *From mechanical loading to collagen synthesis, structural changes and function in human tendon.* Scandinavian Journal of Medicine & Science in Sports, 2009. **19**(4): p. 500-510.
337. Deniz, P., et al., *Use of cyclic strain bioreactor for the upregulation of key tenocyte gene expression on Poly(glycerol-sebacate) (PGS) sheets.* Materials Science and Engineering: C, 2020. **106**: p. 110293.

338. Beynnon, B.D., R.J. Johnson, and B.C. Fleming, *The science of anterior cruciate ligament rehabilitation.* Clin Orthop Relat Res, 2002(402): p. 9-20.
339. Luque-Seron, J.A. and I. Medina-Porqueres, *Anterior Cruciate Ligament Strain In Vivo: A Systematic Review.* Sports Health, 2016. **8**(5): p. 451-5.
340. Johnson, G.A., et al., *A Single Integral Finite Strain Viscoelastic Model of Ligaments and Tendons.* Journal of Biomechanical Engineering, 1996. **118**(2): p. 221-226.
341. Provenzano, P., et al., *Nonlinear Ligament Viscoelasticity.* Annals of Biomedical Engineering, 2001. **29**(10): p. 908-914.
342. van Dommelen, J.A.W., et al., *Nonlinear Viscoelastic Behavior of Human Knee Ligaments Subjected to Complex Loading Histories.* Annals of Biomedical Engineering, 2006. **34**(6): p. 1008-1018.
343. Sun, L., et al., *Effects of Mechanical Stretch on Cell Proliferation and Matrix Formation of Mesenchymal Stem Cell and Anterior Cruciate Ligament Fibroblast.* Stem Cells International, 2016. **2016**: p. 9842075.
344. Gracey, E., et al., *Tendon and ligament mechanical loading in the pathogenesis of inflammatory arthritis.* Nat Rev Rheumatol, 2020. **16**(4): p. 193-207.
345. Dudhia, J., et al., *Aging enhances a mechanically-induced reduction in tendon strength by an active process involving matrix metalloproteinase activity.* Aging Cell, 2007. **6**(4): p. 547-56.
346. Kook, S.H., et al., *Mechanical force induces type I collagen expression in human periodontal ligament fibroblasts through activation of ERK/JNK and AP-1.* J Cell Biochem, 2009. **106**(6): p. 1060-7.
347. Miyaki, S., et al., *Mechanical stretch in anterior cruciate ligament derived cells regulates type I collagen and decorin expression through extracellular signal-regulated kinase 1/2 pathway.* Materials Science and Engineering: C, 2001. **17**(1): p. 91-94.
348. Hannafin, J.A., et al., *Effect of cyclic strain and plating matrix on cell proliferation and integrin expression by ligament fibroblasts.* J Orthop Res, 2006. **24**(2): p. 149-58.
349. Kreja, L., et al., *Effects of mechanical strain on human mesenchymal stem cells and ligament fibroblasts in a textured poly(l-lactide) scaffold for ligament tissue engineering.* Journal of Materials Science: Materials in Medicine, 2012. **23**(10): p. 2575-2582.
350. Wang, J.H., et al., *Mechanoregulation of gene expression in fibroblasts.* Gene, 2007. **391**(1-2): p. 1-15.
351. Dyment, N.A., et al., *A brief history of tendon and ligament bioreactors: Impact and future prospects.* Journal of Orthopaedic Research, 2020. **38**(11): p. 2318-2330.
352. Haus, J. and Z. Halata, *Innervation of the anterior cruciate ligament.* Int Orthop, 1990. **14**(3): p. 293-6.
353. Zimny, M.L., M. Schutte, and E. Dabezies, *Mechanoreceptors in the human anterior cruciate ligament.* Anat Rec, 1986. **214**(2): p. 204-9.
354. Nagelli, C.V. and T.E. Hewett, *Should Return to Sport be Delayed Until 2 Years After Anterior Cruciate Ligament Reconstruction? Biological and Functional Considerations.* Sports Med, 2017. **47**(2): p. 221-232.
355. Çabuk, H. and F. Kuşku Çabuk, *Mechanoreceptors of the ligaments and tendons around the knee.* Clin Anat, 2016. **29**(6): p. 789-95.
356. Gao, F., et al., *A Morphologic and Quantitative Study of Mechanoreceptors in the Remnant Stump of the Human Anterior Cruciate Ligament.* Arthroscopy: The Journal of Arthroscopic & Related Surgery, 2016. **32**(2): p. 273-280.
357. Nayak, M., et al., *Quantitative correlation of mechanoreceptors in tibial remnant of ruptured human anterior cruciate ligament with duration of injury and its significance: an immunohistochemistry-based observational study.* J Orthop Traumatol, 2018. **19**(1): p. 5.

358. Schutte, M.J., et al., *Neural anatomy of the human anterior cruciate ligament.* J Bone Joint Surg Am, 1987. **69**(2): p. 243-7.
359. Katonis, P., et al., *Mechanoreceptors of the posterior cruciate ligament.* J Int Med Res, 2008. **36**(3): p. 387-93.
360. Halata, Z. and J. Haus, *The ultrastructure of sensory nerve endings in human anterior cruciate ligament.* Anatomy and Embryology, 1989. **179**(5): p. 415-421.
361. Kholinne, E., et al., *Mechanoreceptors distribution in the human medial collateral ligament of the elbow.* Orthopaedics & Traumatology: Surgery & Research, 2018. **104**(2): p. 251-255.
362. Gillquist, J., *Knee ligaments and proprioception.* Acta Orthopaedica Scandinavica, 1996. **67**(6): p. 533-535.
363. Sjölander, P., H. Johansson, and M. Djupsjöbacka, *Spinal and supraspinal effects of activity in ligament afferents.* J Electromyogr Kinesiol, 2002. **12**(3): p. 167-76.
364. Solomonow, M. and M. Krogsgaard, *Sensorimotor control of knee stability. A review.* Scand J Med Sci Sports, 2001. **11**(2): p. 64-80.
365. Mora, J.C., R. Przkora, and Y. Cruz-Almeida, *Knee osteoarthritis: pathophysiology and current treatment modalities.* J Pain Res, 2018. **11**: p. 2189-2196.
366. Zhang, S., et al., *Tissue Strain Reorganizes Collagen With a Switchlike Response That Regulates Neuronal Extracellular Signal-Regulated Kinase Phosphorylation In Vitro: Implications for Ligamentous Injury and Mechanotransduction.* Journal of Biomechanical Engineering, 2016. **138**(2).
367. Hoey, D.A., et al., *Primary cilia-mediated mechanotransduction in human mesenchymal stem cells.* Stem Cells, 2012. **30**(11): p. 2561-70.
368. Innocenti, M., *New insights into the formation and the function of lamellipodia and ruffles in mesenchymal cell migration.* Cell Adh Migr, 2018. **12**(5): p. 401-416.
369. Gesink, D.S., et al., *Immunohistochemical localization of beta 1-integrins in anterior cruciate and medial collateral ligaments of human and rabbit.* J Orthop Res, 1992. **10**(4): p. 596-9.
370. Kaneko, D., et al., *Temporal Effects of Cyclic Stretching on Distribution and Gene Expression of Integrin and Cytoskeleton by Ligament Fibroblasts In Vitro.* Connective Tissue Research, 2009. **50**(4): p. 263-269.
371. Munger, J.S. and D. Sheppard, *Cross Talk among TGF-β Signaling Pathways, Integrins, and the Extracellular Matrix.* Cold Spring Harbor Perspectives in Biology, 2011. **3**(11).
372. Tetsunaga, T., et al., *Mechanical stretch stimulates integrin alphaVbeta3-mediated collagen expression in human anterior cruciate ligament cells.* J Biomech, 2009. **42**(13): p. 2097-103.
373. Mousavizadeh, R., et al., *β1 integrin, ILK and mTOR regulate collagen synthesis in mechanically loaded tendon cells.* Scientific Reports, 2020. **10**(1): p. 12644.
374. Tetsunaga, T., et al., *Mechanical stretch stimulates integrin αVβ3-mediated collagen expression in human anterior cruciate ligament cells.* Journal of Biomechanics, 2009. **42**(13): p. 2097-2103.
375. Gilchrist, C.L., et al., *TRPV4-mediated calcium signaling in mesenchymal stem cells regulates aligned collagen matrix formation and vinculin tension.* Proceedings of the National Academy of Sciences, 2019. **116**(6): p. 1992-1997.
376. Meşe, G., G. Richard, and T.W. White, *Gap Junctions: Basic Structure and Function.* Journal of Investigative Dermatology, 2007. **127**(11): p. 2516-2524.
377. Giepmans, B.N.G., *Gap junctions and connexin-interacting proteins.* Cardiovascular Research, 2004. **62**(2): p. 233-245.
378. Maeda, E., et al., *Gap junction permeability between tenocytes within tendon fascicles is suppressed by tensile loading.* Biomech Model Mechanobiol, 2012. **11**(3-4): p. 439-47.
379. Janvier, A.J., E. Canty-Laird, and J.R. Henstock, *A universal multi-platform 3D printed bioreactor chamber for tendon tissue engineering.* J Tissue Eng, 2020. **11**: p. 2041731420942462.

380. Wang, T., et al., *Bioreactor design for tendon/ligament engineering.* Tissue Eng Part B Rev, 2013. **19**(2): p. 133-46.
381. Govoni, M., et al., *Mechanical Actuation Systems for the Phenotype Commitment of Stem Cell-Based Tendon and Ligament Tissue Substitutes.* Stem Cell Reviews and Reports, 2016. **12**(2): p. 189-201.
382. Yu, H.S., et al., *Impact of mechanical stretch on the cell behaviors of bone and surrounding tissues.* Journal of Tissue Engineering , 7 pp. 1-24. (2016), 2016.
383. Salameh, A. and S. Dhein, *Effects of mechanical forces and stretch on intercellular gap junction coupling.* Biochimica et Biophysica Acta (BBA) - Biomembranes, 2013. **1828**(1): p. 147-156.
384. Laurent, C.P., et al., *Towards a Tissue-Engineered Ligament: Design and Preliminary Evaluation of a Dedicated Multi-Chamber Tension-Torsion Bioreactor.* Processes, 2014. **2**(1): p. 167-179.
385. Lee, K.I., et al., *In Vitro and In Vivo Performance of Tissue-Engineered Tendons for Anterior Cruciate Ligament Reconstruction.* The American Journal of Sports Medicine, 2018. **46**(7): p. 1641-1649.
386. Araque-Monros, M.C., et al., *New bioreactor for mechanical stimulation of cultured tendon-like constructs: design and validation.* Expert Review of Medical Devices, 2020. **17**(10): p. 1115-1121.
387. Youngstrom, D.W., J.E. LaDow, and J.G. Barrett, *Tenogenesis of bone marrow-, adipose-, and tendon-derived stem cells in a dynamic bioreactor.* Connective Tissue Research, 2016. **57**(6): p. 454-465.
388. Subramanian, G., et al., *Effect of Uniaxial Tensile Cyclic Loading Regimes on Matrix Organization and Tenogenic Differentiation of Adipose-Derived Stem Cells Encapsulated within 3D Collagen Scaffolds.* Stem Cells International, 2017. **2017**: p. 6072406.
389. Nam, H.Y., et al., *Uniaxial Cyclic Tensile Stretching at 8% Strain Exclusively Promotes Tenogenic Differentiation of Human Bone Marrow-Derived Mesenchymal Stromal Cells.* Stem Cells Int, 2019. **2019**: p. 9723025.
390. Kim, J.G., et al., *Accelerated Versus Non-accelerated Rehabilitation After Primary Anterior Cruciate Ligament Reconstruction Using Hamstring Autografts: A Systematic Review and Meta-analysis of Comparative Studies.* Indian Journal of Orthopaedics, 2021. **55**(2): p. 405-415.
391. Pitman, M.I., et al., *The intraoperative evaluation of the neurosensory function of the anterior cruciate ligament in humans using somatosensory evoked potentials.* Arthroscopy: The Journal of Arthroscopic & Related Surgery, 1992. **8**(4): p. 442-447.
392. Bates, N.A., et al., *Variation in ACL and MCL Strain Before Initial Contact Is Dependent on Injury Risk Level During Simulated Landings.* Orthopaedic Journal of Sports Medicine, 2019. **7**(11): p. 2325967119884906.
393. Howe, J.G., et al., *Arthroscopic strain gauge measurement of the normal anterior cruciate ligament.* Arthroscopy: The Journal of Arthroscopic & Related Surgery, 1990. **6**(3): p. 198-204.
394. Fleming, B.C., et al., *The Strain Behavior of the Anterior Cruciate Ligament During Stair Climbing: An In Vivo Study.* Arthroscopy: The Journal of Arthroscopic & Related Surgery, 1999. **15**(2): p. 185-191.
395. Gumbiner, B.M., *Cell Adhesion: The Molecular Basis of Tissue Architecture and Morphogenesis.* Cell, 1996. **84**(3): p. 345-357.
396. Eyckmans, J. and C.S. Chen, *3D culture models of tissues under tension.* J Cell Sci, 2017. **130**(1): p. 63-70.
397. Nicolas, A., B. Geiger, and S.A. Safran, *Cell mechanosensitivity controls the anisotropy of focal adhesions.* Proceedings of the National Academy of Sciences of the United States of America, 2004. **101**(34): p. 12520-12525.

398. Joshi, S.D. and K. Webb, *Variation of cyclic strain parameters regulates development of elastic modulus in fibroblast/substrate constructs.* J Orthop Res, 2008. **26**(8): p. 1105-13.
399. Juncosa-Melvin, N., et al., *Effects of mechanical stimulation on the biomechanics and histology of stem cell-collagen sponge constructs for rabbit patellar tendon repair.* Tissue Eng, 2006. **12**(8): p. 2291-300.
400. Morita, Y., et al., *Determination of optimal cyclic uniaxial stretches for stem cell-to-tenocyte differentiation under a wide range of mechanical stretch conditions by evaluating gene expression and protein synthesis levels.* Acta Bioeng Biomech, 2013. **15**(3): p. 71-9.
401. Webb, K., et al., *Cyclic strain increases fibroblast proliferation, matrix accumulation, and elastic modulus of fibroblast-seeded polyurethane constructs.* J Biomech, 2006. **39**(6): p. 1136-44.
402. Rahim, M., et al., *Modulators of the extracellular matrix and risk of anterior cruciate ligament ruptures.* Journal of Science and Medicine in Sport, 2017. **20**(2): p. 152-158.
403. Cho, H., et al., *Aging affects response to cyclic tensile stretch: paradigm for intervertebral disc degeneration.* Eur Cell Mater, 2011. **22**: p. 137-45; discussion 145-6.
404. Miller, B.F., et al., *Coordinated collagen and muscle protein synthesis in human patella tendon and quadriceps muscle after exercise.* The Journal of Physiology, 2005. **567**(3): p. 1021-1033.
405. Robbins, J.R., S.P. Evanko, and K.G. Vogel, *Mechanical Loading and TGF-β Regulate Proteoglycan Synthesis in Tendon.* Archives of Biochemistry and Biophysics, 1997. **342**(2): p. 203-211.
406. Susilo, M.E., et al., *Collagen network strengthening following cyclic tensile loading.* Interface Focus, 2016. **6**(1): p. 20150088.
407. Cheema, U., et al., *Engineering Functional Collagen Scaffolds: Cyclical Loading Increases Material Strength and Fibril Aggregation.* Advanced Functional Materials, 2007. **17**(14): p. 2426-2431.
408. Zitnay, J.L., et al., *Accumulation of collagen molecular unfolding is the mechanism of cyclic fatigue damage and failure in collagenous tissues.* Science Advances, 2020. **6**(35): p. eaba2795.
409. Eitzen, I., et al., *A progressive 5-week exercise therapy program leads to significant improvement in knee function early after anterior cruciate ligament injury.* J Orthop Sports Phys Ther, 2010. **40**(11): p. 705-21.
410. Bousquet, B.A., et al., *POST-OPERATIVE CRITERION BASED REHABILITATION OF ACL REPAIRS: A CLINICAL COMMENTARY.* Int J Sports Phys Ther, 2018. **13**(2): p. 293-305.
411. Wang, L. and J.P. Stegemann, *Extraction of high quality RNA from polysaccharide matrices using cetyltrimethylammonium bromide.* Biomaterials, 2010. **31**(7): p. 1612-8.
412. Vennapusa, A.R., et al., *A universal method for high-quality RNA extraction from plant tissues rich in starch, proteins and fiber.* Sci Rep, 2020. **10**(1): p. 16887.
413. Yu, C., et al., *Techniques for the isolation of high-quality RNA from cells encapsulated in chitosan hydrogels.* Tissue Eng Part C Methods, 2013. **19**(11): p. 829-38.
414. White, E.J., et al., *Modified cetyltrimethylammonium bromide method improves robustness and versatility: the benchmark for plant RNA extraction.* Biotechnol J, 2008. **3**(11): p. 1424-8.
415. Thomas, J.M.C., et al., *The Bio-Tribological Characteristics of Synthetic Tissue Grafts.* Proceedings of the Institution of Mechanical Engineers, Part H: Journal of Engineering in Medicine, 2011. **225**(2): p. 141-148.
416. Khassetarash, A., et al., *Fatigue and soft tissue vibration during prolonged running.* Human Movement Science, 2015. **44**: p. 157-167.
417. Funakoshi, M., et al., *Measurement of Whole-Body Vibration in Taxi Drivers.* Journal of Occupational Health, 2004. **46**(2): p. 119-124.
418. McClarren, B. and R. Olabisi, *Strain and Vibration in Mesenchymal Stem Cells.* Int J Biomater, 2018. **2018**: p. 8686794.

419. Friesenbichler, B., et al., *Tissue vibration in prolonged running.* Journal of biomechanics, 2011. **44**(1): p. 116-120.
420. Wakeling, J.M. and B.M. Nigg, *Modification of soft tissue vibrations in the leg by muscular activity.* Journal of Applied Physiology, 2001. **90**(2): p. 412-420.
421. Reda, W. and A. Khedr, *Stump Incorporation for Anterior Cruciate Ligament Reconstruction: A Step Towards a More Anatomical Reconstruction.* Arthrosc Tech, 2017. **6**(4): p. e1303-e1307.
422. Moutzouros, V. and T.R. Jildeh, *Hybrid Remnant-Sparing Anterior Cruciate Ligament Repair-Reconstruction.* Arthrosc Tech, 2021. **10**(7): p. e1717-e1721.
423. Takahashi, T., et al., *A Histological Comparison Between Anterior Cruciate Ligament Remnant Tissue, Anatomically Reconstructed Graft, and Non-Anatomically Reconstructed Graft.* Cureus, 2021. **13**(1): p. e13016.
424. Best, T.M., et al., *Low Intensity Ultrasound for Promoting Soft Tissue Healing: A Systematic Review of the Literature and Medical Technology.* Intern Med Rev (Wash D C), 2016. **2**(11).
425. Fu, S.C., et al., *Low-intensity pulsed ultrasound on tendon healing: a study of the effect of treatment duration and treatment initiation.* Am J Sports Med, 2008. **36**(9): p. 1742-9.
426. Walsh, W.R., et al., *Effects of low-intensity pulsed ultrasound on tendon-bone healing in an intra-articular sheep knee model.* Arthroscopy, 2007. **23**(2): p. 197-204.
427. Warden, S.J., et al., *Low-intensity pulsed ultrasound accelerates and a nonsteroidal anti-inflammatory drug delays knee ligament healing.* Am J Sports Med, 2006. **34**(7): p. 1094-102.
428. Truong, L.K., et al., *Psychological, social and contextual factors across recovery stages following a sport-related knee injury: a scoping review.* British Journal of Sports Medicine, 2020. **54**(19): p. 1149-1156.
429. Xin, Z., et al., *Clinical applications of low-intensity pulsed ultrasound and its potential role in urology.* Transl Androl Urol, 2016. **5**(2): p. 255-66.
430. Watson, T., *Ultrasound in contemporary physiotherapy practice.* Ultrasonics, 2008. **48**(4): p. 321-329.
431. J., D.D. and C.T. E., *The biology of integration of the anterior cruciate ligament.* The Journal of Bone and Joint Surgery. British volume, 2005. **87-B**(7): p. 889-895.
432. Canlong Wang, Y.H., Shichen Zhang, Dengfeng Ruan, Zizhan Huang, Peiwen He, Honglu Cai, Boon Chin Heng, Xiao Chen, Weiliang Shen, , *Application of Stem Cell Therapy for ACL Graft Regeneration.* Stem Cells International, 2021. **2021**: p. 14.
433. Sánchez, M., et al., *Ligamentization of Tendon Grafts Treated With an Endogenous Preparation Rich in Growth Factors: Gross Morphology and Histology.* Arthroscopy: The Journal of Arthroscopic & Related Surgery, 2010. **26**(4): p. 470-480.
434. Mifune, Y., et al., *Therapeutic Potential of Anterior Cruciate Ligament-Derived Stem Cells for Anterior Cruciate Ligament Reconstruction.* Cell Transplantation, 2012. **21**(8): p. 1651-1665.
435. Carlos Vinícius Buarque de Gusmão, J.M.A.a.W.D.B., *Acoustic Therapy as Mechanical Stimulation of Osteogenesis*. Advanced Techniques in Bone Regeneration, ed. A.R.Z.a.J.B.d. Miranda. 2016, IntechOpen.
436. Speed, C.A., *Therapeutic ultrasound in soft tissue lesions.* Rheumatology, 2001. **40**(12): p. 1331-1336.
437. Miller, D.L., et al., *Overview of therapeutic ultrasound applications and safety considerations.* J Ultrasound Med, 2012. **31**(4): p. 623-34.
438. Khanna, A., et al., *The effects of LIPUS on soft-tissue healing: a review of literature.* British Medical Bulletin, 2008. **89**(1): p. 169-182.
439. B. E. Treeby, J.J., E. Martin, B. T. Cox, *From biology to bytes: Predicting the path of ultrasound waves through the human body.* Acoustics Today, 2019. **15**(2): p. 36-44.

440. Maresca, D., et al., *Biomolecular Ultrasound and Sonogenetics.* Annu Rev Chem Biomol Eng, 2018. **9**: p. 229-252.
441. Dholakia, K., B.W. Drinkwater, and M. Ritsch-Marte, *Comparing acoustic and optical forces for biomedical research.* Nature Reviews Physics, 2020. **2**(9): p. 480-491.
442. Furusawa, Y., et al., *Effects of therapeutic ultrasound on the nucleus and genomic DNA.* Ultrasonics Sonochemistry, 2014. **21**(6): p. 2061-2068.
443. Zhou, Y.F., *High intensity focused ultrasound in clinical tumor ablation.* World J Clin Oncol, 2011. **2**(1): p. 8-27.
444. ter Haar, G., *Therapeutic applications of ultrasound.* Progress in Biophysics and Molecular Biology, 2007. **93**(1): p. 111-129.
445. Whittingham, T.A., *Medical diagnostic applications and sources.* Progress in Biophysics and Molecular Biology, 2007. **93**(1): p. 84-110.
446. Tanaka, E., et al., *Low-Intensity Pulsed Ultrasound in Dentofacial Tissue Engineering.* Annals of Biomedical Engineering, 2015. **43**(4): p. 871-886.
447. Rothenberg, J.B., et al., *The Role of Low-Intensity Pulsed Ultrasound on Cartilage Healing in Knee Osteoarthritis: A Review.* PM&R, 2017. **9**(12): p. 1268-1277.
448. Baker, K.G., V.J. Robertson, and F.A. Duck, *A Review of Therapeutic Ultrasound: Biophysical Effects.* Physical Therapy, 2001. **81**(7): p. 1351-1358.
449. Shriki, J., *Ultrasound Physics.* Critical Care Clinics, 2014. **30**(1): p. 1-24.
450. Uzer, G., et al., *Separating Fluid Shear Stress from Acceleration during Vibrations In Vitro: Identification of Mechanical Signals Modulating the Cellular Response.* Cellular and Molecular Bioengineering, 2012. **5**(3): p. 266-276.
451. Vaškovicová, N., et al., *Effects of therapeutic ultrasound on the nuclear envelope and nuclear pore complexes.* Journal of Applied Biomedicine, 2013. **11**(4): p. 235-242.
452. Veronick, J.A., et al., *Mechanically Loading Cell/Hydrogel Constructs with Low-Intensity Pulsed Ultrasound for Bone Repair.* Tissue engineering. Part A, 2018. **24**(3-4): p. 254-263.
453. Harrison, A., et al., *Mode & mechanism of low intensity pulsed ultrasound (LIPUS) in fracture repair.* Ultrasonics, 2016. **70**: p. 45-52.
454. Xavier, C. and L. Duarte, *Ultrasonic stimulation on bone callus: clinical application.* Rev Brazil Orthop, 1983. **18**: p. 73-80.
455. Zhou, S., et al., *Molecular mechanisms of low intensity pulsed ultrasound in human skin fibroblasts.* Journal of Biological Chemistry, 2004. **279**(52): p. 54463-54469.
456. Shimode, K., et al., *Local upregulation of stromal cell--derived factor-1 after ligament injuries enhances homing rate of bone marrow stromal cells in rats.* Tissue Engineering, Part A: Tissue Engineering, 2009. **15**: p. 2277+.
457. Ding, L., et al., *Association of chemokine expression in anterior cruciate ligament deficient knee with patient characteristics: Implications for post-traumatic osteoarthritis.* Knee, 2020. **27**(1): p. 36-44.
458. Warden, S.J., *A New Direction for Ultrasound Therapy in Sports Medicine.* Sports Medicine, 2003. **33**(2): p. 95-107.
459. Ying, Z.M., T. Lin, and S.G. Yan, *Low-intensity pulsed ultrasound therapy: a potential strategy to stimulate tendon-bone junction healing.* J Zhejiang Univ Sci B, 2012. **13**(12): p. 955-63.
460. Lai, W.C., et al., *Low-Intensity Pulsed Ultrasound Augments Tendon, Ligament, and Bone–Soft Tissue Healing in Preclinical Animal Models: A Systematic Review.* Arthroscopy: The Journal of Arthroscopic & Related Surgery, 2021. **37**(7): p. 2318-2333.e3.
461. Franco de Oliveira, R., D.A. Pires Oliveira, and C.P. Soares, *Effect of low-intensity pulsed ultrasound on l929 fibroblasts.* Arch Med Sci, 2011. **7**(2): p. 224-9.

462. Gough, A., et al., *Biologically Relevant Heterogeneity: Metrics and Practical Insights.* SLAS DISCOVERY: Advancing the Science of Drug Discovery, 2017. **22**(3): p. 213-237.
463. Melrose, J., *Glycosaminoglycans in Wound Healing.* Bone and Tissue Regeneration Insights, 2016. **7**: p. BTRI.S38670.
464. Volpi, N., *Therapeutic applications of glycosaminoglycans.* Curr Med Chem, 2006. **13**(15): p. 1799-810.
465. Fu, W., et al., *Mesenchymal stem cells reside in anterior cruciate ligament remnants in situ.* Int Orthop, 2016. **40**(7): p. 1523-30.
466. Nau, T. and A. Teuschl, *Regeneration of the anterior cruciate ligament: Current strategies in tissue engineering.* World J Orthop, 2015. **6**(1): p. 127-36.
467. de Lucas, B., et al., *Ultrasound Therapy: Experiences and Perspectives for Regenerative Medicine.* Genes (Basel), 2020. **11**(9).
468. Liu, D.D., et al., *The role of ultrasound in enhancing mesenchymal stromal cell-based therapies.* STEM CELLS Translational Medicine, 2020. **9**(8): p. 850-866.
469. Zhou, S., et al., *Molecular Mechanisms of Low Intensity Pulsed Ultrasound in Human Skin Fibroblasts*.* Journal of Biological Chemistry, 2004. **279**(52): p. 54463-54469.
470. Carina, V., et al., *Effect of Low-Intensity Pulsed Ultrasound on Osteogenic Human Mesenchymal Stem Cells Commitment in a New Bone Scaffold.* Journal of Applied Biomaterials & Functional Materials, 2017. **15**(3): p. 215-222.
471. Kim, J.Y., et al., *Umbilical cord blood mesenchymal stem cells protect amyloid-β42 neurotoxicity via paracrine.* World J Stem Cells, 2012. **4**(11): p. 110-6.
472. Costa, V., et al., *Osteogenic commitment and differentiation of human mesenchymal stem cells by low-intensity pulsed ultrasound stimulation.* Journal of Cellular Physiology, 2018. **233**(2): p. 1558-1573.
473. Humphrey, J.D., E.R. Dufresne, and M.A. Schwartz, *Mechanotransduction and extracellular matrix homeostasis.* Nature Reviews Molecular Cell Biology, 2014. **15**(12): p. 802-812.
474. Bokhari, A.R. and G.A.C. Murrell, *The role of nitric oxide in tendon healing.* Journal of Shoulder and Elbow Surgery, 2012. **21**(2): p. 238-244.
475. Saini, V. and S. McCormick, *Changes in NO, iNOS and eNOS Expression in MLO-Y4 Cells After Low-intensity Pulsed Ultrasound Treatment With or Without Shear Stress Exposure.* Cellular and Molecular Bioengineering, 2011. **4**(1): p. 91-105.
476. Cheng, B., et al., *PGE(2) is essential for gap junction-mediated intercellular communication between osteocyte-like MLO-Y4 cells in response to mechanical strain.* Endocrinology, 2001. **142**(8): p. 3464-73.
477. Saini, V., S. Yadav, and S. McCormick, *Low-Intensity Pulsed Ultrasound Modulates Shear Stress Induced PGHS-2 Expression and PGE2 Synthesis in MLO-Y4 Osteocyte-Like Cells.* Annals of Biomedical Engineering, 2011. **39**(1): p. 378-393.
478. Attia, M., et al., *Greater glycosaminoglycan content in human patellar tendon biopsies is associated with more pain and a lower VISA score.* Br J Sports Med, 2014. **48**(6): p. 469-75.
479. Fu, S.C., K.M. Chan, and C.G. Rolf, *Increased deposition of sulfated glycosaminoglycans in human patellar tendinopathy.* Clin J Sport Med, 2007. **17**(2): p. 129-34.
480. Xie, Y., et al., *Nanoscale modifications of PET polymer surfaces via oxygen-plasma discharge yield minimal changes in attachment and growth of mammalian epithelial and mesenchymal cells in vitro.* Journal of Biomedical Materials Research, 2002. **61**(2): p. 234-245.
481. Delaine-Smith, R.M. and G.C. Reilly, *Mesenchymal stem cell responses to mechanical stimuli.* Muscles Ligaments Tendons J, 2012. **2**(3): p. 169-80.
482. Sensini, A. and L. Cristofolini, *Biofabrication of Electrospun Scaffolds for the Regeneration of Tendons and Ligaments.* Materials (Basel), 2018. **11**(10).

483. Qasim, S.B., et al., *Electrospinning of Chitosan-Based Solutions for Tissue Engineering and Regenerative Medicine.* Int J Mol Sci, 2018. **19**(2).
484. Snetkov, P., et al., *Hyaluronan-Based Nanofibers: Fabrication, Characterization and Application.* Polymers (Basel), 2019. **11**(12).
485. Vasilieva, T., et al., *Chitosan Plasma Chemical Processing in Beam-Plasma Reactors as a Way of Environmentally Friendly Phytostimulants Production.* Processes, 2021. **9**(1): p. 103.
486. Vasilieva, T., et al., *Hydrolysis of chitin and chitosan in low temperature electron-beam plasma.* Pure and Applied Chemistry, 2016. **88**(9): p. 873-879.